STUDIES ON HOT CORROSION BEHAVIOUR OF CONVENTIONAL AND NANOSTRUCTURED COATINGS

Ph.D. THESIS

by

VISHWAMBHAR NATH SHUKLA

DEPARTMENT OF METALLURGICAL AND MATERIALS ENGINEERING
INDIAN INSTITUTE OF TECHNOLOGY ROORKEE
ROORKEE – 247667, INDIA

DECEMBER, 2013

STUDIES ON HOT CORROSION BEHAVIOUR OF CONVENTIONAL AND NANOSTRUCTURED COATINGS

A THESIS

Submitted in partial fulfilment of the

requirements for the award of the degree

of

DOCTOR OF PHILOSOPHY

in

METALLURGICAL AND MATERIALS ENGINEERING

by

VISHWAMBHAR NATH SHUKLA

DEPARTMENT OF METALLURGICAL AND MATERIALS ENGINEERING
INDIAN INSTITUTE OF TECHNOLOGY ROORKEE
ROORKEE – 247667, INDIA

DECEMBER, 2013

INDIAN INSTITUTE OF TECHNOLOGY ROORKEE
ROORKEE

CANDIDATE'S DECLARATION

I hereby certify that the work which is being presented in the thesis, entitled **"STUDIES ON HOT CORROSION BEHAVIOUR OF CONVENTIONAL AND NANOSTRUCTURED COATINGS"** in partial fulfilment of the requirements for the award of the degree of **Doctor of Philosophy** and submitted in the Department of Metallurgical and Materials Engineering, Indian Institute of Technology Roorkee, Roorkee is an authentic record of my own work carried out during the period from August, 2009 to December, 2013 under the supervision of Dr. R. Jayaganthan, Associate Professor and Dr. V. K. Tewari, Professor, Department of Metallurgical and Materials Engineering, Indian Institute of Technology Roorkee, Roorkee.

The matter presented in this thesis has not been submitted by me for the award of any other degree of this or any other institute.

(**VISHWAMBHAR NATH SHUKLA**)

This is to certify that the above statement made by the candidate is correct to the best of our knowledge.

(V. K. Tewari)
Supervisor

(R. Jayaganthan)
Supervisor

Date:

The Ph.D. Viva-Voce Examination of **Mr. Vishwambhar Nath Shukla,** Research Scholar, has been held on _____

Signature of Supervisor's Chairman, SRC Signature of External Examiner

Head of the Department/ Chairman, ODC

ABSTRACT

Huge amounts of material wastage occur due to high temperature oxidation and erosion of boiler tubes in steam generating system of coal fired boiler and power generation industry, resulting in tube wall thinning and premature failure. Ni-based, Co-based, and Fe-based super alloys have been developed to enhance their high temperature strength and oxidation resistance in high temperature applications. Since these alloys are very costly, a composite system comprising of base material (steel) and wear/corrosion resistant protective surface layer has been proposed as cost effective and most favorable choice of material for combining both mechanical and corrosion resistance properties. Among different approaches employed to ensure longer service life of the components used at elevated temperature, wear and corrosion resistant coatings are widely used to provide protection. It is well known fact that a single material can not provide a combination of both mechanical and corrosion resistance properties. Thermal spray process is widely used to produce wear and corrosion-resistant coatings on the components used in hot section of power generation industry and coal fired boiler as reported in the literature. Fe based high-chromium and nickel containing alloys are extensively used to fabricate corrosion and wear resistant coatings. These FeCr-base coatings are deposited by different thermal spray techniques such as plasma spray process, detonation gun process, high velocity arc spray process (HVAS), and high velocity oxy-fuel process (HVOF). Among all these thermal spray processes, HVOF & HVAS techniques are usually employed due to its high efficiency of deposition and less applications difficulties. HVOF process produces dense coating with higher bond strength and lower oxide content.

Hot corrosion may be defined as an accelerated corrosion, resulting from the presence of salt contaminants such as Na_2SO_4, $Fe_2(SO_4)_3$, NaCl, and V_2O_5 that combine to form molten deposits, which damage the protective surface oxides. At higher temperatures, deposits of Na_2SO_4 are molten (m.p. 884°C) and can cause accelerated attack on boiler steel, the attack is commonly called as hot corrosion. For example, alloys used in gas turbines in aircraft, marine power plants, land-based power generators, boilers, internal combustion engines, fluidized bed combustion and industrial waste incinerators undergo hot corrosion. During hot corrosion, a porous non-protective oxide scale is formed at the surface and sulphides in the substrate. This form of corrosion, unlike oxidation, can consume the material at an unpredictably rapid rate. Consequently, the load-carrying ability of the components reduces quickly, leading eventually to catastrophic failure. For example, boiler steels used for high temperature applications could not meet the requirements of both high-temperature strength and high-temperature erosion–

corrosion resistance, simultaneously. Therefore, thermal spray coatings deposited on 310S alloy substrate provided a significant contribution for combating high temperature oxidation and hot corrosion.

The viable countermeasures against the oxidation and hot corrosion of alloys used in high temperature applications constitute the use of protective coatings. The oxidation and hot corrosion studies of Cr_3C_2-NiCr, FeCr- based conventional and nanostructured coatings developed by HVOF and HVAS spray are limited in the literature. Therefore, oxidation and hot corrosion behavior of austenitic stainless steel designated as 310S as per the manufacturer's specifications, has been investigated with and without the application of thermal spray coatings (Cr_3C_2-NiCr, FeCr- based coatings) in air, Na_2SO_4-60%V_2O_5, Na_2SO_4–82% $Fe_2(SO_4)_3$, at 700 & 900 ^oC, and in actual coal fired boiler environment under cyclic conditions. These alloy substrate (310S) are developed for the high temperature applications such as boilers and gas turbine parts, heat exchangers and piping in chemical industries and high temperature furnace parts.

A thorough investigation on the behaviour of Cr_3C_2-NiCr, FeCr- based conventional and nanostructured coatings in different environment is very essential to choose the suitable coating and substrate for precluding the oxidation and hot corrosion problems manifested in the gas turbine, boiler etc. The results of the present research work are critically analyzed and discussed in light of the existing literature to propose an insight in to the corrosion mechanisms in both coated and bare specimens. The behavior of these coatings in different degrading environments will be helpful in choosing the suitable coating for the hot section components of the thermal power plant.

ACKNOWLEDGEMENT

Every success which is a result of hard efforts never tastes that good if each and every one who participated in it is not acknowledged. First and foremost, I would like to express my gratitude and acknowledgement to almighty God who has given me enthusiasm and passion toward research work. My sincere thanks go to Dr. R. Jayaganthan, and Dr. Vinay Kumar Tewari, Department of Metallurgical and Materials Engineering, Indian Institute of Technology, Roorkee my thesis supervisors for giving me the wonderful opportunity of doing research under them. Their enthusiasm on the problem and encouragement throughout the course of this work is very much appreciable. They have always been available for discussion and guided me to accomplish the objective of this study; they have been an inspiring and driving force during the course of this work. Without their timely help, intellectual input, constructive criticism and painstaking efforts, it would not have been possible for me to complete this thesis in the present form.

I am deeply indebted to Dr. Balbhadra Patruni Vankata Manoj Kumar, for his kind help and everlasting motivation throughout the whole research period.

I would also like to thank Professor S. K. Nath Professor and Head MMED, IIT Roorkee, for his valuable suggestions.

I am great thankful to Dr. Mahadev Chattopadhyay, Calcutta and Dr. O. P. Pandey, Patiala, Panjab who is the spirit and source of inspiration behind this research work**.**

I also wish to thank the whole staff of the Department of Metallurgical and Materials Engineering, Indian Institute of Technology, Roorkee, in particular Mr. Kuldeep Sharma, Mr. Rajinder S. Sharma, Mr. T. K. Sharma, Mr. M. Aslam., Mr Shakti Gupta, Mr S.M. Giri, Mr. Vidya Prakash. Many thanks go to Mr. S.K. Saini, Mr. Rathor, Mr. R. K. Sharma, Mr. Shiv Kumar, Vaibhav Bajpayi and Mr S. D. Sharma of Institute Instrumentation Centre, IIT, Roorkee for helping me in doing XRD, SEM and EDX work.

Thanks are also due to Mr. Sachin Surve without whom this thesis manuscript would not have been in the same format; in fact he has helped a lot. Special thanks are due to Mr. R. Sood, Managing Director, M/s Industrial Processors and Metallizers (IPM), Pvt. Ltd, Delhi, India, for providing the powder and coating facilities.

The discussions and interactions with the colleagues have been very fruitful. Many thank goes to Ph.D. fellows and friends, Mr. Sudhakar Panday, Mr. Ashish Selokar, Mr. Sunkulp Goyal, Mr Vinod Kumar Jinegar, Mr. Nageshwar Rao, Mr Chaitanya Sharma, Mr. Maruf

Husain. At this Moment, I must record my deepest regards and reverence to Almighty and my Parents for their constant support and encouragement.

Finally, I express my indebtedness to "The Lord Hanuman Ji" for all the blessings and kindness. He alone could have (and did) shower on my family and me.

(Vishwambhar Nath Shukla)

TABLE OF CONTENTS

LIST OF FIGURES

LIST OF TABLES

LIST OF RESEARCH PUBLICATION

Research papers published out of the present investigation, in the peer-reviewed journals as well as presented/published in the conferences, are as follows:

(I) REFERRED JOURNALS

1. **V. N. Shukla**, R. Jayaganthan, V. K. Tewari, "Degradation Behavior of Nanostructured Coatings Deposited by High-Velocity Arc Spraying Process in an Actual Environment of a Coal-Fired Boiler", JOM **65(6)** (2013) 784-791.
2. **V. N. Shukla**, R. Jayaganthan, V. K. Tewari, "Environmental Degradation Behavior of high-velocity arc sprayed FeCrBMnSi alloy Coatings in a coal fired boiler, Acta metallurgica sinica (English letters)", **26 (5)** (2013) 602-612.
3. **V. N. Shukla**, V. K. Tewari, R. Jayaganthan, "Comparison of tribological behavior of Cr_3C_2-NiCr coatings deposited by different thermal spray techniques: a review", International Journal of Materials Science and Engineering, **2(1-2)** (2011) 55-58.
4. **V. N. Shukla**, R. Jayaganthan, V. K. Tewari, "Hot corrosion studies of HVOF-sprayed Cr_3C_2-NiCr coating on 310S stainless steel in an actual environment of a coal fired boiler", Advanced Materials Research 585 (2012) 483-487.
5. **V. N. Shukla**, R. Jayaganthan, V. K. Tewari, "Microstructural characterization and cyclic oxidation behavior of HVOF-sprayed Cr_3C_2-NiCr coating on Boiler steel at elevated temperature", Materials Science Forum 736 (2013) 289-300.
6. **V. N. Shukla**, Nidhi Rana, R. Jayaganthan, V. K. Tewari, "Degradation Studies of Wire arc Sprayed FeCrBSiMn alloy Coating in Molten Salt Environment", Procedia Engineering, 2013 (in press).
7. **V. N. Shukla**, R. Jayaganthan, V. K. Tewari, "Degradation behavior of HVOF-sprayed Cr_3C_2-25%NiCr Cermet Coatings exposed to High Temperature Environment", Journal of Materials Engineering and Performance, 2013 (Under review).
8. **V. N. Shukla**, R. Jayaganthan, V. K. Tewari, "Degradation Behavior of High-velocity arc sprayed FeCr based Nanocrystalline alloy Coatings in Molten salt environment", Applied Surface Science, 2013 (Under review).
9. **V. N. Shukla**, R. Jayaganthan, V. K. Tewari, "Role of High-velocity arc sprayed FeCr based Nanostructured coatings in improving High temperature corrosion resistance of 310S steel in presence of Na_2SO_4-82%$Fe_2(SO_4)_3$ salt deposits", Corrosion Science, 2013 (under review).

10. **V. N. Shukla**, R. Jayaganthan, V. K. Tewari, "Degradation Behavior and Microstructural Characterization of HVOF-Sprayed Cr_3C_2-NiCr Cermet Coatings in Molten Salt Environment," International Journal of Materials and Product Technology, 2013 (Under review).

(II) NATIONAL/INTERNATIONAL CONFERENCES PROCEEDINGS

11. **V. N. Shukla**, R. Jayaganthan, V. K. Tewari, "Mechanical and Microstructural properties of HVOF Sprayed Cr_3C_2-25% NiCr Coatings, Microstructure-2011, Department of Metallurgical and Materials Engineering, IIT Roorkee, India, 4-5 Nov, 2011.
12. **V. N. Shukla**, R. Jayaganthan, V. K. Tewari, "Characterizations and Hot corrosion behaviour of HVOF-sprayed Cr_3C_2-NiCr coating on 310S stainless steel in an aggressive environment at 700^0C", Conference on Engineering Coatings: Process, Controls & Applications, EnggCoat-2012, IIT Bombay, India, 9-11 Feb, 2012.
13. **V. N. Shukla**, R. Jayaganthan, V. K. Tewari, "Mechanical and Microstructural characteristics of wire arc sprayed FeCrBSiMn alloy Coatings", The third Asian symposium on Materials & Processing (ASMP 2012), IIT Madras, Chennai,t 30-31 Aug,2012.
14. **V. N. Shukla**, R. Jayaganthan, V. K. Tewari, "Hot corrosion studies of HVOF-sprayed Cr_3C_2-NiCr coating on 310S stainless steel in an actual environment of a coal fired boiler, International conference (AMPCO 2012), Department of Metallurgical and Materials Engineering IIT Roorkee, India, 2-4 Nov, 2012, pp-113.
15. **V. N. Shukla**, R. Jayaganthan, V. K. Tewari, "Hot corrosion behaviour of Wire arc sprayed FeCrBSiMn alloy Coatings on Boiler steel in an aggressive environment" in Science & Technology of materials category in the NMD-ATM 2012, Jamshedpur, 16-19 Nov, 2012, pp.261.
16. **V. N. Shukla**, R. Jayaganthan, V. K. Tewari, "Oxidation behaviour of Wire arc sprayed FeCrBSiMn alloy Coatings in presence of Na_2SO_4-60% V_2O_5 salt deposits" First International Conference on Corrosion in Infrastructure & Chemical Industries CICI-2012, 6-8 December, 2012, ITM Universe, Vadodara, India, pp-75.
17. **V. N. Shukla**, Nidhi Rana, R. Jayaganthan, V. K. Tewari, "Degradation Studies of Wire arc Sprayed FeCrBSiMn alloy Coating in Molten Salt Environment" 7th International Conference on Materials for Advanced Technologies, (ICMAT 2013), Singapore, 30 June -5 July, 2013.

18. **V. N. Shukla**, R. Jayaganthan, V. K. Tewari, "Surface engineering analysis of HVOF sprayed Cr_3C_2-NiCr coating under high-temperature oxidation" International conference on Advancements and futuristic trends in mechanical and materials engineering, AFTMME- 2013, Punjab technical university, Jalandhar, Punjab, India, 3-6 October, 2013, pp-54.

19. **V. N. Shukla**, R. Jayaganthan, V. K. Tewari "Oxidation studies of HVAS-sprayed nanostructured Coatings at elevated temperature" TMS 2014, Annual meeting and exhibition, San Diego, California, 16-20 Feb, 2014 (abstract accepted).

ABBREVIATIONS

BSEI	Back Scattered Electron Image
EDS	Energy Dispersive Spectroscopy
FE-SEM	Field Emission Scanning Electron Microscopy
HVOF	High Velocity Oxy-Fuel
HVAS	High Velocity Arc-Spray
H_v	Vickers Hardness
SEM	Scanning Electron Microscopy
Cr_3C_2-NiCr	Chrome Carbide Nickel Chrome
CC	Conventional Coating
NC	Nanostructured Coating
Wt%	Weight Percentage
XRD	X-ray Diffraction

CHAPTER - 1

INTRODUCTION

Corrosion is defined as the "destruction or deterioration of a material due to its electrochemical reaction with the environment" (Fontana, 2005). It is said that corrosion never stops; corrosion can be fast or slow depending upon its environment. It is estimated that corrosion of metals in USA costs over three hundred billion dollar per year and nearly 40 % of total production of steel in US is used for replacing corroded components (Priyantha et al., 2003). In India, corrosion of metals costs over Rs. 1 lakh crore per annum. For safety or reliability of metallic components, a thorough understanding on their degradation behavior in different corrosive environments is essential (Madhu Chittora, 2008). In today's thermal power plants, the focus is on saving energy or increasing the efficiency. The existing coal power plants are typically 35% efficient, and operate at steam temperature less than 600°C. Most of the materials used in power plants do not have the corrosion resistance strength at elevated temperature required for high temperature operation. The efficiency of plants can be enhanced by designing alloys that can withstand higher temperatures and capable of retaining its mechanical integrity at increased temperature. The efficiency of power plants is a strong function of the steam temperature and pressure. Superalloys have been developed which can provide necessary strength and withstand high temperature and pressure present in the super heaters of advanced boilers, but following problems persist. Since superalloys are currently being used at temperatures close to their melting temperature, the material development is considered to be reached the limit. Further rise in working temperatures may lead to dissolution of the strengthening phases.

When subjected to elevated temperatures in air or oxidizing environments like combustion of in air or excess oxygen, metals and alloys tend to oxidize. "The degradation behaviour of these metals and alloys often rely on the oxidation reaction that develop a protective oxide scale to resist corrosion attack, such as sulphidization, carburisation, ash/salt deposit corrosion etc." (Singh et al., 2006). Therefore, oxidation is considered to be the most important high temperature corrosion process (Lai, 1990). Further, oxidation rate of alloys is reported to increase with increasing temperature. Increased temperature has an adverse effect on the oxidation behaviour of the alloys (Maledi, 2006). The accelerated corrosion of metals and alloys at elevated temperatures in oxidizing gas atmosphere is known as hot corrosion, which results in a porous non-protective scale at the surface (Singh et al., 2005A). Hot corrosion is one of the serious problems for high temperature applications, such as aircraft, marine, industrial and land base gas turbines, boilers and engines. The cause of this type of corrosion is generally due to the presence of

different salts on the superheater surface. During the operation of a boiler in thermal power plants, the evaporated salt in air will deposit directly on materials at elevated temperature, resulting in severe corrosion attack by oxidation, sulfidation and hot corrosion. It has been reported that the corrosion loss for different Fe-Cr-Ni alloys in the presence of salts like NaCl, Na_2SO_4 at elevated temperatures is 30 to 120 times higher than that in absence of salts. The molten deposits of Na_2SO_4, NaCl or V_2O_5 salts are reported to accelerate the corrosion (Eliaz et al., 2002). Moreover, vanadium and its compounds are oxidation catalysts and permit corrosion species in combustion atmosphere to diffuse to the surface and result in further oxidation and damage the surface oxides (Natesan et al., 1976; Sharma et al., 1996). Coal ash corrosion is a major problem for boiler tubes, particularly where coals of high sulphur and chlorine contents are used. The sulphur generated from the coal forms sulphur dioxide and reacts with the volatilised sodium to form sodium sulphate vapour. It subsequently condenses together with fly ash on the superheater and reheater tubes in the boiler and dissolves the chromium oxide in the protecting coating, which allow the base material to react with sulphate ions to form sulphide ions and non-protective oxides (Rapp et al., 1981). Also, in boilers when sodium chloride from air/water reacts with S from fuel and deposits Na_2SO_4 on hot section components, leading to accelerated attack of the alloy substrate. Unacceptable corrosion rates occurred when biofuel fired boiler is operated in steam of 530°C (Salmenoja et al., 1996). The operating temperature and pressure of pulverized coal-fired boilers have to be increased to increase the efficiency of electricity production and to meet the demand for increased electricity (Blum, 1997). But on increasing the operating temperature and pressure of pulverized coal-fired boilers, corrosion accelerated for hot section components. The performance of steels and different alloys in oxidising environment is well established but its behaviour in corrosive environment containing sulphides and chlorides at elevated temperatures have not been systematically investigated.

In coal-fired boilers, solid particles are produced during combustion of heavy oils, synthetic fuels, and pulverized coal and causes erosion of materials (Zhang et al., 2000). One of the most serious problems associated with fludized bed combustors technology is material loss of the combustor wall and the in-bed tubes. The components in boilers suffer severe corrosion or erosion problems resulting in substantial losses. Cheruvu et al., (2006) estimated charges for replacement of hot components to go beyond 35% of the cost of new plant. The data covering one year duration for the boiler tube failure in the coal fired boiler power plant in north western region of India indicates that out of the 89 number of failures, 62 failures were attributed to the erosion-corrosion by fly ash. Moreover, fly ash content of the Indian coal is very high and causes severe erosion-corrosion of the materials in the power plants. In view of the high losses due to erosion-corrosion, it becomes imperative to develop improved protection against such

degradation by exploring newer erosion-corrosion resistant materials for the industrial applications. The corrosion related costs can be considerably reduced using improved techniques of corrosion control.

Ni- based, Fe- based and Co-based superalloys are employed as structural components in different elevated temperature applications owing to the attractive combination of their mechanical properties and resistance to corrosion. To further enhance corrosion resistance and to prolong the service life time of the parts used at elevated temperatures in aggressive chemical environments, the best and cost effective way is to coat them with thin wear and oxidation resistant coatings. The coatings offer the shielding against oxidation and material damage while the beneath material offers the required mechanical strength (Sidhu et al., 2003). Austenitic stainless steels (ASSs) are of prime importance to industry and are estimated to account for more than 70% of production of stainless steels (SSs) due to their excellent combination of corrosion resistance, mechanical strength, durability and fabricability (Sedriks, 1996). They are extensively used as structural materials in chemical, petrochemical, fertilizers, power and nuclear industries. ASSs possess excellent corrosion resistance due to the formation of a self healing passive Cr_2O_3 film on the surface, when exposed to ambient environment (Fontana, 2005).

It is clear from the literature that the thermal spray process has been widely used to produce wear-resistant and corrosion-resistant coatings that provide improved life of components used in coal fired boiler (Wang et al., 2001; Guo et al., 2011, 2011A; Shukla et al., 2011). Minimum damage to the environment is reported to occur in thermal spraying systems in comparison with other coating techniques like physical vapour or chemical vapour deposition, and electroplating techniques (Grewal et al., 2013).

It is necessary to understand the oxidation behaviour of elevated-temperature coatings to widen the use of steel parts without altering mechanical properties of the base materials (Toma et al., 2000). The service life and corrosion resistance of components used at elevated temperature can be improved in two ways: (i) by adding fair amounts of Al, Cr, and Ti to the alloy that promotes resistance to oxidation and corrosion and (ii) by coating the base material with a protective layer (Wang et al., 2002). Furthermore, the role of microstructural features and reaction kinetics of the oxide scales formed at elevated temperatures is critical in estimating the behavior of base alloys/coatings for high temperature use (Matthews et al., 2003; Hussain et al., 1994).

In thermal spraying, the material to be deposited is melted by heat source and propelled towards the surface being coated, where they impact, flatten and solidify. Thermal spraying process can be distinguished on the type of heat source. Sidky and Hocking (1999) have observed that the coatings produced by plasma spray process are porous; this reduces their strength and decreases their corrosion strength and decreases the corrosion strength. High velocity oxy fuel (HVOF) deposition is well accepted thermal spray technology due to flexibility in forming dense and homogeneous microstructure, smooth

surface, uniform deposition thickness, that result in superior bonding strength and hardness (Xiong et al., 2008; Jandin et al., 2003; Fu et al., 2009). The major benefits of HVOF process are the shorter flame residence time, higher velocity and kinetic energy of the feedstock materials/powder (Nicholls et al., 2002). The high velocity arc spray process (HVAS) is also capable to prepare dense, homogeneous microstructure coating with less oxide content and negligible heat transfer to the substrate (Abedini et al., 2006). Metallic coatings and corrosion resistant alloys such as stainless steels are often used to protect boilers from corrosion. The need to protect materials in the energy generation industries caused development of wide variety of corrosion resistant coatings (Streief, 1993).

The present study has been focused to comparatively evaluate the oxidation and hot corrosion behavior of HVOF sprayed Cr_3C_2-NiCr coatings and HVAS sprayed FeCr based conventional and nanostructured coatings on 310S alloy substrate in the laboratory as well as in the actual coal fired boiler environments. The microstructural features of the coatings were correlated with the degradation behavior of coatings. The behavior of these coatings in different degrading environments will be helpful in choosing the suitable coating for the hot section components of the thermal power plant. The following objectives were envisaged for the research work in the present thesis.

1. To study the surfaces of HVOF and HVAS as-sprayed coatings **(**Cr_3C_2-NiCr, FeCr based conventional and nanostructured coating**)** on 310S alloy substrate

2. To determine the oxidation behavior of coated surfaces at ambient and high temperature (700 and 900^oC).

3. To understand the oxidation kinetics of coated surfaces in molten salts such as Na_2SO_4- 60% V_2O_5 and Na_2SO_4- 82% $Fe_2(SO_4)_3$.

4. To study hot corrosion of coated alloys in industrial boiler environment.

5. To characterize the oxide scales of corroded specimens for substantiating the corrosion mechanisms.

The thesis is divided into the following chapters.

First, a comprehensive literature review on thermal spray coatings and their behavior in different corrosion environments is provided in Chapter 2.

In Chapter 3, experimental techniques and procedure employed for applying the coating and their characterization, oxidation studies in air, molten salt environment and in actual coal fired boiler environment are discussed.

Chapter 4 deals with the detailed investigation of 310S alloy substrate and HVOF-sprayed Cr_3C_2-25%NiCr coating, which include characterization and corrosion studies in (i) air and two molten salt environments in the laboratory under cyclic condition at 700 and 900^0 C for 50 cycles, and (ii) coal fired real boiler environments at 700 ±10 ^oC for 1500 h.

Chapter 5 consists of investigation of HVAS-sprayed FeCr based conventional coating, which include characterization and corrosion studies in (i) air and two molten salt environments in the laboratory under cyclic condition at 700 and 900^0 C for 50 cycles, and (ii) coal fired actual boiler environments at 700 ±10 ^oC for 1500 h

The characterization, corrosion studies of HVAS-sprayed FeCr based nanostructured coating in (i) air and two molten salt environments in the laboratory under cyclic condition at 700 and 900^0 C for 50 cycles and (ii) coal fired actual boiler environments at 700 ± 10^oC for 1500 h are discussed in Chapter 6.

Chapter 7 describes the comparative results of all the bare and coated specimens in air, molten salt environments and in actual coal fired boiler environment.

The major conclusions of the present investigation and scope for the future work are listed in Chapter 8.

The following flow chart provides the glimpse of the research work carried out in the present thesis.

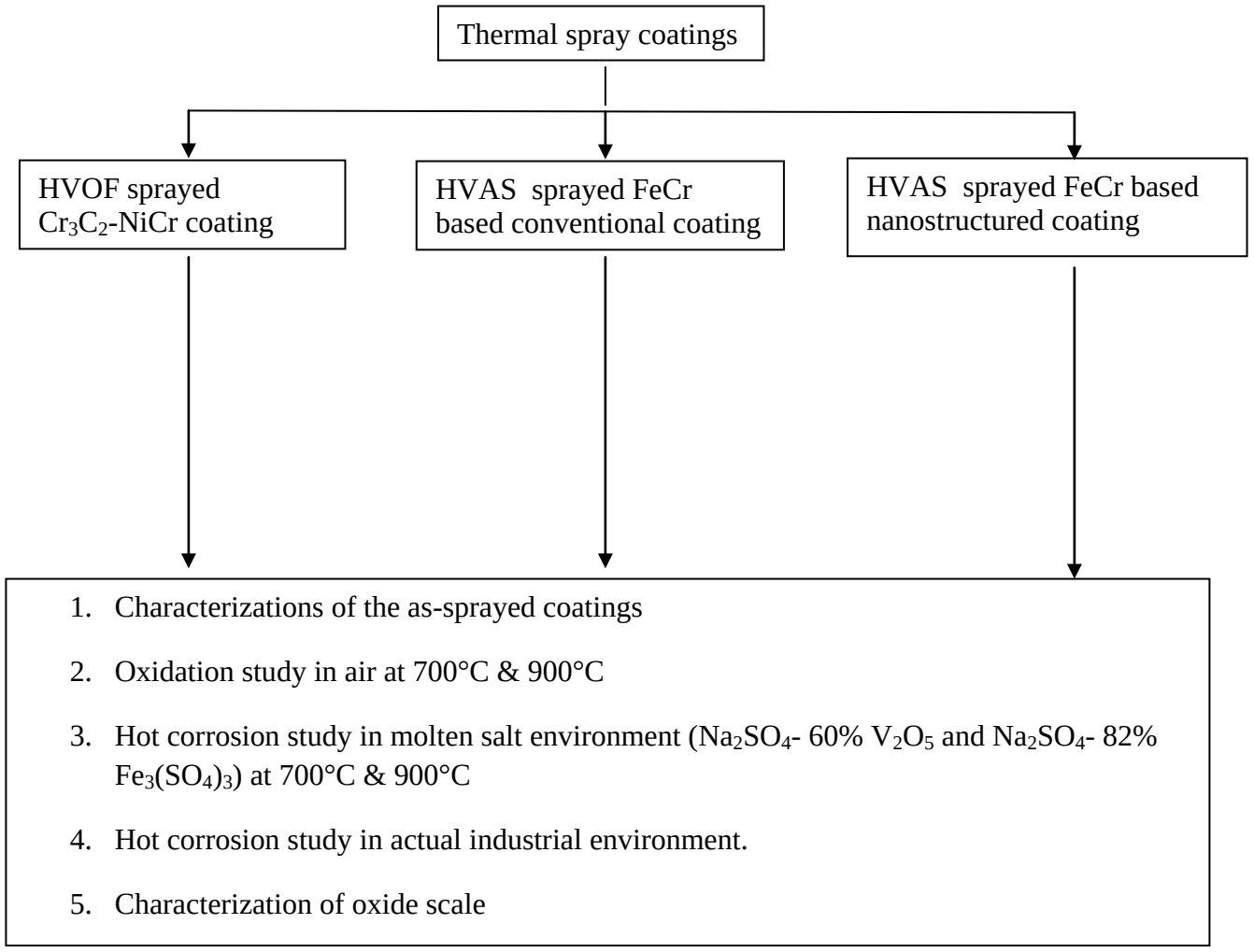

Fig.1.1. Bird's view of the doctoral investigation

CHAPTER - 2

LITERATURE REVIEW

Literature review relevant to the research has been divided into three phases. First phase contains a comprehensive review of the existing literature on high temperature oxidation, hot corrosion and erosion-corrosion along with existing characteristics and mechanisms. In the second phase, critical review regarding the protective coatings and coating deposition processes have been described. The third phase is related to the problem formulation, scope and objectives of the present research work.

2.1 HIGH TEMPERATURE OXIDATION

Metal and alloys exposed to oxygen or oxygen-containing gases at elevated temperatures leads to its degradation and form their corresponding oxides. The oxide scale may be protective if it is adherent, and could preclude further oxidation. Alternatively it may get peeled-off, if the scale is not adherent and results in progressive loss of metals. Almost all the metals are found in nature in the form of an oxide, sulfide, or some other metal compound. Thus all the metals that are derived from ores, when exposed to air at room temperature, form surface compounds, which may be oxides or other compounds, depending upon the contamination in air (Khanna, 2002). It takes from a few hours to a few days to form this oxide layer on the surface, depending upon the type of environment. The rate of the reaction of oxide formation increases many folds, if the sample is exposed to the same atmosphere but at a temperature much higher than the room temperature.

An oxidation reaction between the oxygen gas (O_2) and a metal (M) can be written as:

$$\alpha M(s) + \frac{\beta}{2} O_2(g) \rightarrow M_\alpha O_\beta(s) \qquad (2.1)$$

In the simplest form, oxidation of metal appears as the addition of oxygen to the metal surface. However, the oxidation behavior of metals depends upon various factors and the reaction mechanism involved may prove to be complex (Khanna, 2002).

In the environment if the oxygen potential is larger than oxygen partial pressure of it in equilibrium with oxid e (Kofstad, 1966), reaction would occur with metals and form oxide on its surface. The oxide layer growth may depend upon the accessibility of the metal surface to the oxidizing gas, or on the diffusion of ions or/and electrons. The gas adsorption on the metal surface leads to metal-oxygen reaction as an initial step. Once the reaction proceeds, oxygen would dissolve in the metal and form oxide layer or separate oxide nuclei on the metal surface (Kofstad, 1966).

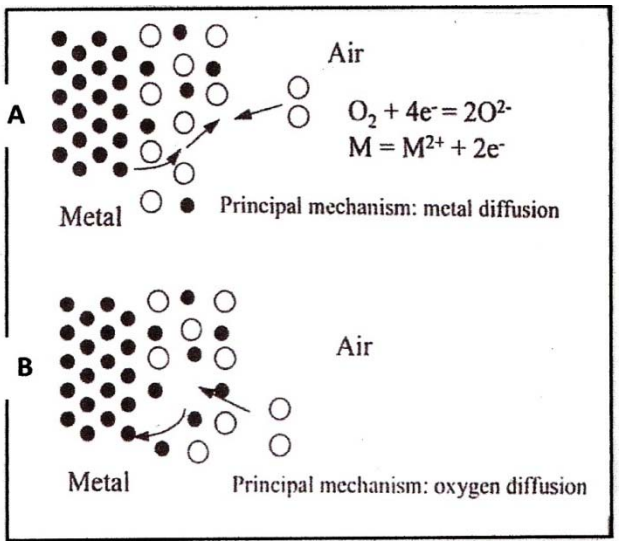

Fig: 2.1 Schematic illustrations of the mechanisms of oxidation at the surface of a metal (Grainger et al., 1989)

If the compound formed on the surface is volatile or continually falls off, the corrosion or oxidation will proceed rapidly, the metal is lost progressively and it ultimately fails. However, if the compound formed on the surface of metal is adherent to the surface, it can act as a barrier for providing protection to the metal from the gas. Solid-state diffusion of the reactants through the coating results in further oxidation but it is very sluggish reaction (Kofstad, 1966). "The metal ions and /or oxygen may diffuse through the barrier layer and could interact chemically to form new oxide at the scale/gas or scale/metal interface" (Stott, 1998). In the first case, Fig.2.1 (A), metal ions and electrons diffuses faster than oxygen ions, which causes the oxide to grow at the outer surface. This mechanism is seen in iron, copper, chromium and cobalt. In the second, Fig.2.1 (B), oxygen ions and electron diffuses through the existing oxide layer faster than metal ions. This causes the oxide layer to grow at the metal/oxide interface, a situation seen in titanium and zirconium.

The load-bearing capability of the original alloy component reduced due to oxidation is one of the serious issues in boiler. Resistance to oxidation at high temperatures is a requisite for alloy component whether used in the coated or uncoated conditions. Therefore, a better understanding of the oxidation resistance of alloy substrate and how it is influenced by the alloy characteristics and exposure conditions are essential for effective design and application of alloy component.

2.1.1 Fundamentals of oxidation

Various alloys are used extensively in high temperature applications. The oxidation resistance of metals can be improved by adding alloying elements so as to be suitable for high temperature application (Khanna, 2002; Bhat et al., 1994). The rate of oxidation at high temperature depends on the oxide layer that forms on the surface of metal (Chawla et al., 2011).

Wagner (1984) has explained the oxidation behavior for an A-B alloy that is forming both AO and BO oxides. When oxides of metals form, their relative position and distribution is determined by thermodynamic properties of the oxides and the alloy, the diffusion processes and reaction mechanisms. The first situation involves immiscible oxides with the more stable oxide growing slowly. With both *AO* and *BO* stable but with rapid growth of *AO* and slow growth of *BO*, the more stable *BO* may nucleate first, but gradually becomes over-whelmed and surrounded by fast-growing *AO*. Figure 2.2 (a) and (b) illustrate the situation.

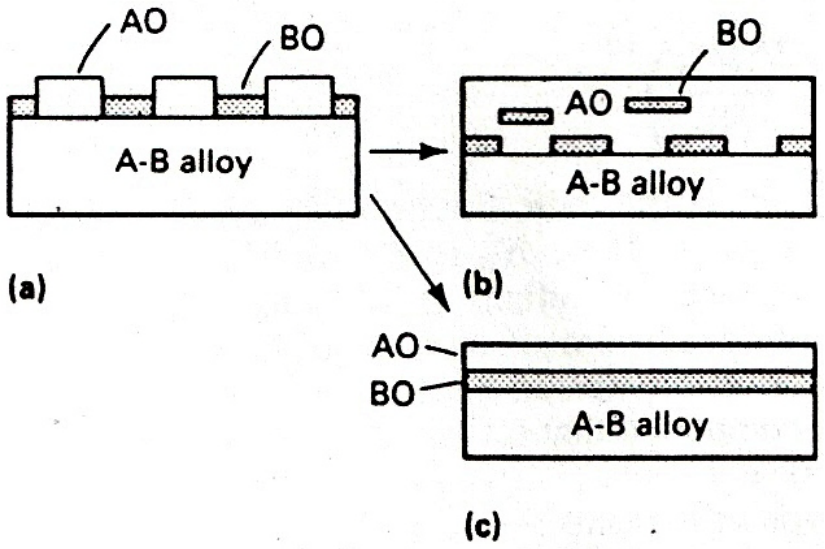

Fig: 2.2 Mechanisms of oxidation at the surface of a metal (Samuel, 1987)

If diffusion in the alloy is rapid, the oxidation proceeds to form an *AO* scale with *BO* islands scattered through it. However, if diffusion in the alloy is slow, the metal becomes depleted of *A* near the metal/oxide interface, while the growth of *BO* continues until it forms a complete layer, undercutting the *AO* (Fig. 2.2 c). Pockets of *AO* at the metal/oxide interface will gradually be eliminated by the displacement reaction:

$$AO + B_{(alloy)} \longrightarrow BO + A_{(alloy)} \qquad (2.2)$$

Because *BO* is thermodynamically more stable than *AO*, this reaction continues even if the oxygen supply is cut off. The second situation involves two oxides that are partially miscible. For alloys rich in *A*, an *AO* scale will form with some *B* ions dissolved sub-stitutionally in the *AO* structure. For alloys rich in *B*, a *BO* layer first forms. If *B* ions diffuse through the scale faster than *'A'* ions, the concentration of *A* ultimately builds up in the scale close to the metal/oxide interface. An *AO* layer then forms underneath the *BO*. On the other hand, if *A* ions diffuses through the original *BO* scale more quickly than *B* ions, the *AO* layer

eventually forms on top of the *BO* layer. In addition, if '*A*' ions diffuse rapidly through *BO* and *B* ions diffuse rapidly through *AO,* alternate layers of *BO/AO/BO/AO* may even form. Further, the spinels, which are double oxides of a metal with +2 valence and a metal with +3 valence, having the general formula $MO.Me_2O_3$ and also having the crystal structure of the mineral spinel ($MgO\text{-}Al_2O_3$), may form.

Nucleation and growth process establishes the formation of oxide layer on the alloy (Stott, 1998)**.** Small nuclei of impinging oxides, which are thermodynamically stable, grow on the surface of the component, when it is exposed to an oxygen rich gas. These oxide nuclei undergo coalescence rapidly to form a complete layer. The rate of oxidation is rapid during the initial stage which causes the alloying elements oxidize and the various oxides formed are proportional to elemental concentration in the alloy.

Li et al. (2003A) have reported that although significant insight has been accumulated on mechanisms of oxidation at elevated temperature, reaction mechanisms are not considerably explained. Oxidation at ambient temperature involves the corrosion of selective elements, oxide scale formation and internal oxidation (Hussain et al., 1994). It is complex phenomena and cannot be understood through the diffusion processes alone.

Plenty of literature exists on high temperature degradation of metals and alloys, which is not possible to review in a sensible manner in such a short space. As an alternative, it is proposed to overview the high temperature phenomenon in context with some current studies conducted by various researchers in the field, which may form basis for the formulation of the problem.

Oxide products have also been found to be more effective in limiting further reaction between the metal or alloy and the high temperature gaseous environment than nitrides and sulfides. Pure chromium and alloys of Fe, Co, and Ni with higher amount of chromium form Cr_2O_3 scales on oxidation at elevated temperatures (Coze et al., 1989; Gesmundo et al., 1988; Haugsrud et al., 2003; Kuiry et al., 1994; Krishna et al., 2002; Kim et al., 2008; Pantony et al., 1968A, 1968B). At lower temperatures, below 1200 ^oC or so, the rate of thickening of the scale follows a parabolic rate law:

$$w^2 \text{ (or } x^2) = k_p t \qquad (2.1)$$

However, deviations from this become apparent at higher temperatures or after very long times. Eventually, the weight of the specimen attains a maximum and starts to diminish, the rate of weight loss asymptotically tends to reach a constant value (linear rate law). It is due to the oxidation of the Cr_2O_3 to the volatile species CrO_3 (Stringer et al., 1972).

Most metals and alloys react with oxygen to oxidise to some extent in gaseous atmospheres. Oxides are generally more thermodynamically stable then reaction products from there species (like N and S) which may be present in the environment. It is therefore common for oxides to form at gas-metal interface (Pettit et al., 1977).

2.1.2 Breakdown of protective scales

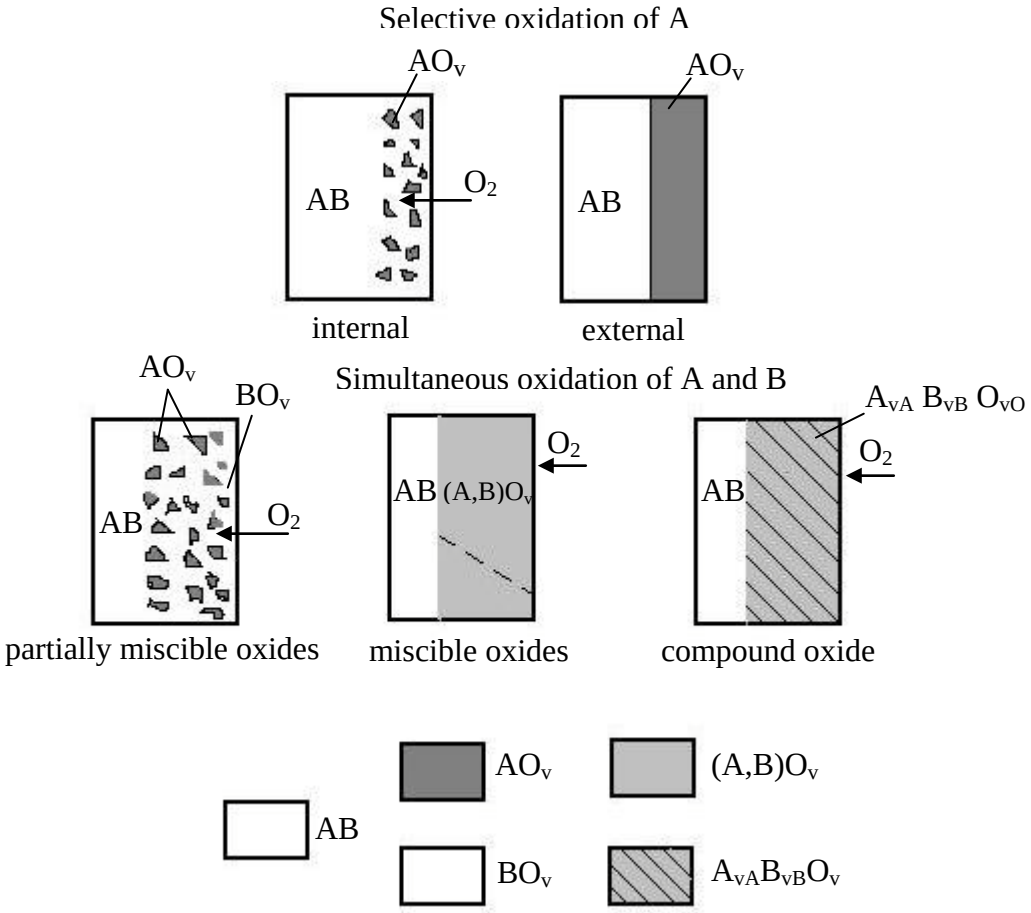

Fig. 2.3 Alloy oxidation mechanisms, with the corresponding morphologies of the oxide layers (Dieter, 2007).

The protective scale formed on alloys by selective oxidation results in depletion of scale-forming element in underlying alloy (Fig. 2.4). The depletion tends to protective scale which become un-stable; degradation of high-temperature alloys are generally more rapid under thermal cycling conditions. Cracking/spalling of protective oxide scale caused due to the mismatch between coefficient of thermal expansion of the oxide scale and alloys (Meier, 1989). Alumina and chromia spelled in high sulfur pressure atmospheres to sulfide channels through the scales (Stott et al., (1985).

2.1.3 Oxidation of Iron and Iron-Based Alloys

Wright (1987) reported alloys intended for skirmishing high temperature environment are designed for protective oxide scale over the surface of alloy. Figure 2.4 schematically represents the oxidation rate of iron-chromium alloys (1000°C, in 0.13 atm oxygen) and depicts the types of oxide scale associated with various alloy types. A useful concept in assessing the potential high-temperature oxidation behavior of an alloy is that of the reservoir of scale-forming element contained by the alloy in excess of the minimum level (around 20 wt% for iron-chromium alloys at 1000°C, according to Fig.2.4). The more likely the service conditions are to cause repeated loss of the protective oxide scale, alloys required for scale-forming element for continuous protection is very high. Cr-Mo steels are best choice for the moderate temperature applications. Mo is used to provide good creep strength at elevated temperatures, while Cr forms a chromium-rich scale to provide oxidation resistance to steel. In case of stainless steel (with more than 12% Cr), protective chromia layer is formed on the surface provides oxidation resistance.

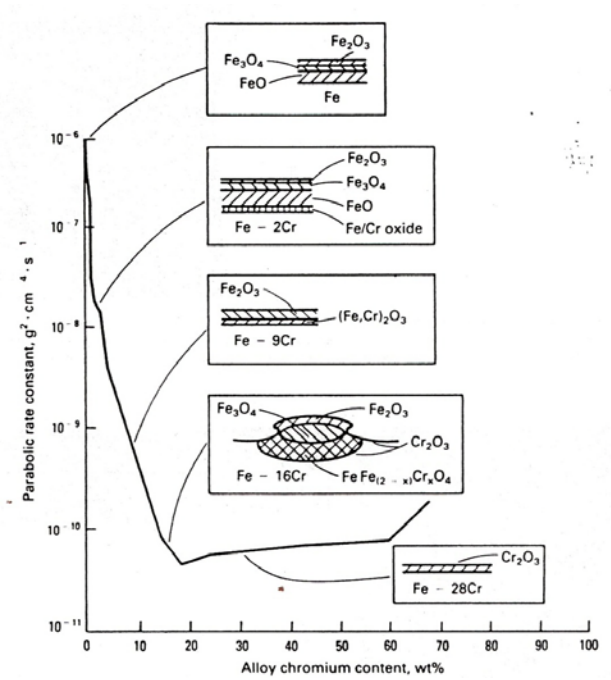

Fig.2.4 Schematic of the variation with alloy chromium content of the oxidation rate and oxide scalestructure, based on isothermal studies at 1000°C in 0.13 atm oxygen (Wright, 1987)

Khalid et al (1999) conducted similar studies for comparison of oxidation behaviour of Incoloy 825 and Incoloy 800H at high temperature. Incoloy 800H showed better oxidation resistance than Incoloy 825. Coarse Ti-rich inclusions, showed less dissolution of Ti in the alloy is responsible for poor corrosion resistance of Incoloy 825.

Sidhu (2003) carried out high temperature oxidation studies on the GrA1, T11 and T22 boiler steels in air at 900^0C. He reported that Mo containing T22 steel showing least resistance to oxidation. It is due to the formation of a low melting point MoO_3 phase. Low melting point phase (795^0C) causes the removal of the protective oxide scale, resulting in accelerated oxidation of the steel.

2.2 HOT CORROSION

Accelerated oxiadation generally occours in Metals and alloys when they are covered with molten salt in aggressive environment at elevated temperature, this is known as hot corrosion (Shih et al., 1989). According to Eliaz et al. (2002) and Khanna et al. (1998), the presence of salt contaminants damage the protective oxide scale. Hot corrosion is observed in incinerators, boilers, gas turbines and mufflers of internal combustion engines (Choquet et al 1987; Colot et al., 1997; Coze et al., 1989; Das et al., 2002; DeMasi-Marcin et al., 1994). In gas turbines, sulphur and sodium impurities present in fuel and in combustion air, reacts to form sodium sulphate (Na_2SO_4) during the combustion stage in heat engines. If the percentage of sulphate exceeds the saturation vapour pressure in case of turbine blades at the operating temperature (700-1100°C), Na_2SO_4 will be deposited on the surface (Khanna et al., 1998, Dooley et al., 1975, Conner et al., 1994, Fairman et al., 1962; Frances et al., 1985).

Hot corrosion is generally divided into two forms of attacks firstly High temperature hot corrosion(Type-I) and secondly Low temperature hot corrosion (Type-II), as reported by Eliaz et al. (2002) and Khanna et al. (1998)**.** Composition of alloy and thermo-mechanical condition, temperature and temperature cycles, contaminant composition and flux rate, velocity and gas composition affect these corrosion (Eliaz et al., 2002 and Pettit at al., 1987).

*2.2.*1 High Temperature Hot Corrosion (HTHC)-Type I

High temperature hot corrosion is found to occur mainly within temperature range of 850-950°C, when the salt gets deposited on metal or alloy in liquid state (Khanna, 2002, Hancock, 1987, Wright, 1987 and Eliaz et al., 2002). Na_2SO_4 is dominant salt in Type-I hot corrosion due to its high thermodynamic stability. For example, Na_2SO_4 when combined with V_2O_5, a eutectic is formed with a melting point of 550°C, a very aggressing environment is formed (Tiwari, 1997).

*2.2.*1 Low Temperature Hot Corrosion (LTHC)-Type II

Low temperature hot corrosion occurs when the temperature is below the melting point of Na_2SO_4. This form of hot corrosion is mainly observed within the temperature ranging from 650-800°C (Eliaz et al., 2002). Wright (1987) reported high partial pressure of SO_3 in gaseous phase is required in the Type-II reactions to occur, in contrary to High temperature hot corrosion. The formation of $Na_2SO_4 \pm NiSO_4$ eutectics has been reported for nickel-based super alloys, the morphology of attack is pitting when

the LTHC takes place, low temperature corrosion shows little inter-granular attack, and a layered type of corrosion scale (Misra, 1986). Chromium (25-40%) and silicon are particularly beneficial in coatings for protection against Type II corrosion.The type of corrosion attack can be classified as type I or type II, based on the nature of attack, and not the temperature. Low-temperature hot corrosion is characterized by a pitting attack (Stringer, 1998).

2.2.3 Sequence of Hot Corrosion Degradation

The hot corrosion degradation of hot section components usually involves two distinct stages of attack (Pettit and Meier, 1985; Pettit and Giggins, 1987), namely, an initiation (incubation) stage and propagation stage. Such conditions are depicted schematically in Fig.2.5.

2.2.3.1 The Initiation Stage

Alloys can not be immune to hot corrosion attack indefinitely although there are some alloy compositions that require a long initiation times before the hot corrosion process moves from the initiation stage to the propagation stage. During the initiation stage of hot corrosion, superalloys are degraded at rates similar to the alloys degraded in the absence of the deposits. Elements in the alloy are oxidized and electrons are transferred from metallic atoms to the reducible substances in the deposit. Consequently, the reaction product that grows beneath the deposit on the alloy surface usually exhibits features resulting from the gas–alloy reaction (Pettit and Giggins, 1987). Numerous factors affecting the hot corrosion process moves from the initiation stage into the propagation stage as shown in Fig. 2.5. These factors also play the vital role in determining the type of reaction product that is formed in the propagation stage. This fact is responsible for variety of hot corrosion processes that have been observed when superalloys are exposed to different environments (Pettit and Meier, 1985).

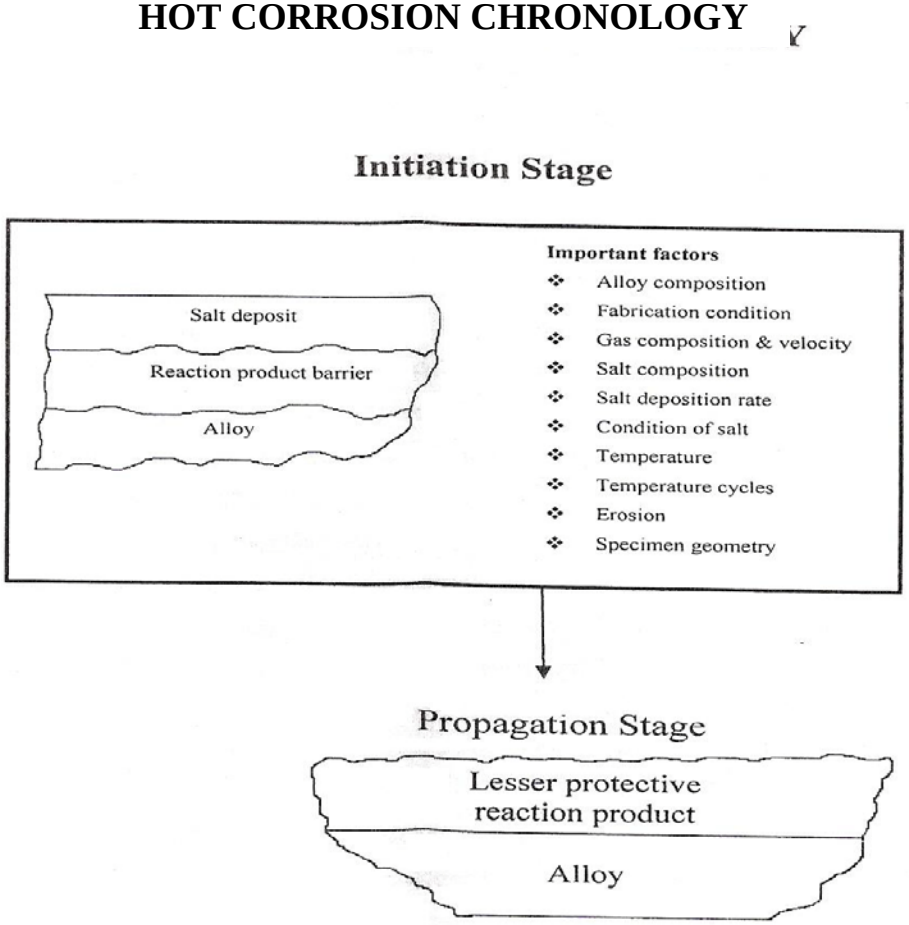

Fig. 2.5 Schematic diagram showing the conditions that develop during hot corrosion attack. (Pettit and Meier, 1985).

2.2.3.2 The Propagation Stage

The propagation stage of the hot corrosion is the stage for which the superalloy must be removed from service. This stage always leads to higher corrosion rates than for the same superalloy in the initiation stage (Pettit and Meier, 1985 and Pettit and Giggins, 1987). Since superalloys always contain elements that have high affinities for oxygen, an oxygen gradient is established across the deposit. Hence, an important effect of the deposit is to separate the superalloy from the gas environment. This situation usually results in a lower oxygen activity over the surface of the alloy than what would have been established in the absence of a deposit (Pettit and Meier, 1984; Pettit and Giggin, 1987).

2.2.4 Chemistry of salts

2.2.4.1 Chemistry and Phase Stability of Na_2SO_4 Salt

Rapp (1986 and 2002) described that oxyanion melts of alkali nitrates, carbonates, hydroxides and sulphates exhibit an acid base character whereby the acid components may be considered as $NO_2(g)$, $CO_2(g)$, $H_2O(g)$ or $SO_3(g)$, respectively.

Although the use of the Lux-Flood selection of NO_3^-, CO_3^{2-}, OH^- and SO_4^{2-} as the basic components is common for such fused salts, the oxide ion can be alternatively selected as the Lewis base in common for all of these salts (Rapp, 1986 and 2002). For a melt of pure Na_2SO_4 (m.p. 884°C), there exists the equilibrium as given below:

$$Na_2SO_4 \rightarrow Na_2O + SO_3(g) \qquad (2.4)$$

According to Rapp (1986), Stability of the oxide scale Cr_2O_3, with respect to dissolution as shown in Fig. 2.6. The two abscissa scales at the bottom and top of figure provide alternate parameters for melt basicity (or acidity).

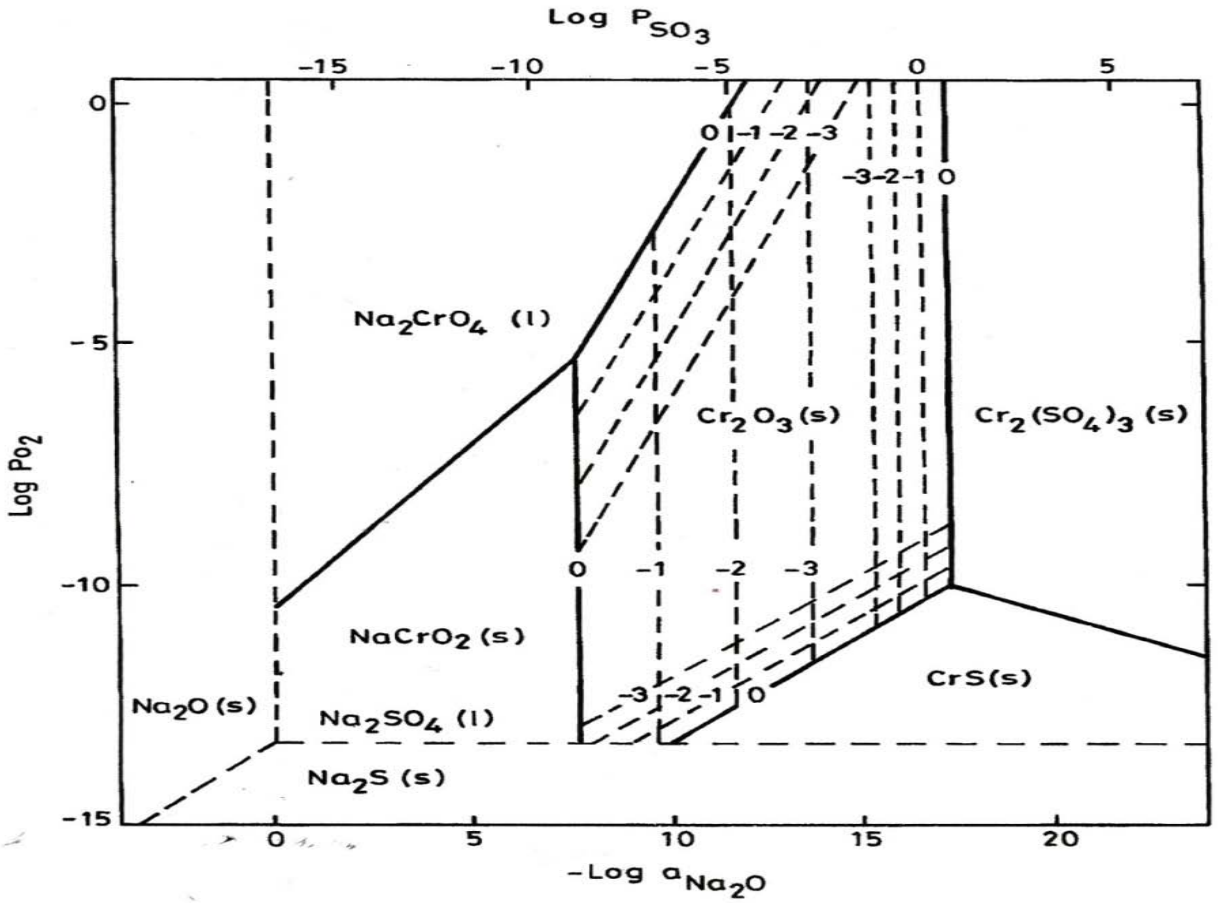

Fig. 2.6 Na-Cr-S-O phase diagram for 1200K (Rapp, 1986)

2.2.4.2 Vanadate Solution Chemistry

As reported by Hwang and Rapp (1989), vanadium is unique, in that it forms a low-melting oxide V_2O_5. This low melting temperature (670°C under 1 atm of oxygen) results from the peculiar crystal structure of the compound in which vanadium is 5-coordinated with oxygen and in which there occur four different vanadium-oxygen bond lengths. Rapp and Goto (1981) have reported that the presence of such multivalent metal ions in a fused salt deposit could greatly aggravate the hot corrosion rate either by counter diffusion of the multivalent cations or else by electron hopping. They would provide the fast transport of charge through the salt film.

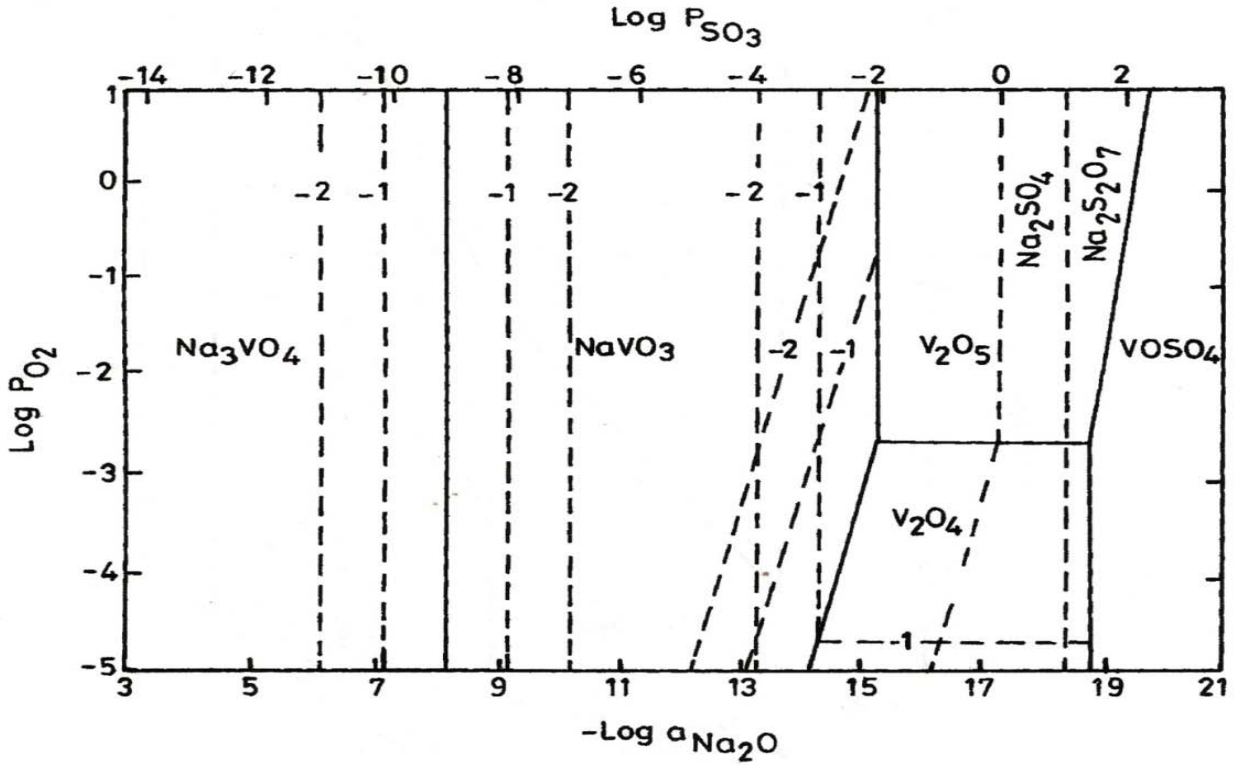

Fig. 2.7 Phase stability diagram for Na-V-S-O phase diagram at 900°C (Hwang and Rapp, 1989)

The diagram showing the phase stability for the Na-V-S-O system at 900°C reported by Hwang and Rapp (1989) has been shown in Fig. 2.7. The dashed lines present the isoactivity lines for the vanadate species in the salt solution. They determined the dependence of the equilibrium concentrations of various vanadate solutes in the sodium sulphate-vanadate solutions on the melt basicity by considering following equilibrium reactions:

$$Na_2SO_4 \rightarrow Na_2O + SO_3 \qquad (2.5)$$

$$Na_3VO_4 \rightarrow Na_2O + NaVO_3 \qquad (2.6)$$

$$2NaVO_3 \rightarrow Na_2O + V_2O_5 \qquad (2.7)$$

The equilibrium concentration of each vanadium compound varies continuously with melt basicity. Na_3VO_4 is the dominant component in the melt at basicity less than 8.2 and V_2O_5 is dominant at basicity greater than 16.3. For basicities between 8.2 and 16.3, $NaVO_3$ is the most important vanadium solute (Hwang and Rapp, 1989).

2.2.4.3 Chemistry of Salts in the Combustion of Coal/Fuel Oils

It is not possible to remove sulphur from coal or fuel oil completely and economically, also it is not possible to prevent the formation of SO_2 during combustion (Nelson et al., 1959). According to Khanna and Jha (1998), the sulphur present in coal yields SO_2 on combustion which gets partially oxidizes to SO_3. The NaCl reacts with SO_3 and water vapour at ambient temperature to yield Na_2SO_4 as below:

$$2NaCl + SO_3 + H_2O \rightarrow Na_2SO_4 + 2HCl(g) \qquad (2.9)$$

Inspite of high melting point (884^0C) of pure Na_2SO_4 in presence of dissolved salts e. g. NaCl or other metal sulphates, its melting point is lowered. Na_2SO_4 can further reacts with SO_3 to form sodium pyrosulphate, $Na_2S_2O_7$ with melting point (m. p.) of 401 ^{o}C:

$$Na_2SO_4 + SO_3 \rightarrow Na_2S_2O_7 \qquad (2.10)$$

Small amounts of vanadium may be present in fuel oils, which on combustion forms V_2O_5. This may further react with Na_2SO_4 to form low melting sodium vanadates, which are highly corrosive.

$$xNa_2SO_4 + V_2O_5 \rightarrow (Na_2O)_x.V_2O_5 + xSO_3 \qquad (2.11)$$

Thus metals and alloys in combustion gases are exposed to various corrosives such as O_2, SO_2/SO_3, molten salts, e.g. Na_2SO_4 or sulphate mixtures, sodium vanadates, NaCl etc. (Khanna and Jha, 1998). These vapours condense with fly ash on the re-heater tubes in the boiler. Corrosion occurs due to the fluxing action of molten salts deposited on the on the surface of the tubes, causing hot corrosion, accompanied by Sulphidation (Beltran and Shores, 1972; Rapp et al., 1981).

2.2.4.4 ELEMENTS AFFECTING HOT CORROSION OF METALS/ALLOY

The alloying elements, presence of S and Cl^- in the deposit and the temperature play important roles in hot corrosion (Khanna et al., 1998; Eliaz et al., 2002; Jena et al., 1984; Khalid et al., 1999). Chromium is very effective as a alloying elements for imparting hot corrosion resistance of materials (Otsuka et al., 2002).. Otsuka et al. (2002) have suggested that Ce, La, Zr, Y, and Sc significantly increases resistance because of improvement of adhesion between alloys and the protective oxide.

Sulphur-induced hot corrosion is generally known as sulphidation (Khanna et al., 1998 and Wright, 1987). Sulphidation is a specific form of hot corrosion but the attack does not always take place via sulphidation. At high temperatures, sulphide phases are found substantially beneath the molten

deposits. Once these sulphides starts oxidizing ,the resulting phases are not protective because of SO_2 evolution (Khanna et al., 1998).

The presence of chlorine may also affect the hot corrosion of alloys. Cl_2 concentrations in the ppm range may increase the propensity of oxide scales (e.g. Al_2O_3 and Cr_2O_3) on alloys to crack and spall (Khanna et al., 1998). Further, large concentrations of chloride in the deposit causes rapid removal of Al and Cr from alloys by the formation of volatile metal chlorides in the low oxygen pressure regions. The chloride-induced effect is significant between 700 and 1000°C. Temperature is an extremely important factor. The onset temperature of catastrophic attack, "threshold temperature"' generally occurs near the melting point of the salt or salt mixture. As temperature is increased further, the rate of diffusion-controlled processes increases and reaches a maximum at about 980°C for most alloys.

According to Kofstad (1988), during combustion vanadium get oxidized to form higher valence vanadium oxides (V_2O_4 and V_2O_5), which react with sodium salts to form low melting point sodium vanadates (lowest M.P. 535 ^oC) such as $(Na_2O)_xV_2O_4(V_2O_5)_{12-x}$, $(Na_2O)_5(V_2O_4)_x(V_2O_5)_{12-x}$, $NaVO_3$, $Na_4V_2O_7$ and Na_3VO_4. The details of vanadate reaction mechanisms are discussed by Koftad (1988). Hwang and Rapp (1989) studied the solubility of oxides in the mixed sodium sulphate-vanadate solution containing 30 mole% vanadates. They reported that the basicity of the melt, oxygen partial pressure and proportion of V^{5+} and V^{4+} states of vanadate in the sulphate-vanadate solution decide the solubilities of oxides**.**.

Sidhu, (2003) studied the hot corrosion behaviour of boiler tube steels in air and molten salt environments of Na_2SO_4-60%V_2O_5 at 900 ^oC. They found that all the steels show lesser resistance in the aggresive environment than in air. They reported that the presence of sodium, vanadium and sulphur accelerates the rate of corrosion of boiler steels in the molten salt environment. (Sidhu et al., (2007) evaluated degradation behaviour of HVOF sprayed NiCrBSi and Cr_3C_2-NiCr coatings in the presence of the Na_2SO_4-60%V_2O_5 salt mixture. He reported that Cr_3C_2-NiCr coating gets oxidized partially whereas in case of NiCrBSi coating, only the top layer of the coating gets oxidized.

2.3 SOME STUDIES ON POWER PLANT ENVIRONMENTS

The availability of electrical power and the development of millions of devices that use it have made electricity the energy of choice in contemporary industrial societies. It is estimated that in the United States approximately 70% of the electricity is produced in fossil power plants, 15% in nuclear power plants, 12% in hydraulic power plants and the remainder from other types of sources (Viswanathan et al., 1989; Chawla et al., 2011A, Rajan et al., 2006). The fuels used in fossil-fired plants are petroleum, natural gas and coal. Natural gas is generally pure and does not constitute a hot corrosion threat, unless firing is substoichiometric in reducing NO_x emission. Petroleum fuels is corrosive to boilers if contain

alkali sulfates or vanadium oxides, both of which are highly corrosive to metals in the combustion chamber and hot gas passages. However, coal contains impurities such as chlorides, sulfur and alkali metals, which are extremely corrosive. Different authors have reported that accumulation /condensation of salts on the boiler tubes in coal fired boilers is main cause for rigorous wastage of tube materials. These salts containing sulfates of potassium and sodium easily liquefy at the operating temperatures results in severe hot corrosion of boiler tubes (Nelson et al., 1959; Rapp, 1986; Backman et al., 1987; Salmenoja et al., 1996; Lee et al., 1990 & 2002).

Metallic components in coal based energy generation systems are subjected to severe corrosive atmospheres. The gaseous environments containing sulphur, oxygen and carbon cause material degradation at fast rate and due to which components life is reduced. (Goebel et al., 1970A, 1970B & 1973; Mobin et al., 1996; Sarkar et al., 2006; Hara et al., 1991; Harris et al., 1955; Iyer et al., 1987 &1987A; Johnson et al., 1978; Kai et al., 1998, and Wang, 1988, Li et al., 1996, Malik et al., 1983, 1987 & 1988, Choudhury et al., 1998, Manoj et al., 2005 & 2005A). The phenomenon of accelerated corrosion at high-temperatures occurs because of deposition of fly ashes during combustion of coal. Ashes have high concentrations of compounds of sodium, vanadium and sulphur, mainly as Na_2SO_4–V_2O_5 complex and sodium–vanadates mixtures. These impurities are also present in residual oils used as fuel (Kerby et al., 1972 & 1973, Khajavi et al., 2004; Kohi et al., 1979; Kolta et al., 1972, Lambert et al., 1991; Nanni et al., 1987). Some of these mixtures of compounds have melting points (480 to 510°C) lower than the metallic surface temperatures and turn into liquid state which increases the corrosion rates (Cuevas-Arteaga et al., 2004).

According to Khanna (2002) the hot corrosion plays an key role in determining the life of boiler components. A schematic of a coal-fired boiler showing as two main parts susceptible to hot corrosion is presented in Fig.2.8. Water wall fireside corrosion occurs mainly due to reducing (substoichiometric) conditions caused by incomplete combustion of coal particles and molten salt attack. Reducing conditions lower the melting point of deposited salt and increase its ability to dissolve the normal oxide scales. Further, local disruption of the normal oxide film on the wall tubes through fluxing by molten salt can lead to accelerated oxidation or oxidation-sulphidation.

.

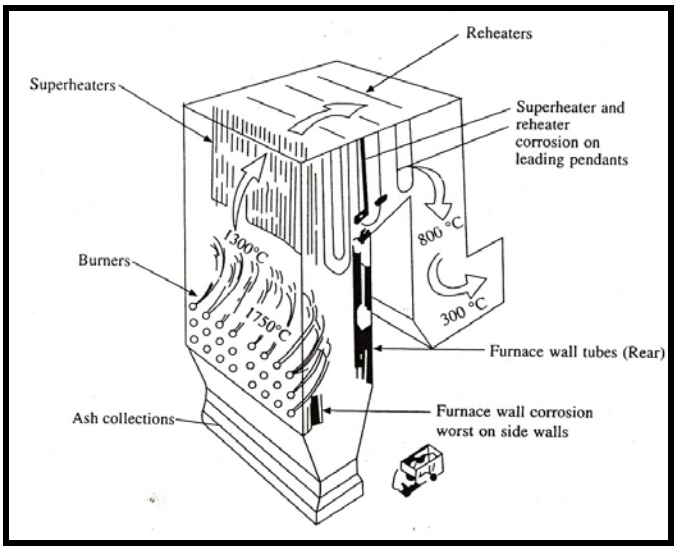

Fig. 2.8 Schematic illustration of coal fired boiler (Khanna, 2002 and Marriott, 1990)

As suggested by Khanna et al. (1998), the sulphur present in coal and fuel oils yields SO_2 on combustion which is partially oxidised to SO_3. The NaCl (either as impurities in the fuel or in the air) reacts with SO_3 and water vapours at combustion temperatures to yield Na_2SO_4 as below:

$$2NaCl + SO_3 + H_2O \rightarrow Na_2SO_4 + 2HCl(g) \qquad (2.12)$$

At lower temperatures Na_2SO_4 can further react with SO_3 to form sodium pyrosulphate, $Na_2S_2O_7$ with melting point (m. p.) of 401°C:

$$Na_2SO_4 + SO_3 \rightarrow Na_2S_2O_7 \qquad (2.13)$$

Small amounts of vanadium may be present in fuel oils, which on combustion forms V_2O_5. This may further react with Na_2SO_4 to form low melting sodium vanadates, which are highly corrosive.

$$xNa_2SO_4 + V_2O_5 \rightarrow (Na_2O)_x.V_2O_5 + xSO_3 \qquad (2.14)$$

Thus metals and alloys in combustion gases are exposed to various corrosives such as O_2, SO_2/SO_3, molten salts, e.g. Na_2SO_4 or sulphate mixtures, sodium vanadates, NaCl (Khanna et al., 1998 & 2005). The fireside corrosion of superheaters in coal-fired boilers has restricted lower steam temperatures (Khanna, 2002). The enhanced corrosion of the superheater tubes is generally associated with the deposition of ash along with molten salts on the tube walls as illustrated in Fig.2.9.

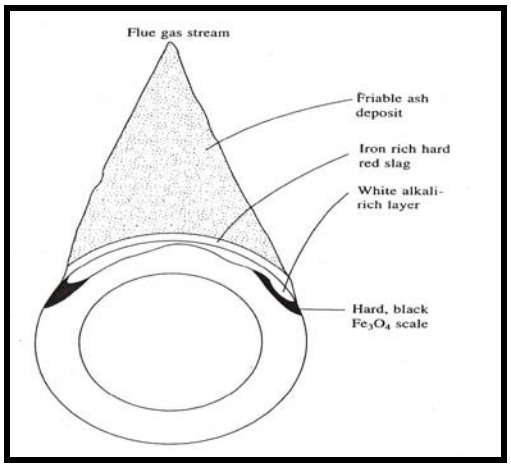

Fig. 2.9 Enhanced corrosion of superheater, associated with the formation of a molten deposit on the tube walls (Khanna, 2002)

Moujahid (1987) observed severe ash corrosion and cracks on the cast iron chains of moving grate used for air burning of coal. Coal ash in liquid state at 1300°C is strongly acidic and dissolves the basic spinel layers which formed on the chains at elevated temperature. The fused ash embeds coal particles and also reduces the thermal efficiency of the equipment. Drastic enhancement in ash corrosion rate has been attributed to the mechanical damages.

2.4 PREVENTIVE MEASURES AGAINST HOT CORROSION

Fuels with sulphur and other impurities cause hot corrosion which significantly reduces the life of components (Sharma, 1996). Corrosion and its associated losses cannot be eliminated completely. However, using better corrosion techniques almost one-fourth of annual corrosion related costs can be saved (Koch et al., 2002; Priyantha et al., 2003).

Preventive measures against losses in metals due to corrosion should be cost effective and ensure safety (Chatterjee et al., 2001).

Corresponding to the variety of corrosive environments, numbers of countermeasures have been developed to avoid excessive material damage. Heath et al. (1997) grouped the countermeasures into following categories:

1. Alloy selection: A large number of Fe, Ni- and Co-based alloys exist today especially designed for good resistance to oxidation, sulphidation or corrosion by ash/salt deposits.
2. Design aspect: Improve temperature distribution (avoid hot spots), avoid excessive deposition of ash and slags by use of soot blower, rapping, screens etc.
3. Chemical additives: Neutralisation of corrosive components in the flue gases by injecting additives such as limestone and dolomite.
4. Shielding: SiC tiles in waste incinerations, other type of refractory linings

5. Coatings: Different coating techniques are applied to protect the critical surface areas from corrosive gases, including co-extrusion, chromising, weld overlay and thermal spray coatings.

In general alloying elements which can improve the hot corrosion resistance of materials such as Cr, Al, etc., often have a negative effect on the mechanical properties in high temperature environments and are expensive (Wu and Okuyama, 1996). As reported by Goebel et al. (1973), the corrosion control in highly aggressive applications requires careful selection of materials.

2.5 ROLE OF COATINGS

A coating can be defined as a layer of material, formed naturally or synthetically or deposited artificially on the surface of an object made of another material, with the aim of obtaining required technical or decorative properties (Sidhu et al., 2006D). The coatings at high temperature develop a protective oxide layer on the metal surface to limit section loss by oxidation (Souza et al., 2007; Singh et al., 2005B; Xue et al., 2002; Fernando et al., 2003, Goward et al., 1998, Kim et al., 2004). Generally, these protective oxides (namely $A1_2O_3$, Cr_2O_3, and SiO_2) minimize the diffusion of gaseous or liquid species towards the component and conversely to prevent elemental diffusion from the alloy towards the external surface where they could react with the substrate (Smeggil et al., 1983). Moreover, inter-diffusion effects between coating and substrates are supposed to be minimum as far as the properties of the coated component are concerned (Mevrel et al., 1989).

Today in order to fulfill the reqirement for extended component lives, higher operating temperature and more fuel-efficient power plants, coatings are playing a key role. About $3/4^{th}$ of all the components used in jet engines are coated (Zhang et al., 2000). Efforts are now being made to develop high temperature degradation resistant coatings by various methods. (Shirvani et al., 2003). Sundararajan et al (2003) advocated the needs for applying thermal spray coatings on the boiler components.

2.5.1 Coating Processes

The commonly employed methods used for coating deposition have been enlisted in Fig.2.10 (Bhushan and Gupta, 1991). Nicoll (1984) reported that PVD, CVD and thermal spraying are mostly employed from production point of view. CVD process is costlier since it is a non-line-of-site process, proper masking and tooling are the major considerations during designing. Inclusion of pack particles in coating is another shortcoming of the CVD process, which lead to coating failure.

A large number of nanostructured coatings fabricated by different coating techniques of different compositions has been studied for various high temperature applications and tribological behaviour by several investigators. Thermal spraying systems cause less damage to the environment in comparison with other techniques such as PVD, CVD, and electroplating techniques.

2.5.2 Thermal Spray Process

Thermal spraying is a dry state based coating technique offering fast and convenient manner of growing thick coatings of metals and cermets on almost any of substrate by high deposition rates (Singh et al., 2005A, & 2005B; Sidhu et al., 2005A, 2005B, 2006A, 2006B, 2006C, 2006E, 2006F, 2006G, 2006H). The earliest records for thermal spraying are patents by the Swiss engineer M.U. Schoop, originating in the early 1900s (Bunshah, 2001).Thermal spraying is a generic technique whereby droplets of molten and partially-molten material are generated and projected at the substrate to form the coating. The droplets undergo little interaction with the substrate, merely adhering to the roughened surface through physical means to form an “overlay” coating. Generally, any material which does not decompose, sublimate, vaporize, or dissociate on heating, can be easily thermally sprayed. In the generalized thermal spray process, the coating material in wire, rod or powder form is fed into a high temperature heat source, where it is heated close to, or in excess of its melting temperature. A high velocity accelerating gas or combustion gas stream accelerates the droplets of material to the substrate, where they impact and spread across the surface to form a “splat”, Fig. 2.11 (Matthews, 2004**).** The oxidation time during thermal spray coating is short (Fig.2.12) typically less than 0.01 s, and can occur in either the solid or molten state.

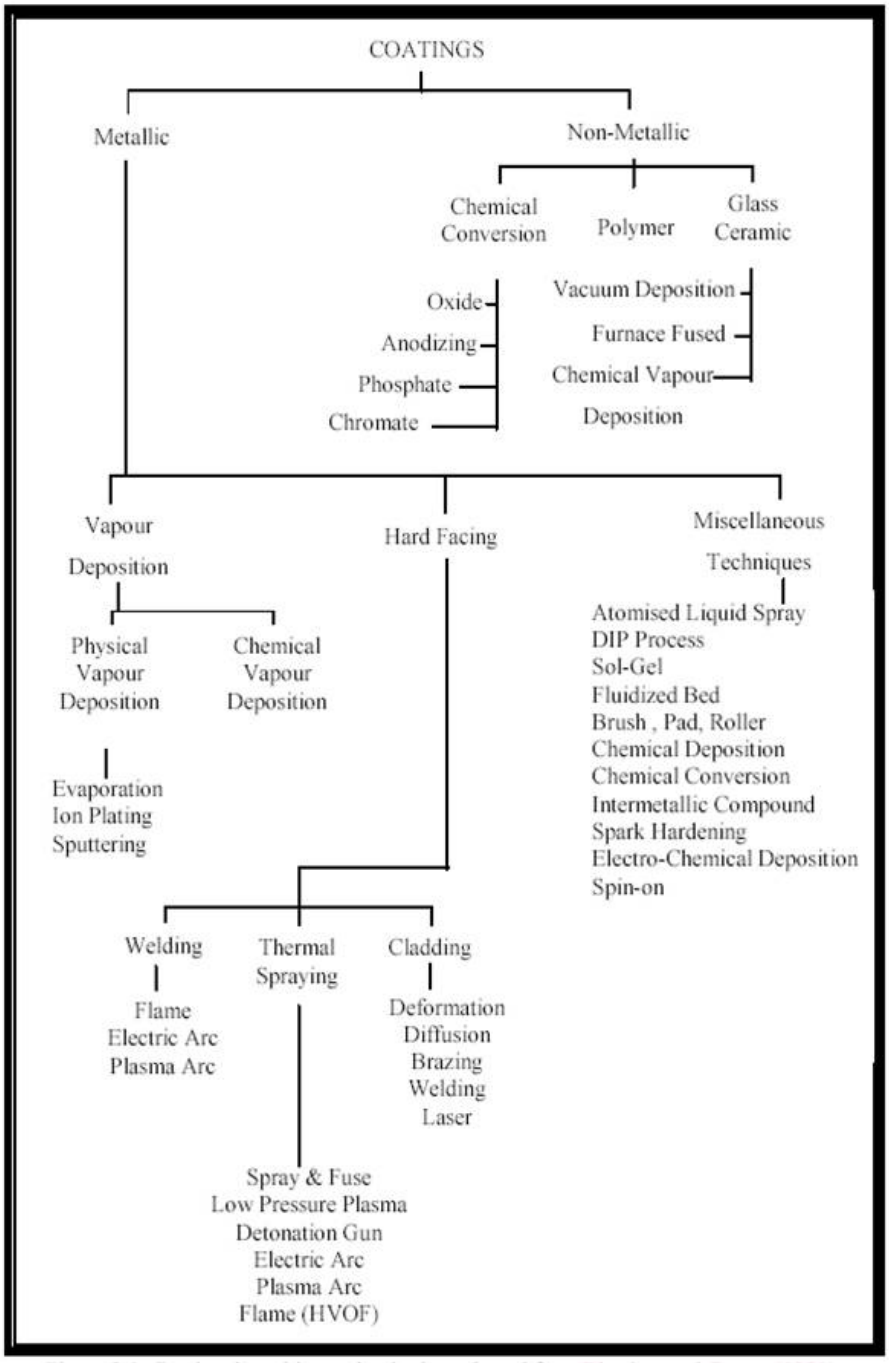

Fig.2.10 Coating deposition technology, (Bhushan and Gupta, 1991)

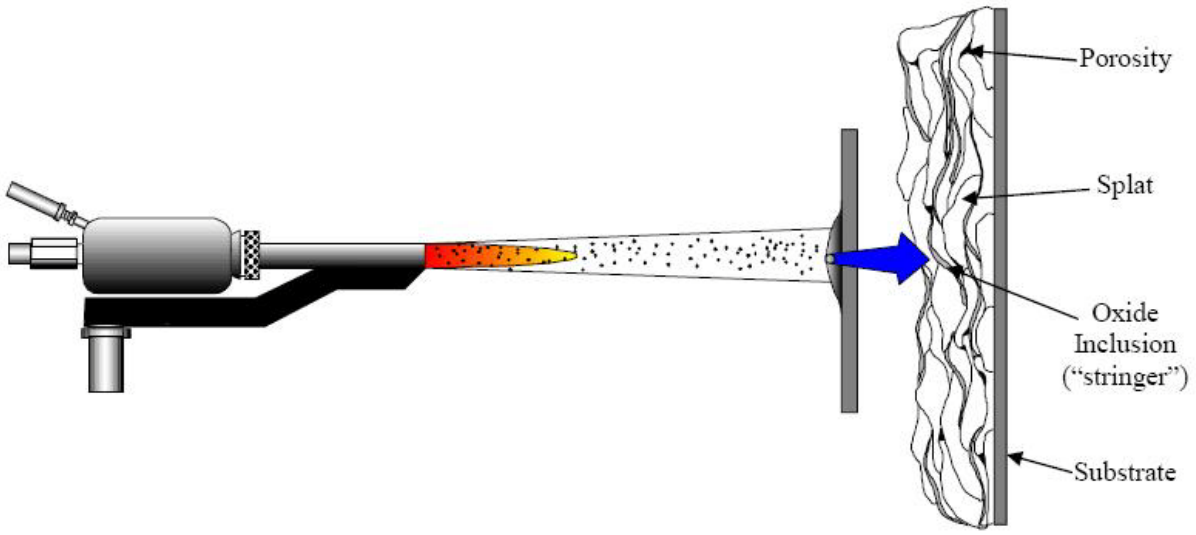

Fig.2.11 Schematic development of the thermal spray process and mechanism of coating build-up (Matthews, 2004).

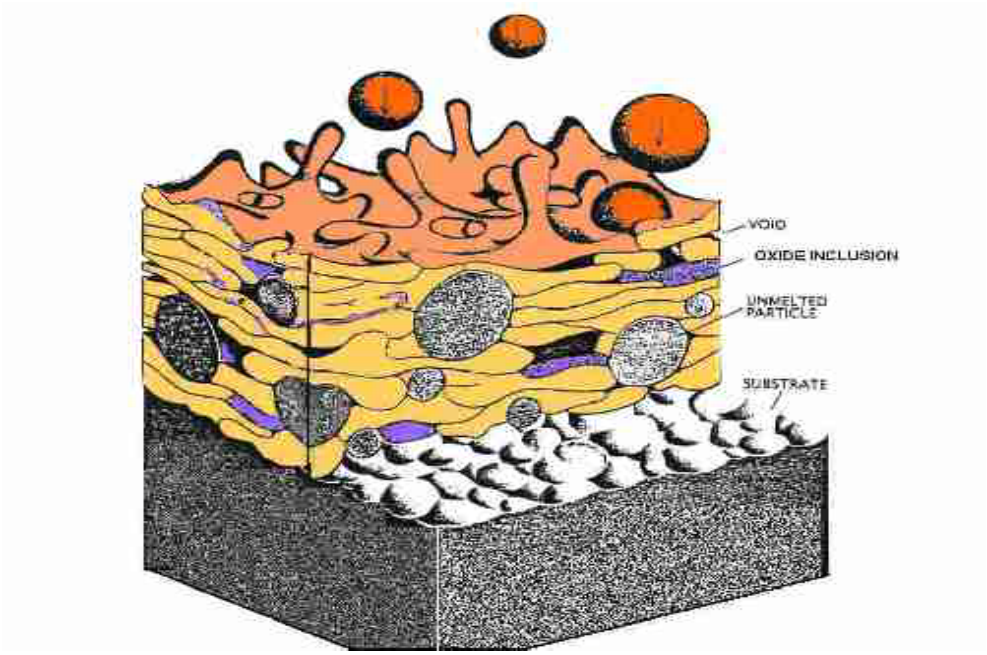

Fig.2.12 Coating deposition and the oxidation process (Herman, 1988).

Kuroda et al., (2008) classified the various thermal spray processes in terms of velocity and particle temperature (Fig.2.13).Similarly, Gledhill et al. (1999) proposed the schematic diagram (Fig.2.14) showing un-melted particles, splats, voids and in coming particles with un-melted core along the cross-section through a thermally sprayed coating. In the 70's due to development of the thermal plasmas and to

fulfill the increasing demand of wear resistant and high temperature application materials the technology is expanded (Knotek, 2001).

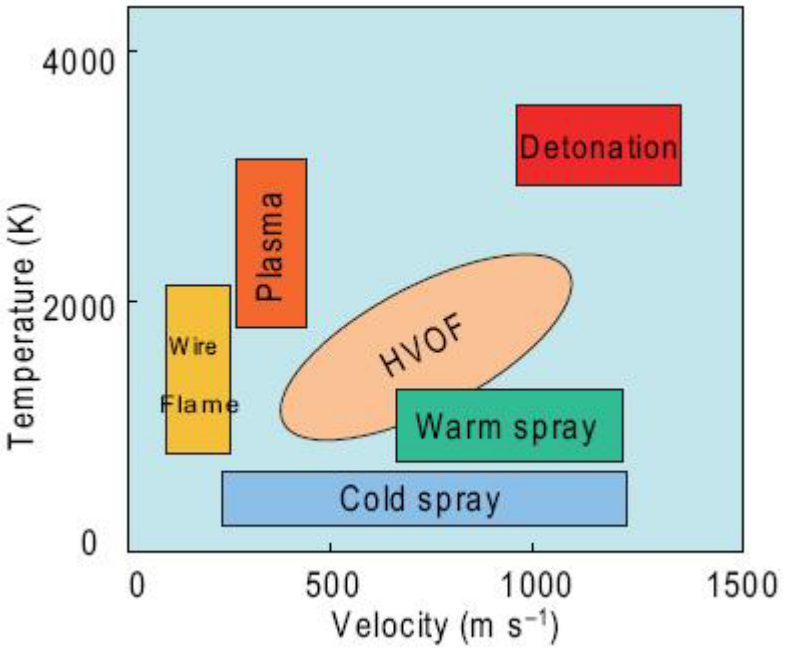

Fig. 2.13 Comparison of various thermal spray processes in terms of particle temperature and velocity (Kuroda et al., 2008).

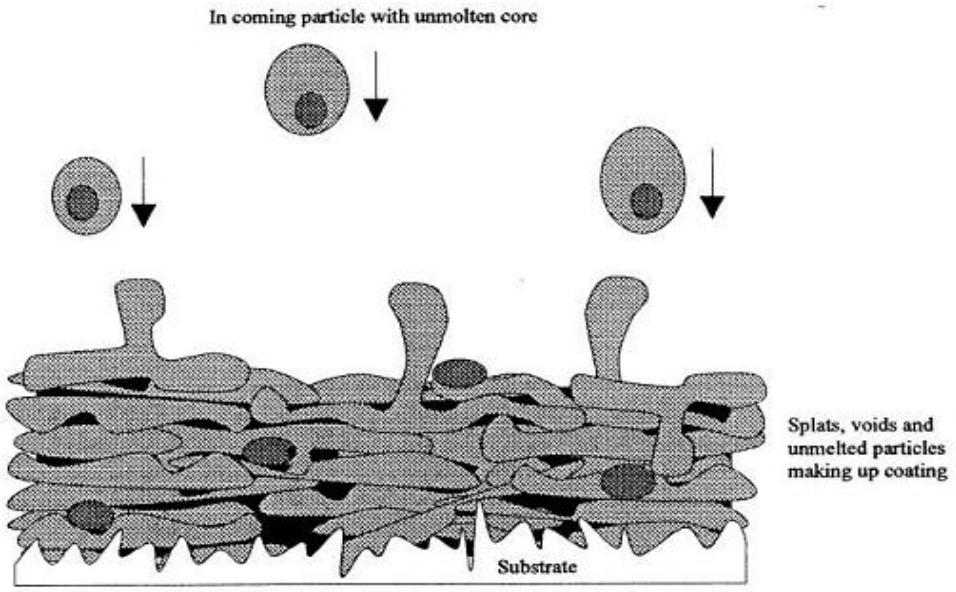

Fig.2.14 Schematic diagram showing a cross-section through a thermally sprayed coating (Gledhill et al., 1999)

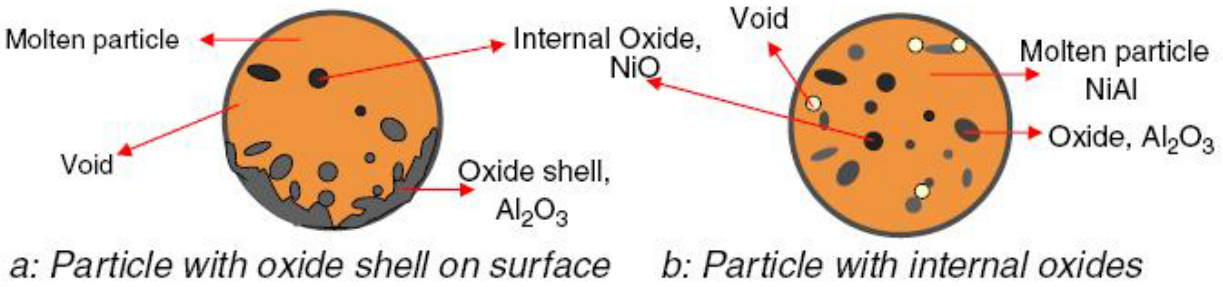

Fig. 2.15: Schematics for oxidation of particles, in-flight. (Deshpande et al., 2006)

Deshpande et al. (2006) proposed that, during in-flight oxidation, oxide layer is formed on the molten particle. However, when the temperature of particle reduced during later part of the reaction, these oxides tend to solidify due to which a oxide shell was formed around the droplet (Fig.2.15).

Literature reveals that the thermal spray technique was widely used to fabricate wear and corrosion-resistant coatings, which improve service life time and corrosion/wear resistance of the component of gas turbines, power generation industry, steam turbine, coal fired boiler. The flexibility in spray dimensions and faster rate of deposition are some of the characteristics of thermal spray coatings. The types of thermal sprays depend on the type of heat sources employed and are classified as shown in figure 2.16

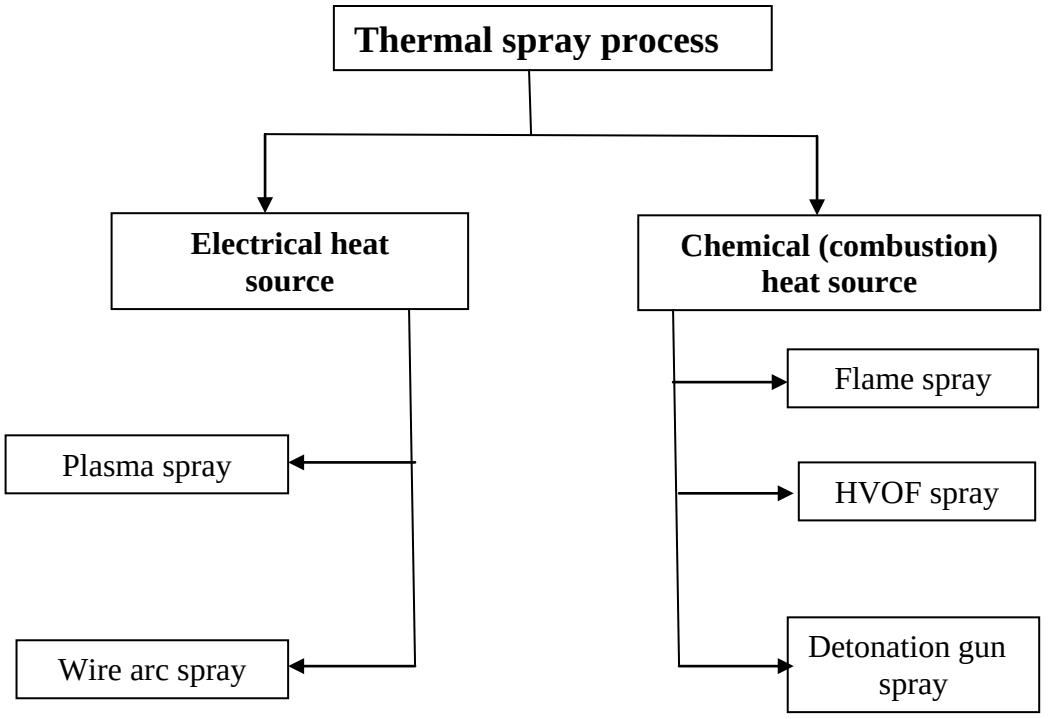

Figure 2.16: Classification of thermal spray process of coating

2.6 HIGH VELOCITY OXY-FUEL (HVOF) THERMAL SPRAYING

During the 1980s, High velocity oxy-fuel (HVOF) process was developed. HVOF process belong to the family of thermal spray techniques, which are capable of producing dense coatings and superior bond strength. (Sahraoui et al., 2004; Murthy et al., 2007, Mahesh et al., 2008; Lima et al., 2007; Li et al., 2002; Korpiola et al., 1996; Hazoor et al., 2006). The schematic cross section of HVOF gun is shown in fig. 2.17. In HVOF spray process, powder is melted by the use of combustion of fuel gas with oxygen and is propelled at a very high velocity by the use of compressed air towards the substrate. During HVOF process, hypersonic gas velocities of about 1800 ms^{-1} and the flame temperature of above 2800^0C are achieved. “High velocity oxy fuel (HVOF) deposition technique is preferred for the deposition of cermet coatings as compared to other thermal spray processes such as plasma spray, detonation gun spray, flame spray due to its ability to develop coatings with dense and homogeneous microstructure, uniform deposition thickness, smooth surface, superior bonding strength and hardness (Shukla et al 2013).

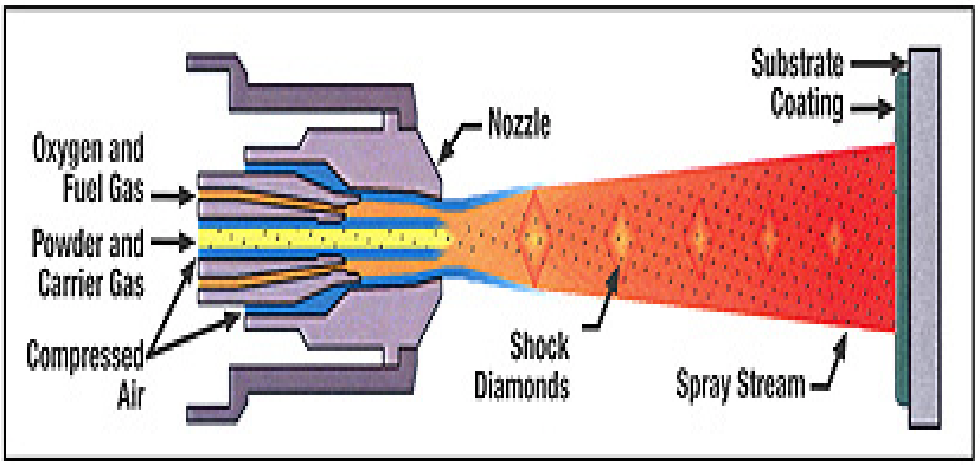

Fig: 2.17 Schematic diagram of HVOF gun (High Velocity Oxygen Fuel Thermal Spray Process)

Thermal spray technology is extensively used to fabricate wear and corrosion-resistant coatings on steel substrates in industry, which improves service life time and high performance of coated steel (Hawthorne et al., 1999; Haugsrud et al., 2003; Hao Du et al., 2007; Gurrappa et al., 1999, 2000, 2001, 2003 & 2006). The HVOF coatings are widely used for high-temperature corrosion and wear resistance in power generation industry, oil-refining industry, heat treatment rolls, coal burning boiler tubes, and aerospace industry, (He et al., 2001; Stein et al., 1999; Li et al., 2004; Sidhu et al., 2006A, 2006C, 2006G, 2006F &2006H; Gang et al., 2006). Cr_3C_2-NiCr coatings deposited on different substrates by different thermal spray techniques has been studied by various researchers.

Literature review reveals that the high temperature oxidation of the cermet coatings is influenced by factors such as the size and distribution of the carbide particles, the morphology of the starting powder, and the coating process. The influence of microstructural features on the corrosion resistance of HVOF sprayed Cr_3C_2-NiCr coatings and the mechanisms by which coatings oxidized in high temperature environment with respect to time is scarce in the literature.

2.7 HIGH VELOCITY ARC-SPRAY (HVAS) THERMAL SPRAYING

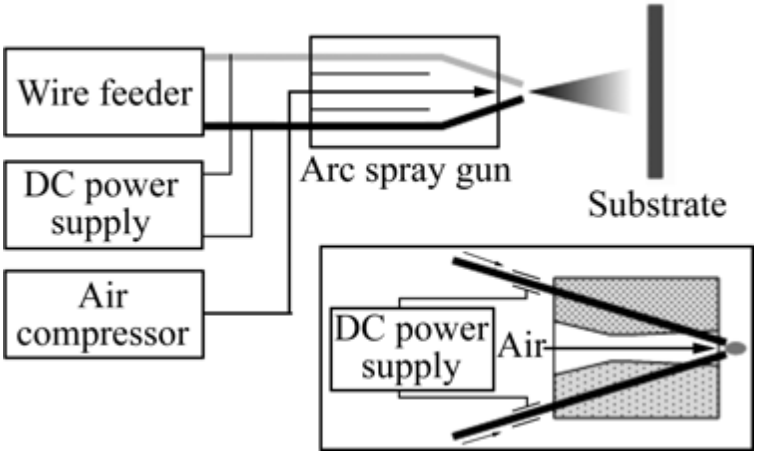

Fig.2.18 Schematic diagram of HVAS (Chen et al., 2008)

High velocity Arc spray is one form of thermal spray process, instead of combusting fuel as heat source to melt the feedstock material (like HVOF), electric discharge arc is used to directly melt the coating material (Fig. 2.18). The coating process consists of two consumable coating wires of identical or different materials that are continuously fed into a gun. Both the wires have opposite electric polarity, an electric arc is formed between the two wires to complete the electric circuit. Due to the electric arc, temperature rises and both the wires melts. The molten material is then propelled on to the substrate by compressed air. The coating wire material must be electrically conductive. HVAS process is preferred for the deposition of FeCr base coatings on bare substrate compared to other thermal spray techniques such as plasma spray, detonation gun spray, flame spray owing to its capability to develop coatings with dense, homogeneous microstructure with lower oxide content and minimal heat transfer to the substrate, cost effectiveness, high efficiency of the process. Table 2.1 shows some of the important characteristics associated with these thermal spray techniques (Bhushan and Gupta, 1991; Sobolev et al., 2004; Wagner et al., 1984).

Table 2.1. Important characteristics associated with thermal spray techniques

Deposition Technique	**Heat source**	**Propellent**	**Material feed type**	**Spray Gun temp. (^{0}C)**	**Particle velocity m/s**	**Coating materials**	**Relative bond strength**	**Porosity level% volume**
ctric Arc	Arc between electrodes	Air	Wire	6000	240	Ductile materials	Good	8-15
Plasma Arc Spraying	Plasma Arc	Inert Gas	Powder	16000	120-600	Metallic, ceramic, plastic and compounds	Very Good to Excellent	2-5
Low Pressure Plasma Spraying	Plasma Arc	Inert Gas	Powder	16000	900	Metallic, ceramic, plastic and compounds	Excellent	<5
Spray & Fuse	-	-	Powder	-	-	Fusible metals	Excellent	<0.5
Flame Spraying	Oxyacetylene/ Oxy hydrogen	Air	Powder	3000	30-120	Metallic and ceramics	Fair	10-20
Detonation Gun Spraying	Oxygen/ Acetylene/ Nitrogen Gas Detonation	Detonation Shock Waves	Powder	4500	800-1200*	Metallic, ceramic, plastic and compounds	Excellent	0.1 to 1
High Velocity Oxy-fuel (HVOF)	Oxy-propylene/ hydrogen/ propane/LPG	Combustion Jet	Powder/ wire	3000	800	Metallic and ceramic	Excellent	0.1-2

2.8 PROBLEM FORMULATION

2.8.1 Scope

Materials degradation at high temperatures is a serious problem in several high tech industries. Attempts to increase the efficiency of steam generating plant by raising the final steam temperature above

600°C and the use of gas turbines for the production of cheap electric power have made working conditions more severe for the materials (Thilkan et al., 1967, Mukhopadhyay et al., 1998 & 1999).

It has been learnt from the literature that high temperature corrosion and erosion problems needs to be arrested through some other preventive means; prominent among them being controlling process parameters, use of inhibitors, application of protective coatings etc. as there lies little scope in improvement of the combustion environments. In Indian context, this is even more relevant as the Indian coal is found to have high ash content (Sharma, 1996). Further, the use of inhibitors is not easily viable due to practical implications in injecting these inhibitors in the combustion chamber along with the fuel in an actual industrial environment (Tiwari and Prakash, 1996 and Gitanjaly et al., 2002 & 2003). In this regard, it is further learnt from the published literature that one possible, practical, reliable and economically viable way to control or prevent the high temperature corrosion and erosion problems of the superheaters and reheaters of the boilers is an application of a thin layer of corrosion resistant coatings having good thermal conductivity.

Due to the continuously rising cost of the corrosion resistance materials such as superalloys as well as increased material requirements, the coating techniques play important role in the recent times. Therefore, the use of protective thermal spray coatings has been identified as a potential area for the present research. Porosity, stress generation and interlayer separation between the different deposited layers are the prominent parameters to be considered for selecting a particular process for deposition of the corrosion resistant coating. The easiness, economy and convenience of operations are the other major factors that must be considered for applying the coatings to industrial installations.

The high temperature corrosion behavior of the coatings deposited by HVOF and HVAS process is very limited in the literature so far. Chromium based metallic coatings are frequently considered for the protection against oxidation, corrosion, wear and erosion at high temperatures. Therefore, the present research work is envisaged to make a detailed investigation of HVOF and HVAS sprayed coatings (Cr_3C_2-25%NiCr, FeCr based conventional and nanostructured coatings) on 310S alloy substrate subjected to oxidation, hot corrosion and actual boiler environments. It is very essential to investigate the hot corrosion behavior of thermal sprayed coatings deposited on ASS 310S to assess its suitability for high temperature applications. Most industrial processes involve the use of metals and alloys at elevated temperature followed by cooling to room temperature numerous times. The operating conditions in such plants are mostly cyclic, rather than to isothermal processes. Therefore, oxidation under cyclic conditions is more realistic approach (Hocking, and Sidky, 1987). Relatively fewer studies are reported under cyclic conditions, which actually simulate the working conditions of boilers and gas turbines. Owing to the

aforementioned views, the present work has been focused to address the issues as given in following section.

2.8.2 Objectives

1. The present research work is focused on studying the high temperature (700 ^{o}C & 900^{o}C) oxidation (Air), hot corrosion in Na_2SO_4-60%V_2O_5 and Na_2SO_4-82%$Fe_3(SO_4)_3$ environment in the laboratory tube furnace and actual coal fired boiler environment on 310S in bare conditions and after application of HVOF sprayed Cr_3C_2-25%NiCr, FeCr based conventional and nanostructured coatings on the 310S.
2. To compare the oxidation and hot corrosion performance of the HVOF and HVAS sprayed coatings with bare substrate (310S) and assess its suitability for using it in the boiler super-heaters and re-heaters, and for other future hot section components to be used in similar corrosive environments.
3. To understand and propose mechanisms for the high-temperature corrosion of the alloy substrate and coated alloys, wherever possible. As far as the testing in air environment is concerned, the study could also provide useful information regarding the adhesion of the coatings and the spalling tendency of their oxide scales apart from air oxidation behaviour of the coatings.
4. To establish the behaviour of these coatings and bare substrate in the actual working conditions in which they may be used, the coatings are investigated in the operational environment of the coal fired boiler at Guru Nanak Dev Thermal Plant, Ropar, Punjab, India.
5. In both the laboratory as well in industrial environments, the experiments are planned to conduct under cyclic conditions as it provides the severest conditions for testing and represents the actual industrial environment where breakdown and shutdown occur frequently.
6. The Cr_3C_2-25%NiCr, FeCr based conventional and nanostructured coatings, deposited on the 310S alloy substrate, after high temperature air oxidation and hot corrosion studies were characterized by the techniques such as XRD, FE-SEM/EDS, & X-ray mapping to render an insight into the corrosion mechanisms based on the morphology of the corroded products formed on the coated specimens. The similar characterizations studies were performed for the corroded uncoated specimens.
7. To summarize the important contributions made in the present work on HVOF and HVAS sprayed coatings on 310S alloy substrate and highlight the scope for future work in the high temperature corrosion of coatings.

CHAPTER - 3

Experimental Procedure and Characterization Techniques

This chapter presents experimental techniques and procedures employed for deposition and characterization of coatings. A detailed description of high temperature oxidation studies in air as well as in molten salt environments and erosion-corrosion studies in an actual industrial environment is given in this chapter. The methods for analyzing the corrosion products are discussed.

3.1 SELECTION OF SUBSTRATE MATERIALS

Austenitic stainless steel 310S (boiler steel) have been selected for the present study as the substrate material after consultation with GGSSTP Plant, Roop Nagar, India. The actual chemical composition of 310S ASS has been determined using Optical Emission Spectrometer (Thrmo Jarrel Ash, TJA181/81, U.S.A); which is reported in Table 3.1. The 310S alloy finds application in steam boilers, heat exchangers and furnace equipment.

Table 3.1. Chemical composition (wt.%) of 310S alloy substrate

Chemical composition (wt.%) of 310S alloy									
C	**Cr**	**Ni**	**Mn**	**Si**	**Cu**	**Mo**	**P**	**S**	**Fe**
0.0409	25.18	19.14	1.32	0.486	0.189	0.177	0.0202	0.004	Balance

3.2 DEVELOPMENT OF COATINGS

3.2.1 Preparation of Substrate Materials

Specimens having dimension 20 mm X 15 mm X 5 mm were cut from the base alloy sheets. The polished specimens were grit blasted by alumina (Grit 45) particles prior to deposition of coatings by HVOF and HVAS thermal spray techniques for developing better adhesion between the substrates and the coatings.

3.2.2 Feedstock Materials for the Coatings

Three types of commercially available feedstock materials namely Cr_3C_2-NiCr (TAFA 1375VM), FeCrBMnSi (TAFA 95 MXC), FeCrWNbMoBCMnSi (TAFA 140 MXC) were chosen for HVOF and HVAS thermal spray coating on 310S alloy substrates. The chemical composition of the feedstock materials are reported in Table 3.2.

Table 3.2. Chemical composition (wt %) of feedstock materials for the coatings

Chemical composition (wt %) of feedstock material											
Feedstock material	Cr	Cr_3C_2	Ni	W	Nb	Mo	B	C	Mn	Si	Fe
Cr_3C_2-25%NiCr (TAFA 1375VM)	5	75	20	-	-	-	-	-	-	-	-
FeCrBMnSi (TAFA 95 MXC)	< 29	-	-	-	-	-	< 4	-	< 2	< 2	Bal.
FeCrWNbMBCMnSi (TAFA 140MXC)	< 25	-	-	< 15	< 12	< 6	< 5	< 4	< 3	< 2	Bal.

Table 3.3 Spray parameters as employed during HVOF spraying.

Spraying parameters	**Cr_3C_2-25%NiCr coating**
Oxygen flow rate (scfh)	1850
Oxygen pressure (psi)	210
Fuel gas (kerosene) flow rate (slph)	22.7
Fuel gas (kerosene) pressure (Kgf/cm^2)	170
Carrier gas (N_2) flow rate (slpm)	10
N_2 pressure (psi)	50
Stand-off distance (mm)	300
Powder feed rate (gm/min)	80

Table 3.4 Spray parameters as employed during HVAS spraying.

Spraying parameters	**CC and NC coating**
Spray Rate (kg/hr/125 amps)	4
Coverage (wire consumption, kg/m^2/100 microns)	1.2
Stand-off distance (inches)	5

3.2.3 Formulation of coatings

The HVOF thermal spray technique was used to fabricate Cr_3C_2-25%NiCr coatings and HVAS process was used to apply conventional FeCrBMnSi alloy (CC) and nanostructured FeCrWNbMBCMnSi alloy (NC) coatings on 310S alloy substrate at M/s Industrial Processors and Metallizers (IPM), Pvt. Ltd, Delhi, India using standard parameters (Shukla et al. 2012 & 2013). The process parameters for the HVOF and HVAS processes employed for applying the coatings are summarized in Table 3.3 and 3.4, respectively.

3.3 CHARACTERIZATION OF THE COATINGS

3.3.1 Specimen preparation

The as-coated 310S alloy substrate coupons were cut with a diamond cutter (Buehler's Precision Diamond Saw, Model ISOMET 1000, USA) across its cross-section and subsequently hot mounted using Buehler's transoptic powder (20-3400-080). Subsequently, the mounted specimens were polished manually by standard polishing using emery papers followed by cloth polishing using 0.05 μm alumina powder suspension.

3.3.2 Measurement of Coating Thickness

The thickness of the coating was monitored during the coating processes. The thickness was monitored with a Minitest-2000 thin film thickness gauge (made in Germany, precision ±1 μm). Efforts were made to obtain the coatings with uniform thickness. The thickness of some of the as-coated specimens (nanostructured as well as conventional coatings) were further verified by cutting along the cross-section and mounted (as explained in Section 3.3.1). A field emission scanning electron microscope (FE-SEM) (FEI Quanta 200F, the Netherlands) was employed to obtain images of the cross-sectioned samples surfaces. The average coating thickness was measured from the BSE images at different locations and reported in Chapters 4, 5 and 6.

3.3.3 Measurement of Porosity

Zeiss Axiovert 200 MAT inverted optical microscope was used to capture polished images of the coated surfaces. The porosity was measured from the microstructures using image analysis software Zeiss Axiovision Release 4.1, (Germany)" (Shukla et al. 2013). The average porosity values are reported in Chapters 4, 5, and 6.

3.3.4 Measurement of Bond strength

The bond strength of as-sprayed coating was tested using a portable pull-off adhesion tester. The top surface of coated specimen (80mm x80mm x10mm) was joined with loading fixture using polymerized glue and subjected to increasing tensile stresses until the coating failed. Tensile load exerted by the machine was recorded continuously. The average porosity values are reported in Chapters 4, 5, and 6.

3.3.5 Measurement of Microhardness

For obtaining microhardness of the thermal sprayed coatings, the specimens were cut, mounted and polished as explained in section 3.3.1. The micro hardness of the coatings was determined using Vickers hardness tester (VHM-002 Walter UHL, Germany) at 300 grams load for 15 s. Each reported value of the microhardness is the average value of five measurements". These microhardness values are plotted as a function of distance from the coating/substrate interface and incorporated in Chapters 4, 5, and 6.

3.3.6 Measurement of Surface Roughness

The surface characteristics of coated and bare specimens were studied using roughness tester (Mitutoyo SJ-400, Japan). The average of surface roughness (R_a) measured at five different locations are reported in Chapters 4, 5 and 6.

3.3.7 X-Ray Diffraction (XRD) Analysis

Phase analysis of surfaces of bare, as sprayed and oxidized samples was done using X-ray diffractometer (XRD, Bruker AXS D-8, Germany) with CuK_α radiation (Fig. 3.1). The scanning speed of 2^o/min was maintained in 2θ range of 20^o - 100^o. The grain size of the nanostructured coatings was estimated using Scherrer formula (Cullity, 1970) as follows:

$$D = 0.9\,\lambda / B\,\text{Cos}\theta \quad \ldots\ldots\ldots\ldots\ldots\ldots\ldots\ldots\ldots\ldots \quad (3.1)$$

The grain size values of the nanostructured thin coatings are presented in Chapter 6.

3.3.8 Field Emission-Scanning Electron Microscopy (FE-SEM) and Energy Dispersive Spectroscopy (EDS) Analysis

3.3.8.1 Surface Morphology/EDS Analysis

The surface morphologies of the feedstock materials and as-coated coupons were studied using FE-SEM fitted with EDAX Genesis software attachment (Fig. 3.2); with an aim to understand the morphology of the coating powders and to identify inclusions, un-melted, partially melted particles and pores in the as sprayed coatings. FE-SEM/EDS analysis of the as coated specimens is reported in Chapter 4, 5 and 6 of the present study.

3.3.8.2 Cross sectional analysis

The sample was prepared as explained in the section 3.3.1. The analysis was carried out using a FE-SEM equipped with Energy Dispersive Spectroscopy (EDS). The back scattered electron images were taken and the EDS analysis was performed across the cross section to ascertain elemental composition (weight %) at different points as well as to identify the presence of various elements along the cross-section of the coatings.

3.3.8.3 X-ray mapping analysis

To obtain cross-sectional analysis of the different elements present, the bare, as sprayed and oxidized samples were cut along the cross-section, mounted and polished in accordance with the procedure already discussed in section 3.3.1. X-ray mapping analysis of FE-SEM images was also done to understand elemental distribution of the coated surface.

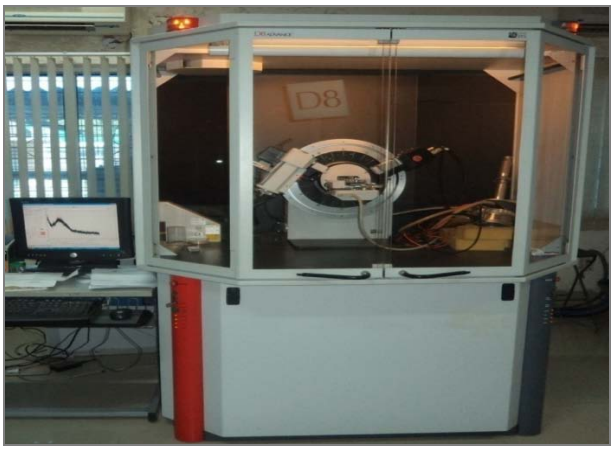

Fig. 3.1: A photograph of D8 advanced X-ray diffractometer used in the present study.

Fig. 3.2: A photograph of FEI Quanta 200F scanning electron microscope used in the present study.

Fig. 3.3: A photograph of TECNAI G2 transmission electron microscope used in the present study.

3.3.9 Transmission Electron Microscopy

TEM images and SAED patterns of the feedstock material (140MXC) as well as nanostructured alloy coating (NC) were recorded on FEI TECNAI G2 (Fig. 3.3) electron microscopes. TEM analysis of the feedstock material (140MXC) as well as nanostructured alloy coating (NC) is reported in Chapter 6 of the present study.

3.4 HIGH TEMPERATURE OXIDATION AND HOT CORROSION STUDIES

3.4.1 Experimental

Prior to oxidation studies, the bare and coated specimens were polished to obtain similar surface conditions. Physical dimensions and weight of the polished specimens were measured. The specimens were kept in an alumina boat and inserted into hot zone of the furnace maintained at a constant temperature. Oxidation studies were conducted at 700^{o}C and 900^{o}C in a silicon carbide tubular furnace. One hour holding time in the furnace in still air was given, followed by cooling for 20 minutes at room temperature". Following this, weight changes were measured at the end of each cycle using a precision electronic balance (Shimadzu AUX 220, Japan) with 0.1mg sensitivity. All oxidation and hot corrosion studies were carried out for 50 cycles. The reproducibility in the experiments was established by repeating hot corrosion experiments for three cases.

3.4.2 Oxidation Studies in Air

The oxidation tests at 700^{o}C and 900^{o}C were performed on bare 310S alloy substrate (mirror polished) as well as coated alloys in laboratory silicon tube furnace up to 50 cycles as discussed in section 3.4.1.

3.4.3 Hot Corrosion Studies in Molten Salt (Na_2SO_4-60%V_2O_5 & Na_2SO_4 - 82%$Fe_2(SO_4)_3$)

3.4.3.1 Coating of Molten Salt

The as coated as well as bare specimens (mirror polished) were prepared for studies as discussed in section 3.4.1. The specimens were then heated in an oven up to 250^{o}C and a salt mixture of Na_2SO_4-60%V_2O_5 and Na_2SO_4 - 82% $Fe_2(SO_4)_3$ dissolved in distilled water was coated on all the six surfaces of warm polished specimens with the help of a hair brush. A salt coating of 3-5 mg/cm^2 was maintained. FE-SEM morphology and EDS compositional analysis of Na_2SO_4, V_2O_5 and $Fe_2(SO_4)_3$ salts are shown in Figure 3.4, 3.5 and 3.6, respectively. The salt coated specimens and alumina boats were dried in an oven for 3 hours at 100^{o}C and weighed before being exposed to hot corrosion tests.

3.4.3.2 Hot Corrosion Studies

The bare 310S alloy substrate as well as coated coupons after application of salt coating were subjected to hot corrosion in the laboratory furnace at 700^0C & 900^0C for 50 cycles as discussed in section 3.4.1.

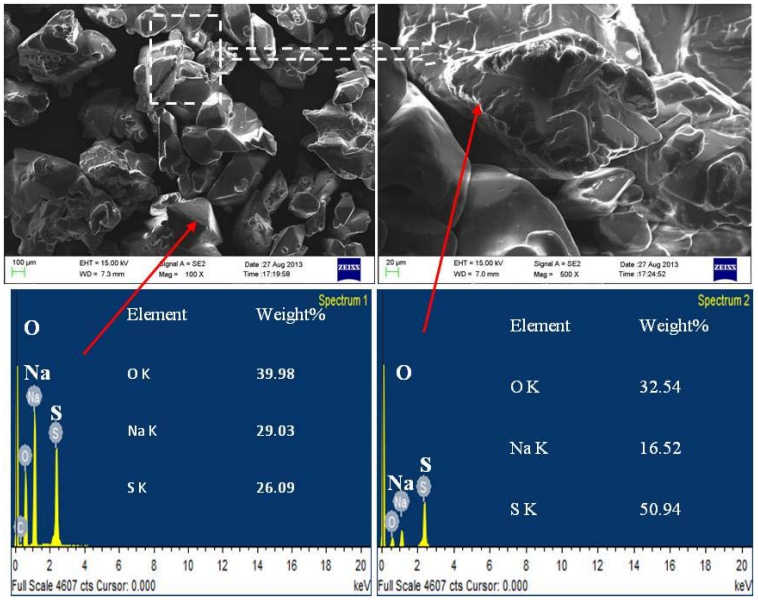

Fig. 3.4 FE-SEM morphology and EDS compositional analysis of Na_2SO_4 salt.

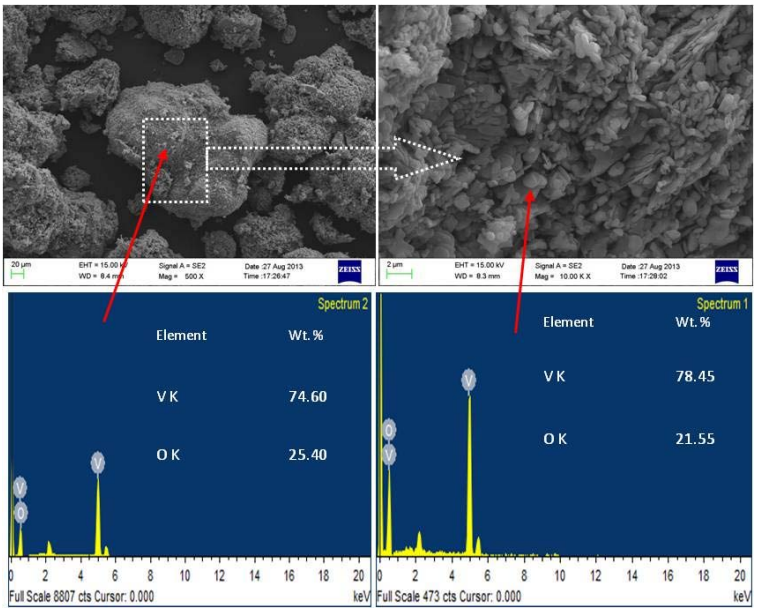

Fig. 3.5 FE-SEM morphology and EDS compositional analysis of V_2O_5 salt.

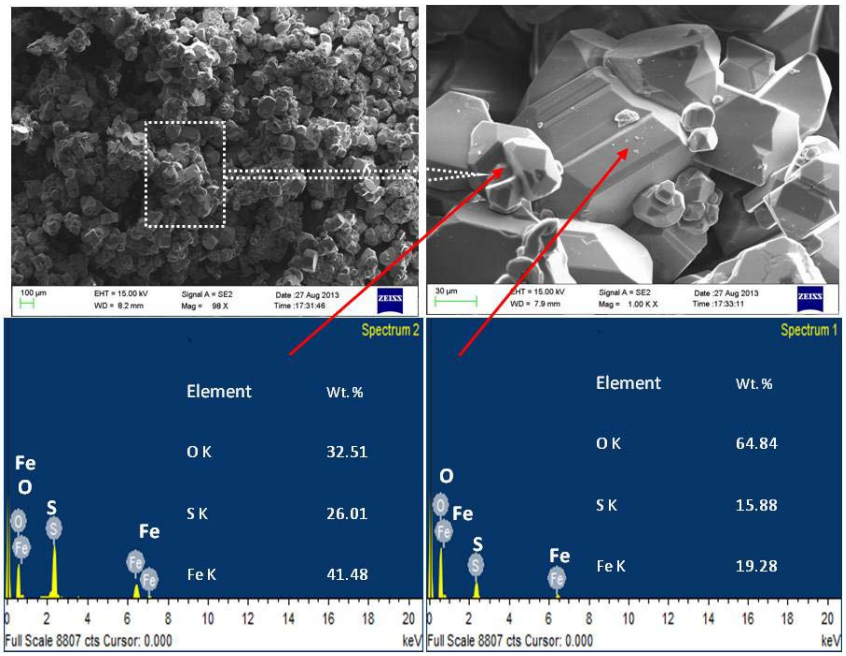

Fig. 3.6 FE-SEM morphology and EDS compositional analysis of $Fe_2(SO_4)_3$ salt.

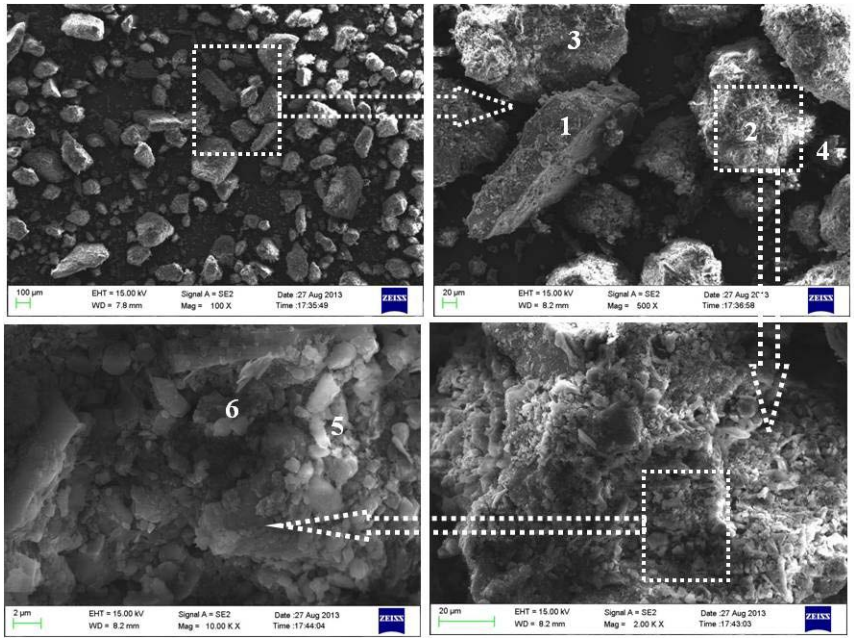

Fig. 3.7 FE-SEM morphology and EDS compositional analysis of fly ash inside the GGSSTPP boiler.

Table 3.5: Compositional analysis of ash and flue gases inside the GGSSTPP boiler (Fig 3.5)

Elements	Point of analysis (Weight % of elements)					
	1	2	3	4	5	6
C K	59.49	23.31	67.17	50.92	42.76	69.03
O K	31.19	51.31	28.09	15.12	44.06	25.07
Na K	0.06	0.10	0.05	-	0.89	0.80
Mg K	0.13	0.22	0.09	-	-	0.14
Al K	4.37	10.05	1.97	3.09	6.14	1.95
Si K	4.86	12.86	2.24	14.99	5.62	2.26
S K	-	-	0.08	-	0.12	-
Cl K	0.30	0.42	0.05	3.16	0.34	0.74
K K	0.11	0.34	0.26	14.63	0.18	0.05
Ca K	0.39	1.51	67.17	50.92	42.76	0.22
Fe K	59.49	23.31	28.09	15.12	44.06	0.24

Table 3.6 Coal analysis data

Constituent	Weight percentage
Total moisture (inherent + surface)	10.43
Inherent moisture	7.55
Ash	34.74
Ash on fire basis (actual)	33.64
Volatile metal	21.59
GC_v (gross calorific value) in kcal/kg	4187
GC_v on fire basis in kcal/kg	4055
Net GC_v in kcal/kg	3834
Unburnt carbon in fly ash	1.35
Unburnt carbon in bottom ash	5.75

3.4.4 Studies in coal fired industrial boiler environment

In order to understand the hot corrosion behavior, erosion-corrosion studies under cyclic conditions were done for the coated and uncoated alloy specimens in the middle zone of superheater of the Stage-II Boiler of GGSSTP Plant, Roopnagar,India. The estimated temperature in the middle zone of the superheater was 700 ± 10 ^{0}C, while volumetric flow of flue gases was estimated to be around 700 ton/h. The SEM/EDS analysis of the fly ash of GGSSTPP boiler is shown in Fig. 3.7 (Table 3.5). The chemical analysis of the coal used in GGSSTPP is given in Table 3.6 (Bala et al., 2012). The specimens were hanged in the boiler. The coated as well as bare alloy substrate was polished. Physical dimensions and weight of the specimens were measured before exposing them to the boiler environment. The coated as well as bare specimens were then hanged with the help of a stainless steel wire through the

soot blower dummy points at 27 m height from the base of the boiler. The specimens were exposed to the combustion environment for 3 cycles. Each cycle consisted of 500 hours heating followed by 1 hour cooling at ambient conditions. After completion of each cycle, the specimens were carefully observed for any change in the surface texture, further it has been washed by acetone and weight of the specimens were measured subsequently using an Electronic Balance with sensitivity of 0.1mg. The chemical analysis of the flue gas and ash present inside the GGSSTPP boiler is given in Table 3.7(Bala et al., 2012).

Table 3.7: Chemical analysis of ash and flue gases inside the GGSSTPP boiler

Ash		Flue Gases (Volumetric flow, 231 m^3/sec)	
Constituent	Wt. %age		
Silica	54.70	Constituent	Value relative to flue gases
Fe_2O_3	5.18	SO_x	236 mg/m^3
Al_2O_3-Fe_2O_3/Al_2O_3	29.56	NO_x	1004 $\mu g/m^3$
Calcium oxide	1.48	CO_2	12%
Magnesium oxide	1.45	O_2	7%
SO_3	0.23	40% excess air was supplied to the boiler for the combustion of coal.	
Na_2O	0.34		
K_2O	1.35		
Ignition loss	4.31		

3.5 ANALYSIS OF CORROSION PRODUCTS IN INDUSTRIAL ENVIRONMENT

All the specimens subjected to oxidation, hot corrosion as well as in the boiler environment were analyzed for the characterization of corrosion products. The surface and cross-section of the corroded specimens were analyzed using various analytical techniques such as XRD, FE-SEM/EDS, and X-ray mapping analyses.

Weight change analysis was not useful for predicted corrosion behavior of experiments conducted in coal fired boiler due to suspected spalling and ash deposition on the samples. Also, the weight change was also influenced by the erosion due to ash. Based on these facts, the corrosion was monitored by measuring sample thickness after 1500 hours. The extent of corrosion is expressed as corrosion rate in mils/year (mpy).

CHAPTER - 4

Cr_3C_2-25%NiCr COATING

In this chapter, characterization, oxidation and hot corrosion behavior of Cr_3C_2-25%NiCr coatings deposited on 310S alloy substrate by high velocity oxy fuel (HVOF) process as well as bare alloy substrate 310S are described in this chapter. The cyclic oxidation behavior and hot corrosion were investigated at an elevated temperature of 700^0C and 900^0C in air, Na_2SO_4-60%V_2O_5, Na_2SO_4-82%$Fe_2(SO_4)_3$ molten salt environments for 50 cycles and in actual coal fired boiler for 1500 hours. The weight change measurements for coated and bare substrate were made to substantiate its oxidation kinetics through the evaluation of the parabolic rate constants, thereby evaluating protective nature of the coatings. The microstructural characteristics of corroded products were studied using XRD, FE-SEM/EDS and X-ray mapping to understand the mode of oxidation and hot corrosion.

4.1CHARACTERIZATION OF THE ALLOY SUBSTRATE (310S)

4.1.1 Microstructure of the alloy substrate

Optical microstructures and FE-SEM images of the 310S alloy substrate are shown in Fig. 4.1, which are explained with reference to atlas of microstructures for industrial alloys (Metals handbook, 1975 and Metals handbook, 1990). The 300-series alloys are Fe-Cr-Ni grades containing 16 to 26% Cr and 6 to 22% Ni. The other alloying elements such as Mo, Cu, Si, Al, Ti, Nb, Ta and N are added to improve resistance to pitting & crevice corrosion, SCC and hot corrosion. It is observed that 310S alloy substrate shows single phase austenitic grain structure and there are no carbides as seen from Fig.4.1.

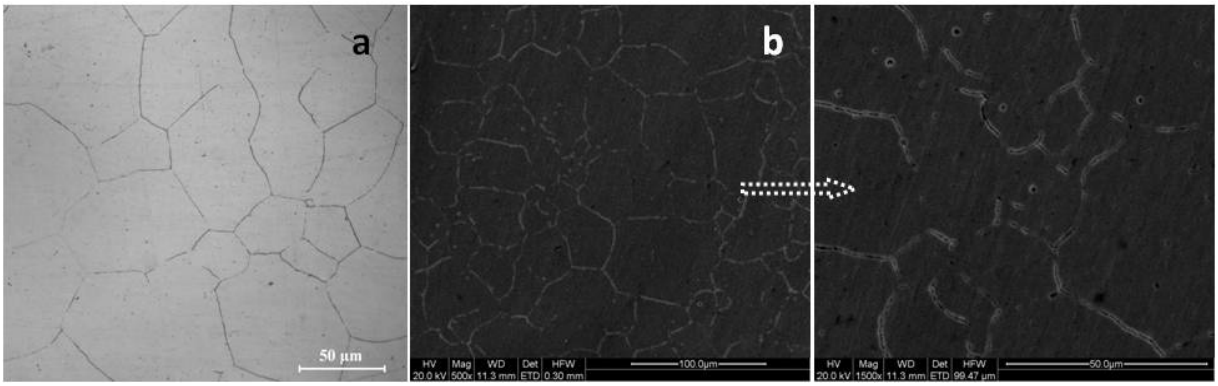

Fig.4.1 Optical (a) and Fe-SEM (b) micrographs showing the microstructure of the alloy substrate (310S)

4.1.2 Surface roughness of the alloy substrate

The polished surface of the specimen is very smooth and the surface roughness (R_a) was around 0.04 µm (Fig. 4.2).

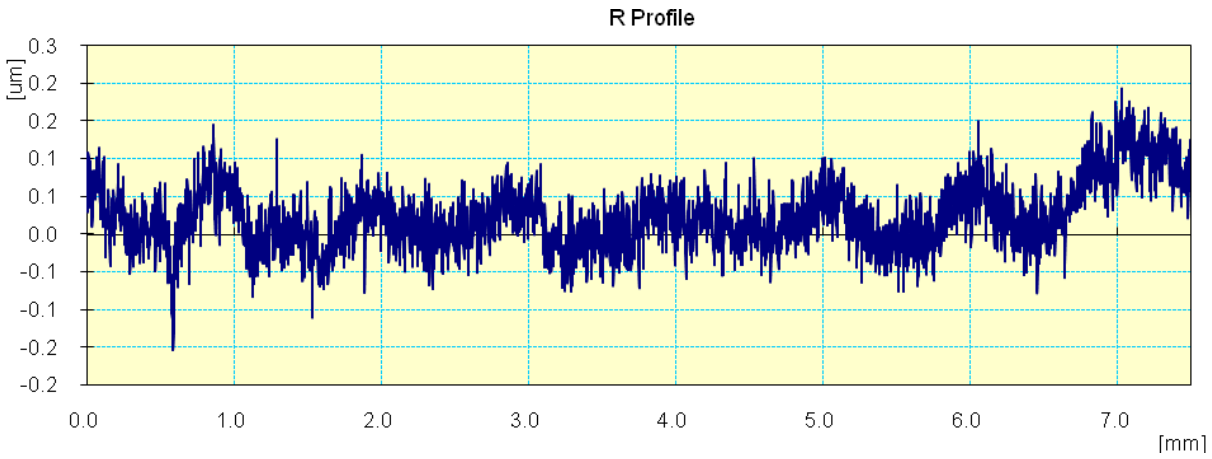

Fig 4.2: Roughness profile of the polished surface

4.2 CHARACTERIZATION OF THE COATING

4.2.1 Introduction

Among various thermal spray process, high velocity oxy fuel (HVOF) deposition is attractive to deposit Cr_3C_2-NiCr on steel because of its capability to render uniform and dense coatings with smooth surface, homogeneous microstructure, high harness and bonding strength (Kaur et al., 2009; Guilemany et al., 1994, 1996, 2001 and 2006, Wirojanupatump et al., 2001; Sidhu et al 2006B; Wang et al., 2002).

In the present work, HVOF sprayed Cr_3C_2-25%NiCr coatings deposited on 310S substrate for its high temperature applications have been characterized. Particularly, the microstructure, porosity, coating thickness, phase formation, microhardness of the deposited coatings have been characterized using FE-SEM/EDS, X-ray mapping, and XRD and Vickers indentation.

4.2.2 Experimental Details

The details of the substrate material, coating formulation and characterization of the coating are discussed in Chapter 3 (Experimental chapter) of the thesis.

4.2.3 Results

4.2.3.1 Coating powder

4.2.3.1.1 Morphology of the coating powder

A cermet powder of nominal composition Cr_3C_2-25%NiCr (TAFA 1375VM) with particle size -~50 µm was used. Figure 4.3 shows irregular morphology of powders. SEM images of powders further show

uniformly distributed grains of chrome carbide-rich ceramics, while the nickel chrome-rich binder phase attaches ceramic grains. Interconnecting networks of ceramic grains within each powder particle can also be observed in Fig, 4.3.

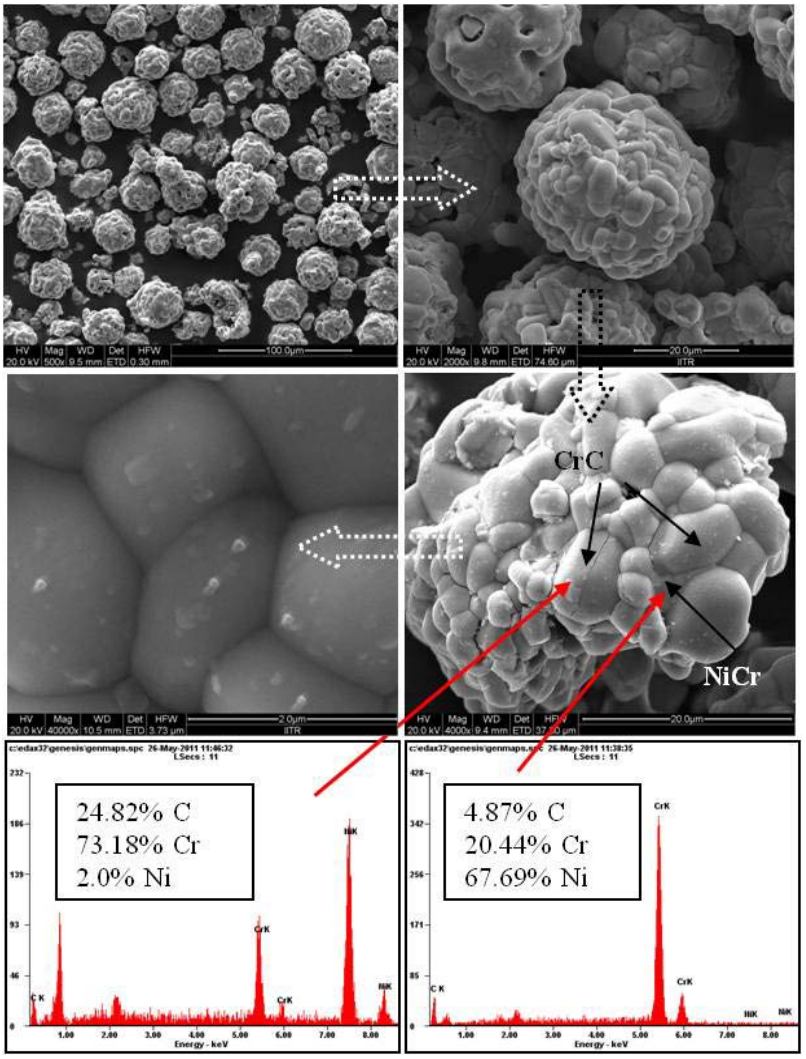

Fig 4.3: FE-SEM micrographs showing the morphology of Cr_3C_2–NiCr powder used for developing coatings.

4.2.3.2 Surface roughness and cross section of the coating

The surface of the as-sprayed coated specimen was rough and the average surface roughness (R_a) was around 7 µm (Fig. 4.4).

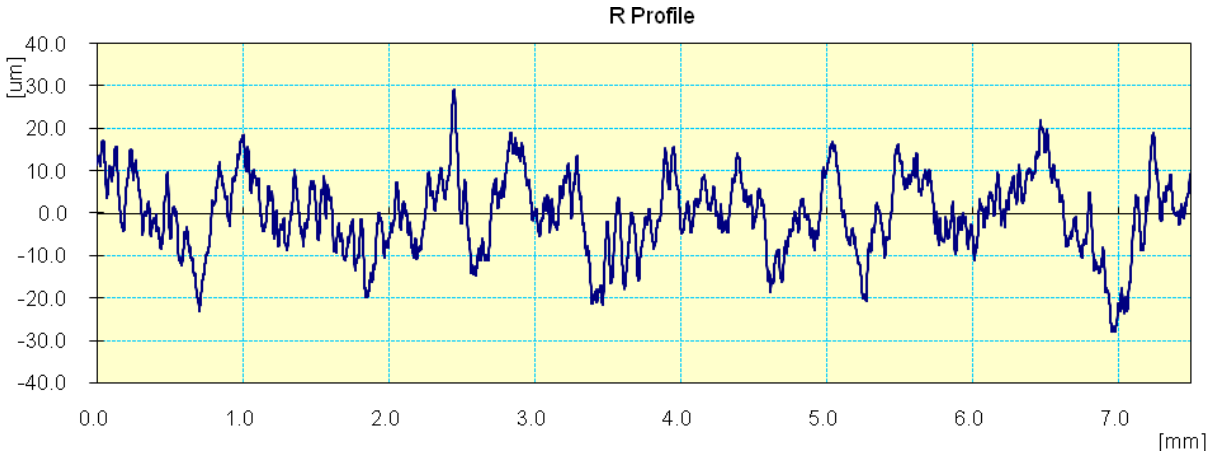

Fig 4.4: Surface roughness profile of the as-sprayed coating (Cr_3C_2–25%NiCr).

BSE image of cross-section of the mounted sample (Fig. 4.5a) shows dense, uniform and adherent splats like structure. There are no signatures of cracks or gaps at the coating-substrate interfaces. This indicates improved adhesion of the coatings on the substrate. The average thickness of Cr_3C_2–25%Nir coating is 265±19 µm approximately. .

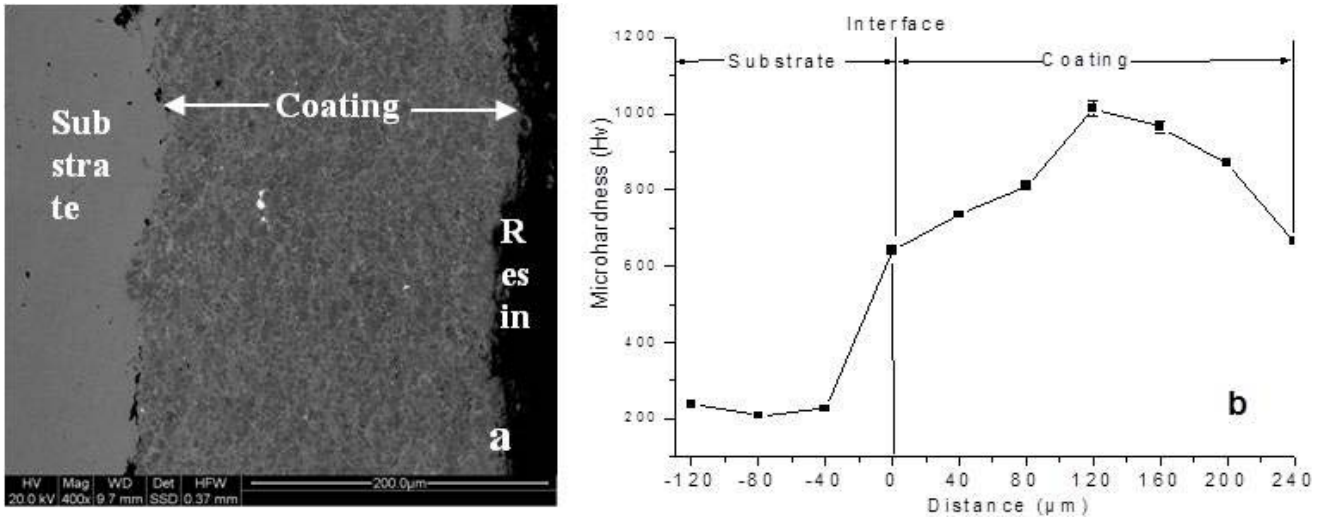

Fig 4.5: (a) Cross sectional micrograph of as-sprayed Cr_3C_2–25%NiCr coating, (b) Variation of microhardness across the cross section of the coating.

4.2.3.3 Porosity of the coating

The coating porosity significantly influences corrosion or high temperature oxidation as it provides selective pathway through which corrosion species tend to penetrate coating to the substrate. High kinetic energy of incident particles are expected to render coatings with few pores and voids in HVOF process. Porosity of the HVOF sprayed coatings is found to be less than 0.97%, which reveals that coating was very dense. The small amount of porosity is attributed to high kinetic energy of incident powder particles. Sidhu et al. (2006) and Guilemany et al. (2006) also reported similar kind of low porosity.

4.2.3.4 Bond strength of the coating

The bond strength of Cr_3C_2–25%NiCr coating was measured on three specimens as discussed in section 3.3.4. The coating failed at the substrate-coating interface while remaining bonded to the adhesive. Average bond strength of 10,000 Psi is observed for the Cr_3C_2–25%NiCr coating.

4.2.3.5 Microhardness of the coating

Microhardness of the Cr_3C_2-25%NiCr coatings was determined across the cross-sectioned samples and is shown in Fig.4.5b. The microhardness of the substrate was varied from 205 Hv to 240 Hv; but for the coatings, it is found to vary with the distance from the coating–substrate interface. The maximum microhardness of the coating is found to be 1014 Hv.

4.2.3.6 X-ray diffraction (XRD) analysis

The XRD analysis of the Cr_3C_2-25%NiCr powders and Cr_3C_2-25%NiCr coating (Fig 4.6) indicates that the powder mainly consisted of Cr_3C_2 and NiCr whereas Cr_3C_2, Cr_7C_3 and Cr were present as the main phase in the coating.

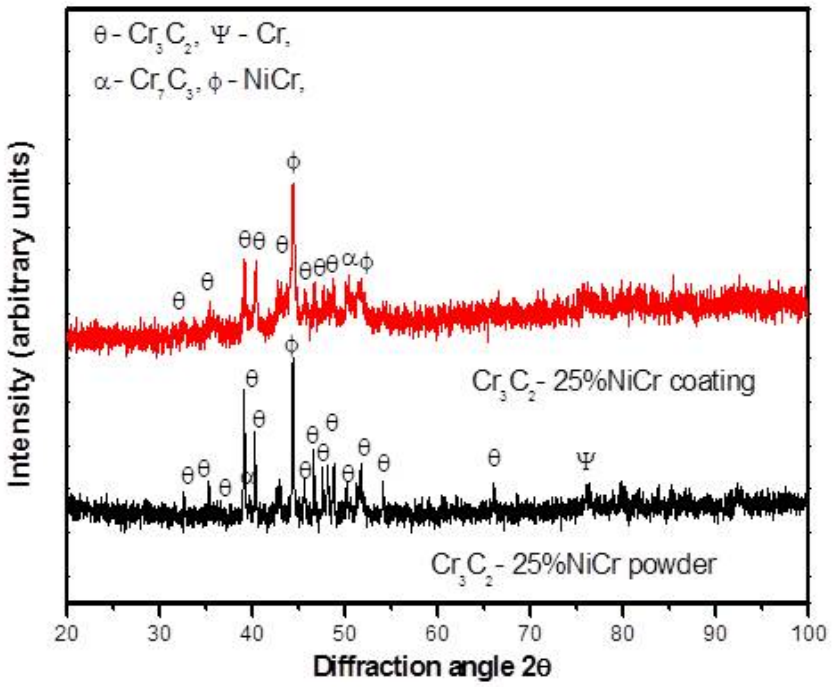

Fig 4.6: XRD patterns for Cr_3C_2–25%NiCr powder and as-sprayed coating

4.2.3.7 FE-SEM/EDS analysis of the coating

4.2.3.7.1 Surface morphology of the coating

FE-SEM micrographs showing the surface microstructures of the as sprayed coating are provided in Fig. 4.7 (a, b). The surfaces of coating show incompletely melted as well as few unmelted particles and free from cracks (Fig.4.7). The microstructures revealed that HVOF sprayed Cr_3C_2–25%NiCr coating consist of irregular shaped splats having low oxide content which are interconnected. The presence of oxides can be ascribed to in-flight oxidation occurred during spraying process. Accordingly, the EDS data showed the small amount of oxygen. The marginal presence of oxygen in the composition of coating indicates the chances of the formation of oxides in the coatings (Chatha et al., 2012). The white region is NiCr binder phase whereas dark grey region is carbides. The as-sprayed coating (Fig 4.7b) consisted of uniformly distributed chromium carbide-rich ceramic grains (Cr-75.25, C-19.98, Ni-2.25, O-2.22) attached with nickel chrome-rich binder phase (Ni-50.98, Cr-32.92, C-1.83, O-1.83). Fracture of particles of carbide is also observed in the HVOF coating, which occurs upon incidence of powder particles on the substrate under high velocities.

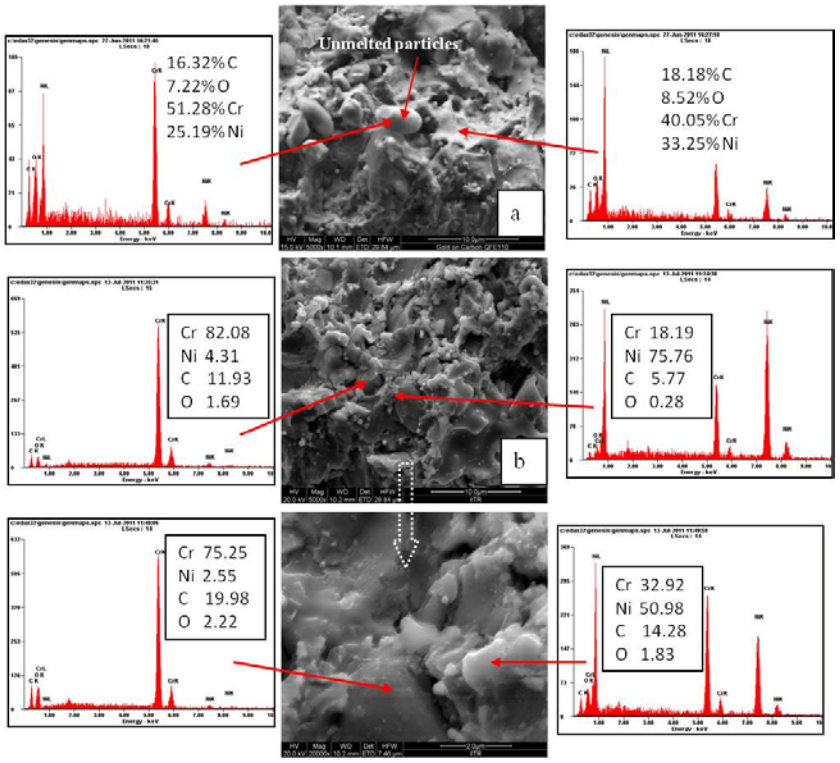

Fig 4.7: Micrograph showing the surface morphology and EDS analysis for the (a,b) as sprayed Cr_3C_2–NiCr coatings.

4.2.3.7.2 Cross-sectional analysis and X-ray mapping

The BSE images at the cross-section of HVOF sprayed Cr_3C_2–25%NiCr coating on 301S alloy substrate by FE-SEM/EDS and the results are shown in Fig. 4.8. Dense uniform and adherent splats like structure with some unmelted particles and pores can be noted. X-ray mapping of the coating was carried out at several points along the cross-section are shown in Fig. 4.8. It is clear that the large part of the deposit is covered with Cr_3C_2. X-ray mapping of the coating shows (Fig. 4.9) distribution of elements of powder and diffusion of small amount of Fe from the substrate.

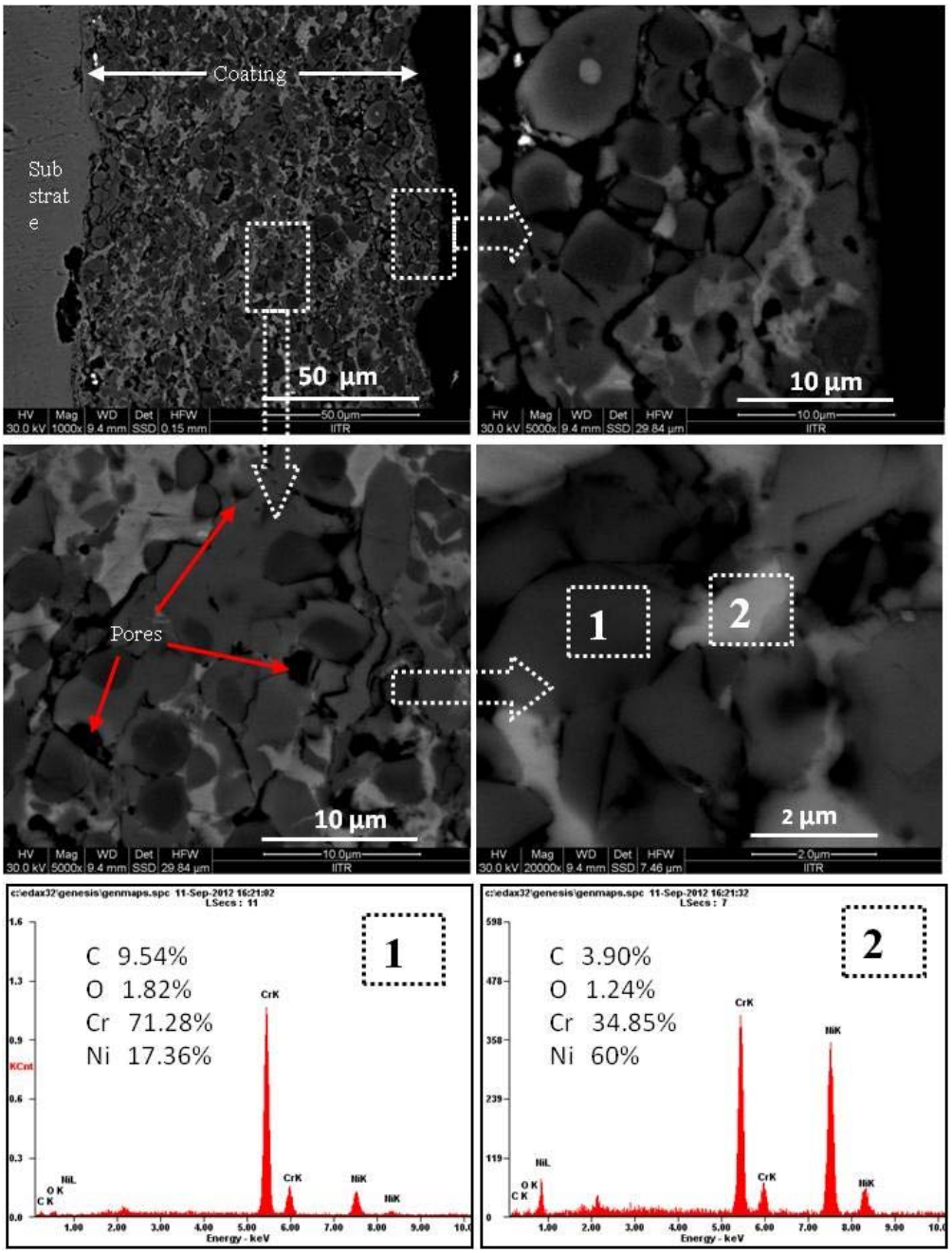

Fig 4.8: Cross sectional micrograph showing the morphology of the developed Cr_3C_2-NiCr coating,

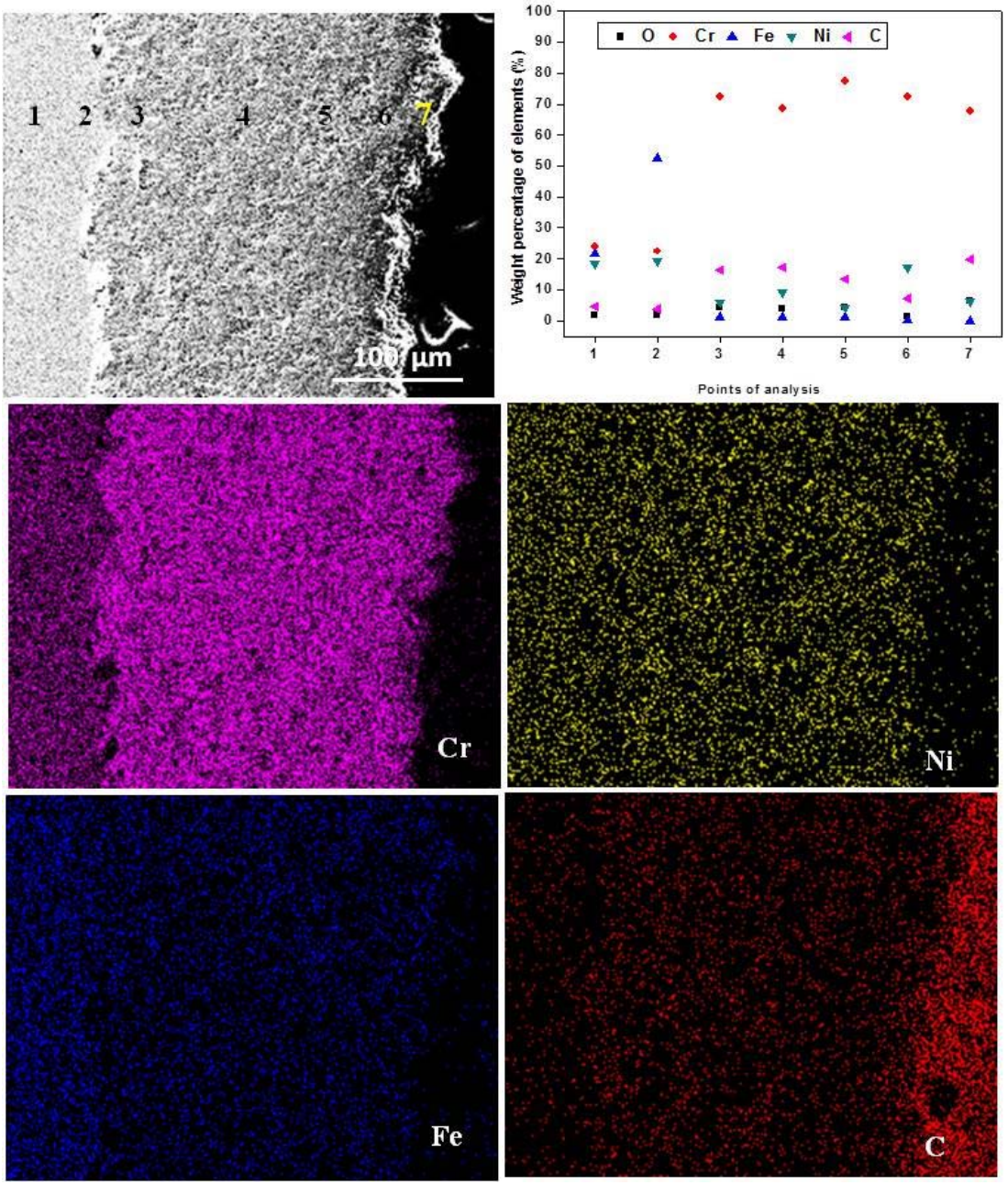

Fig.4.9 Fe-SEM/EDS analysis across the cross-section and x-ray mapping of as-sprayed Cr_3C_2–25%NiCr coating on 310S alloy substrate.

4.2.4 Discussion

The Cr_3C_2–25%NiCr coating appears uniform and cracks are not observed. The cross-sectional morphologies shown in Fig. 4.8 reveal that the coating exhibits uniform distribution of carbide particles and metallic binder phase. Limited porosity existed at the interface between flattened particles of melted carbide (Fig.4.8), which can be attributed to high impact velocity of the coating particles. Dense coatings are known to provide better corrosion resistance than the porous coatings. It is also known that pores form along the splat boundaries (Seo et al., 2007). The micropores in the coatings can lead to reactive corrosion (Choi et al., 2002) through which corrosion species penetrate coating and cause rapid corrosion attack. SEM images of as sprayed and polished surface morphology of as sprayed Cr_3C_2–25%NiCr coating are provided in Fig.4.7. The as sprayed surface is rough, dense, flat and free from cracks and shows the presence of partially melted particles. The microhardness of HVOF sprayed Cr_3C_2–25%NiCr coating has been found to be high when compared against that of the substrate (Fig.4.5b). Variation in microhardness the coating is probably due to the presence of porosity, un-melted and partially melted particles. The X-ray diffraction pattern of the coating powder shows Cr_3C_2 and NiCr as major phases, in accordance with the findings of (Kamal et al., 2009). The XRD pattern of as-sprayed Cr_3C_2-25%NiCr coating indicates that Cr_3C_2, Cr_7C_3 are produced by partial decomposition of the initial Cr_3C_2 phase during the HVOF spraying process. Similar findings of the presence of carbides phases in the microstructure of HVOF Sprayed coatings were reported by Mathews et al., 2003 & 2013 and Chatha et al. 2012.

4.2.5 Conclusions

HVOF process has been used to deposit Cr_3C_2-25%NiCr coating on 310S alloy substrate and the coating was characterized for their microstructural characteristics and hardness. The following are the major conclusions:

- The C_3C_2-25%NiCr coatings exhibit a dense structure with the 0.97% porosity.
- EDS analysis indicates no change in elemental composition between coating and initial powder is observed.
- The absence of cracks and gaps at the interface suggests good adhesion of the coatings with the substrate.
- The microhardness of the Cr_3C_2–25 NiCr coating varied from 775 HV to 1014 HV because of homogeneously dispersed high volume fraction of carbides.

4.3 OXIDATION STUDIES IN AIR

4.3.1 Introduction

Oxidation of metals or alloys takes place when they are heated in presence of corrosion species such as air or oxygen. An oxidation reaction is represented by the interaction of metals with oxygen to form oxides (Birks, 1983; Bittel, 1969). Iron based high chromium or nickel alloys and Cr_3C_2-NiCr cermets are preferred for fabricating corrosion and wear resistant coatings on steel components used in hot section of waste incineration boilers, electric furnaces and fossil fuel-fired boilers (Matthews et al., 2008, 2009 & 2013; Mohanty et al., 1996; Morimoto et al., 2006; Kaur et al., 2011, Barbooti et al., 1988, Erning et al., 1999; Eroglu et al., 1997, He et al., 2000 & 2002; Kamal et al., 2009, 2009A, 2009B). Among various approaches used to enhance corrosion resistance thereby improve the life of high temperature components in corrosive environments , the best and cost effective one is is to coat with thin wear and oxidation resistant coatings (Bluni et al., 1996, Grunling et al., 1992, Rahman et al., 2013).

While microstructural characteristics and oxidation behavior of HVOF sprayed Cr_3C_2-NiCr coatings is well reported, the degradation mechanisms of coating in high temperature environment as a function of very short exposure periods in air under cyclic condition is limited in the literature. In this context, the present study has been focused to understand the microstructural changes and degradation behavior of HVOF sprayed Cr_3C_2-25%NiCr coatings after exposure of 10 and 50 hours at 900^0C. Several analytical techniques such as FE-SEM/EDS, XRD and thermo gravimetric techniques, have been used.

4.3.2 Experimental details

The substrate material, coating formulation and the oxidation studies are explained in detail in section 3.1, 3.2.3 and 3.4.1.

4.3.3 Results

4.3.3.1 Weight change measurements

Figure 4.10 (a) shows the weight change for the coated and uncoated specimens oxidized at 700^oC in air up to 50 cycles. The uncoated specimen reached a steady state with long exposure time. During early oxidation period, the oxidation of free surface of both coated and bare substrate led to high rate of oxidation. The coated specimen exhibited relatively higher weight gain during initial period subjected to oxidation (first 15 cycles) as compared to the subsequent cycles up to 50. It can be attributed o the formation of protective oxide films, during the initial cycles, which stops further oxidation during the latter cycles. The weight gain per unit area after oxidation of uncoated specimen has shown a gradual increase with some spalling up to 50 cycles. The weight gain in the case of the oxidized coated specimen was lower than the uncoated specimen. Figure 10 (b) shows the square of weight gain per unit area (mg^2

/cm^4) versus number of oxidation cycles. It is clear that the trend in growth of oxide scale can be estimated to a parabolic relationship in case of Cr_3C_2–NiCr-coated substrate, whereas uncoated substrate also follow the parabolic rate law but with little deviation. The parabolic rate constants Kp values for the bare substrate and Cr_3C_2–NiCr-coated alloy substrate after 50 cycles at 700^{o}C were 15 x 10^{-12} $g^2cm^{-4}s^{-1}$ and 8.4 x 10^{-12} $g^2cm^{-4}s^{-1}$, respectively. The Kp value is lower for the coated specimen as compared to that of uncoated specimen, which indicates that coating shows better oxidation resistance.

Figure 4.10 (c) shows the weight change for the coated and uncoated specimens oxidized at 900^{o}C in air up to 50 cycles. The coated specimen has undergone lesser overall weight gain when compared against uncoated counterparts. The steady state reached after a high rate of increase in weight during the initial 10 cycles; whereas gradual increase in weight gain with some spalling up to 50th observed for uncoated specimen,. The square of weight gain per unit area (mg^2 /cm^4) for coated and uncoated specimens is provided in Fig. 10(d). The trend in oxide growth can be estimated to parabolic relationship in both the uncoated as well as Cr_3C_2–NiCr-coated substrates. The parabolic rate constants K_p values for the bare substrate and Cr_3C_2–NiCr-coated alloy substrate were 41.3 x 10^{-12} $g^2cm^{-4}s^{-1}$ and 13 x 10^{-12} $g^2cm^{-4}s^{-1}$, respectively. The K_p value for the coated specimen was found to be one-third of the K_p value of the uncoated specimen, which indicates that coating shows a improved oxidation resistance.

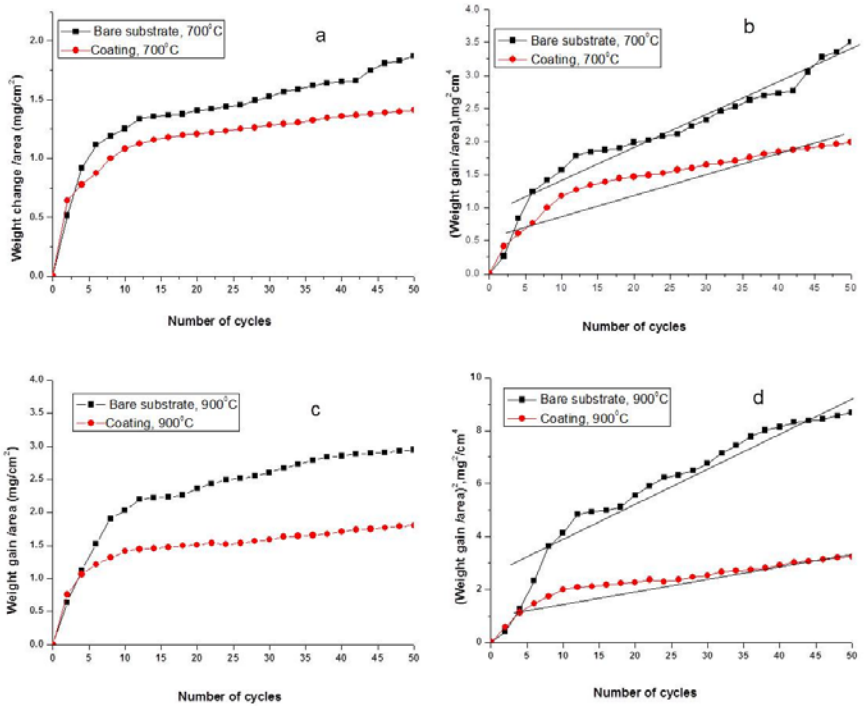

Fig 4.10: (a,c) Weight gain after oxidation per unit area versus number of cycles and (b,d) Weight gain after oxidation per unit area)^2 Vs number of cycles, at 700 & 900^{0}C in air.

4.3.2.2 FE-SEM/EDS analysis

4.3.2.2.1 Surface morphology of the scales

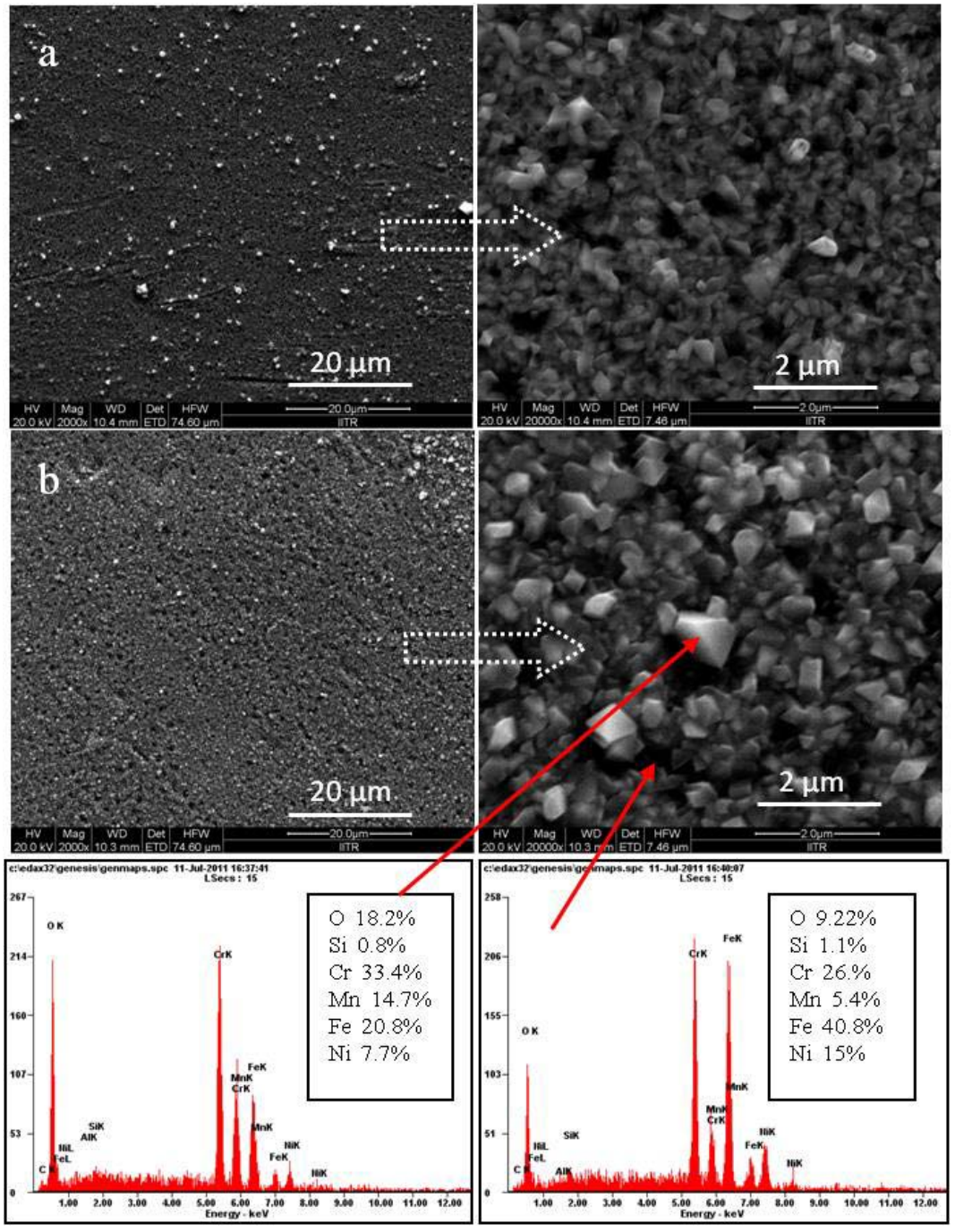

Fig 4.11: Surface morphology of bare substrate after (a) 10 h, and (b) 50 h oxidation cycles at 700^0C.

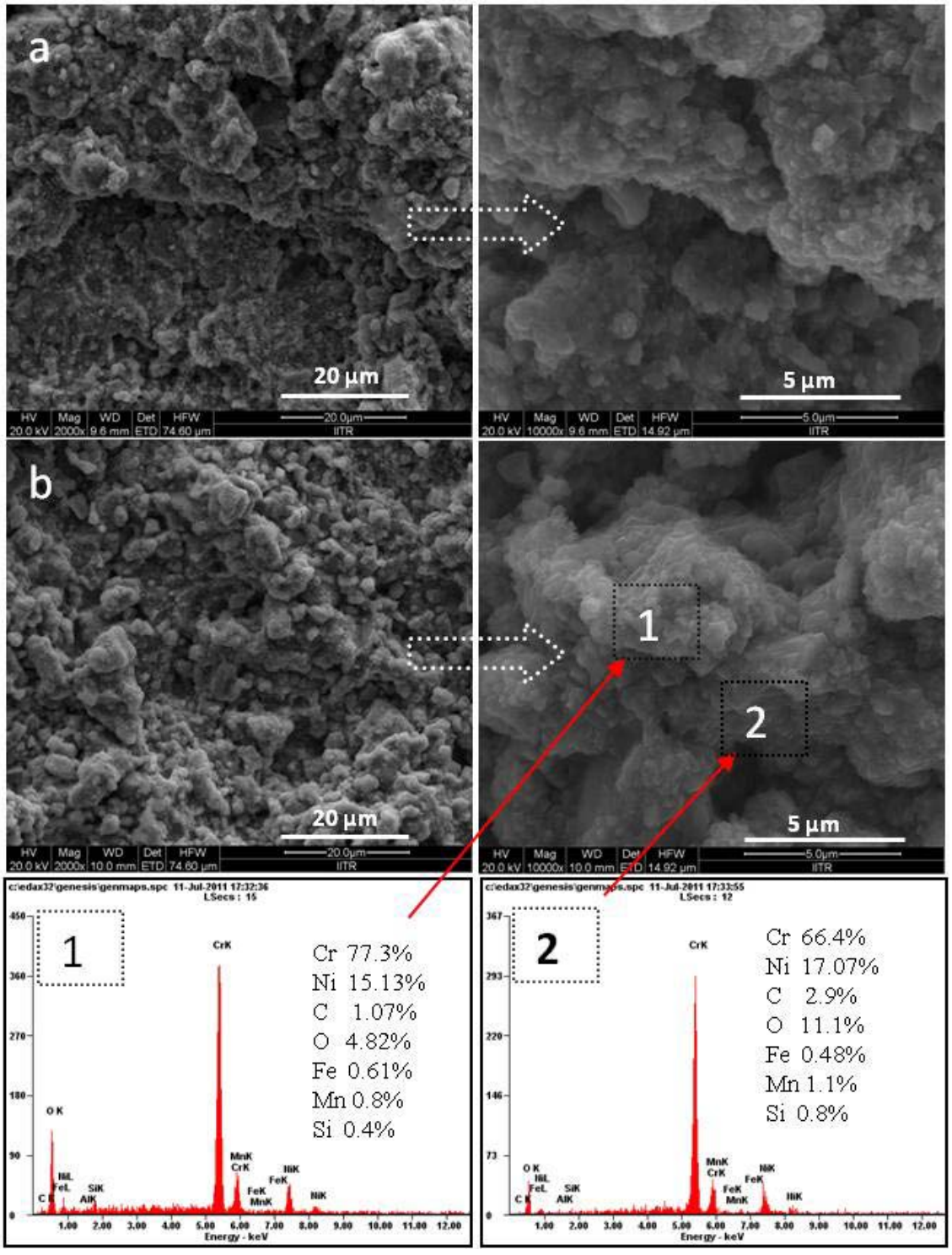

Fig 4.12: Surface morphology of coated specimen after (a) 10 hours, and (b) 50 hours oxidation cycles at 700^0C.

FE-SEM/EDS images of the surface morphology of the uncoated and coated specimens oxidised in air for 10, and 50 cycles at 700^0C under cyclic conditions are shown in Fig. 4.11 and Fig 4.12, respectively. The scale formed on the bare substrate was rich with oxides of chromium and iron. Minor amount of Mn, Si, Ni has also been detected in the oxide scale. Micrograph of the oxidized coated specimen appears to be dense, consisting of spongy nodules. The surface scale mainly consisted of oxides of chromium and nickel. The observation of small amounts of Fe, Si, Mn suggests their diffusion from the substrate to the coating. The increase in concentration of Cr_2O_3 in the oxide scale of the coatings occurs with progress of the oxidation at high temperature, 700^0C.

Surfaces of bare and coated specimens after oxidization at 900^0C for 10, and 50 cycles are shown in Fig. 4.13 and 4.14, respectively. FE-SEM analysis of the uncoated surface indicates loosely bound oxide particles after 10 cycles of oxidation, while thick layers of oxides are found after oxidation at 50 cycles. EDS analysis indicates the major presence of Cr, O, Fe along with minor presence of C, Mn, Ni, and Si (see Fig. 4.13a). The cracks observed after oxidation for 50 cycles indicate spalling of the oxide scales. The presence of Fe_2O_3 in spalled scale has been reported to be non-protective by Sidhu et al., 2007 and Kaur et al., 2009 during high temperature oxidation of Superfer 800H (Fe-based superalloy) and boiler steel. The surface of the oxidized coated specimen appears as consisting of spongy nodules after oxidation for 10 cycles (Fig 4.14a). EDS analysis of nodules indicates Cr, O, C, Ni. Minor amount of Fe, Si, and Mn have also been detected in the oxide scale, which reveals inter diffusion of alloying elements from the substrate into the coating after 10 cycles. These results of inter diffusion of alloying elements to the coating are in good agreement with the findings of Kaur et al., 2009. With increase in number of cycles to 50 (Fig 4.14b), oxidized surface also shows platelets. EDS analysis suggests that these platelets are mainly oxides of chromium. Further, the EDS analysis of the nodules shows the major presence of Cr, O and Ni.

It may be mentioned that the formation of protective scale during the initial cycle of 10 cycles over the coated specimens as observed in the present work were not reported earlier. The thickness of protective scale has increased up to 50 cycles. No spallation of protective scales on the coated specimens was observed under thermal cyclic conditions. On the other hand, the oxide scale formed on the bare substrate is not adherent and it peeled-off under thermal cyclic conditions (Fig. 4.13b).

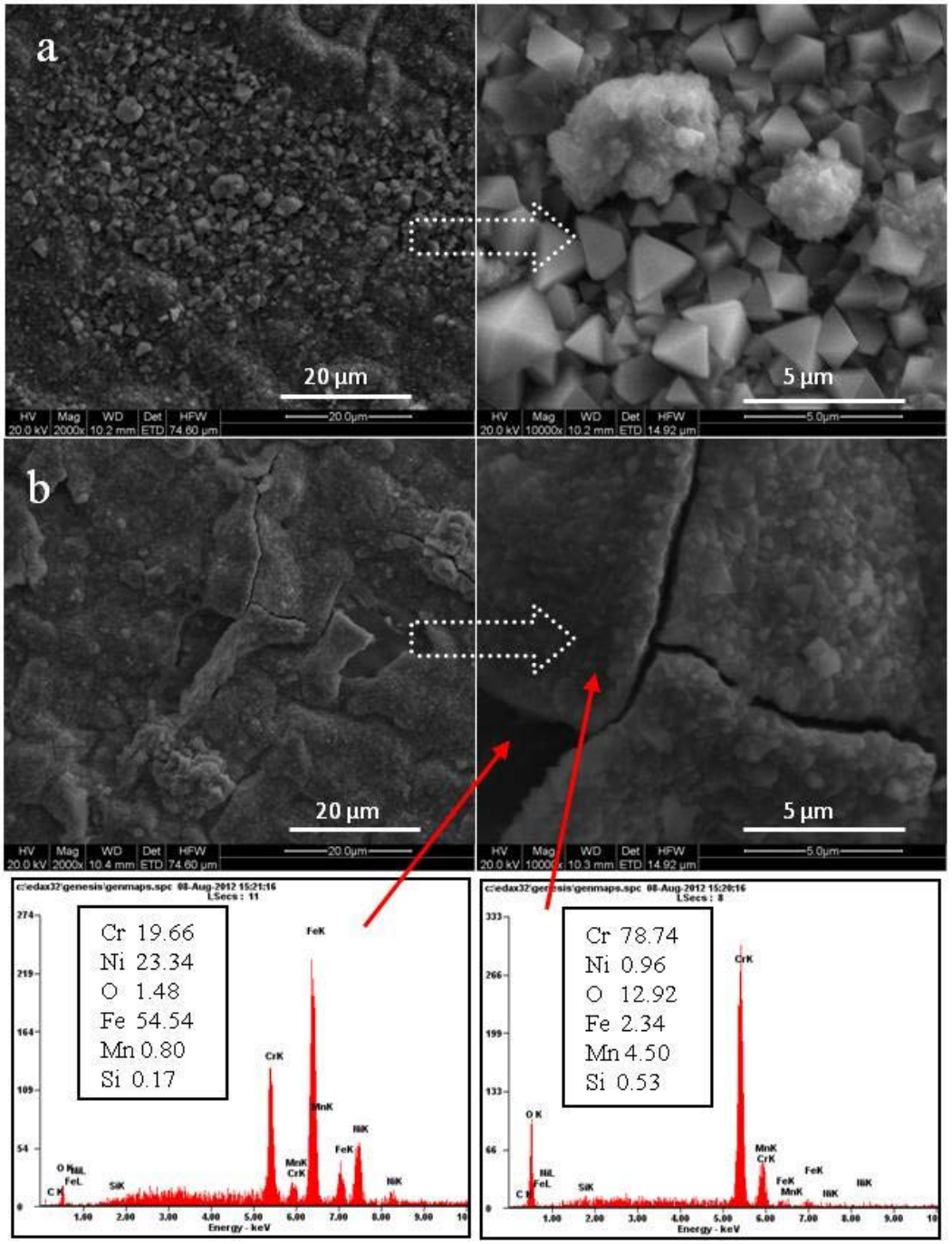

Fig 4.13: Surface morphology of bare substrate after (a) 10 h, and (b) 50 h oxidation cycles at 900^0C in air.

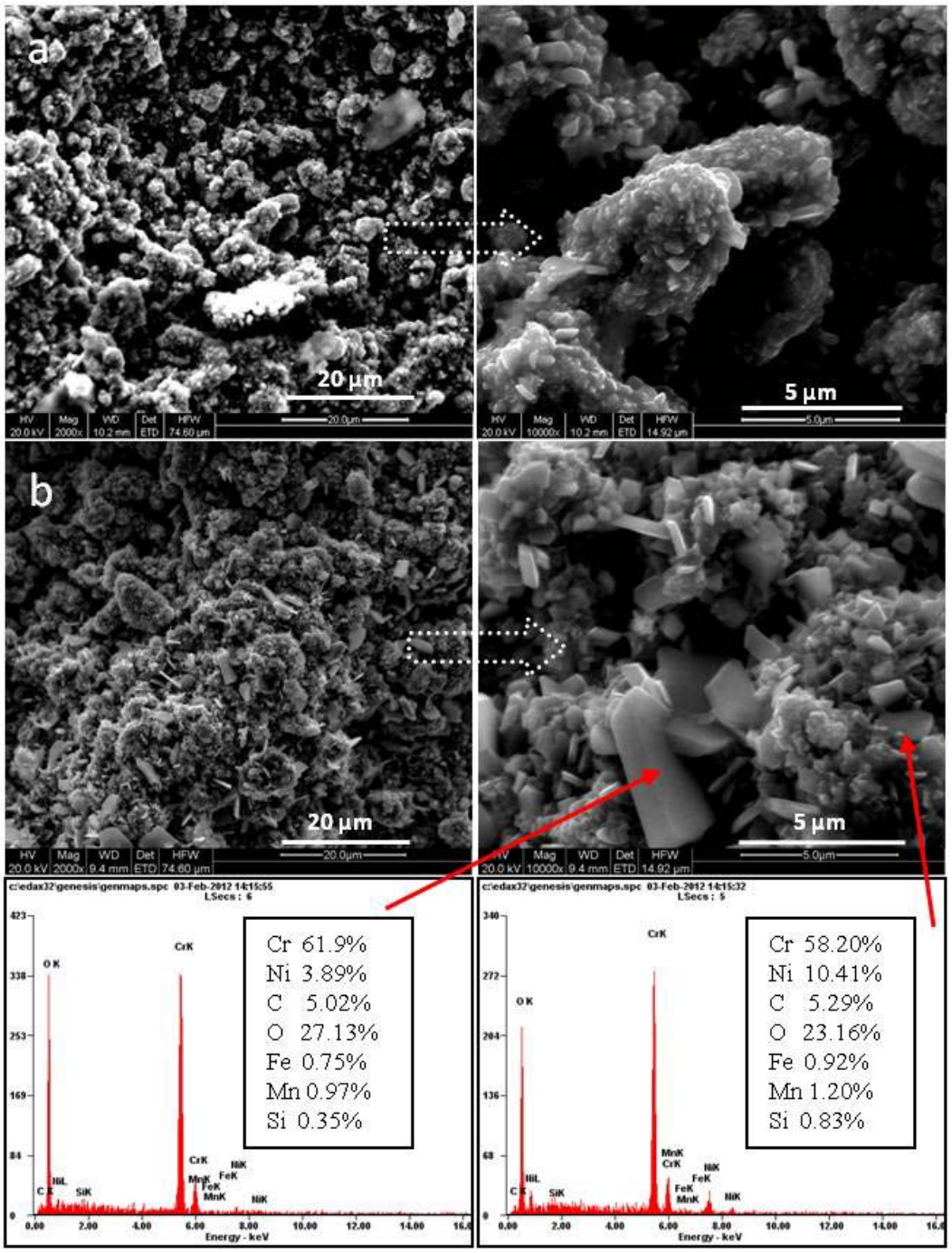

Fig 4.14: Surface morphology of coated specimen after (a) 10 h, and (b) 50 h oxidation cycles at 900^0C.

4.3.2.2.1 Cross-sectional analysis and X-ray mapping of the scale

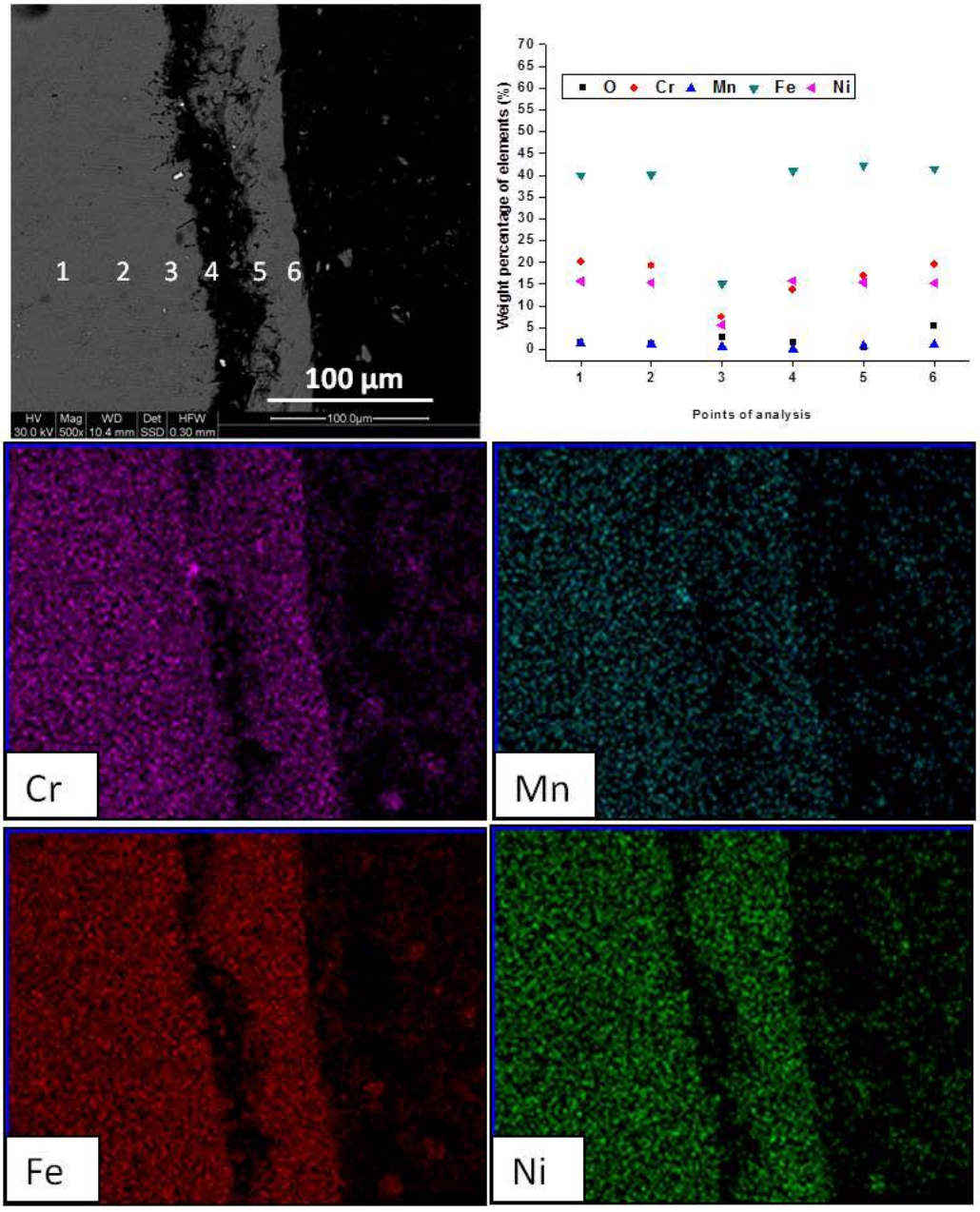

Fig.4.15 Fe-SEM/EDS analysis across the cross-section and X-ray mapping of the alloy substrate subjected to cyclic oxidation at 900 ^{o} C in air after 50 cycles.

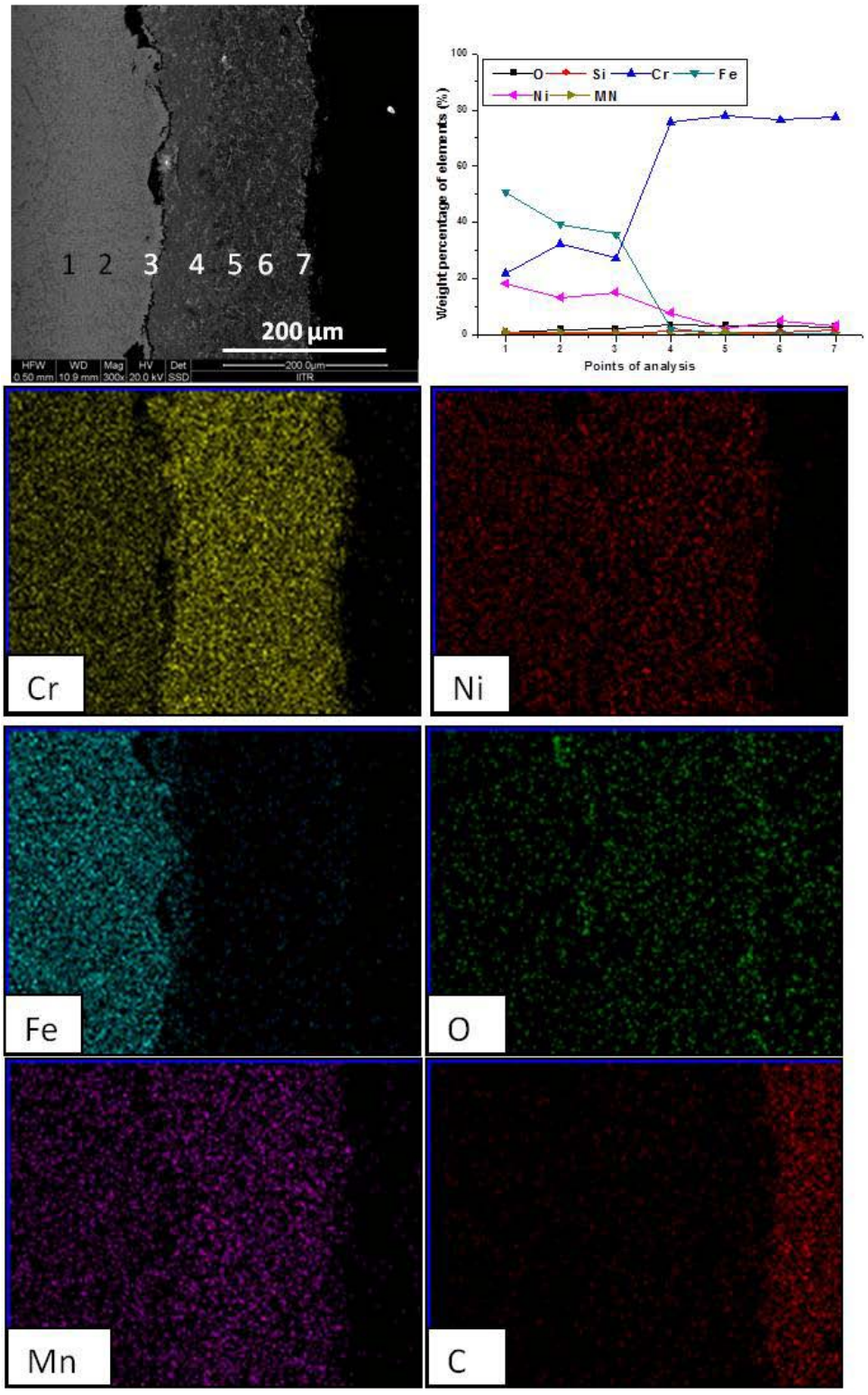

Fig.4.16 Fe-SEM/EDS analysis across the cross-section and x-ray mapping of Cr_3C_2–25%NiCr coating subjected to cyclic oxidation at 900 ^{o} C in air after 50 cycles.

FE-SEM analysis of the oxide scale carried out at several points along the cross section of oxidized uncoated and HVOF-sprayed coated specimens subjected to 50 cycles of oxidation at 900^{o}C in air is shown in Fig.4.15 & 4.16. The scale on the surface of uncoated specimen is light in appearance, porous and fragile, as shown in Fig. 4.15. The scale of the coated specimen is found to be continuous, dense, and adherent (Fig. 4.16). Chatha et al. reported the presence of cracks in the HVOF sprayed Cr_3C_2-NiCr coatings after high temperature oxidation studies (Chatha et al., 2012). EDS analysis of the scale of the bare specimen shows the presence of O, Fe, Cr, Mn and Si, while that of coated specimen scale indicates the presence of Cr, Ni, O, Mn, Si and Fe. X-ray mapping of different elements of the cross section of the coated specimen subjected to 50 cycles of oxidation in air at 900^{o}C (see Figure 4.16) also reveals the presence of O, Cr, Mn, Ni, Si and Fe throughout the coating. The presence of Fe, Mn and Si on top surface of the coating is probably due to their diffusion in to the coating through substrate-coating interface.

4.3.2.3 X-ray diffraction analysis (XRD) analysis

XRD patterns of the scale formed on bare and coated specimens during cyclic oxidation are shown in Fig. 4.17 and 4.18, respectively. Various phases identified from the X-ray diffraction (XRD) patterns of the oxidized bare specimen in air at 700^{o} C after 50 cycles are shown in Fig 4.17. Austenite phase was observed as the major phases, while Cr_2O_3 and Fe_2O_3 were also present in the oxide scale. XRD diffractograms for the coated specimen after 50 cycles of exposure to air at 700^{o}C revealed the formation of Cr_2O_3 and Cr_3C_2 as very strong phases, NiCr, Cr_7C_3, NiC and $Cr_{23}C_6$ as low intensity phases (Kaur et al., 2008; Kamal et al., 2009). The major and minor phases identified from XRD analysis of bare and Cr_3C_2–NiCr-coated specimens during cyclic oxidation in air at 900^{o}C after 50 cycles are shown in Fig. 4.18 respectively. XRD analysis of uncoated surfaces indicates the presence of Cr_2O_3, Fe_3O_4 and austenite phase as major phase, whereas $(Cr,Mn,Fe)_3O_4$ as minor phase. Similar finding has been reported by Hsu et al., 2000. XRD analysis of coated surfaces after oxidation for 50 hour indicates the presence of Cr_2O_3, Cr_3C_2, $NiCr_2O_4$ as major phases and NiCr, Cr_7C_3 and $Cr_{23}C_6$ as minor phases. The austenite and oxides of Fe are absent at any stage of the oxidation. Kaur et al., 2009 reported Cr_2O_3 and Cr_7C_3 as very strong phases but $NiCr_2O_4$ phase is absent after oxidation of the Cr_3C_2-NiCr coating at 700^{0}C for 50 cycles. Kamal et al., reported Fe_2O_3 as a result of diffusion of Fe from Ni-based superalloy substrate into the detonation-gun-sprayed Cr_3C_2-NiCr coating after oxidation at 900^{0}C for 100 cycles (Kamal et al. 2009). The formation of nickel chromium oxide or chromium oxide-rich scale in the present study probably acted as obstacle to the internal diffusion of oxygen into the coating.

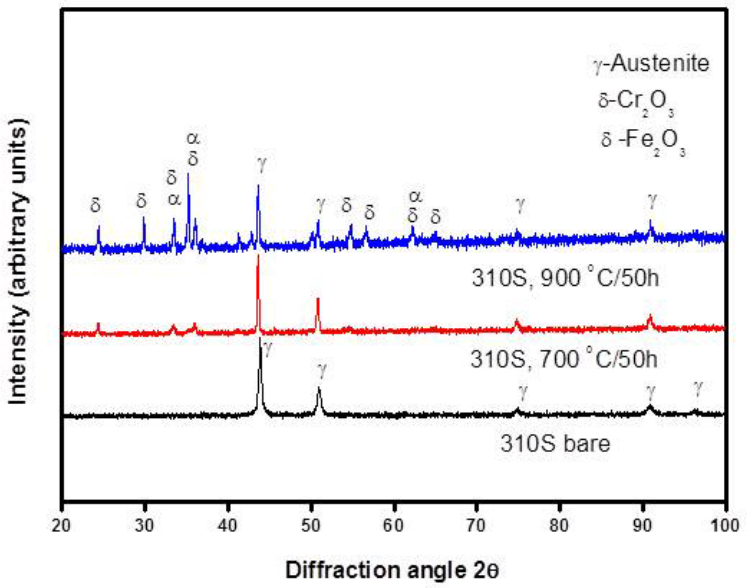

Fig 4.17: The XRD patterns of the scale formed on bare substrate after cyclic oxidation of 50 cycles in air at 700^0 C and 900^0 C.

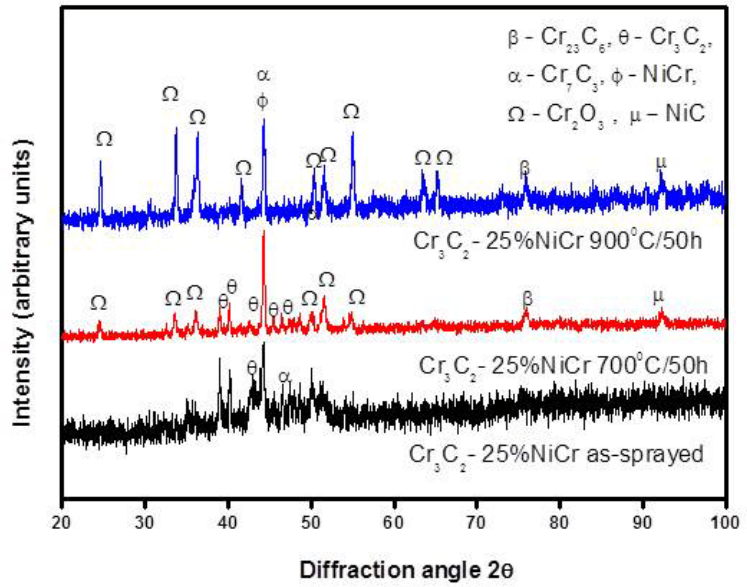

Fig 4.18: The XRD patterns of the scale formed on coated specimen after cyclic oxidation of 50 cycles in air at 700^0 C and 900^0 C.

4.3.4 Discussion

Although high temperature oxidation behavior of Cr_3C_2-NiCr coatings deposited on different substrates are well studied, the formation of different phases, interdiffusivity of alloying elements, and protective nature of scales formed under shorter exposure periods to high temperature environment (700 ^oC & 900^oC) are completely different as evident from the XRD, SEM/EDS, and X-ray mapping results obtained in the present work.

Figure 4.8 shows the cross section morphology of the Cr_3C_2-NiCr coating on 310S alloy substrate and shows characteristic splat like, layered morphology because of the deposition and solidification of molten droplets. The microhardness profiles of the Cr_3C_2-NiCr coatings on 310S alloy substrate change with the distance from coating-substrate interface. They ranged from 740 to 1014 Hv (4.5b). The hardness change was due to the formation of oxides.

HVOF sprayed coating in high temperature environment depends on various factors like porosity, oxides, splat size, splat shape, inclusions etc. The elevated temperature cyclic oxidation behavior of Cr_3C_2-NiCr coated specimens follows a parabolic trend as observed in Fig 4.10. The parabolic kinetic behavior is because of the diffused mechanism operating at high temperature under cyclic condition.

The divergence from the parabolic behavior of cyclic oxidation is due to the development and fast growth of oxides (Choi et al., 2002). The accelerated weight gain of the coated specimens was noted only during initial cycles. This can be probably due to the rapid development of oxides along the coating-splat boundaries and penetration of oxidizing species along the splat boundaries/open pores. However, weight gain was minimized subsequently due to densification and obstructed movement of oxidizing species to the inner portion of the coating.

The high temperature performance of Cr_3C_2–NiCr coating in air depends on the formation of a protective oxide scale. This oxide scale forms a solid diffusion barrier that precludes further interaction of oxygen with the beneath coating. Since the coating is in direct contact with oxygen, the reaction rate is initially rapid. When the coating is exposed to high temperature, the scale grows and becomes continuous resulting in increasingly difficult diffusion of corrosion species. Experimental results from the present study confirm that Cr_3C_2–NiCr coating possesses good oxidation resistance at high temperature and can be preferred for components to use in high temperature oxidative environments.

It evident from the XRD results of the oxidized coated surfaces that Cr_2O_3, Cr_3C_2, $NiCr_2O_4$ as major phases and NiCr, Cr_7C_3 and $Cr_{23}C_6$ as minor phases (Fig. 4.18). The presence of these phases is further supported by EDS and X-ray mapping analysis (Fig. 4.16).The formation of protective oxide layers such as Cr_2O_3 and spinel of nickel and chromium is responsible for imparting resistance against

high temperature oxidation. The possible oxidation mode of the Cr_3C_2-NiCr coated specimen at 900^0C after 50 cycles is shown in schematically in Fig. 4.19

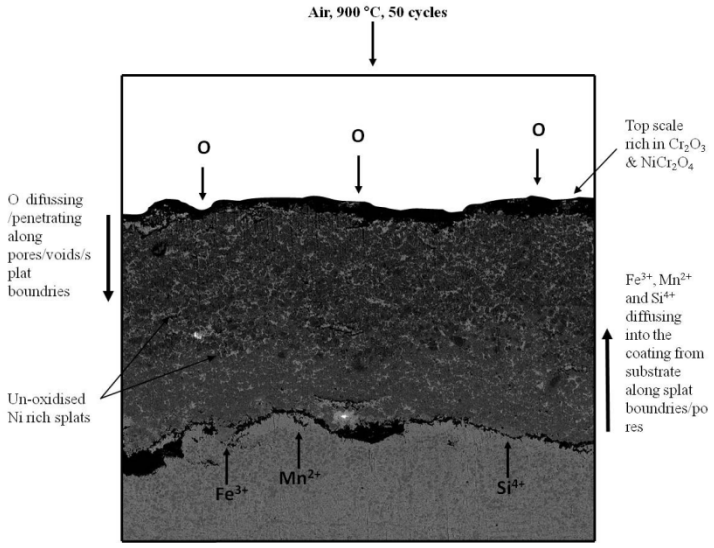

Fig 4.19: Schematic of the proposed oxidation mechanism of Cr_3C_2–25%NiCr coated 310S alloy substrate at 900^0 C in air after 50 cycles.

4.3.5 Conclusions

- The parabolic rate constant value, during oxidation, was found to be one-half (at 700^0C) and one-third (at 900^0C) for the coated specimen as compared to that of uncoated specimen, which indicates that coating shows better oxidation resistance.
- The splat and globular morphology of the as deposited coatings provides relatively high density to the coatings, which is essential for achieving resistance to oxidation.
- The formation of protective oxide layers such as Cr_2O_3 and spinel of nickel and chromium is responsible for imparting resistance against high temperature oxidation on the coated specimen.
- The diffusion controlled reaction upon formation of Ni spinels and Cr_2O_3 films on the coatings surface limits the diffusion of aggressive species such as air and other impurities in to the coatings.
- The oxidation behavior of coated samples was found to obey parabolic rate law.

4.4 HOT CORROSION STUDIES IN MOLTEN SALT ENVIRONMENTS

4.4.1 Introduction

Degradation of metals costs the United States more than the cost of annual floods and fires according to recent estimates (Priyantha et al., 2003; T. S. Sidhu et al., 2006). Hot corrosion is a serious problem in gas turbines, steam turbine, steam boilers, power generation industry, fossil fuel-fired boilers, and industrial waste incinerators, which results in degradation of the materials at vary fast rate, leading eventually to their catastrophic failures (Bornstein et al., 1969, 1970 & 1975; Sidhu et al., 2006F; Smith et al., 1999; Sidky et al., 1987, Seal et al., 1994, Scrivani et al., 2001 Castello et al., 2000; Chattopadhyay et al., 1970; Kofstad et al., 1990; Levy et al., 1989 & 1993**;** Lin et al 1984; Lindgren et al., 1987; Natesan et al., 1985). Vanadium, sulphur, and sodium are present as impurities in the residual fuels. In the combustion system, sodium, vanadium and sulphur present in the fuel react with each other and form molten sulphate-vanadate deposits as well as complex vanadates, which are extremely corrosive to the components used in hot section of combustion system (Kamal et al., 2009B; Sidhu et al., 2004; Luthra et al., 1980, 1982 &1985, Shi et al., 1993 & 1993A)Thermally sprayed Cr_3C_2–NiCr cermets are extensively used to mitigate corrosion and wear in high temperature application such as gas turbines, steam turbine, steam boilers, power generation industry, aerospace industry, oil-refining industry, heat treatment rolls, heat exchangers and piping in chemical industry and fossil fuel-fired boilers, where WC based composites are not suitable (Matthews et al., 2003, Wang et al., 1996).

The most common cermet coatings are WC-CO, WC-COCr, and Cr_3C_2-NiCr,which are deposited by detonation gun process, plasma spray process, and High velocity oxy-fuel process. Among all these thermal spray processes, HVOF is one of the most promising methods due to its very high deposition rate, strong adhesion to substrates, high cohesive strength, high hardness with a high volume fraction of carbide being preserved during the spraying due to its moderate process temperature and high gas velocity (Chatha et al., 2012).

The influence of microstructural features on the high temperature degradation behavior of HVOF sprayed Cr_3C_2-NiCr coatings and the governing mechanisms of coatings degrading under short exposure periods (10 cycles, 50 cycles) by an accelerated testing is scarce in the literature. The reaction kinetics and microstructural evolution of the oxide scales morphology, during high temperature degradation, are vital for evaluating performance of the materials in high temperature applications. Therefore, the present work has been focused to study the microstructural changes and high temperature degradation behavior of high velocity oxy-fuel (HVOF) sprayed Cr_3C_2-25%NiCr coatings. The coated as well as uncoated

specimens were exposed to molten salt (Na_2SO_4-60%V_2O_5 & Na_2SO_4-82% $Fe_2(SO_4)_3$) environment at 700^{o}C & 900^{o}C under cyclic conditions.

FE-SEM/EDS, XRD were used to characterize the corroded coated and uncoated samples. Thermogravimetric technique was used to study the kinetics of degradation. The variation in microstructure observed for the coated and uncoated samples upon high temperature degradation was used to establish the governing mechanisms for the failure of coatings.

4.4.2 Experimental details

Details about substrate material, coating formulation and the oxidation studies are provided in sections 3.1, 3.2.3 and 3.4.1.

4.4.3 Results

4.4.3.1 Weight change measurements

Figure 4.20 (a) shows weight change (mg/cm^2) for the coated as well as uncoated specimen during cyclic oxidation in Na_2SO_4-V_2O_5 up to 50 cycles at 700 ^{0}C. In case of uncoated specimen, a steady state in oxidation rates occurred with longer exposure time. Few fluctuations are also observed. The oxide scales is loosely bound fragile and porous. The oxide scale on the coated substrate was blackish grey in colour after 50 cycles of oxidation. It is apparent that spallation was absent with the scale being adherent. Initially, oxidation rate was high due to the oxidation of free surface of both coated and uncoated substrate. It can also be observed that the slope of the weight gain versus number of cycles plot is higher for the coated specimen during first 20 cycles, thereafter slope does not change much up to 50 cycles. It can be attributed to the protective oxide film formation during the initial cycles, which precludes further oxidation in the latter cycles. Weight gain per unit area after oxidation for uncoated specimen has shown a gradual increase with some spalling up to 50 cycles.

The diffusion pathways are decreased due to increased size of oxide grains resulting in a slow oxidation rate. Thus, the oxidized coated specimen has lower in weight gain than the uncoated specimen. In Figure 4.20(a), the weight gain/unit area were plotted to determine the conformance with the parabolic rate law. The square of weight change (mg^2 /cm^4) versus number of cycles shows a parabolic relationship for Cr_3C_2–NiCr-coated 310S alloy substrate, whereas uncoated substrate deviated from the parabolic rate law (see Fig. 4.20 (b)). The parabolic rate constants K_p values for the bare substrate and Cr_3C_2–NiCr-coated alloy substrate after 50 cycles of high temperature oxidation were calculated from the slope of linear regression fitted line, and found to be 18.3x 10^{-11} $g^2cm^{-4}s^{-1}$ and 10.2x 10^{-11} $g^2cm^{-4}s^{-1}$, respectively. The K_p value for the bare substrate was found to be nearly twice of the K_p value of the coated specimen, which indicates that coating shows a better hot corrosion resistance.

Weight change plots for the bare alloy substrate as well as the Cr_3C_2–25%NiCr coated specimen subjected to molten salt (Na_2SO_4-60% V_2O_5) environment at 900^0C for 50 hours are shown in Fig. 4.20(c). 310S bare alloy substrate exhibit higher weight gain as compared to Cr_3C_2–25%NiCr coated specimens. In Fig. 4.20(d), the square of weight gain per unit area (mg^2 /cm^4) versus number of cycles for bare and coated specimens is plotted. The parabolic rate constants K_p values for the bare substrate and Cr_3C_2–NiCr-coated alloy substrate after 50 cycles of high temperature oxidation were calculated from the slope of linear regression fitted the line, and found to be 55x 10^{-11} $g^2cm^{-4}s^{-1}$ and 33.8 x 10^{-11} $g^2cm^{-4}s^{-1}$, respectively. The K_p value for the bare substrate was found to be nearly twice of the K_p value of the coated specimen, which indicates that coating shows a better hot corrosion resistance.

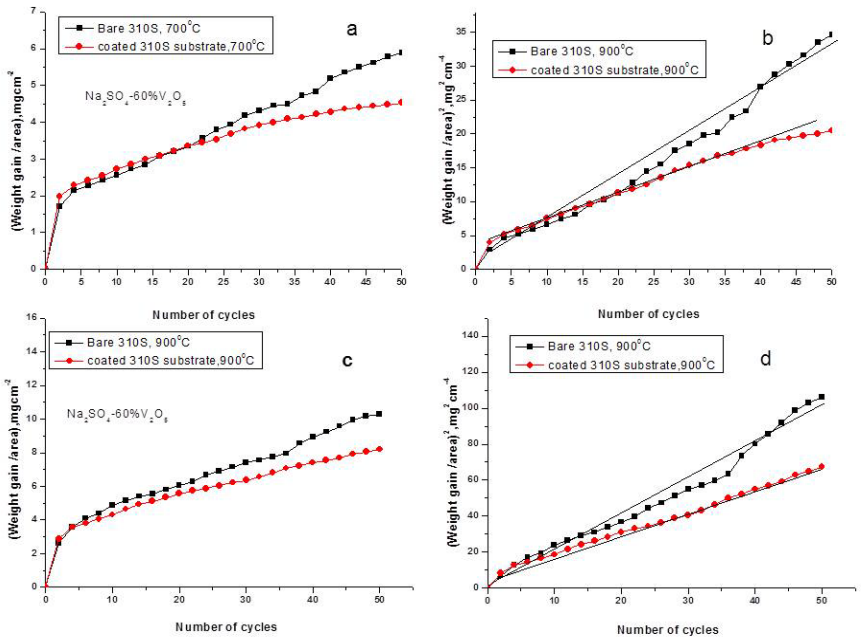

Fig 4.20: (a,c) Weight gain after oxidation per unit area Vs number of cycles and (b,d) Weight gain after oxidation per unit area)^2 Vs number of cycles, for the bare and coated specimens subjected to hot corrosion in molten salt (Na_2SO_4-60% V_2O_5) environment at 700^0C & 900^0C for 50 cycles.

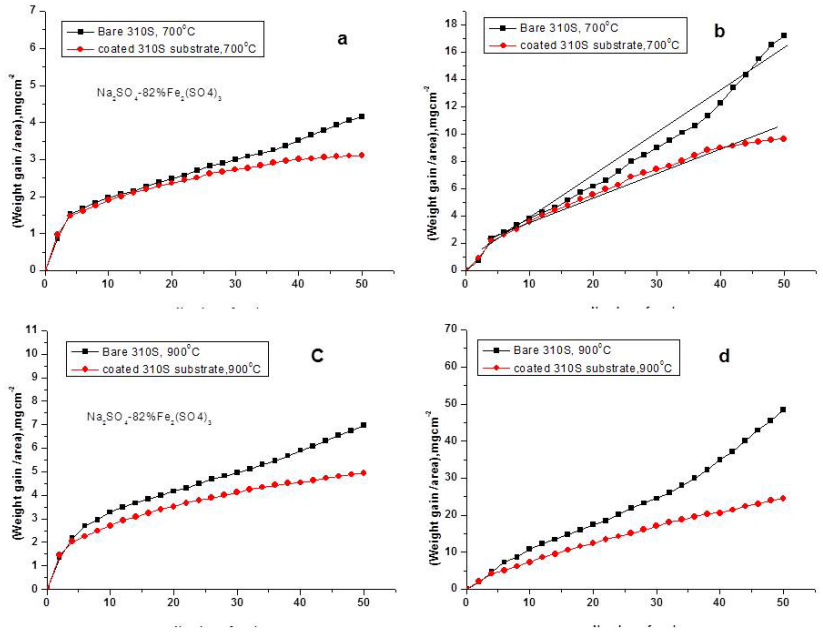

Fig. 4.21: (a,c) Weight gain after oxidation per unit area Vs number of cycles and (b,d) Weight gain after oxidation per unit area)^2 Vs number of cycles, for the bare and coated specimens subjected to hot corrosion in molten salt (Na_2SO_4-82% $Fe_2(SO_4)_3$) environment at 700^{0}C & 900^{0}C for 50 cycles.

Figure 4.21(a) shows weight change (mg/cm^2) for the coated and uncoated specimens subjected to oxidation at 700 ^{0}C in Na_2SO_4-82% $Fe_2(SO_4)_3$ up to 50 cycles. In case of uncoated specimen, a steady state in oxidation rates occurred with longer exposure time. It is apparent that spallation was absent with the scale being adherent. Initially, oxidation rate was high due to the oxidation of free surface of both coated and uncoated substrate. It can also be observed that the slope of the weight gain versus number of cycles plot is higher for the coated specimen during first 30 cycles, thereafter slope does not change much up to 50 cycles. It can be attributed to the protective oxide film formation during the initial cycles, which precludes further oxidation in the latter cycles. Weight gain per unit area after oxidation for uncoated specimen has shown a gradual increase with some spalling up to 50 cycles.

Figure 4.21 (b) shows a parabolic relationship occurs in case of Cr_3C_2–NiCr-coated 310S alloy substrate, whereas uncoated substrate deviates from the parabolic rate law. The parabolic rate constants K_p values for the bare substrate and Cr_3C_2–NiCr-coated alloy substrate after 50 cycles of high temperature oxidation were calculated from the slope of linear regression fitted the line, and found to be 8.6x 10^{-11} $g^2cm^{-4}s^{-1}$ and 5 x 10^{-11} $g^2cm^{-4}s^{-1}$, respectively. The K_p value for the bare substrate was found to be nearly twice of the K_p value of the coated specimen, which indicates that coating shows a better hot corrosion resistance.

Weight change plots for the bare alloy substrate as well as the Cr_3C_2–25%NiCr coated specimen subjected to molten salt (Na_2SO_4-60% V_2O_5) environment at 900^{0}C for 50 hours are shown in Fig. 4.21C.

310S bare alloy substrate exhibit higher weight gain as compared to Cr_3C_2–25%NiCr coated specimens. In Fig. 4.21(d), the square of weight gain per unit area (mg^2 /cm^4) versus number of cycles for bare and coated specimens is plotted. The parabolic rate constants K_p values for the bare substrate and Cr_3C_2–NiCr-coated alloy substrate after 50 cycles of high temperature oxidation were calculated from the slope of linear regression fitted the line, and found to be 24.4x 10^{-11} $g^2cm^{-4}s^{-1}$ and 12.7 x 10^{-11} $g^2cm^{-4}s^{-1}$, respectively. The K_p value for the bare substrate was found to be nearly twice of the K_p value of the coated specimen, which indicates that coating shows a better hot corrosion resistance.

4.4.2.2 FE-SEM/EDS analysis

4.4.2.2.1 Surface morphology of the scales

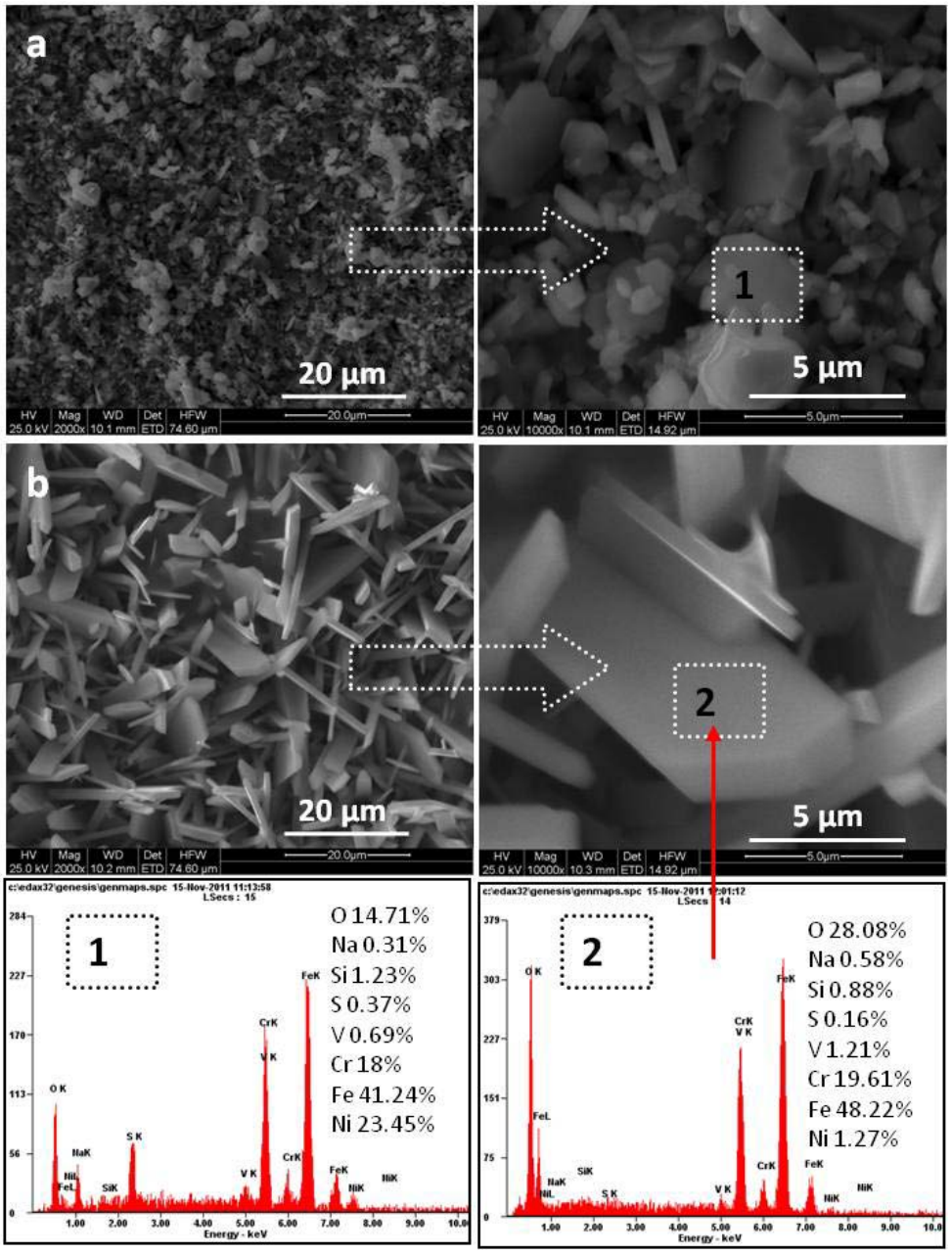

Fig 4.22 Surface scale morphology and EDS analysis for bare substrate subjected to hot corrosion in molten salt (Na_2SO_4-60% V_2O_5) environment at 700^0C for (a) 10 cycles and (b) 50 cycles.

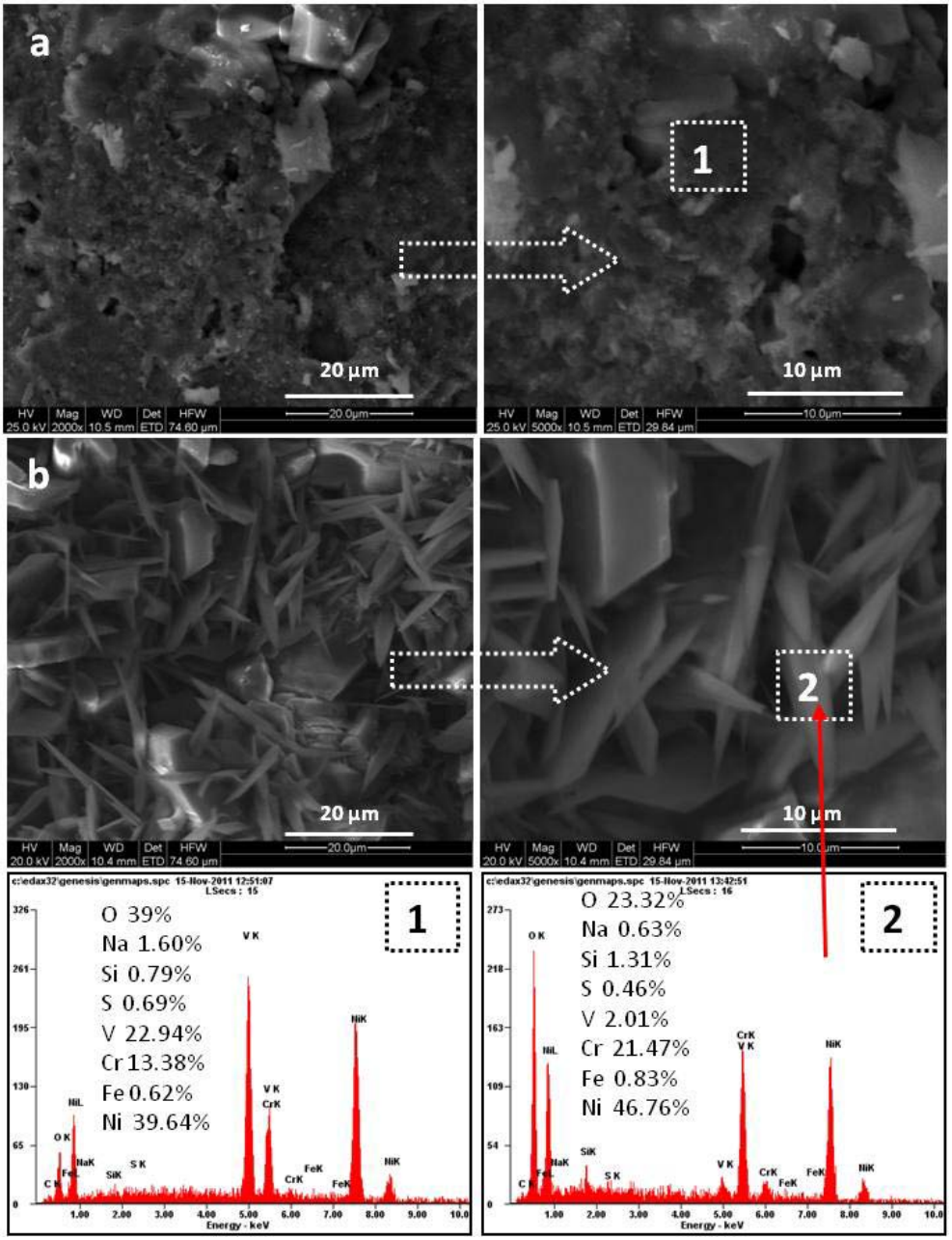

Fig 4.23: Surface scale morphology and EDS analysis for HVOF-sprayed Cr_3C_2–25%NiCr coating subjected to hot corrosion in molten salt (Na_2SO_4-60% V_2O_5) environment at 700^0C for (a) 10 cycles and (b) 50 cycles.

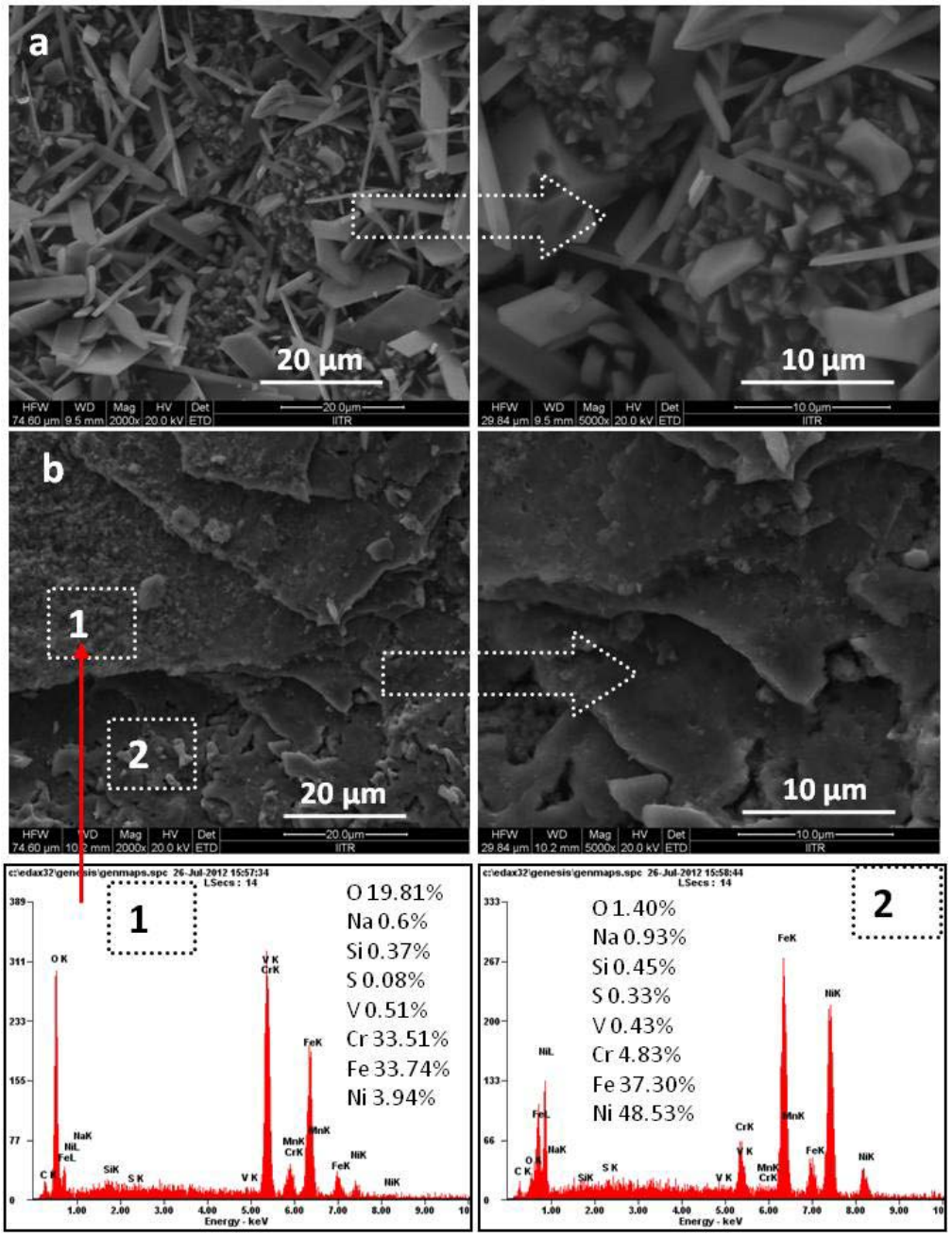

Fig 4.24: Surface scale morphology and EDS analysis for bare substrate subjected to hot corrosion in molten salt (Na_2SO_4-60% V_2O_5) environment at 900^0C for (a) 10 cycles and (b) 50 cycles.

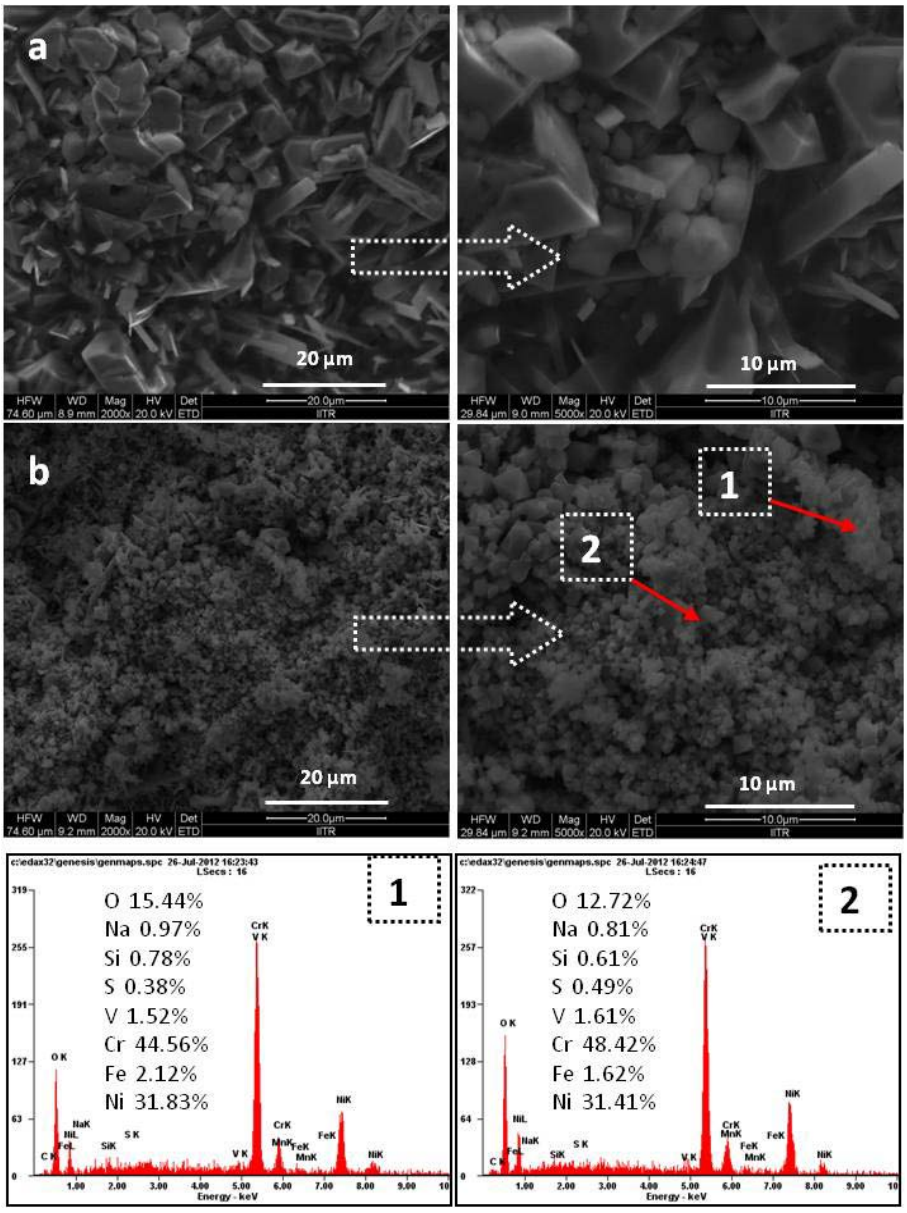

Fig 4.25: Surface scale morphology and EDS analysis for HVOF-sprayed Cr_3C_2–25%NiCr coating subjected to hot corrosion in molten salt (Na_2SO_4-60% V_2O_5) environment at 900^0C for (a) 10 cycles and (b) 50 cycles.

Detailed analysis of surfaces of uncoated and coated specimens after degradation in molten salt (Na_2SO_4-60% V_2O_5) environment at 700°C is shown in Fig. 4.22 and 4.23, respectively and detailed analysis of surfaces of uncoated and coated specimens after degradation in molten salt (Na_2SO_4-60% V_2O_5) environment at 900°C is shown in Fig. 4.24 and 4.25, respectively. FE-SEM analysis of the uncoated surface indicates loosely bound oxide particles after 10 cycles of oxidation at 700^oC (Fig. 4.22a) and 900^oC (Fig. 4.24a).The microstructure consists of mixture of large elongated and small irregular shaped particles for the uncoated surface after 10 cycles of oxidation at 700^oC (Fig. 4. 22a), while sharp

elongated and small irregular shaped particles appeared at 900^{o}C (Fig. 4.24a). With increased exposure to 50 cycles, particles became elongated in their size at 700^{o}C and completely covered oxide later appeared spalling at 900^{o}C. EDS analysis shows the major presence of Fe, Cr and Ni along with minor presence of Si, V, Na, and S throughout the composition of the scale along with oxygen. It indicates the possibility of formation of oxide of Fe , Ni and Cr. EDS analysis indicates that after 50 cycles, wt% of Fe, Cr and O has increased in oxide scale in both cases of 700^{o}C (Fig 4.22b) and 900^{o}C and (Fig. 4. 24b). The presence of Fe_2O_3 in spalled scale has been reported to be non-protective by Kaur et al. (2009) during cyclic oxidation of SAE-347H steel in molten salt environment at 700^{0}C.

The surface of the hot corroded coated specimen appears as consisting of spongy nodules after oxidation for 10 cycles at 700^{o}C (Fig. 4.23a) and irregular shaped particles at 900^{o}C (Fig. 4.25a). EDS analysis of scale indicates the presence of Ni, V, Cr, O. Minor amount of Na, Fe, Si, and S have also been detected in the oxide scale, which reveals inter diffusion of alloying elements from the substrate into the coating in both cases of 700^{o}C (Fig. 4. 23b)and 900^{o}C (Fig 4.25b). These results of inter diffusion of alloying elements to the coating are in good agreement with the findings of Kaur et al.(2009) and Kamal et al.(2009) during high temperature oxidation of Cr_3C_2–NiCr coated boiler steel and superalloy specimens. With increase in number of cycles to 50, oxidized surface also shows platelets, the presence of which increased in specimen surfaces oxidized for 50 cycles at 700 ^{o}C (Fig 4.23b) and completely covered surface with negligible spalling at 900^{o}C (Fig. 4.25b) . EDS analysis suggests that these platelets could be mainly oxides of chromium. Further, the EDS analysis of the nodules shows the major presence of Cr, O and Ni in both cases of 700^{o}C (Fig. 4.23b) and 900^{o}C (Fig. 4.25b).

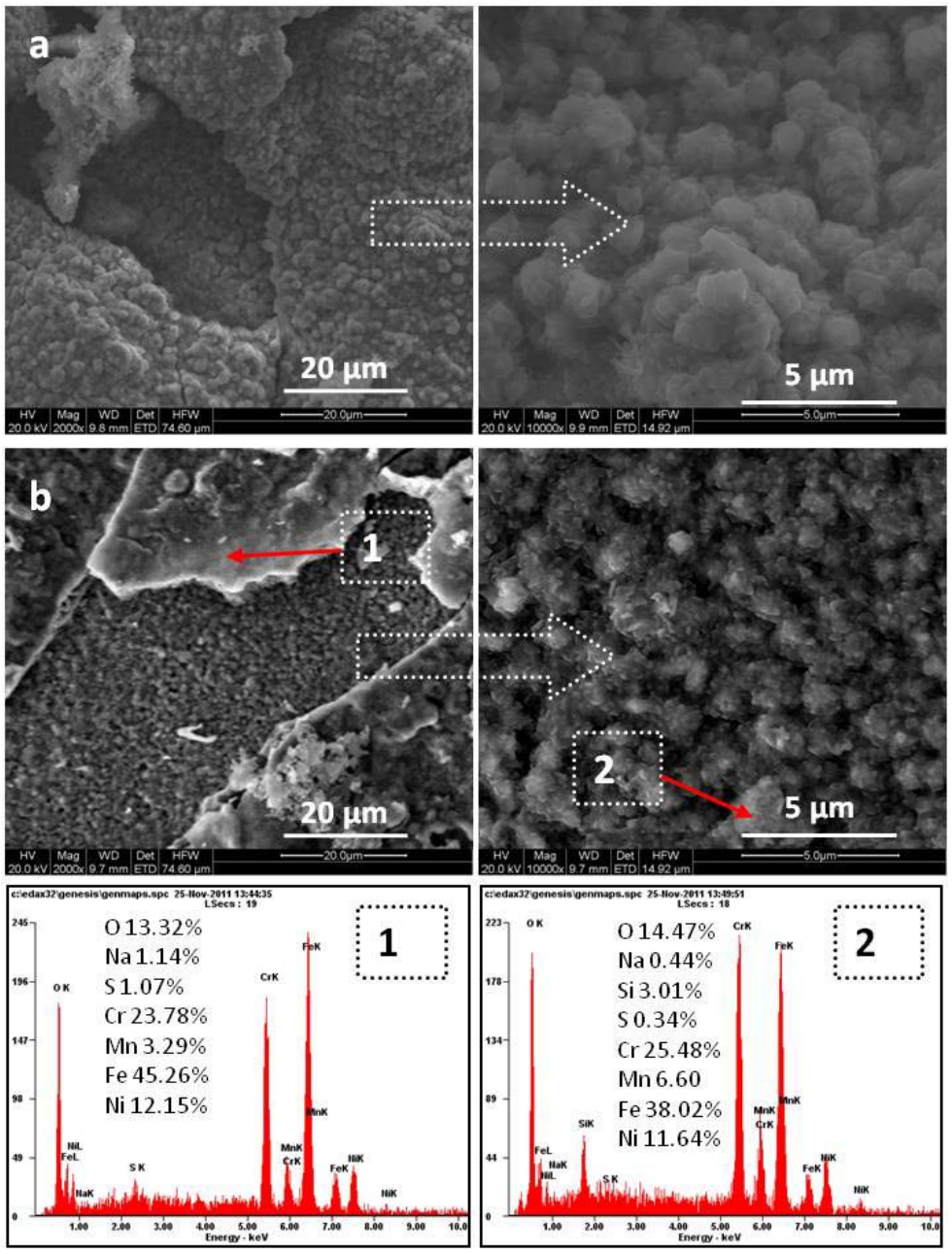

Fig 4.26: Surface scale morphology and EDS analysis for bare substrate subjected to hot corrosion in molten salt (Na_2SO_4 - 82% $Fe_2(SO_4)_3$) environment at 700^0C for (a) 10 cycles and (b) 50 cycles.

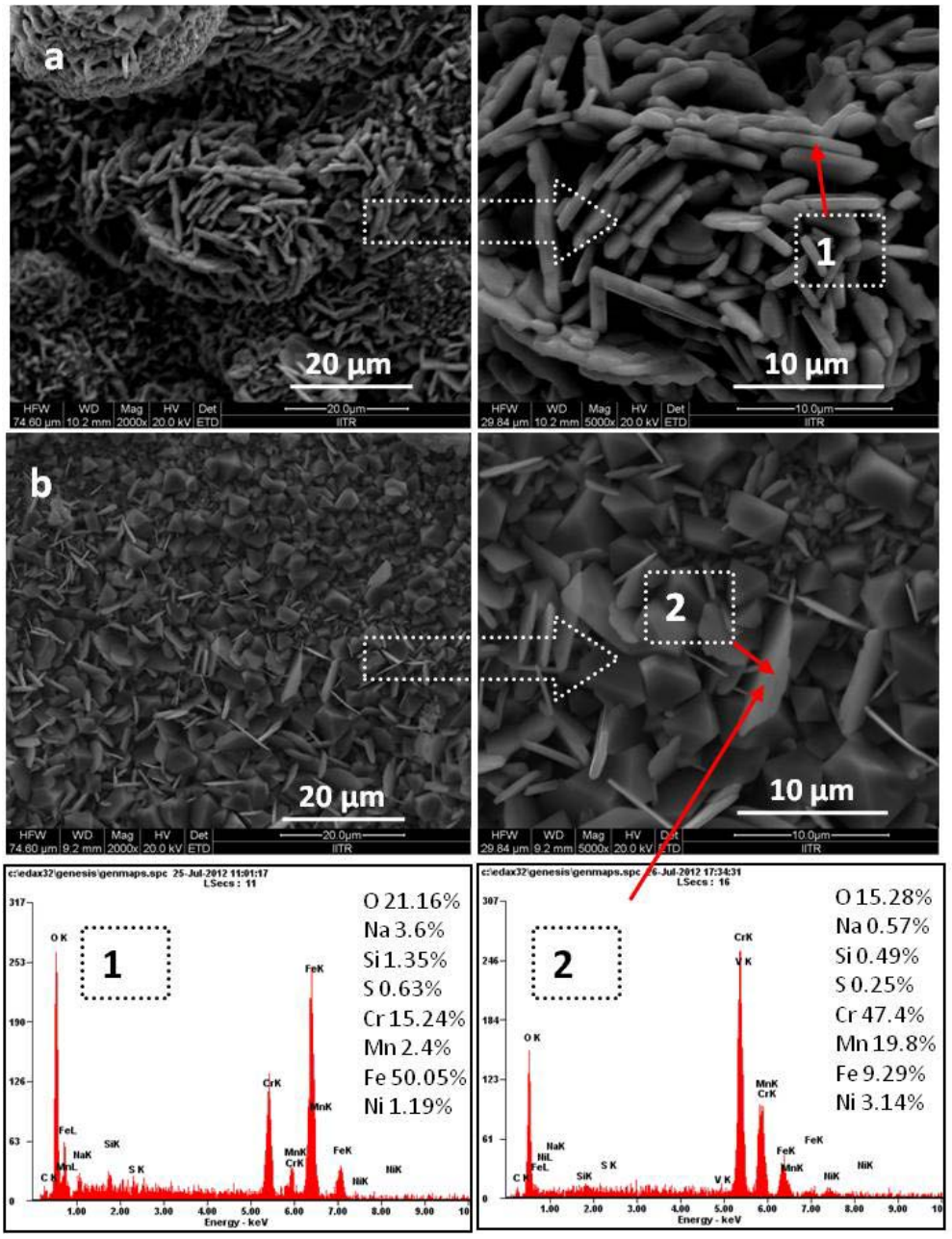

Fig 4.27: Surface scale morphology and EDS analysis for bare substrate subjected to hot corrosion in molten salt (Na_2SO_4 - 82% $Fe_2(SO_4)_3$) environment at 900^0C for (a) 10 cycles and (b) 50 cycles.

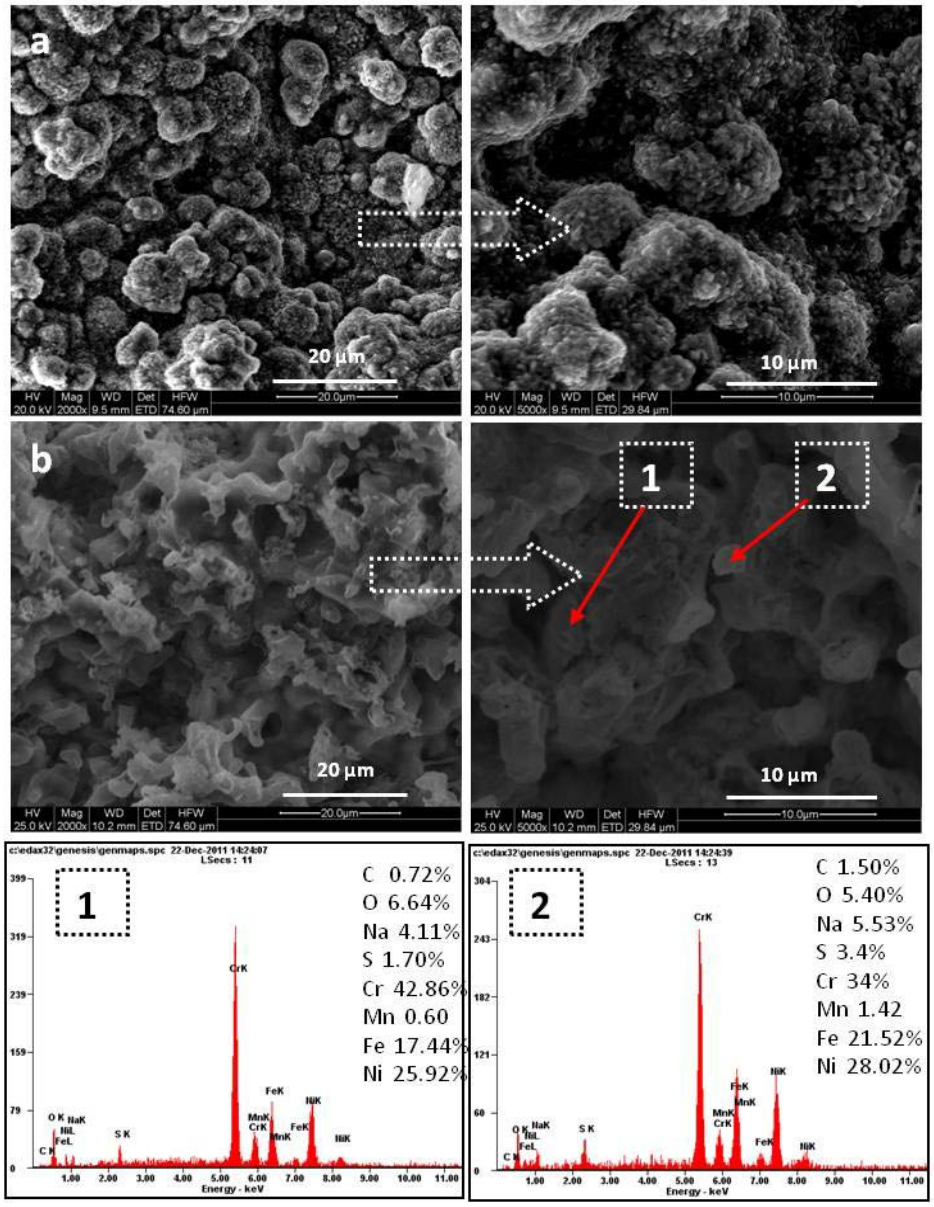

Fig 4.28: Surface scale morphology and EDS analysis for HVOF-sprayed Cr_3C_2–25%NiCr coating subjected to hot corrosion in molten salt (Na_2SO_4 - 82% $Fe_2(SO_4)_3$) environment at 700^0C for (a) 10 cycles and (b) 50 cycles.

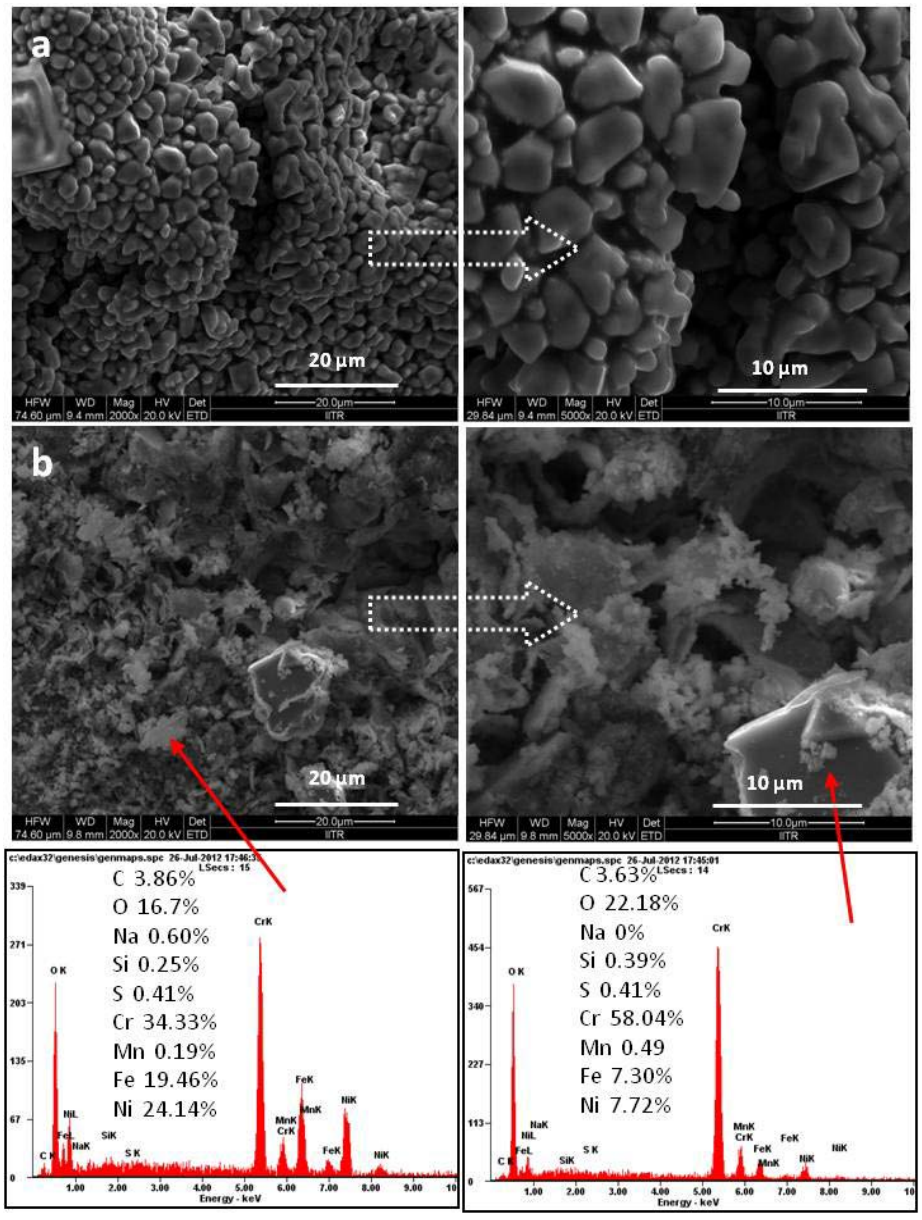

Fig 4.29: Surface scale morphology and EDS analysis for HVOF-sprayed Cr_3C_2–25%NiCr coating subjected to hot corrosion in molten salt (Na_2SO_4 - 82% $Fe_2(SO_4)_3$) environment at 900^0C for (a) 10 cycles and (b) 50 cycles.

Detailed analysis of surfaces of both uncoated & coated specimens exposed to molten salt (Na_2SO_4-82%$Fe_2(SO_4)_3$) environment at 700^0C and 900^0C under cyclic conditions for 10 and 50 cycles is shown in Figs. 4.26-4.27 and Figs. 4.28-4.29, respectively. The surface of uncoated specimen after heating at 700^oC for 10 cycles shows porous oxide layer consisting of globular particles (Fig. 4.26a),

whereas breaking of smooth and thick layers can be found after 50 cycles of oxidation (Fig. 4.26b). EDS analysis indicates the major presence of Cr, O, Fe along with minor presence of B, Mn, Na, S and Si. It is interesting to see the considerable change in the morphology of oxide surfaces when heated at 900^{o}C. Figure 4.27a shows the platelet morphology of the oxide surface after 10 cycles of oxidation at 900^{0}C. With increase in cycles to 50, the surface consists of mixture of irregularly shaped and thin platelet particles (Fig. 4.27b). EDS analysis suggests that the oxide particles are rich in iron after 10 cycles, whereas the oxide particles are rich in chromium after 50 cycles. This indicates that both morphology and chemistry of the oxide particles change with number of cycles and temperature. The surface of the hot corroded coated specimen appears as consisting of globular particles after oxidation for 10 cycles at 700^{o}C (Fig. 4.28a), while thin and small interconnected particles appears after 50 cycles of oxidation (Fig. 4.28b). EDS analysis indicates the presence of elements from salts in addition to elements from cermet coating and substrate.(Fig. 4.28b). After oxidation at 900^{o}C for 10 cycles, strongly connected and irregularly shaped particles formed on the surface (Fig.4.29a). With prolonged oxidation of 50 cycles, loosely connected large particles were formed (Fig. 4.29b).

4.4.2.2.1 Cross-sectional analysis and X-ray mapping of the scale

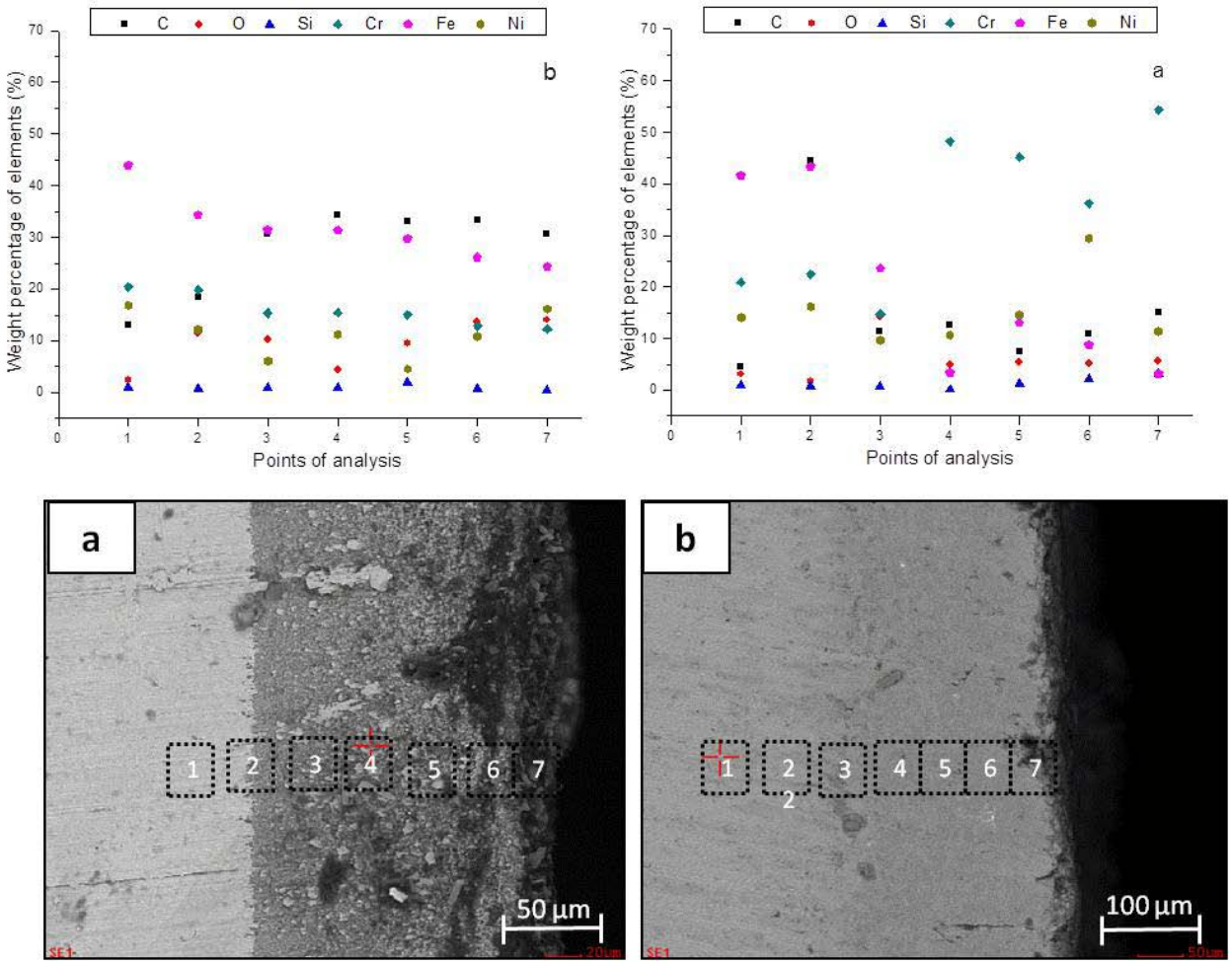

Fig 4.30: Morphology of oxide scale across the cross section of (a) bare, and (b) coated specimens, subjected to hot corrosion in molten salt (Na_2SO_4-60% V_2O_5) environment at 900^0C for 50 cycles.

Oxide scale morphologies along with variation of elemental composition across the cross section of the coated and uncoated specimens subjected to oxidation at 900 ^{0}C after 50 cycles in Na_2SO_4-60% V_2O_5 are shown in Fig. 4.30, while that in Na_2SO_4 - 82% $Fe_2(SO_4)_3$ are shown in Fig. 4.31. Thick and light colored scale formed on the surface of uncoated specimen in Na_2SO_4-60% V_2O_5 (Fig 4.30(a)), while non-uniform and more fragile scale formed on the surface of uncoated specimen in Na_2SO_4 - 82% $Fe_2(SO_4)_3$ (Fig. 4.31(a)). X-ray mapping analysis shows mainly iron along with chromium, nickel, and silicon on the oxide scale.

It is to note that even after 50 cycles of oxidation, the scale was dense and adherent and retained contact with the substrate in case of coated specimen in both salts. The oxide scale contains chromium, nickel and oxygen. This observation suggests formation of oxides and carbides of chromium in the oxide

scale (see Fig. 4.30 (b) and Fig. 4.31 (b)). It suggests that the nickel diffused from substrate to coating while chromium diffused from coating to substrate.

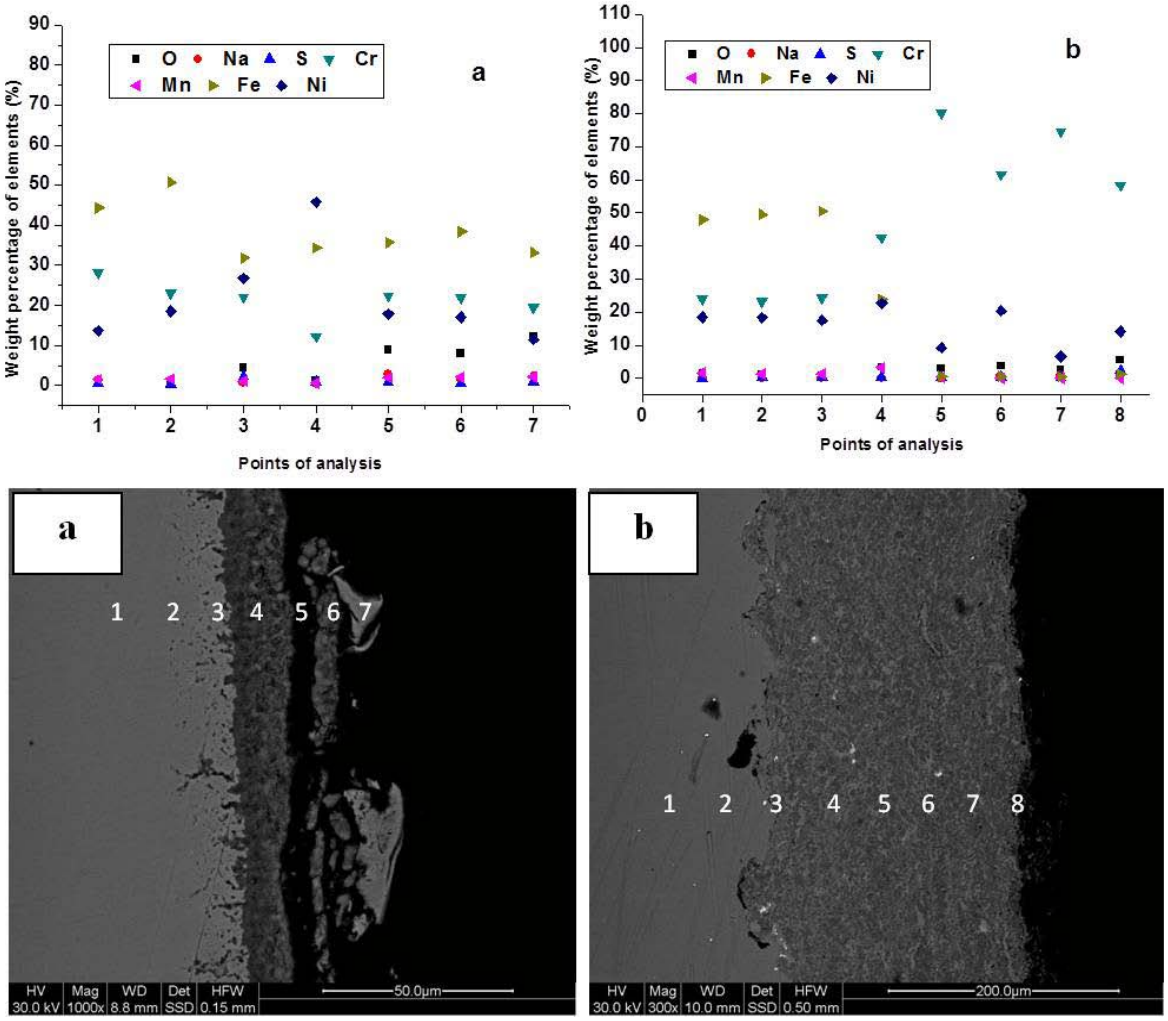

Fig 4.31: Morphology of oxide scale across the cross section of (a) bare, and (b) coated specimens, subjected to hot corrosion in molten salt (Na_2SO_4 - 82% $Fe_2(SO_4)_3$) environment at 900^0C for 50 cycles.

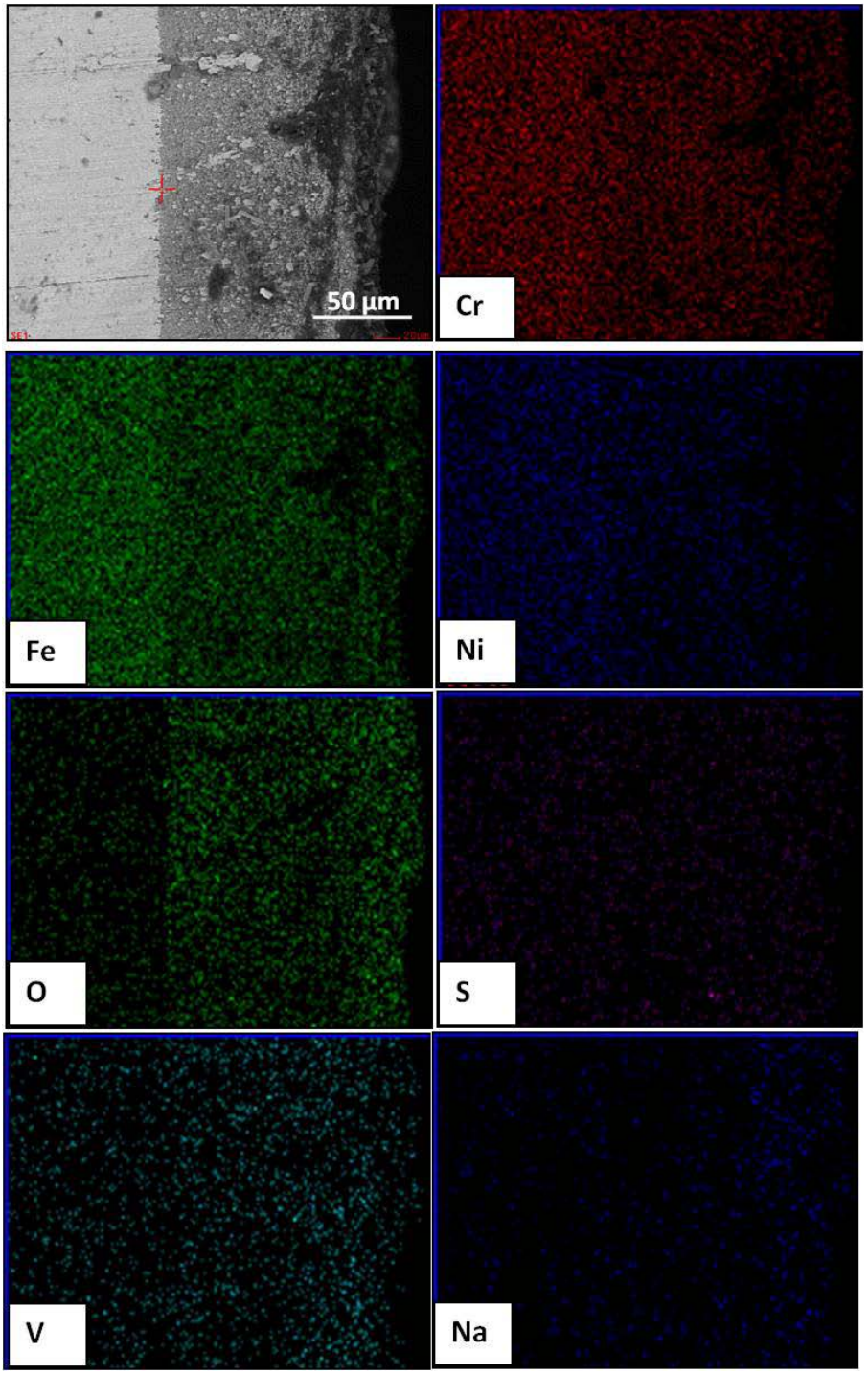

Fig 4.32: Composition image (SE) and X-ray mapping of the cross section of the bare alloy substrate subjected to hot corrosion in molten salt (Na_2SO_4-60% V_2O_5) environment at 900^0C for 50 cycles.

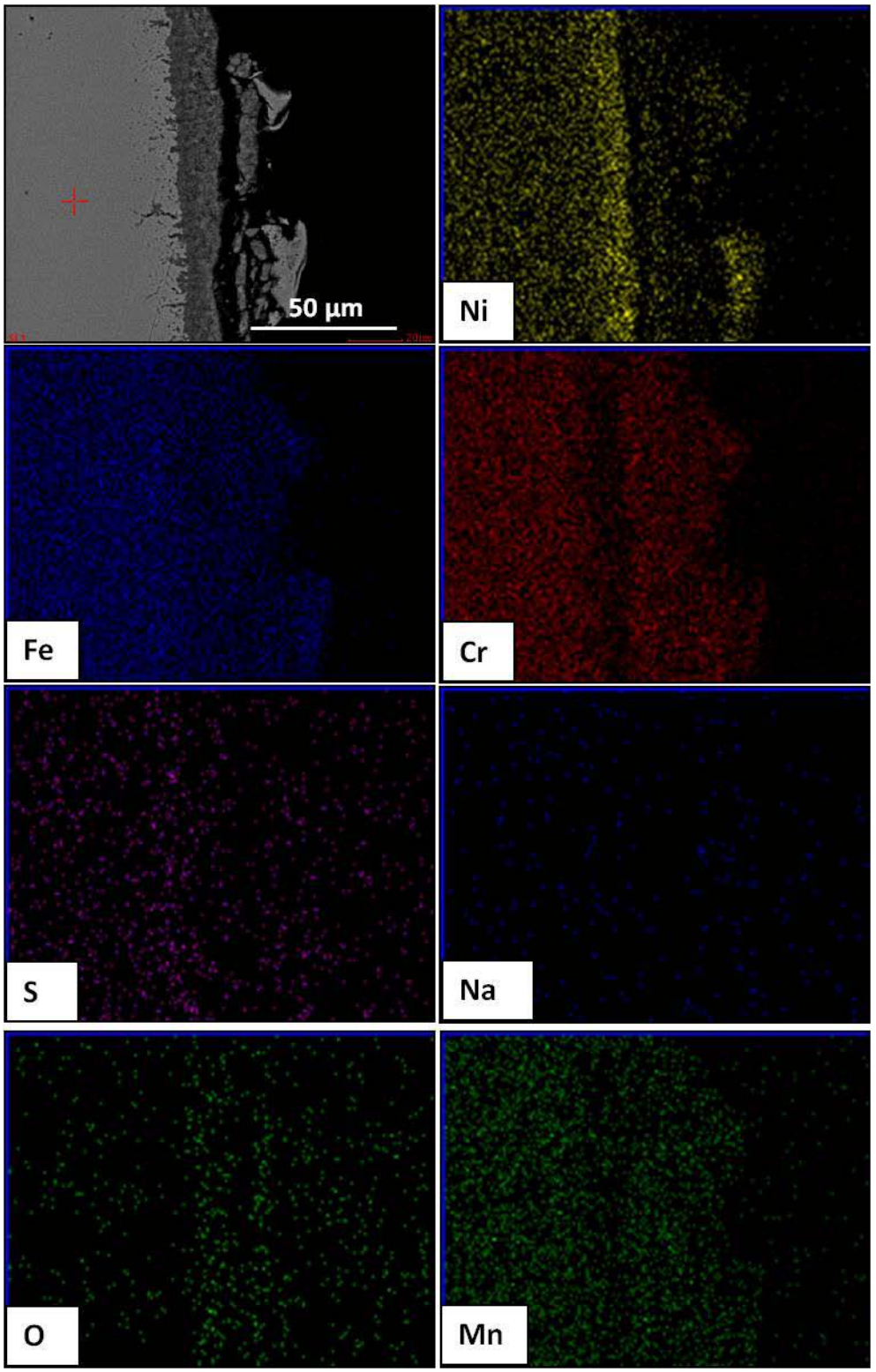

Fig 4.33: Composition image (SE) and X-ray mapping of the cross section of the bare alloy substrate subjected to hot corrosion in molten salt (Na_2SO_4 - 82% $Fe_2(SO_4)_3$) environment at 900^0C for 50 cycles.

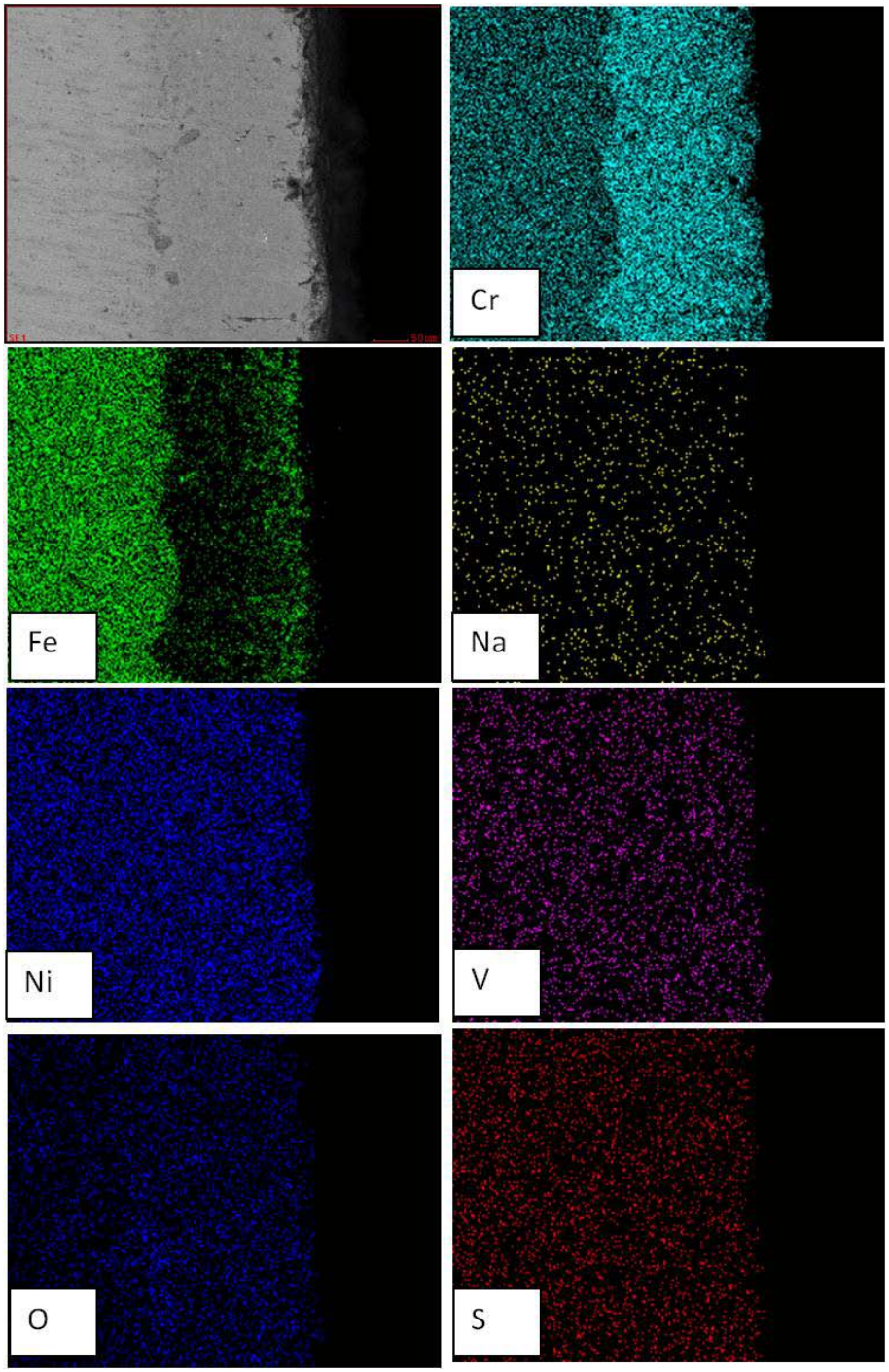

Fig 4.34: Composition image (SE) and X-ray mapping of the cross section of the coated specimen subjected to hot corrosion in molten salt (Na_2SO_4-60% V_2O_5) environment at 900^0C for 50 cycles.

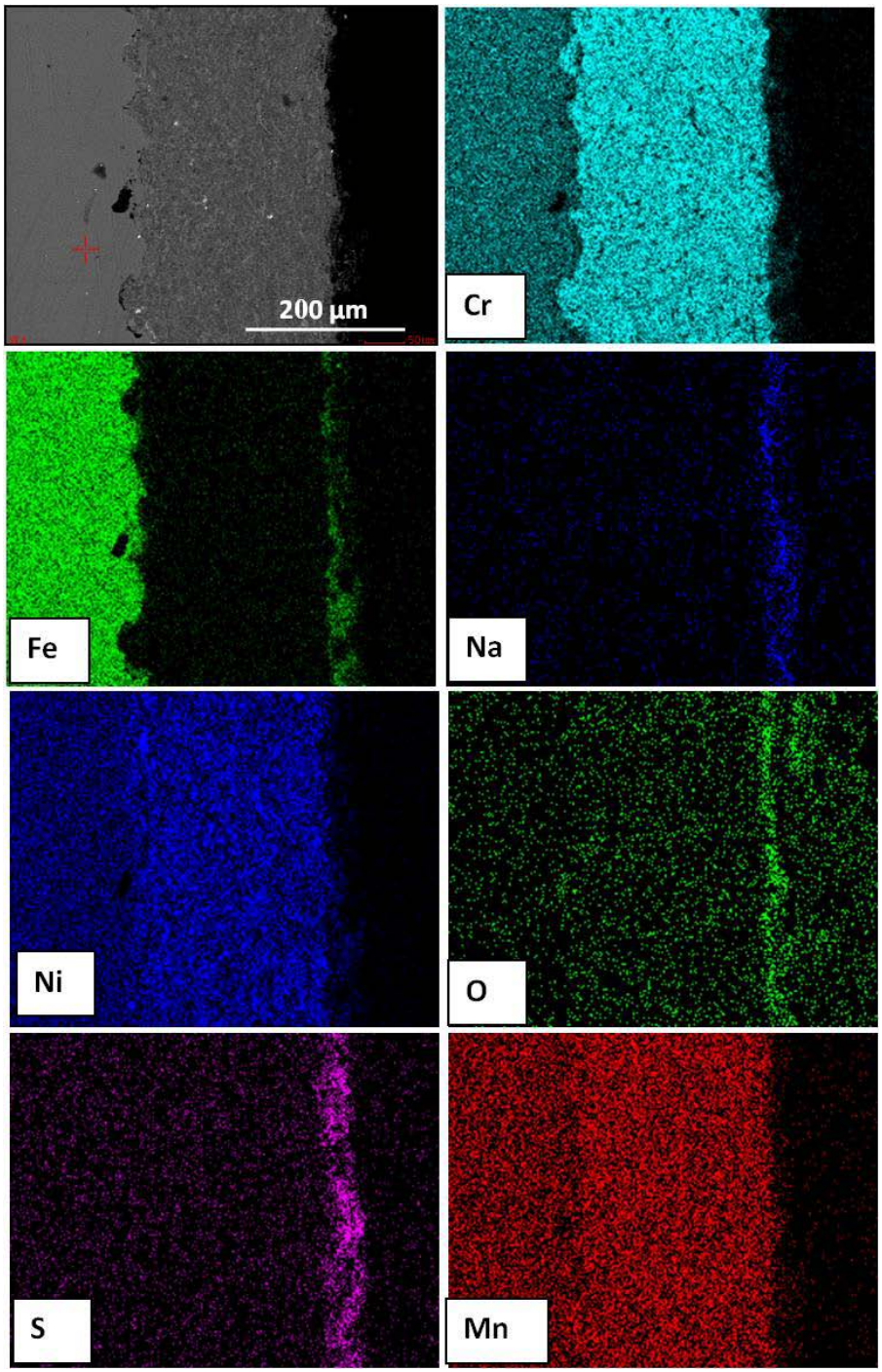

Fig 4.35: Composition image (SE) and X-ray mapping of the cross section of the coated specimen subjected to hot corrosion in molten salt (Na_2SO_4 - 82% $Fe_2(SO_4)_3$) environment at 900^0C for 50 cycles.

The performance of HVOF coating on the high temperature oxidation behavior in two different molten salt environments is discussed. X-ray mappings of cross sections of surfaces of bare specimen and coated specimens after 50 cycles of oxidation at 900 ^{0}C in Na_2SO_4-60% V_2O_5 are respectively shown in Figs. 4.32 and 4.34, while that in Na_2SO_4-82% $Fe_2(SO4)_3$ salt are respectively represented in Figs. 4.33 and 4.35.

Cross sections show that bare specimens are not susceptible to oxidation in both salt environments (Figs. 4.32 and 4.33). The damaged, fragile and non-adherent oxide scales are apparent in both salts. The distribution of elements from salt environments as wells as steel alloy in X-ray mapping indicate diffusion of corrosion species into the specimen. In case of coated specimens, the coating was intact with the substrate and uniformly thick without any signs of cracks (Fig. 4.34 and 4.35).Thus, the coating was susceptible to the exposed to the investigated hot corrosion environments. X-ray mappings of the cross sections of the coated specimens reveal distribution of elements from coating/substrate like Cr, Ni, Fe along with elements from salts like Na, S, O and/or V. Furthermore, it is interesting to observe the significant presence of Fe, Na, S and O only on the outer most surface of the coating in specimens subjected to hot corrosion in Na_2SO_4 - 82% $Fe_2(SO_4)_3$ environment (see Fig. 4.35). This suggests that the diffusion of salt was restricted only to the outer surface of the coating, while the other part of the coating was not affected to a large extent. However, the oxide scale formed during high temperature oxidation in Na_2SO_4 – 60% V2O5 salt consisted of the distribution of elements from salt in addition to that from coating or substrate. Literature also supports that the salt containing vadanadium is aggressive in effecting the oxide surfaces at high temperature (Khanna and Jha, 1998).

The adherent and crack-free oxide scales obtained on the surface of coated specimens after hot corrosion necessarily highlight superior performance of HVOF coating in Na_2SO_4 – 60% V_2O_5 and Na_2SO_4 - 82% $Fe_2(SO_4)_3$ salts. Particularly, the investigating coating was not affected by the Na_2SO_4 - 82% $Fe_2(SO_4)_3$ salt environment at high temperature.

4.4.2.3 X-ray diffraction analysis (XRD) analysis

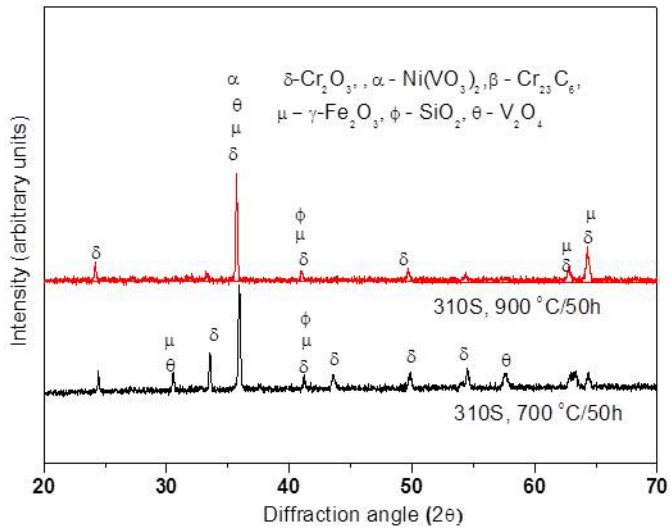

Fig 4.36: The XRD patterns of the scale formed on bare alloy substrate, subjected to hot corrosion in molten salt (Na_2SO_4-60% V_2O_5) environment at 700^{0}C & 900^{0}C for 50 cycles.

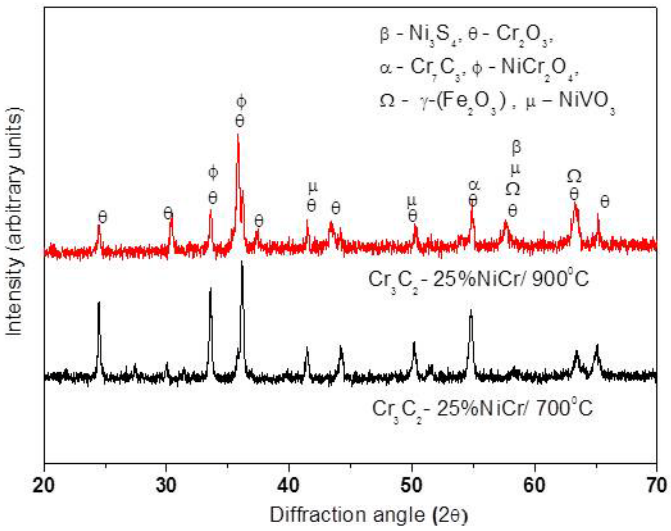

Fig 4.37: The XRD patterns of the scale formed on coated specimen, subjected to hot corrosion in molten salt (Na_2SO_4-60% V_2O_5) environment at 700^{0}C & 900^{0}C for 50 cycles.

XRD patterns of the scale formed on uncoated and coated specimens after 50 cycles of oxidation at 700 ^{0}C & 900 ^{0}C in Na_2SO_4-60% V_2O_5 are shown in Figures 4.36 and 4.37, respectively. Similarly, XRD patterns of scale formed on bare and coated specimens after 50 cycles of oxidation at 700 ^{0}C & 900 ^{0}C in (Na_2SO_4 - 82% $Fe_2(SO_4)_3$) are shown in Figures 4.38 and 4.39, respectively.

The XRD diffractograms for the uncoated specimen subjected to cyclic oxidation at 900 ^{0}C in Na_2SO_4-60% V_2O_5 revealed Austenite phase as main phases, whereas Cr_2O_3, SiO_2, V_2O_4, $Ni(VO_3)_2$ and Fe_2O_3 was also revealed in the oxide scale (4.36). The absence of $Ni(VO_3)_2$ can be noted in XRD pattern for uncoated specimen after oxidation at 900^{o}C in (Na_2SO_4 - 82% $Fe_2(SO_4)_3$). The XRD diffractograms for the coated specimen subjected to cyclic oxidation at 900 ^{0}C in Na_2SO_4-60% V_2O_5 revealed the formation of Cr_2O_3 and Cr_7C_3 as very strong phases, Ni_3S_4, $Ni(VO_3)_2$, Fe_2O_3, and $NiCr_2O_4$ spinel as low intensity phases (Fig. 4.37). The absence of $Ni(VO_3)_2$ can be noted in XRD patterns of coated specimen subjected to cyclic oxidation at 900 ^{0}C in (Na_2SO_4 - 82% $Fe_2(SO_4)_3$).

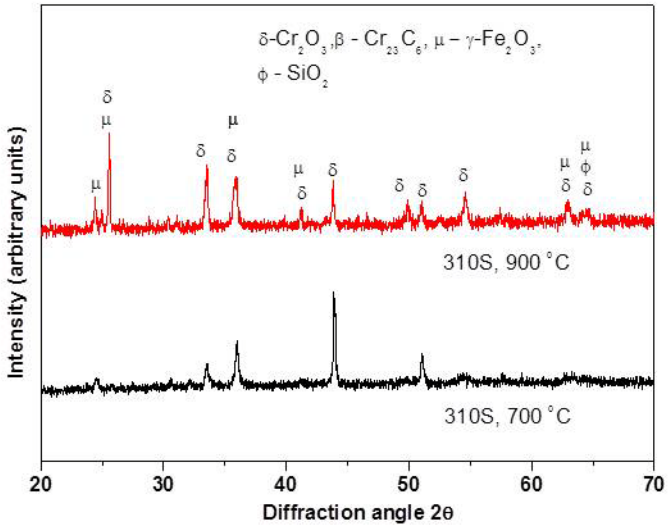

Fig 4.38: The XRD patterns of the scale formed on bare alloy substrate, subjected to hot corrosion in molten salt (Na_2SO_4 - 82% $Fe_2(SO_4)_3$) environment at 700^{0}C & 900^{0}C for 50 cycles.

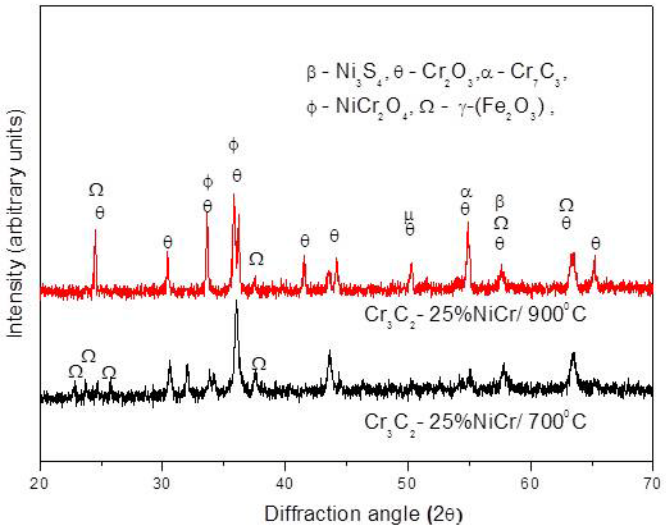

Fig 4.39: The XRD patterns of the scale formed on coated specimen, subjected to hot corrosion in molten salt (Na_2SO_4 - 82% $Fe_2(SO_4)_3$) environment at 700^0C & 900^0C for 50 cycles.

4.4.4 Discussion

The weight gain curves for HVOF gun sprayed Cr_3C_2-25%NiCr coated and bare 310S alloy substrate followed nearly a parabolic behavior (Fig. 4.20 & 4.21). A minor deviation from the parabolic rate law was probably due to the cyclic growth of the oxide scale. The higher weight gain of the specimens during initial period of oxidation was due to the rapid development along boundaries of splat and within the open pores, subsequently gradual increase in weight. The parabolic rate constant for the bare alloy substrate is found to be greater than the coated specimens. The nature of fit parabolic rate law, for hot corrosion experiments are shown in (Fig.4.20)

The phases identified from XRD analysis of the oxidized uncoated specimen subjected to cyclic oxidation in air at 700 ^{0}C in Na_2SO_4-60% V_2O_5 after 50 cycles are shown in Fig 4.36. Austenite phase was observed as the main phases, whereas Cr_2O_3, SiO_2, V_2O_4 and Fe_2O_3 were also revealed in the oxide scale. The XRD diffractograms for the coated specimen subjected to cyclic oxidation in air at 700 ^{0}C in Na_2SO_4-60% V_2O_5 (Fig 4.37) revealed the formation of Cr_2O_3 and Cr_7C_3 as very strong phases, Ni_3S_4, Ni $(VO_3)_2$, Fe_2O_3, and $NiCr_2O_4$ spinel as low intensity phases.

The composition analysis of surfaces of Cr_3C_2–NiCr -coated substrate indicates that Cr_2O_3 phase is mainly present in the oxide scale along with NiO, Fe_2O_3, and SiO_2, which clearly reveals the diffusion of these elements from substrate. The predominant phases formed on the surface of uncoated

substrate oxidised at 700 ^{0}C in air up to 50 cycles are Cr_2O_3 and Fe_2O_3, where as NiO, V, S, Na and SiO_2 present as weak phases.

EDS analysis of cross section of corroded Cr_3C_2–NiCr -coated specimens reveals the variation in elemental composition after oxidation, the chromium rich elements are present in the uppermost part of coating.

The slow growth of thermodynamically stable chromium oxide scale as shown in Fig 9, might have acted as barrier to the inward diffusion of corrosion species into the coating. Fe and Si are clearly visible in top surface of the coating, which confirms the diffusion of this element from the substrate to the top coating surface.

The present investigation suggeststhat Cr_3C_2–NiCr coating can provide higher hot corrosion resistance at high temperature. Schematic diagram of the proposed oxidation mechanism of Cr_3C_2–25%NiCr coated 310S alloy substrate subjected to hot corrosion in molten salt (Na_2SO_4-60% V_2O_5) & (Na_2SO_4 - 82% $Fe_2(SO_4)_3$) environment at 700^{0}C & 900^{0}C for 50 cycles are shown in Fig. 4.40 & 4.41, respectively.

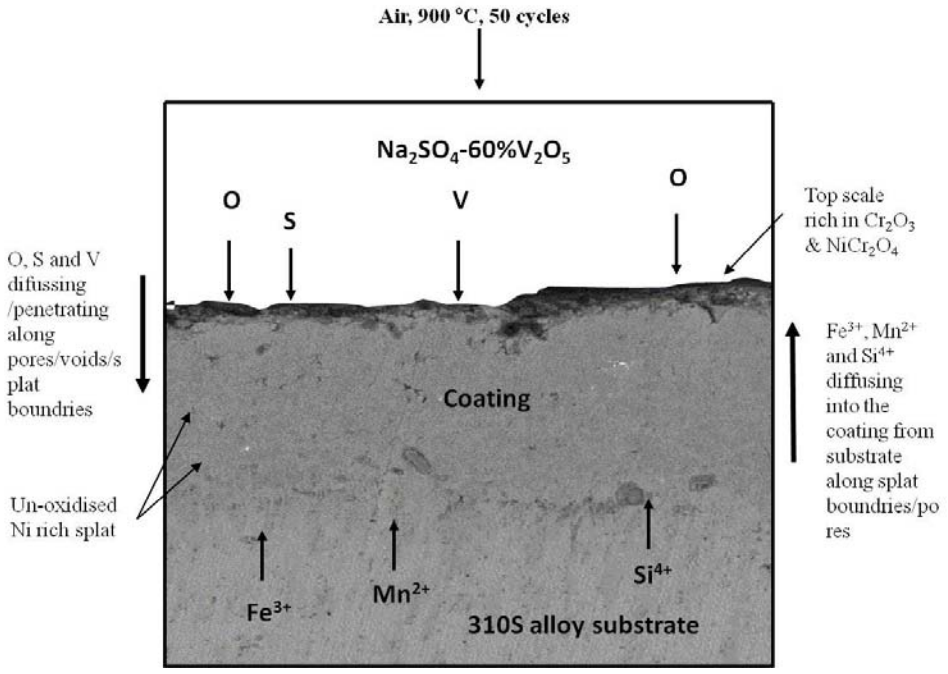

Fig 4.40: Schematic of the proposed oxidation mechanism of Cr_3C_2–25%NiCr coated 310S alloy substrate subjected to hot corrosion in molten salt (Na_2SO_4-60% V_2O_5) environment at 700^{0}C & 900^{0}C for 50 cycles.

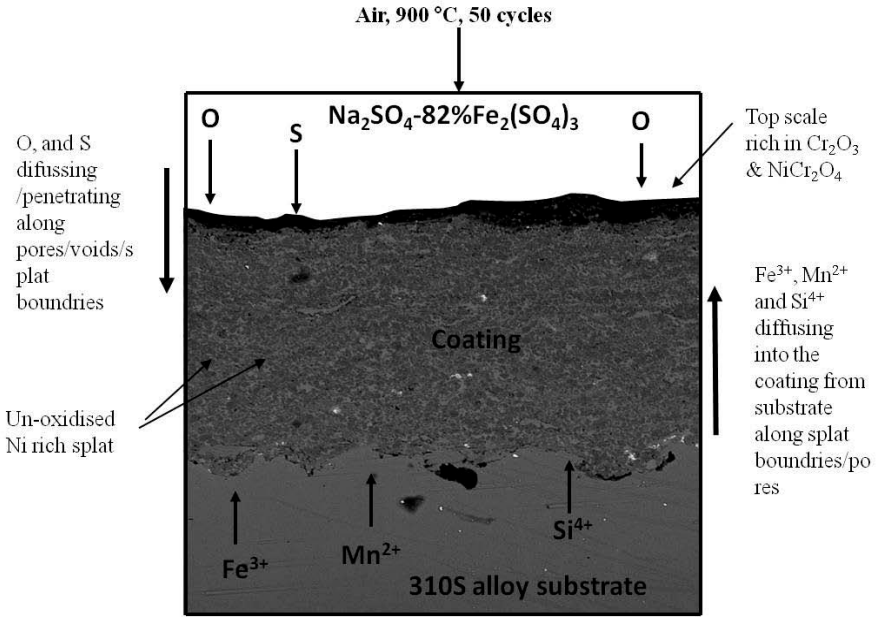

Fig 4.41: Schematic of the proposed oxidation mechanism of Cr_3C_2–25%NiCr coated 310S alloy substrate subjected to hot corrosion in molten salt (Na_2SO_4 - 82% $Fe_2(SO_4)_3$) environment at 700^0C & 900^0C for 50 cycles.

4.4.5 Conclusions

- In this work, Cr_3C_2-25NiCr coatings were deposited successfully on 310 alloy substrate by the HVOF-spraying process.
- The coated specimen showed a higher hot corrosion resistance subjected to cyclic oxidation in air at 700 ^{0}C in molten salt environment ($N_{a2}S_{O4}$-60% $_{V2O5}$) after 50 cycles with its uncoated counterpart.
- The formation of protective dense oxides of chromium, nickel and their spinel might have contributed for the better hot corrosion resistance in the coated specimen. The scale formed on the surface of the coating was adherent with some sign of minor cracks.
- The splat and globular morphology of the as deposited coatings provides relatively high density to the coatings, which is essential for achieving oxidation resistance of the coatings.
- The formation of protective oxide layers such as Cr_2O_3 and spinel of nickel and chromium is responsible for imparting resistance against high temperature oxidation on the coated specimen.
- The diffusion controlled reaction upon formation of Ni spinels and Cr_2O_3 films on the coatings surface limits the diffusion of aggressive species such as air and other impurities in to the coatings.
- The oxidation behavior of coated samples was found to obey parabolic rate law.

4.5 EROSION-CORROSION STUDIES IN ACTUAL INDUSTRIAL ENVIRONMENT

4.5.1 Experimental details

The substrate material, coating formulation and the oxidation studies are explained in detail in sections 3.1, 3.2.3 and 3.4.1.

4.5.2 Results

4.5.2.1 Weight change measurements

The weight change for the alloy substrate and for the HVOF sprayed Cr_3C_2-25NiCr coating on 310S SS were -14.392 and 6.831 $mgcm^{-2}$, respectively. This small weight gain in case of coated specimen can be attributed due to the oxidation and deposition of ash particles on exposed surfaces.

4.5.2.2 FE-SEM/EDS analysis

4.5.2.2.1 Surface morphology of the scales

FE-SEM images with EDS analysis for the coated and uncoated specimens when exposed to coal fired boiler after 1500 hours at 700 ± 10^0 C are shown in Fig. 4.42. EDS analysis reveals the presence of ash deposits on the surface of substrate (Fig. 4.42a). The scale formed on alloy substrate was porous and less adherent and consists mainly of Fe, Cr, Ni and O, with considerable amount of Al, S, Na, C and Si. The scale was removed due to particle impact. Spalling and cracking were observed in case of alloy substrate along with presence of pits and hills as shown in Fig 4.42a. The Cr_3C_2-25NiCr coatings deposited on 310S by the HVOF-spraying process behaved very well in the boiler environment. The scale was adherent and minor spalling observed at the edges of the coated specimen. The scale is made up of Cr, C, Ni and O, with considerable amount of Al, S, Fe, Mn and Na. EDS analysis confirmed the presence of ash deposited on the coating surface (Fig 4.42b). Similar observations were reported by Sidhu et al. (2004). The thickness loss of alloy substrate and coating is due to the impact of fly ash in the air blast as shown in Fig. 4.43.

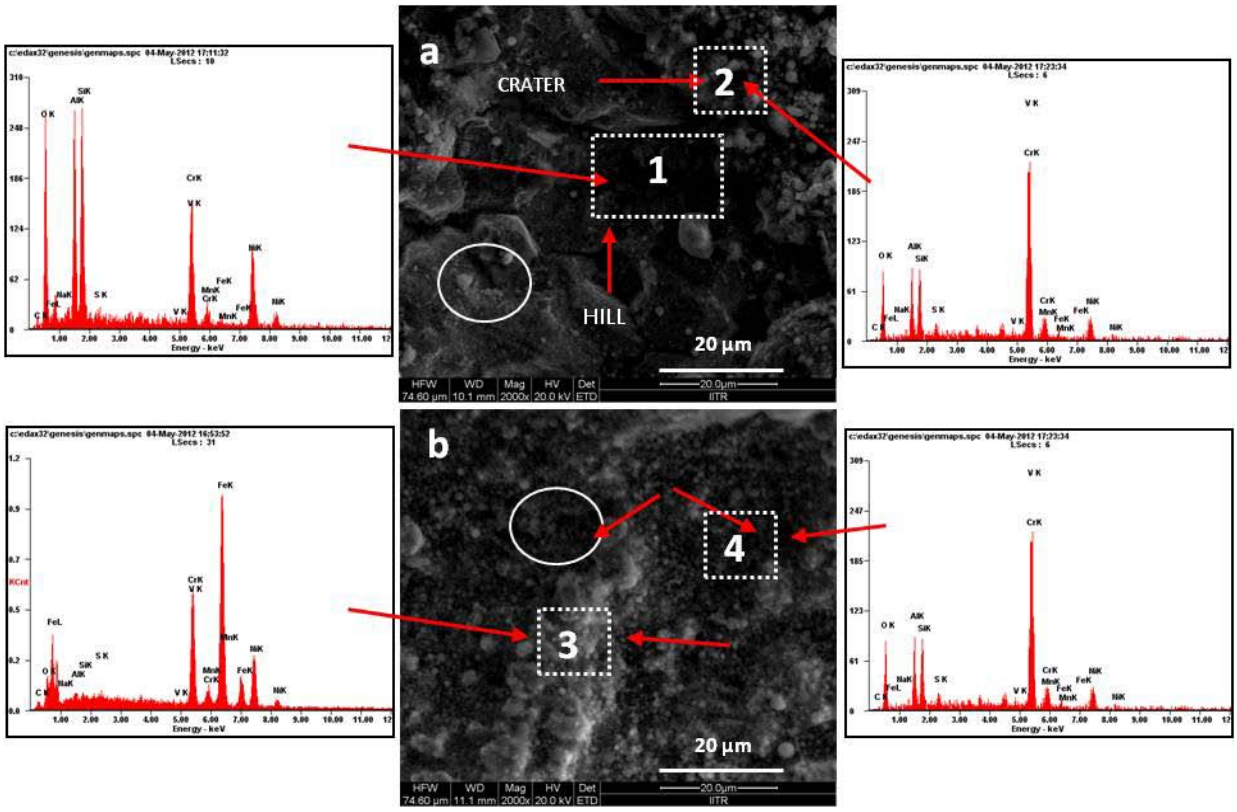

Fig 4.42: FE-SEM/EDS Surface analysis of (a) 310S alloy substrate and (b) Cr_3C_2 -25%NiCr coated alloy substrate exposed to superheater of the coal fired boiler 700±10 ^{0}C for 1500 hours.

4.5.2.2.1 Cross-sectional analysis and X-ray mapping of the scale

The thickness of metal lost for the alloy substrate and for the HVOF sprayed Cr_3C_2-25NiCr coatings on 310S were 0.34 and 0.11 mm, respectively, and the rates of thickness loss were 78.233 and 25.310 mpy, respectively. The scale was very fragile resulting in spalling of oxide scale (Fig 4.43a). Wang also observed severe spalling of the oxide scale during cyclic study of 2.25Cr-1Mo steel at 740^0 C in coal-fired boiler (wang et al., 1988). Craters and hills were formed on the surface exposed to superheater of the coal-fired boiler after 1500 hours at 700±10^0 C, revealing the combined effect of erosion and corrosion due to presence of flue gases and fly ash. Coating was quite adherent/intact and there was no sign of crack development in the coating (Fig. 4.43b).

The cross-sectional analyses by X-ray mapping of different elements of the bare and coated specimens subjected to degradation in coal fired boiler at 700 ± 10 ^{o} C for 1500 hours are shown in Fig. 4.44 and 4.45 respectively. The oxide scale of coated specimen mainly consists of oxides of Cr, Ni, whereas S and Na have diffused in to the coating (Shukla et al., 2012). The coating performed well and protected the 310S substrate material.

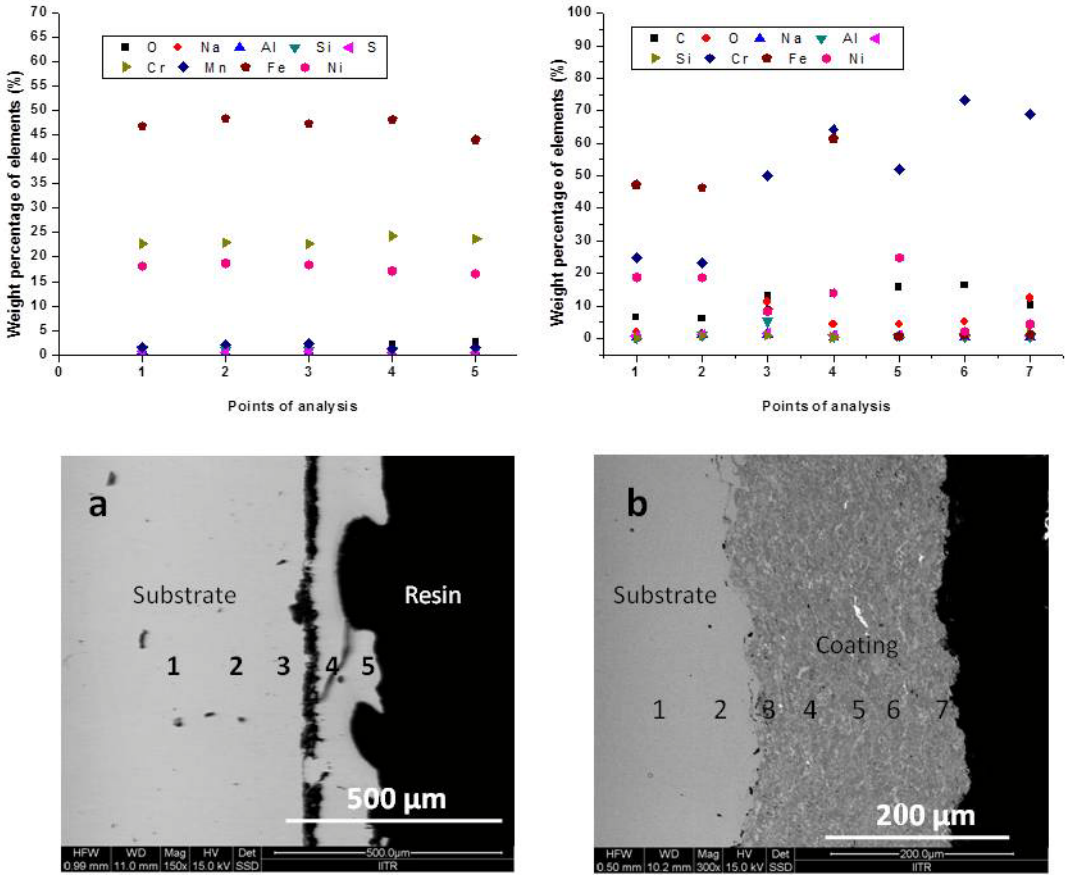

Fig 4.43: Morphology of oxide scale across the cross section of (a) 310S alloy substrate, and (b) Cr_3C_2- 25%NiCr coated alloy substrate exposed to superheater of the coal fired boiler at 700±10 ^{0}C for 1500 hours.

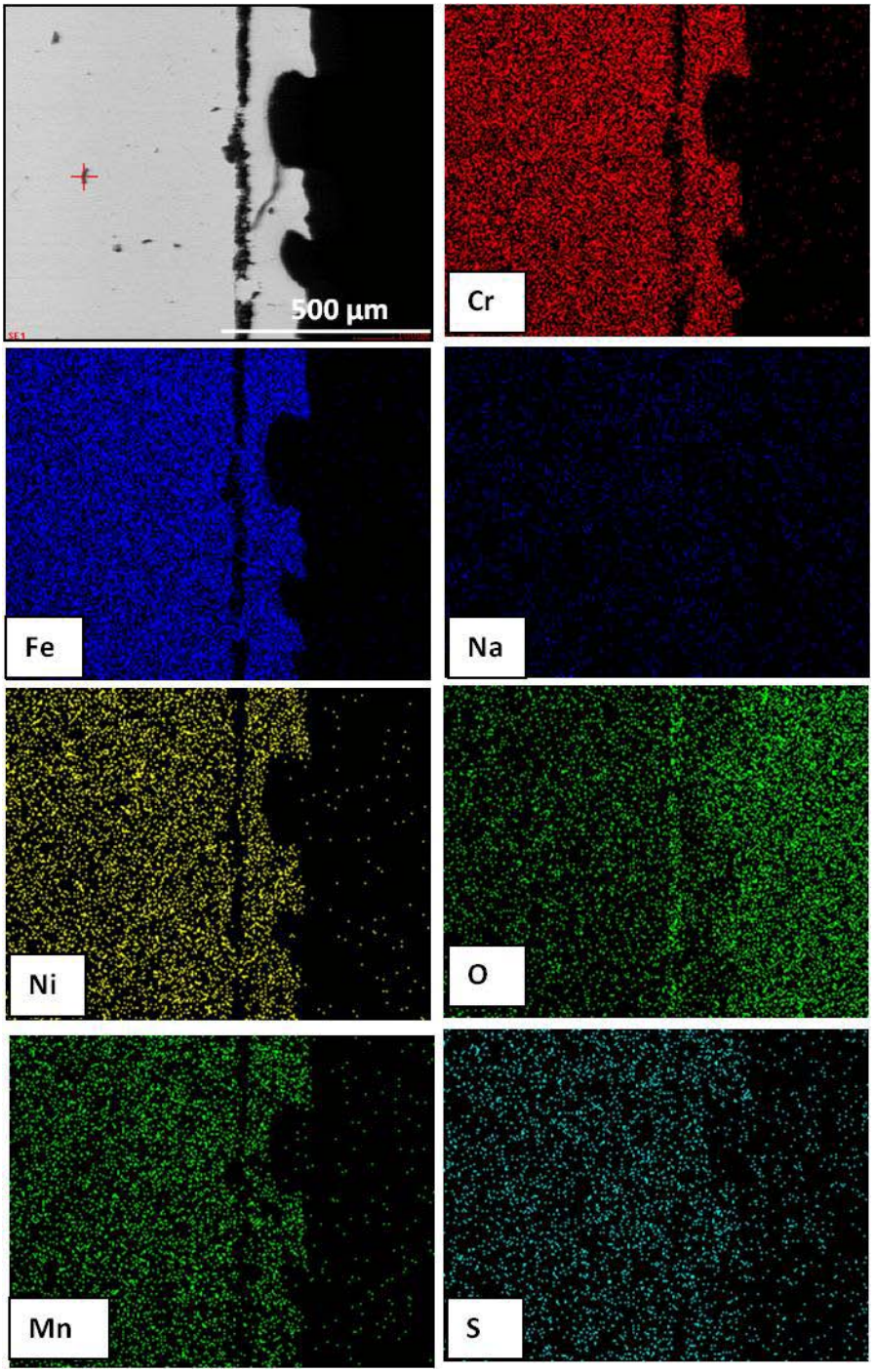

Fig 4.44: Composition image (SE) and X-ray mapping of the cross section of the bare alloy substrate subjected to subjected to hot corrosion in actual boiler environment at 700±10 ^{0}C for 1500 hours.

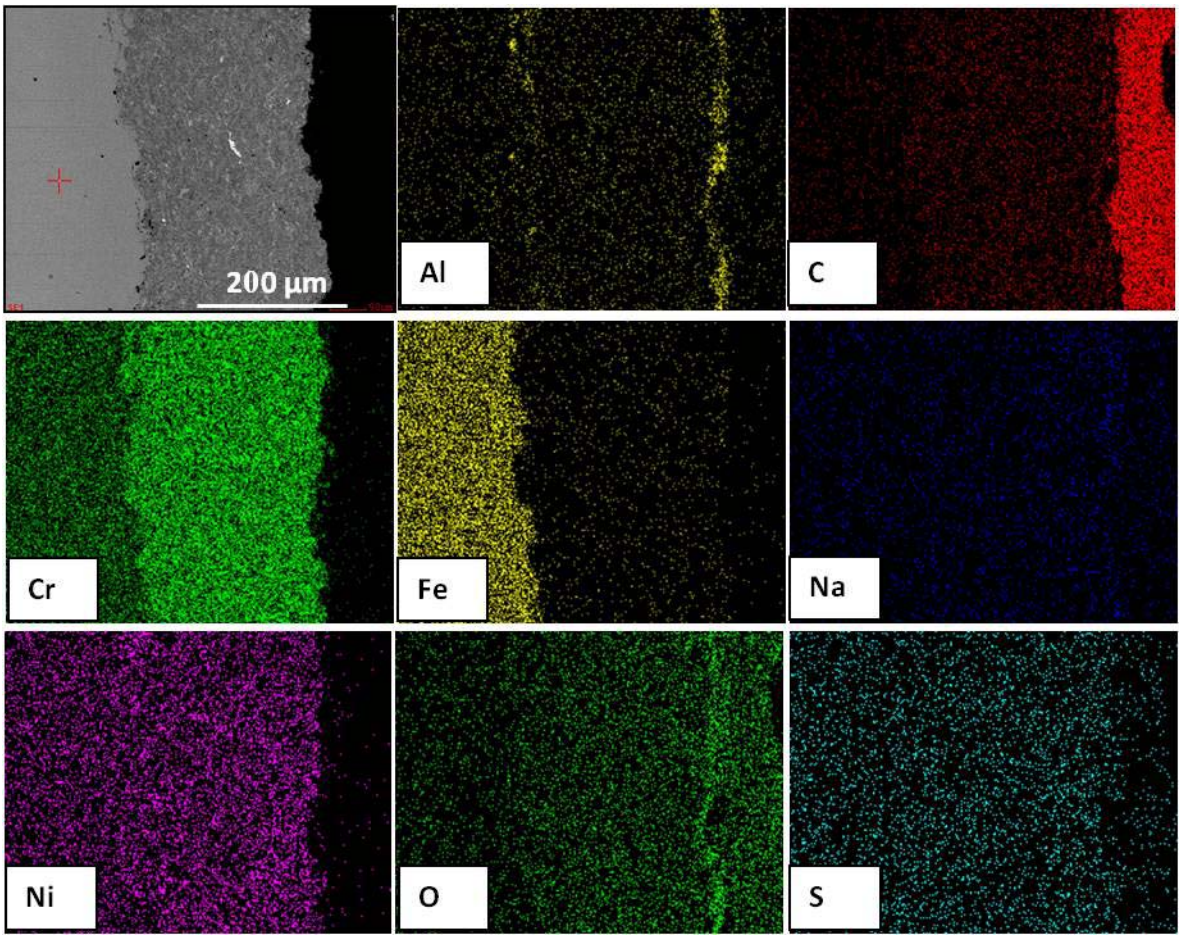

Fig 4.45: Composition image (SE) and X-ray mapping of the cross section of the coated specimen subjected to subjected to hot corrosion in actual boiler environment at 700±10 ^{0}C for 1500 hours.

4.5.2.3 X-ray diffraction analysis (XRD) analysis

The XRD patterns of the scale formed on uncoated and coated specimens after hot corrosion in actual boiler environment at 700±10 ^{0}C for 1500 hours are shown in Fig. 4.46. The major and minor phases detected at the surface of the specimens are shown in the XRD graph. The various phases identified from the X-ray diffraction (XRD) patterns of the corroded uncoated specimen subjected to real environment of boiler at 700±10 ^{0}C are shown in Fig 4.46. Cr_2O_3 and Fe_2O_3 are observed as the major phases. The XRD diffractograms for the coated specimen subjected to hot corrosion in actual boiler environment at 700±10 ^{0}C for 1500 hours revealed the formation of Cr_2O_3 as very strong phases whereas Ni_3S_4 and Fe_2O_3 are present as low intensity phases.

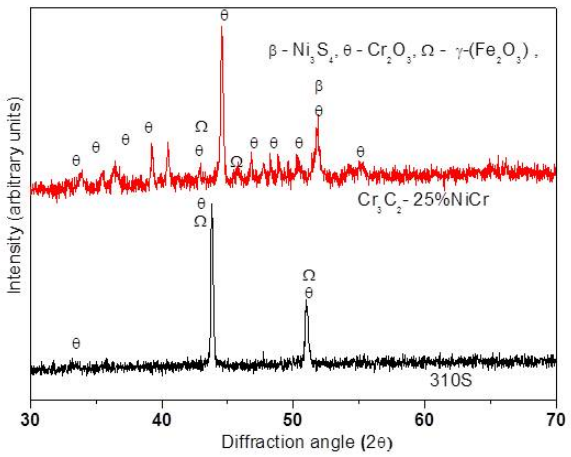

Fig 4.46: The XRD patterns of the scale formed on (a) bare and (b) coated specimens, subjected to hot corrosion in actual boiler environment at 700±10 ^{0}C for 1500 hours.

4.5.3 Discussion

The less weight gain of uncoated substrate compared against coated specimen is probably due to oxide scale spallation in the real coal fired boiler environment and molten salt fluxing along with oxide scale erosion. The general ash deposit obtained on the boiler super heater surface is $Na_2O.V_2O_4.5V_2O_5$, which melts at 550^{0}C. Also, above the melting point, this material corrodes metals by long-term contact (Sidhu and Prakash, 2006P). The accumulation of low melting point salts from flue gas on the fire side surface of the boiler tubes indicates hot corrosion and is considered a route cause for tube material wastage (Sidhu et al., 2005 C).

4.5.4 Conclusions

- Accelerated oxidation occurred for bare 310S alloy. The spalling of the oxide scale occurred during in real boiler environment at 700±10 °C. The steel suffered from larger weight loss than coated specimen.

- The HVOF sprayed Cr_3C_2–NiCr coating was successful in keeping adherence on the steel in real boiler environment at 700±10 °C.

- The coated substrate exhibited improved resistance to erosion and oxidation than uncoated specimen.

- The formation of Cr_2O_3 rich oxide scale probably contributed to the improved resistance to oxidation and erosion.

- Cr_3C_2-25NiCr coated specimens exhibited excellent oxidation and wear/spallation resistance.

CHAPTER - 5

FeCr based conventional coating

Characterization, oxidation and hot corrosion behavior of FeCr based conventional coatings deposited on 310S alloy substrate by High velocity arc spray process (HVAS) are described in this chapter. The cyclic oxidation r and hot corrosion studies were performed at an elevated temperature of 700^{0}C and 900^{0}C in air, Na_2SO_4-60%V_2O_5, Na_2SO_4-82%$Fe_2(SO_4)_3$ molten salt environments for 50 cycles and coal fired actual boiler environments at 700 ±10^{o}C for 1500 hours, respectively. The weight change measurements for coated and bare substrate were made to substantiate its oxidation kinetics through the evaluation of the parabolic rate constants, thereby evaluating protective nature of the coatings. The microstructural characteristics of the corroded products were analysed by using techniques such as XRD, FE-SEM/EDS and X-ray mapping to understand the mode of oxidation and hot corrosion.

5.1CHARACTERIZATION OF THE COATING

5.1.1 Introduction

Huge amounts of material wastage occurs due to high temperature oxidation and erosion of boiler tubes in steam generating system of coal fired boiler and power generation industry, resulting in tube wall thinning and premature failure (Kaur et al., 2011; Singh et al., 2005A). It is known that a single material can not satisfy variable needs of industry with combination of both mechanical and corrosion resistance properties. Therefore, a composite system comprising of base material and wear/corrosion resistant protective surface layer could be the most favorable choice for combining both mechanical and corrosion resistance properties.

Literature reveals that the thermal spray process was extensively used to fabricate wear and corrosion-resistant coatings, which improve service life time and wear/corrosion resistance of the component used in hot section of gas turbines, steam turbine, power generation industry, coal fired boiler. HVAS process is preferred for the deposition of FeCr base coatings on bare substrate compared to other thermal spray techniques such as plasma spray, detonation gun spray, flame spray owing to its capability to develop coatings with dense, homogeneous microstructure with lower oxide content and minimal heat transfer to the substrate, cost effectiveness, high efficiency of the process (Abedini et al., 2006; Jandin et al., 2003, Xiong et al., 2008; Cheng et al., 2009) Therefore, a composite system comprising base material and FeCr based protective surface layer is the best choice in combining material properties.

In spite of the progress made so far, a systematic investigation is necessary to further improve mechanical properties and resistance to oxidation and hot corrosion and of coatings. Limited information

on the use of HVAS sprayed conventional FeCrBMnSi alloy (CC) coatings in the literature. In the present work, coatings have been characterized in terms of microstructure, porosity, thickness of coating, phase evolution and microhardness properties using several analytical techniques such as FE-SEM/EDS, X-ray mapping and XRD in order to provide an experimental basis and to enlarge applications of HVAS sprayed FeCr based alloy coatings in the coating industries.

5.1.2 Experimental Details

The details of the substrate material, coating formulation and characterization of the coating are discussed in Chapter 3.

5.1.3 Results

5.1.3.1 Morphology of the coating powder

The morphology of the feedstock wire material used for coating and as-sprayed coatings was investigated by FE-SEM. Fig. 5.1(a) shows the cross sectional view of cored wire and Fig. 5.1(b) shows the morphology of the irregular shaped initial feedstock powder particles present inside the cored wire.

5.1.3.2 FE-SEM/EDS analysis of the coating

FE-SEM images of the CC coating are shown in Fig. 5.2(a, b). The coating exhibits dense morphology without any micro cracks. The loose particles were not found in the coatings. The globules of sprayed splats are observed in the coatings. Fe, Cr are observed as major elements and Si, Mn, O, B as minor elements are observed in the EDS results of the coatings.

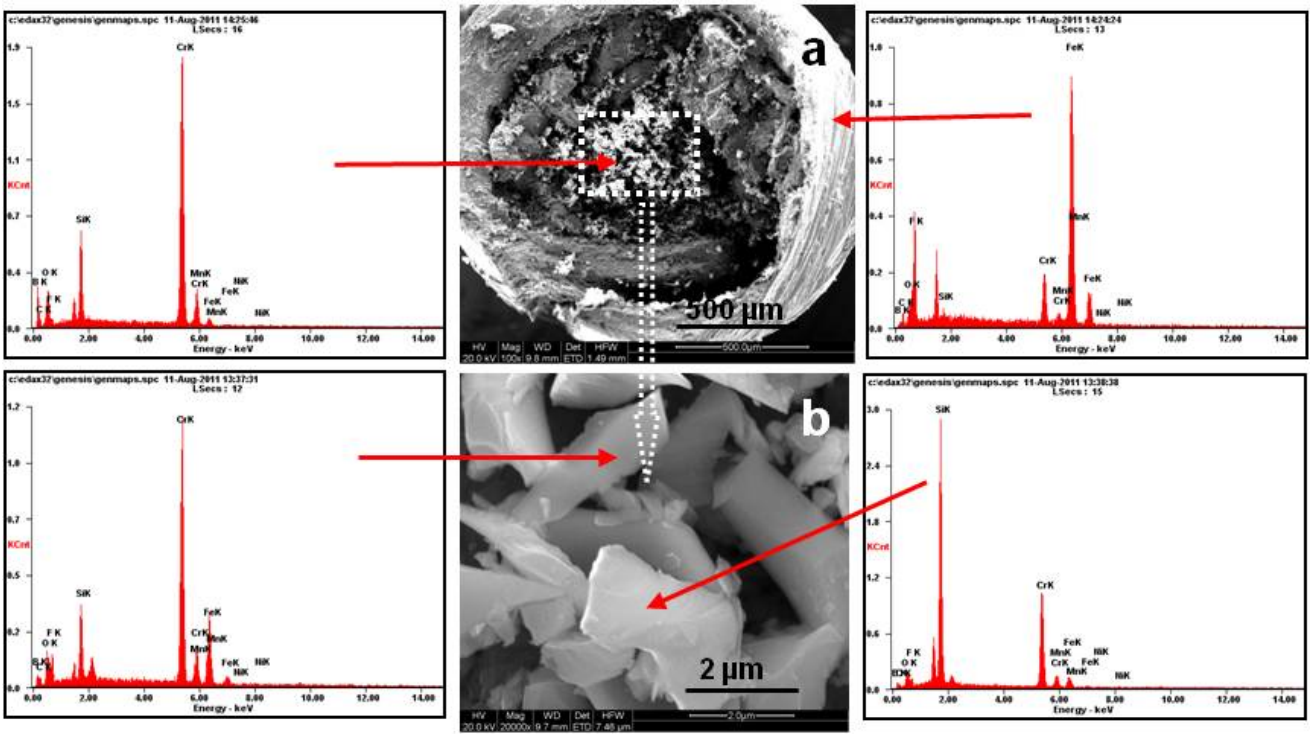

Fig 5.1: FE-SEM/EDS with EDS analysis showing the inclined cross section of cored wire (TAFA 95MXC).

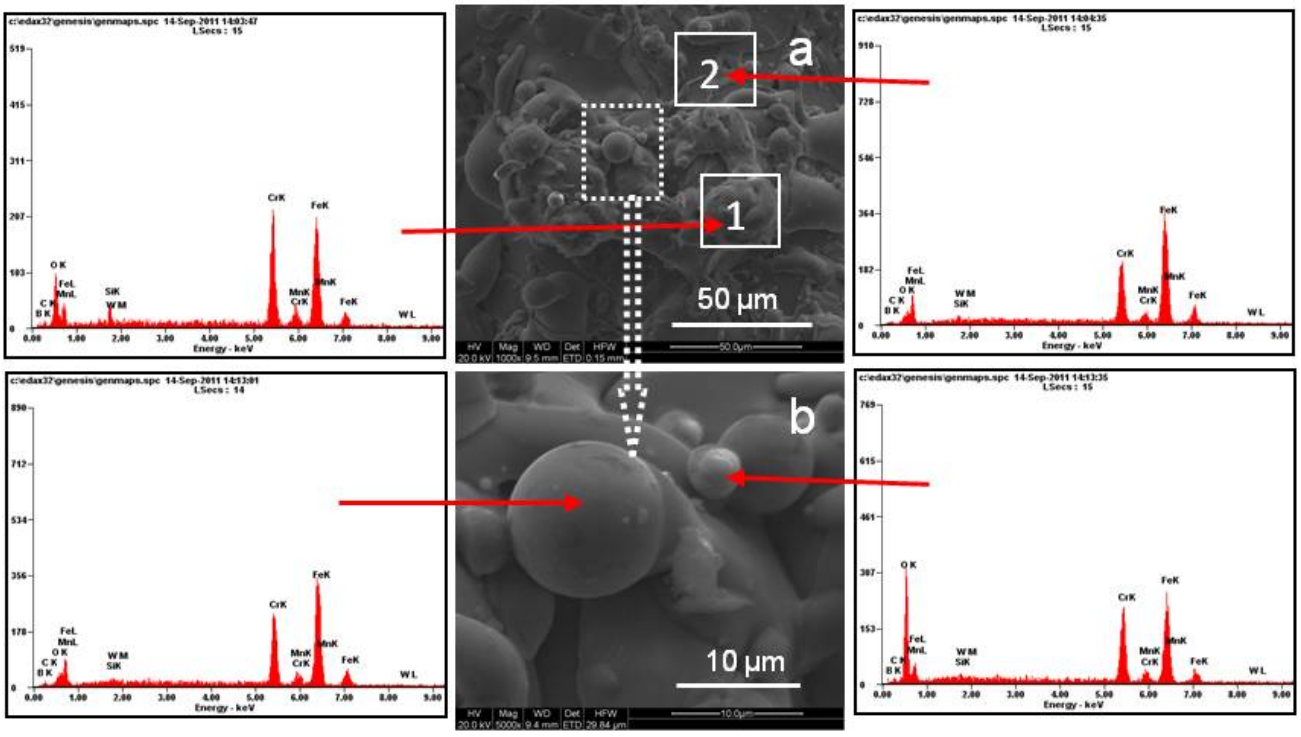

Fig 5.2: FE-SEM/EDS with EDS analysis showing the surface morphology for the as-sprayed coating on 310S substrate.

5.1.3.3 Surface roughness of the coated specimen (CC)

The surface of the as-sprayed coated specimen (CC) was rough and the average R_a value was around 26.59 µm (Fig. 5.3).

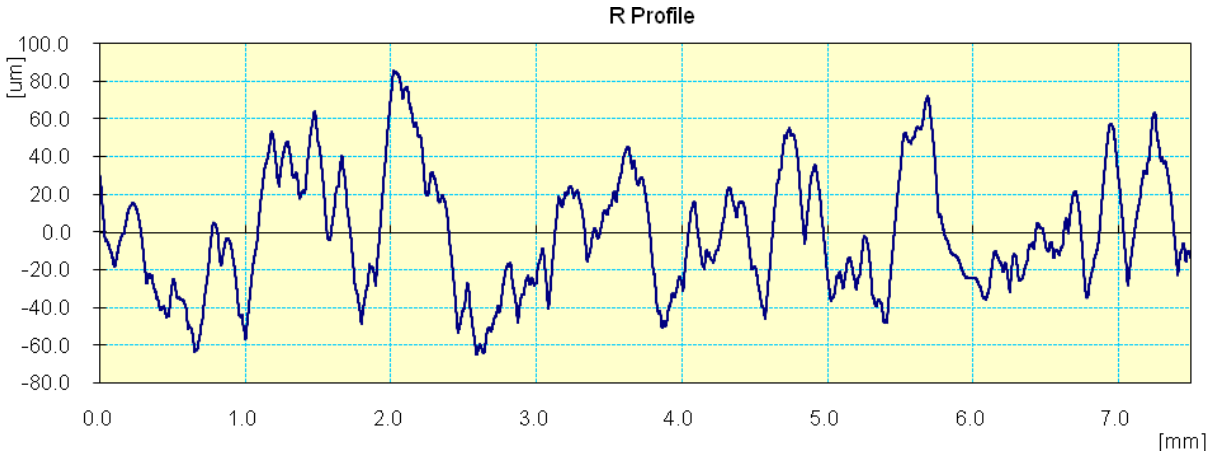

Fig 5.3: Surface roughness profile of the as-sprayed coating(CC).

5.1.3.4 Porosity of the coating

The coating porosity influences corrosion or high temperature oxidation as it provides preferential ways through which corrosion products can penetrate the coating and reach the substrate thereby reduce corrosion resistance of coating. The porosity of the HVOF sprayed coatings is found to be less than 3.4%, which reveals that coating is dense.

5.1.3.5 Bond strength of the coating

The bond strength of CC coating was measured on three specimens as discussed in section 3.3.4. An average strength of 6k psi was found for the CC coating.

5.1.3.6 Microhardness of the coating

Micro hardness of the FeCrBMnSi alloy coating was determined across the cross-sectioned samples. The microhardness data of the coatings are compiled in Fig.5.4b, it was found to be in the range of 630-1060 HV. It varies with distance from the coating–substrate interface. The maximum microhardness measured for the coating is about 1060 Hv.

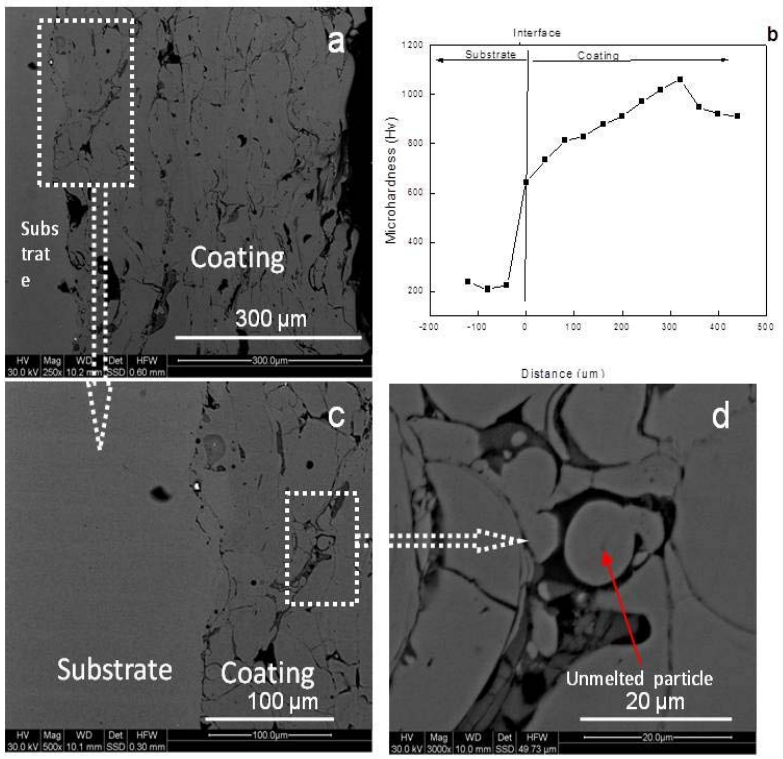

Fig 5.4: Cross sectional micrograph showing the morphology of the developed coating

5.1.3.7 X-ray diffraction (XRD) analysis

XRD pattern of the as-sprayed FeCrBMnSi coating shown in Fig. 5.5 reveals the presence of FeCr phase on the as-sprayed coating surface.

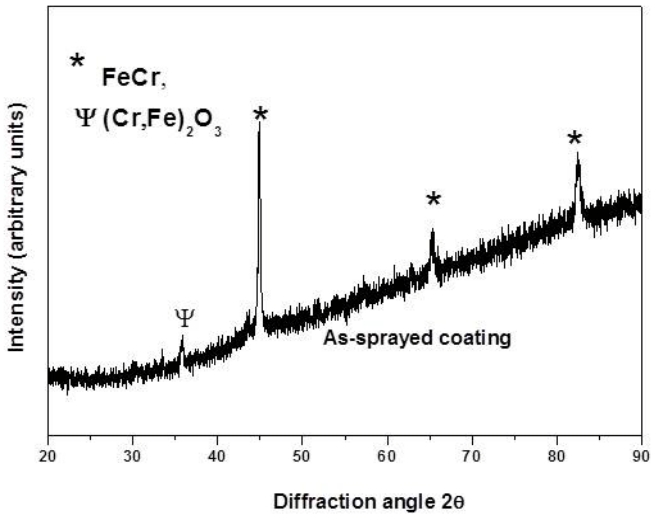

Fig 5.5: XRD diffraction for the as-sprayed coating

5.1.3.8 Cross-sectional analysis and X-ray mapping

The BSE images at the cross-section of CC coating on 301S alloy substrate by FE-SEM/EDS and the results are shown in Fig. 5.4a & 5.6. It clearly shows the formation of dense uniform and adherent splats like structure with some unmelted particles and pores. The major portion of CC coating is covered with Fe and Cr. Elemental X-ray mapping of the coating shows (Fig. 5.7) that the coating area is found to be rich with the main elements of the coating powder. Elemental mapping also indicates diffusion of small amount of Ni from the substrate to the coating.

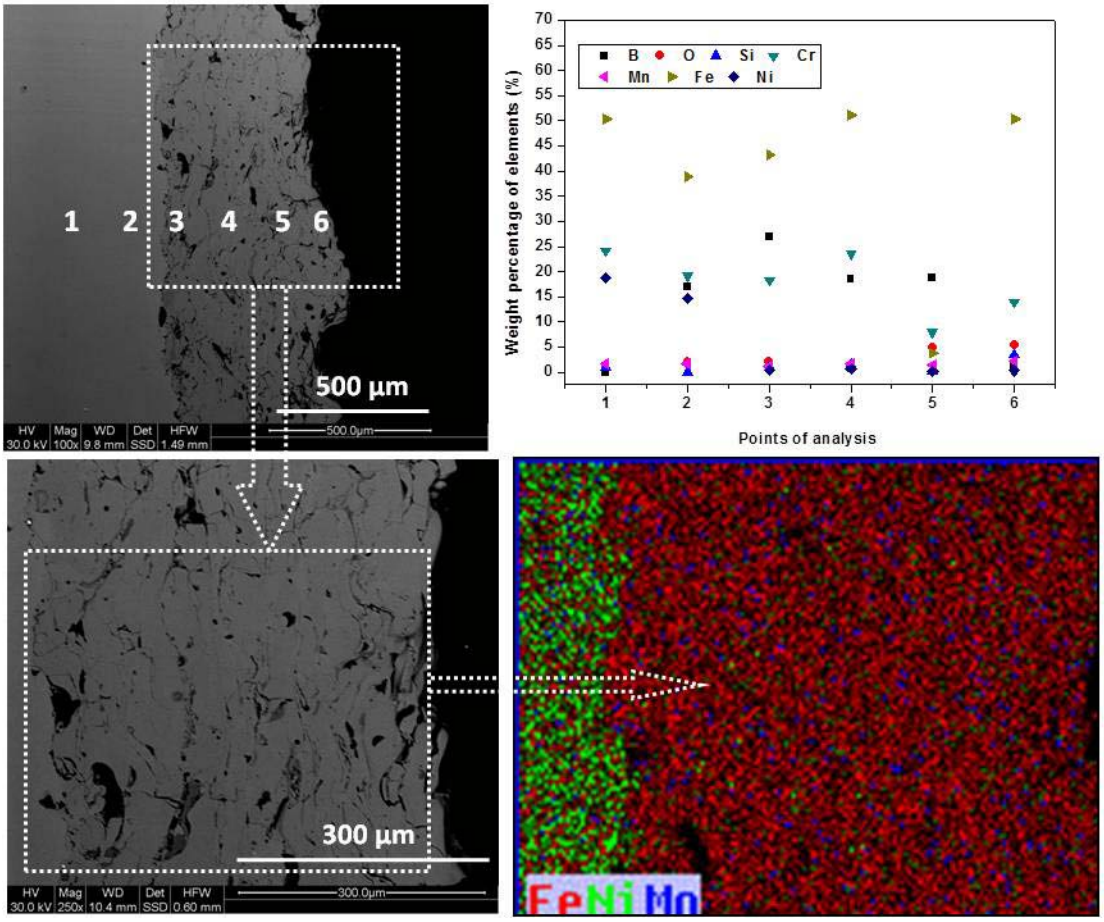

Fig.5.6 FE-SEM/EDS analysis at the cross-section of as sprayed coated specimen (CC).

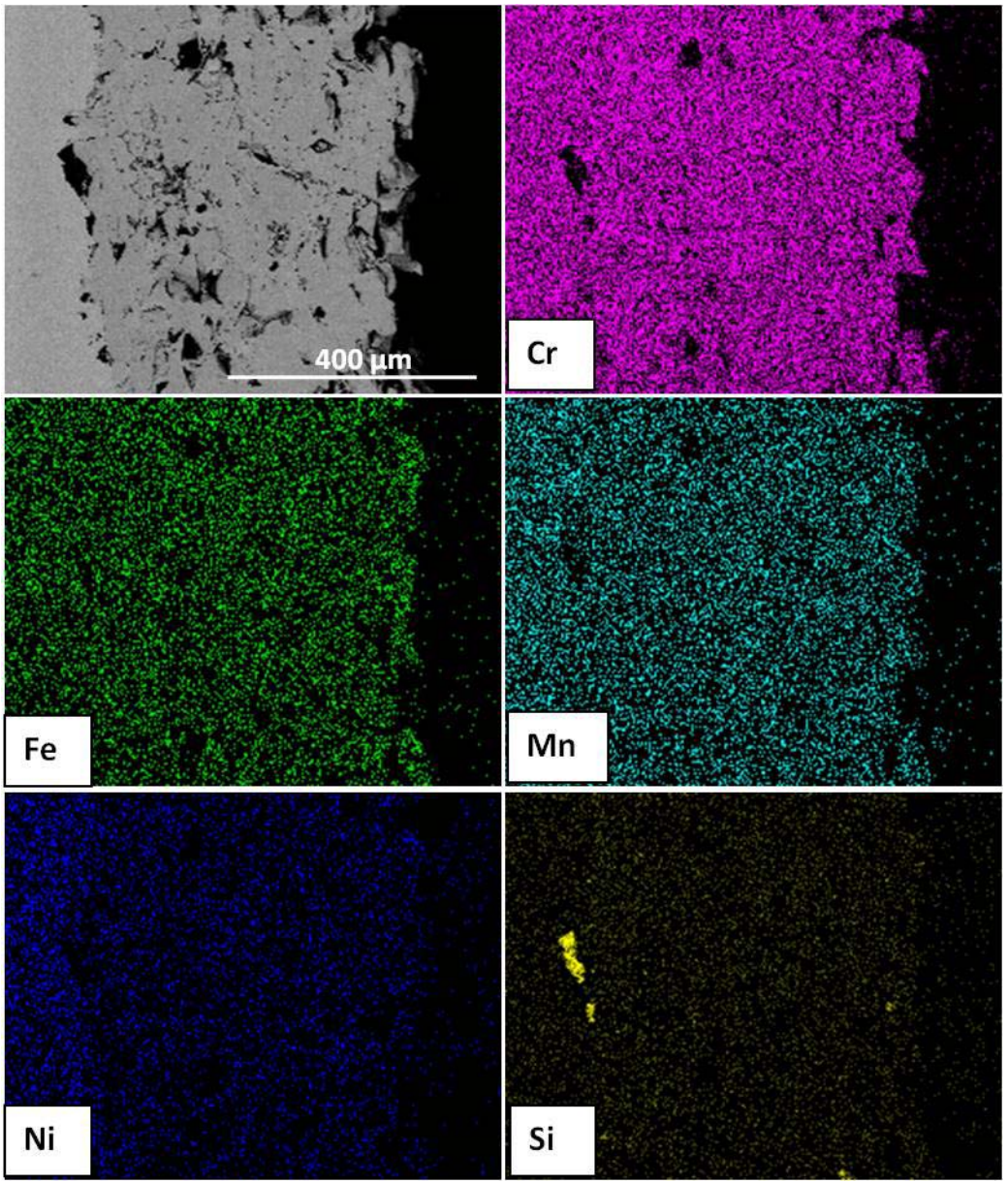

Fig.5.7 X-ray mapping of as-sprayed coated specimen (CC) on 310S alloy substrate.

5.1.4 Discussion

Experimental results indicate that uniform and crack-free coating was obtained by HVAS coating of FeCrMnBSi on steel substrate. The micropores in the coatings have a significant role to play as far as the corrosion of thermal spray coatings is concerned, as they can provide a pathway to the reactive corrosive elements (Choi et al., 2002) through which the corrosion species can penetrate the coating to reach the substrate and may cause rapid corrosion attack. However, the black contrast regions observed in Fig, 5.6 reveals small amount of porosity on the coated surface. Porosity measurements also indicate 3.5% porosity. Such a small amount of porosity was probably due to high velocity of incident particles and did

not affect the strength of the coating. FE-SEM micrographs corresponding to the surface morphology of as- sprayed and polished surface morphology of as sprayed coating are shown in Fig.5.2. The HVAS surface also shows incompletely melted particles. The microhardness of HVAS coating was high as compared to the bare substrate (Fig.5.4b). The observed variation in microhardness of the coating was probably due to the presence of un-melted and partially melted particles.

5.1.5 Conclusions

The HVAS process was employed to deposit FeCrBMnSi alloy (CC) coatings on 310S alloy substrate The coatings were characterized for their microstructural characteristics, and mechanical properties. Major observations are listed here.

- FeCrBMnSi alloy (CC) coatings on 310S were fabricated by the HVAS process.
- A good adhesion of the coatings with the substrate was evident as there is no sign of cracks and gaps at the interface.
- The as-sprayed coatings consisted of smooth and dense structure.
- The microhardness of the as sprayed coating was found to be in the range of 630–1060 Hv.

5.2 OXIDATION STUDIES IN AIR

5.2.1 Introduction

Corrosion is a major problem in superheater of coal fired boilers. Degradation of components occurs due to high temperature oxidation and hot corrosion of boiler tubes in steam generating system of power generation industry. Large amounts of wastage of material due to the combustion of fuels are commonly observed in superheaters. There is a wide contribution of thermal sprayed coatings for the protection of turbine engine and boiler tubes against high temperature corrosion (Kim et al., 1996, 1998 & 2002, Klimenko et al., 1979; Ko et al., 2002, Li et al., 1996, 2000, 2004, Mitra et al., 1993, Sidhu et al., 2005A). In recent times, interest has been increasing in producing iron-based alloy coatings owing to their high strength and hardness, superior resistance to wear and corrosion. The degradation mechanisms of high velocity arc sprayed FeCr based alloy coatings exposed to high temperature environment at 700ºC and 900^0C under cyclic conditions is scarce in the literature.

Limited information is available on the influence of microstructural characteristics on the oxidation behavior of CC coatings and material degradation mechanisms of coatings at high temperature environment (700^0C & 900^0C) when exposed to short periods (10 cycles, 30 cycles) in air under cyclic condition is limited in the literature. So, the present study has been aimed to study the microstructural changes and degradation behavior of CC coatings after exposure of 10, 30, 50 hours at 900^0C by using FE-SEM/EDS, XRD, and thermo gravimetric techniques, respectively. The microstructural features of the coatings were correlated with the degradation behavior of coatings.

5.2.2 Experimental details

The substrate material, coating formulation and the oxidation studies are explained in detail in section 3.1, 3.2.3 and 3.4.1.

5.2.3 Results

5.2.3.1 Weight change measurements

The weight change (mg/cm^2) versus number of cycles plot for the coated coupons during cyclic oxidation at 700ºC and 900^oC, in air environment are shown in Fig. 5.8a. The coated coupons show significant weight change at 900ºC as compared to at 700ºC. The coated coupons approaches a steady state after a gradual increase in weight during the initial 20 cycles of the study at 700^oC. However, weight gain is high with some spalling in the coatings up to 50 cycles at high temperature (900ºC). The weight gain did not increase rapidly for coated coupons after exposure at 700^oC for 50 hours, confirming the higher corrosion resistance of the coatings. A parabolic relationship is observed for the oxide growth in the coatings at 700ºC and 900ºC (Fig.5.8b). The degradation kinetics of coatings at 700ºC and 900ºC

follows approximately parabolic relationship as observed in the present work. The calculated parabolic rate constants K_p values of the coated specimens are 3.61 x 10^{-12} $g^2cm^{-4}s^{-1}$ and 15.2 x 10^{-12} $g^2cm^{-4}s^{-1}$ at 700^{o}C and 900^{o}C, respectively. The K_p value for the coated specimen at 900ºC is higher than that of the sample exposed at 700ºC. The degradation of coatings at the beginning is chemically controlled due to the large thermodynamic driving force available for the formation of oxides. As and when the oxide covers the whole surface of the coatings, the reaction kinetics transforms to diffusion controlled mode, in which the oxide scale acts as a diffusion barrier. It precludes further degradation of coatings due to lack of direct contact between coating and atmosphere.

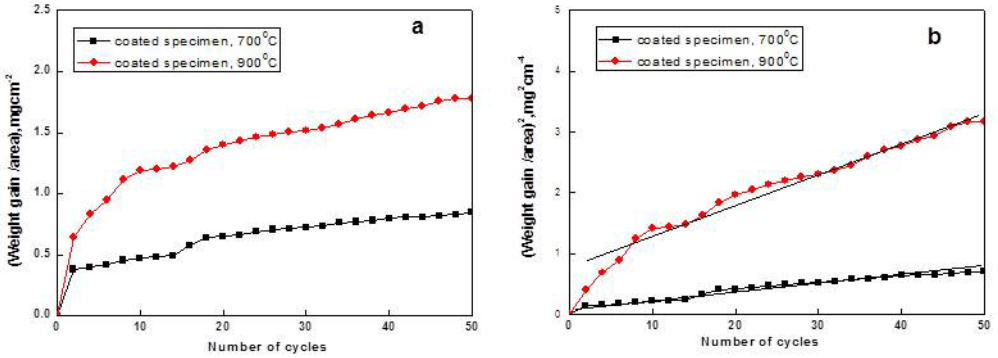

Fig 5.8: Weight gain/area versus number of cycles and (Weight gain/area)^2 versus number of cycles plot (a, b) for the coated specimen (CC), after cyclic oxidation of 50 cycles in air at 700º C and 900^0 C.

5.2.3.2 FE-SEM/EDS analysis

5.2.3.2.1 Surface morphology of the scales

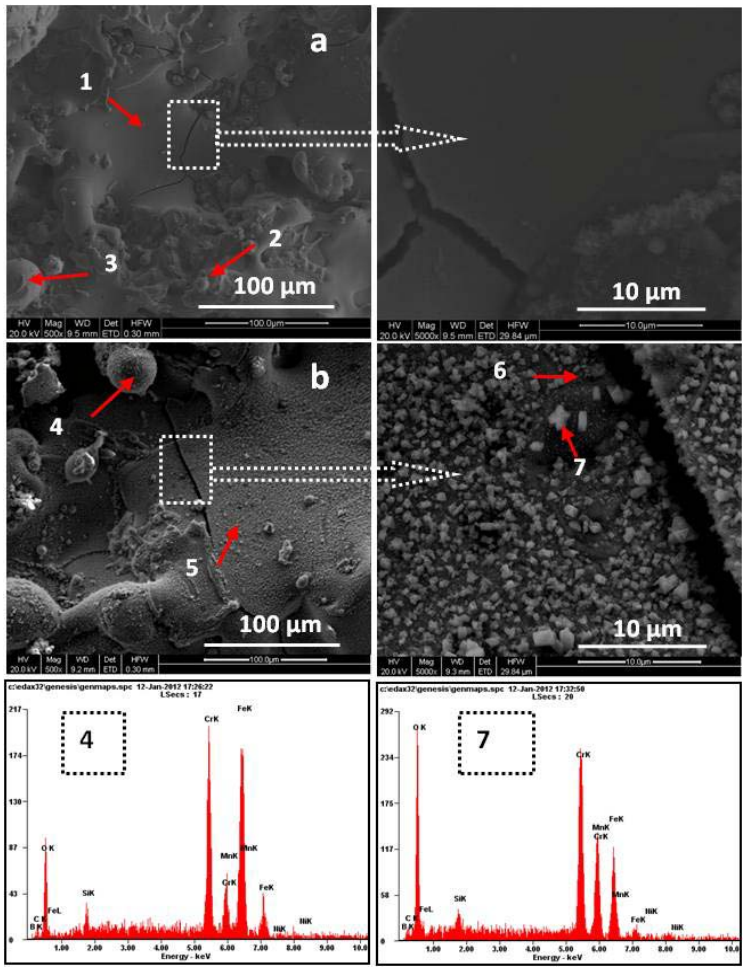

Fig 5.9: Surface morphology of coated specimen (CC) after (a) 10 h, and (b) 50 h oxidation cycles at 700^0C.

Table 5.1: EDS analysis results (wt. %) corresponding to Fig. 5.9 for the coated specimen subjected to cyclic oxidation in air at 700º C.

Elements	Fe	Cr	B	Si	Mn	Ni	O
1	52.59	23.63	12.80	1.66	1.63	0.58	4.19
2	52.98	23.19	11.62	1.60	1.78	0.51	4.88
3	53.48	24.19	10.81	1.81	2.10	0.52	4.43
4	50.50	27.58	0	2.22	6.46	0.81	8.20
5	35.53	30.89	7.28	1.51	8.61	1.36	12.17
6	15.93	26.58	17.43	1.07	14.45	0.71	18.98
7	53.21	23.57	6.45	1.64	2.97	1.36	8.76

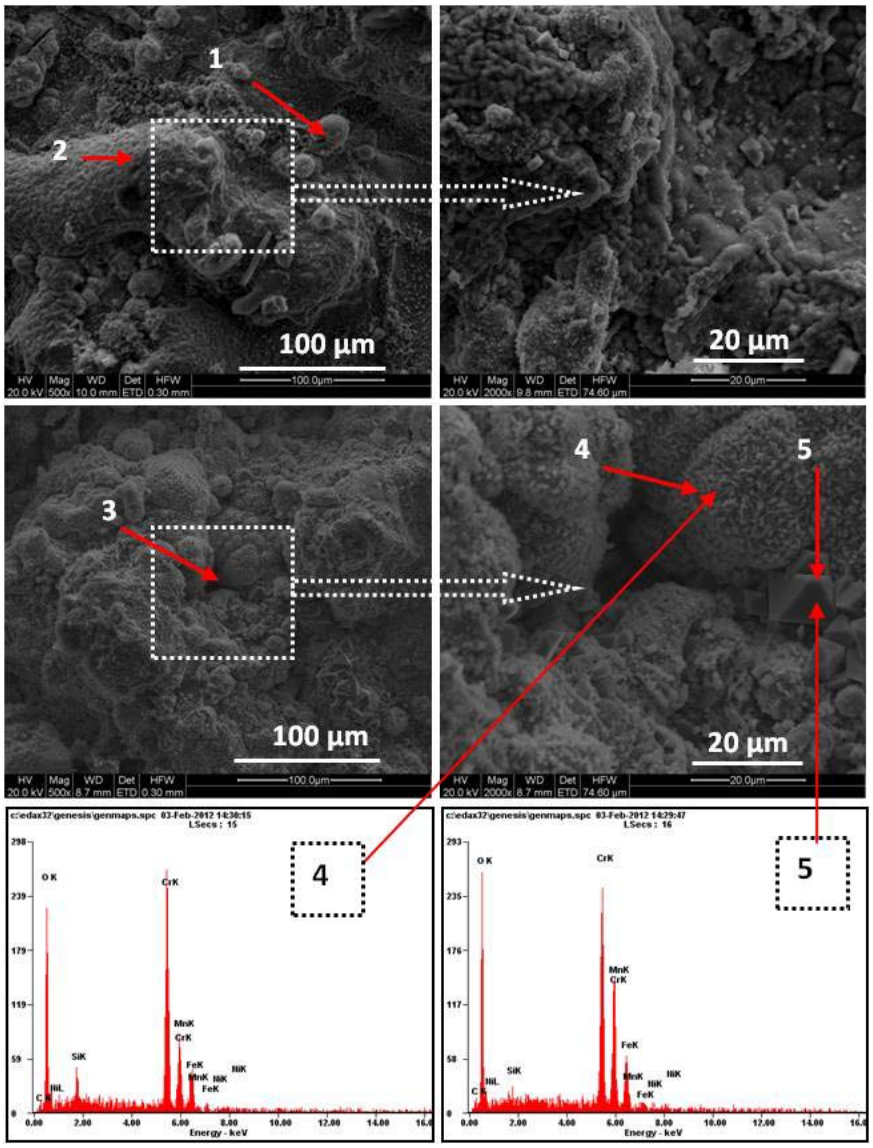

Fig 5.10: Surface morphology of coated specimen (CC) after (a) 10 h, and (b) 50 h oxidation cycles at 900^0C.

Table 5.2: EDS analysis results (wt. %) corresponding to Fig. 5.10 for the coated specimen subjected to cyclic oxidation in air at 900º C.

Elements	Fe	Cr	B	Si	Mn	Ni	O
1	56.34	24.51	1.31	0	3.69	0.86	13.28
2	4.39	51.33	2.11	1.05	25.45	1.40	13.97
3	23.74	57.49	0	0.34	15.64	1.05	1.58
4	5.76	48.20	0	0.83	42.86	0.26	2.09
5	13.43	43.78	4.98	2.76	11.36	1.05	22.63

Morphology of surfaces of oxidised coatings at 700ºC and 900^0C as a function of different exposure periods is shown in Fig. 5.9 and Fig. 5.10, respectively. FE-SEM analysis of the coated surface at 700ºC indicates some micro crack and free oxide particles upon 10 cycles of oxidation (Fig 5.9a). The thick

layers of oxides are observed after 50 cycles (Fig. 5.9b). The major presence of Cr, O, Fe along with minor presence of B, Mn, and Si in the coatings is observed as evident from EDS analysis (see Table 5.1). The spalling of the oxide scales is observed after degradation of the coatings as shown in (Fig. 5.9a, b).

The globular morphology is observed on surface of the oxidized coated specimen at 900ºC after 10 cycles of oxidation (fig 5.10a). It indicates the presence of Cr, O, Fe as well as minor amount of B, Si, and Mn (see Table 5.2). On the other hand, the surface is completely covered by globular morphology after oxidation for 50 cycles (Fig 5.10b). The globular morphology of the coatings shows the major presence of Fe, Cr, O. The presence of $(Cr, Fe)_2O_3$ (see Fig. 5.12) is evident from XRD results of coated specimen after 50 cycles of oxidation at high temperatures. The corroded products showed the formation of $(Cr, Fe)_2O_3$ after 50 cycles of oxidation of the coatings at 700^{o}C and 900^{o}C.

The cross-sectional analyses and X-ray mapping of different elements of the coated coupons subjected to cyclic oxidation in air at 900^{o}C after 50 cycles are shown in Fig. 5.11. Figure 5.11 indicates that the scale mainly consists of oxides of Fe and Cr along with significant amounts of Ni. The continuous, dense morphology of the oxide scale is observed and it is adherent to the substrate. The scale mainly consists of oxides of Cr and Fe as shown in Fig. 5.11.

5.2.3.2.2 Cross-sectional analysis and X-ray mapping of the scale

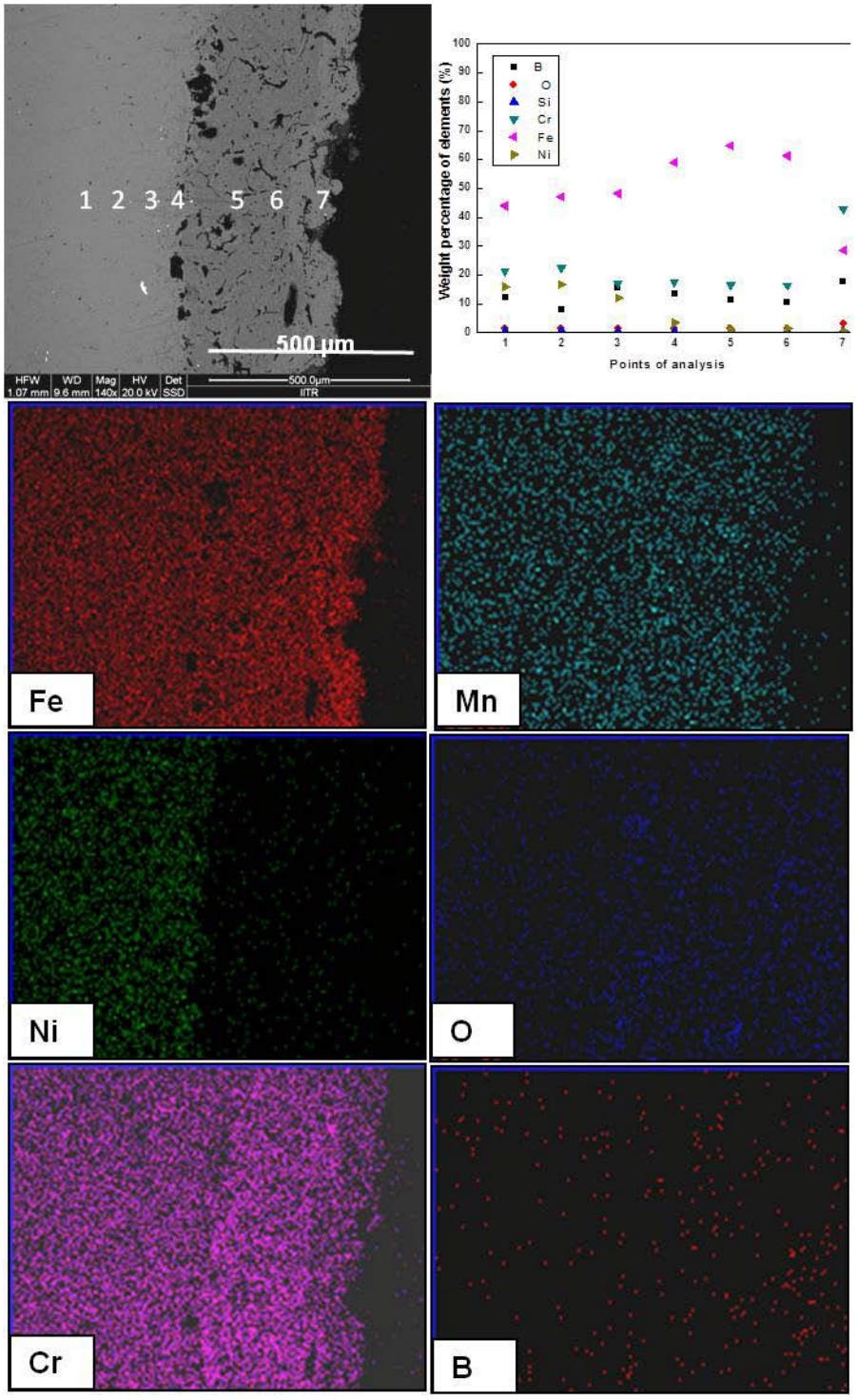

Fig.5.11 Fe-SEM/EDS analysis across the cross-section and X-ray mapping of the coated specimen (CC) subjected to cyclic oxidation at 900 ^{o} C in air after 50 cycles.

5.2.3.3 X-ray diffraction analysis (XRD) analysis

Various phases identified by XRD analysis of the oxidized uncoated specimen at 700^{o} C and 900^{0}C in air after 50 cycles are shown in Fig 5.12. The XRD diffractograms for the coated specimen after 50 cycles of exposure to air at 700^{o}C indicates the formation of Cr_2O_3, FeCr, and Fe_2O_3 phases.

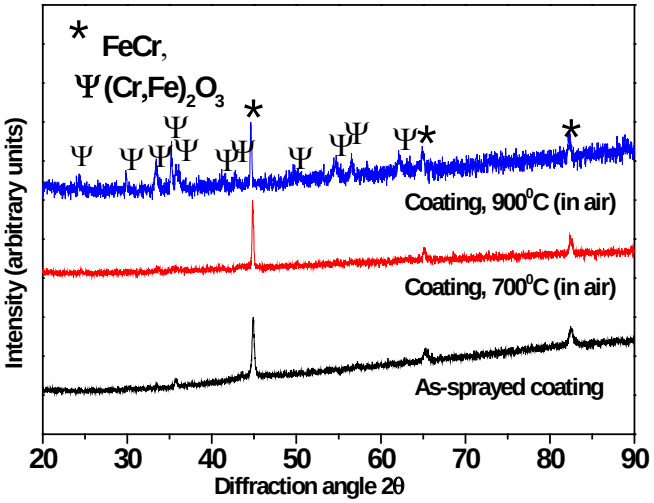

Fig 5.12: The XRD patterns of the scale formed on coated specimen (CC) after cyclic oxidation of 50 cycles in air at 700^{0} C and 900^{0} C.

5.2.4 Discussion

Although high temperature oxidation behavior of coatings are well studied, the formation of different phases, interdiffusivity of alloying elements, and protective nature of scales formed under shorter exposure periods to high temperature environment (700 ^{o}C & 900^{o}C) are completely different as evident from the XRD, SEM/EDS, and X-ray mapping results obtained in the present work. The behavior of HVAS sprayed coatings at high temperatures depends on the various factors like porosity, inclusions, oxides and size and shape of the splat microstructures. The high temperature cyclic oxidation behavior of coated specimens follows a parabolic trend as evident from the results of thermogravimetric data reported in Fig 5.8. Such a trend is attributed to the diffusion mechanism operating at high temperature cyclic conditions. The possible oxidation modes of the HVAS sprayed specimen (CC) at 900^{0}C after 50 cycles are schematically represented in Fig. 5.13.

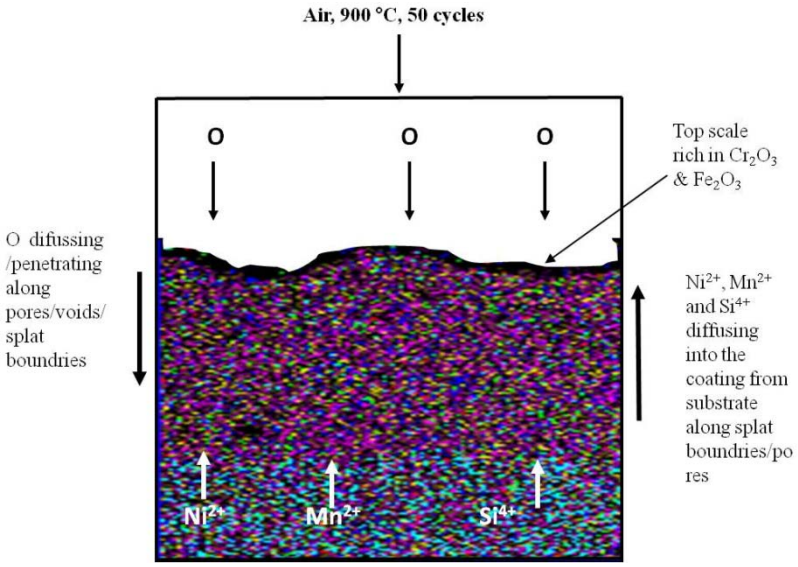

Fig 5.13: Schematic of the proposed oxidation mechanism of coated specimen (CC) at 900^0 C in air after 50 cycles.

5.2.5 Conclusions

- The parabolic rate constant value during oxidation was found to be one-half (at 700^0C) and one-third (at 900^0C) for the coated specimen as compared to that of uncoated specimen, which indicates that coating shows better oxidation resistance.
- FeCrBMnSi alloy coating exhibited excellent oxidation and wear/spallation resistance.
- The oxide of Fe and Cr preclude high temperature oxidation of the coatings.The formation of protective oxide layers such as Cr_2O_3 is responsible for imparting resistance against high temperature oxidation on the coated specimen.
- The diffusion controlled reaction upon formation of Cr_2O_3 films on the coatings surface limits the diffusion of aggressive species such as air and other impurities in to the coatings.
- The oxidation behavior of coated samples was found to obey a parabolic rate law.

5.3 HOT CORROSION STUDIES IN MOLTEN SALT ENVIRONMENTS

5.3.1 Introduction

Ni-based, Co-based and Fe-based super alloys have been developed to improve strength at elevated temperature and resistance to oxidation. Since these alloys are very costly, a composite system comprising of base material (steel) and wear/corrosion resistant protective surface layer has been proposed as most favorable choice of material for combining both mechanical and corrosion resistance properties as reported in the literature. Literature reveals that the thermal spray process is widely used to produce wear and corrosion-resistant coatings on the components used in hot section of power generation industry and coal fired boiler (Bala et al., 2012).

Thermal spraying systems cause little damage to the environment as compared to other deposition techniques such as physical vapor deposition (PVD), chemical vapor deposition (CVD), and electroplating techniques (Grewal et al., 2013). Nanostructured materials have received considerable interest for the enhanced corrosion and wear resistance (He et al., 2002). Recently, there has been increasing interest in producing Fe-base alloy coatings due to their high strength and hardness, superior wear and corrosion resistance (Wielage et al., 2013; Bakare et al., 2012). HVAS process is preferred for the deposition of FeCr base coatings on bare substrate compared to other thermal spray techniques due to its cost effectiveness (operating lower cost), high deposit efficiency and less applications difficulties (Xiong et al., 2008).

Studies on the degradation mechanisms of high velocity arc sprayed FeCr based alloy coatings exposed to molten salt (Na_2SO_4-60%V_2O_5) environment at 700^0C and 900^0C under cyclic conditions have not been reported so far. The reaction kinetics and microstructural changes of the oxide scales formed at high elevated temperatures in aggressive environment determine the failure of the components used in high temperature applications. Therefore, the present work has been focused to study microstructural changes and high temperature degradation behavior of FeCr-based coatings exposed to (Na_2SO_4-60%V_2O_5) molten salt environment at high temperatures (700ºC and 900^0C) for different periods. FE-SEM/EDS, XRD and thermogravimetric techniques were used to substantiate the mechanisms governing the high temperature degradation of materials.

5.3.2 Experimental details

The substrate material, coating formulation and the oxidation studies are explained in detail in section 3.1, 3.2.3 and 3.4.1.

5.3.3 Results

5.3.3.1 Weight change measurements

Weight change per unit area (mg/cm^2) versus number of cycles plots for the coated specimens exposed to molten salt (Na_2SO_4-60%V_2O_5) environment at 700^0C and 900^0C under cyclic conditions after 50 cycles is shown in Fig. 5.14. During the initial period, the oxidation of free surface of coated substrate resulted in a high oxidation rate. It has been observed that the coated specimen showed relatively higher weight gain in the early cycles subjected to oxidation, during first 20 cycles, were comparatively more as compared to the subsequently cycles up to 50. It can be attributed the development of shielding oxide films, during the initial cycles, which precludes further oxidation in the latter cycles.

The increased oxide grain size led to reduced density for the diffusion pathways, which resulted in a slow oxidation rate. Thus, the weight gain in the case of the oxidised coated specimen was lower than the uncoated specimen (310S alloy aubstrate). The weight gain/unit area results shown in Fig. 5.14(a) confirm parabolic rate law. The square of weight change (mg^2/cm^4) data Figure 5.14b indicates that the oxide growth can be approximated to a parabolic relationship in case of CC coated substrate, while no such law can be applied for the uncoated substrate. After 50 cyles of high temperature oxidation at 700^0C and 900^0C, the parabolic rate constants K_p values for the CC coating were calculated from the slope of linear regression fitted the line, and found to be 5.9 x 10^{-11} $g^2cm^{-4}s^{-1}$ and 9.36 x 10^{-11} $g^2cm^{-4}s^{-1}$, respectively. The K_p value for the bare substrate was found to be nearly twice of the K_p value of the coated specimen, which indicates that coating shows a better hot corrosion resistance.

Weight change plots for coated specimen (CC) subjected to molten (Na_2SO_4-82% $Fe_2(SO_4)_3$) salt environment at 700^0C and 900^0C for 50 hours are shown in Fig. 5.15(a). The CC coating exhibits less weight gain than uncoated specimens. The square of weight gain per unit area (mg^2/cm^4) data shown in Fig. 5.15(b) reveals that the parabolic rate constants K_p values for the CC coating after 50 cycles of high temperature oxidation at 700^0C and 900^0C were 4.14 x 10^{-11} $g^2cm^{-4}s^{-1}$ and 7.61 x 10^{-11} $g^2cm^{-4}s^{-1}$, respectively.

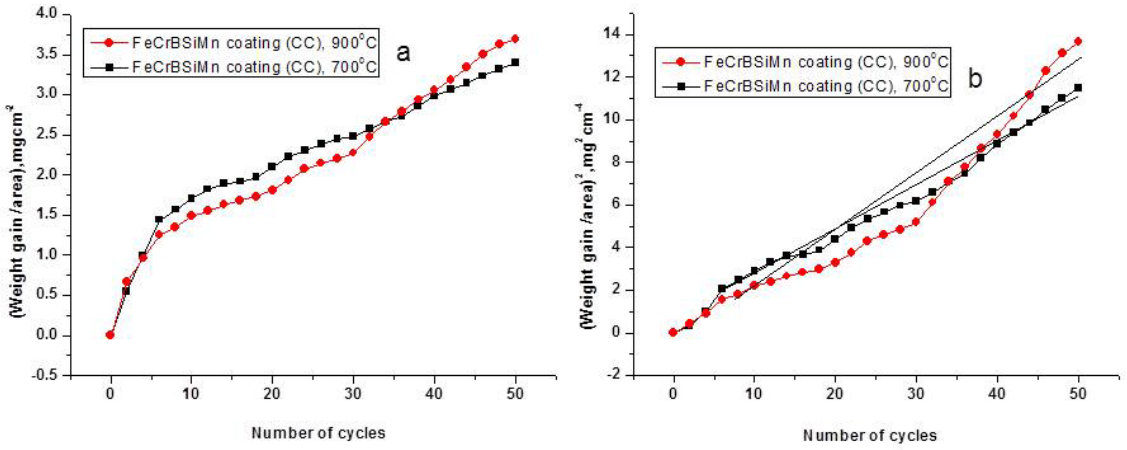

Fig 5.14: (a) Weight gain after oxidation per unit area versus number of cycles and (b) Weight gain after oxidation per unit area)^2 versus number of cycles, for coated specimens (CC) subjected to hot corrosion in molten salt (Na_2SO_4-60% V_2O_5) environment at 700^{0}C & 900^{0}C for 50 cycles.

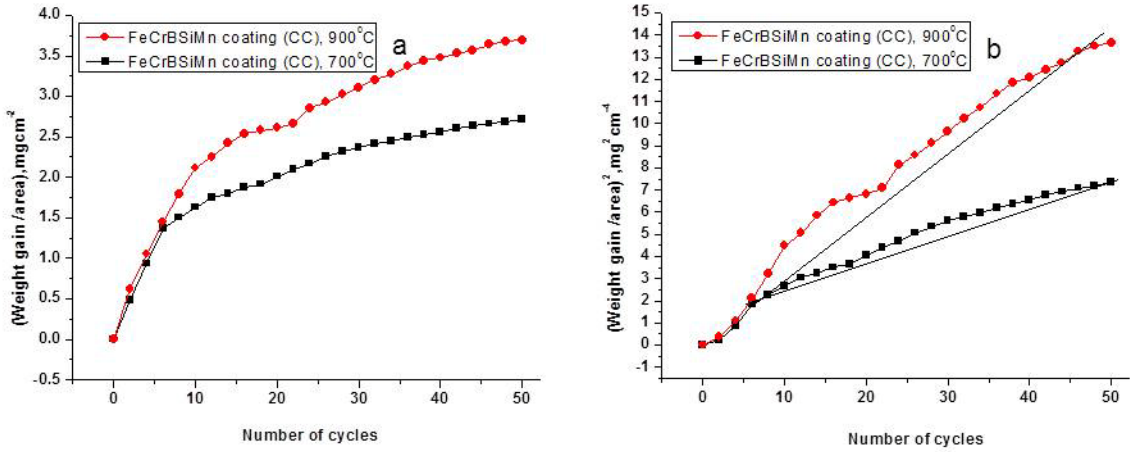

Fig 5.15: (a) Weight gain after oxidation per unit area versus number of cycles and (b) Weight gain after oxidation per unit area)^2 versus number of cycles, for the coated specimens (CC) subjected to hot corrosion in molten salt (Na_2SO_4-82% $Fe_2(SO_4)_3$) environment at 700^{0}C & 900^{0}C for 50 cycles.

Table 5.3: EDS analysis results (wt. %) corresponding to Fig. 5.16 for the FeCrBMnSi alloy coating exposed to molten salt (Na_2SO_4-60%V_2O_5) environment at 700^0C under cyclic condition (a) after 10 hours, (b) after 50 hours

Elements	B	O	Na	Si	S	V	Cr	Mn	Fe	Ni
1	0.00	3.80	0.65	0.24	0.09	1.70	47.93	7.86	34.57	0.34
2	21.36	9.86	0.41	0.64	0.27	2.38	30.63	4.13	27.37	0.70
3	0.00	4.86	0.00	0.36	0.16	1.74	30.38	1.30	60.12	1.09
4	12.66	21.20	1.10	0.49	0.51	2.18	15.93	2.92	38.39	0.81
5	0.00	25.51	1.76	0.11	0.70	2.27	15.08	3.35	46.64	1.12
6	0.00	11.66	5.41	0.74	1.55	2.41	21.40	4.34	50.79	0.69
7	0.00	1.60	1.12	0.14	0.72	1.91	24.03	4.34	65.31	0.83

Table 5.4: EDS analysis results (wt. %) corresponding to Fig. 5.17 for the FeCrBMnSi alloy coating exposed to molten salt (Na_2SO_4-60%V_2O_5) environment at 900^0C under cyclic condition (a) after 10 hours, (b) after 50 hours..

Elements	B	O	Na	Si	S	V	Cr	Mn	Fe	Ni
1	25.16	21.37	6.55	0.81	0.61	4.16	11.88	2.07	19.33	0.62
2	14.50	24.91	28.32	0.29	21.75	2.16	2.0	0.81	2.13	0.31
3	10.76	20.40	4.73	0.41	0.78	2.39	21.85	2.02	30.63	0.93
4	12.89	12.21	14.08	3.14	1.10	29.82	7.39	2.38	13.58	0.92
5	28	20.85	23.63	0.22	20.53	0.35	0.98	0.61	0.81	0.24
6	3.94	1.96	3.85	0.17	0.13	7.33	48.84	5.76	26.48	0.00

5.3.3.2 FE-SEM/EDS analysis

5.3.3.2.1 Surface morphology of the scales

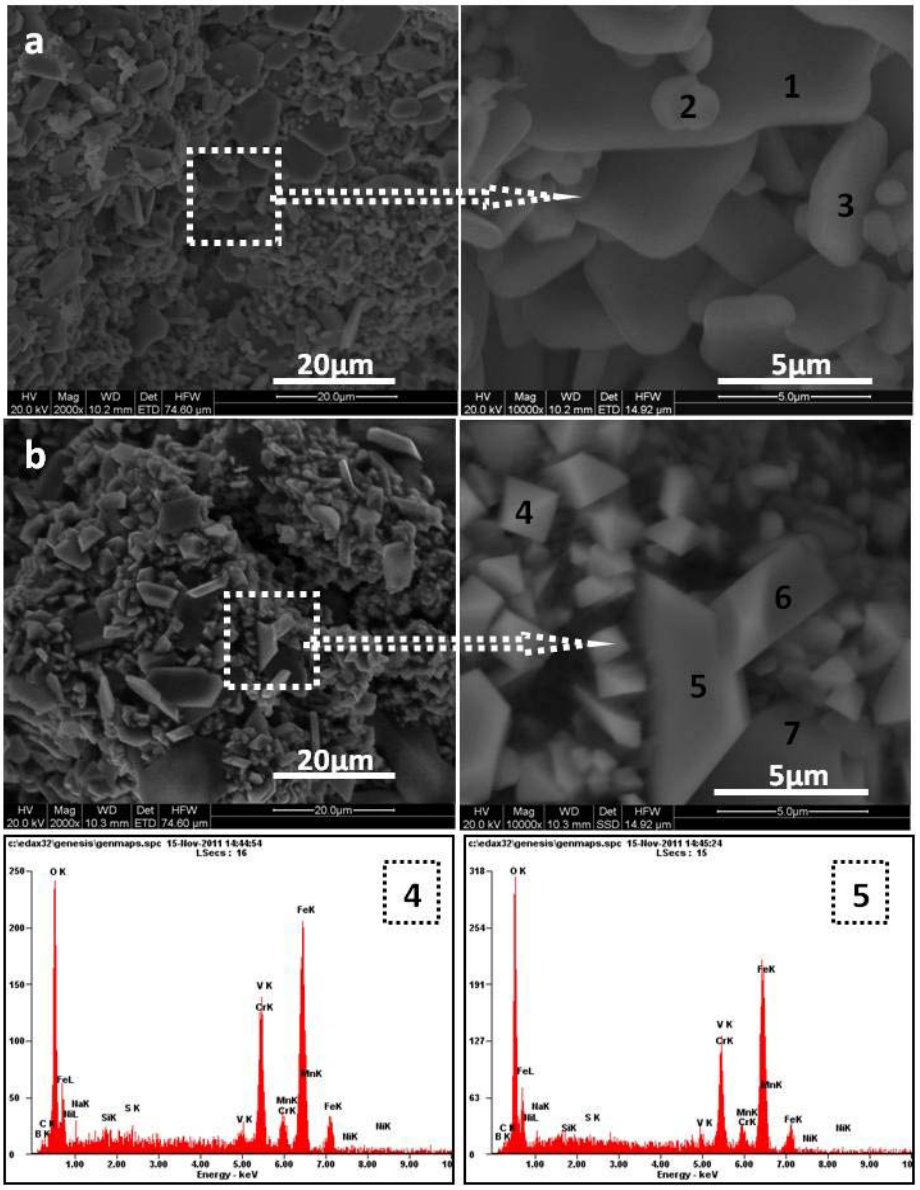

Fig 5.16: Surface scale morphology and EDS analysis for the coated specimens (CC) subjected to hot corrosion in molten salt (Na_2SO_4-60% V_2O_5) environment at 700^0C for (a) 10 cycles and(b) 50 cycles.

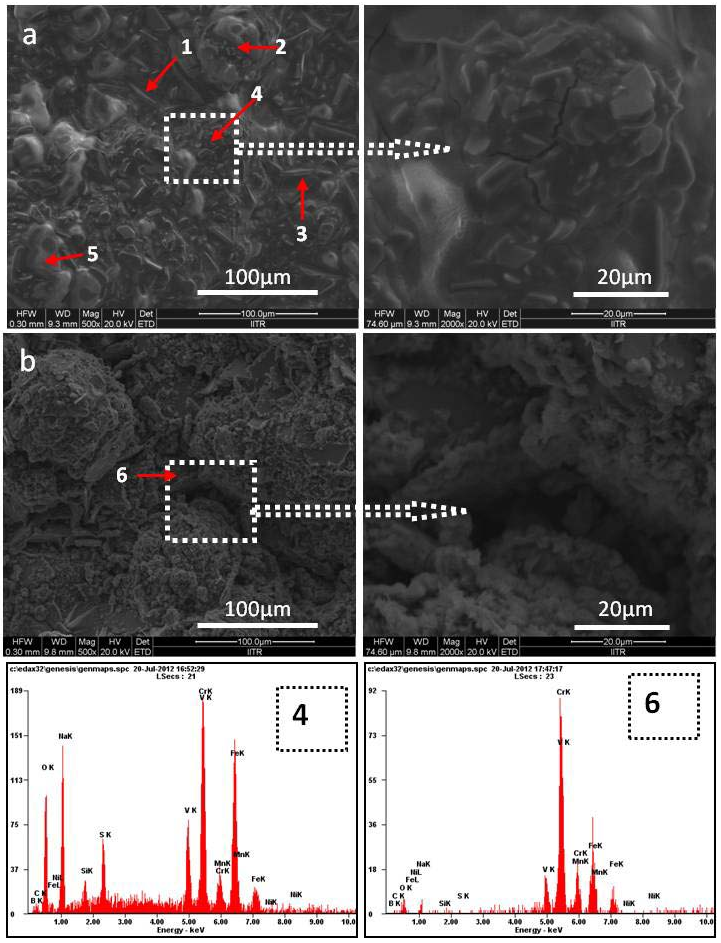

Fig 5.17: Surface scale morphology and EDS analysis for the coated specimens (CC) subjected to hot corrosion in molten salt (Na_2SO_4-60% V_2O_5) environment at 900^0C for (a) 10 cycles and (b) 50 cycles.

Detailed analysis of surfaces of coated specimens (CC) exposed to molten salt (Na_2SO_4-60%V_2O_5) environment at 700^0C and 900^0C under cyclic conditions for 10, and 50 cycles is shown in Fig. 5.16 and Fig. 5.17 respectively. FE-SEM analysis of the coated surface of CC at 700ºC indicates loosely bound oxide particles after 10 cycles of oxidation (Fig 5.16a), while the thick layers of oxides are found after oxidation after 50 cycles (Fig. 5.16b). EDS analysis listed in Table 5.3 indicates the major presence of Cr, O, Fe along with minor presence of B, Mn, V, Na, S and Si. The cracks observed after oxidation for 30 and 50 cycles indicate that there is no spalling of the oxide scales.

The surface of the oxidized coated specimen of CC at 900ºC appears as consisting of spongy nodules after oxidation for 10 cycles (fig 5.17a). EDS analysis of surface indicates Cr, O, Fe, and B. Minor amount of Mn, V, Na, S and Si are detected in the oxide scale (Table 5.4). With increase in number of cycles to 30, the number of nodules has increased. However, the surface is completely covered by the

nodules after oxidation for 50 cycles (Fig 5.17b). The voids formed on the surface indicate the spalling of oxide scale.

The surfaces of coated specimens (CC) subjected to molten (Na_2SO_4-82%$Fe_2(SO_4)_3$) salt environment at 700^0C and 900^0C under cyclic conditions for 10 and 50 cycles are shown in Figs. 5.18 and Figs. 5.19, respectively. The surface after oxidation at 700^0C for 10 cycles shows oxide particles of irregular shape (Fig. 5.18a). With increase in number of cycles to 50, the bonding of oxide particles to the surface increased. The particles are also grown in their size.(Fig. 5.18b). No change is observed in the EDS analysis of the oxide surfaces obtained after 10 and 50 cycles.

SEM images of nanostructured coated samples after heating at 900^0C for 10 cycles indicates considerable spalling and breaking of oxide surface. High magnification image in Fig. 5.19a shows dense irregular shaped oxide particles. The surface after heating for 50 cycles shows large numbers of dispersed platelet oxide particles (Fig. 5.19b).

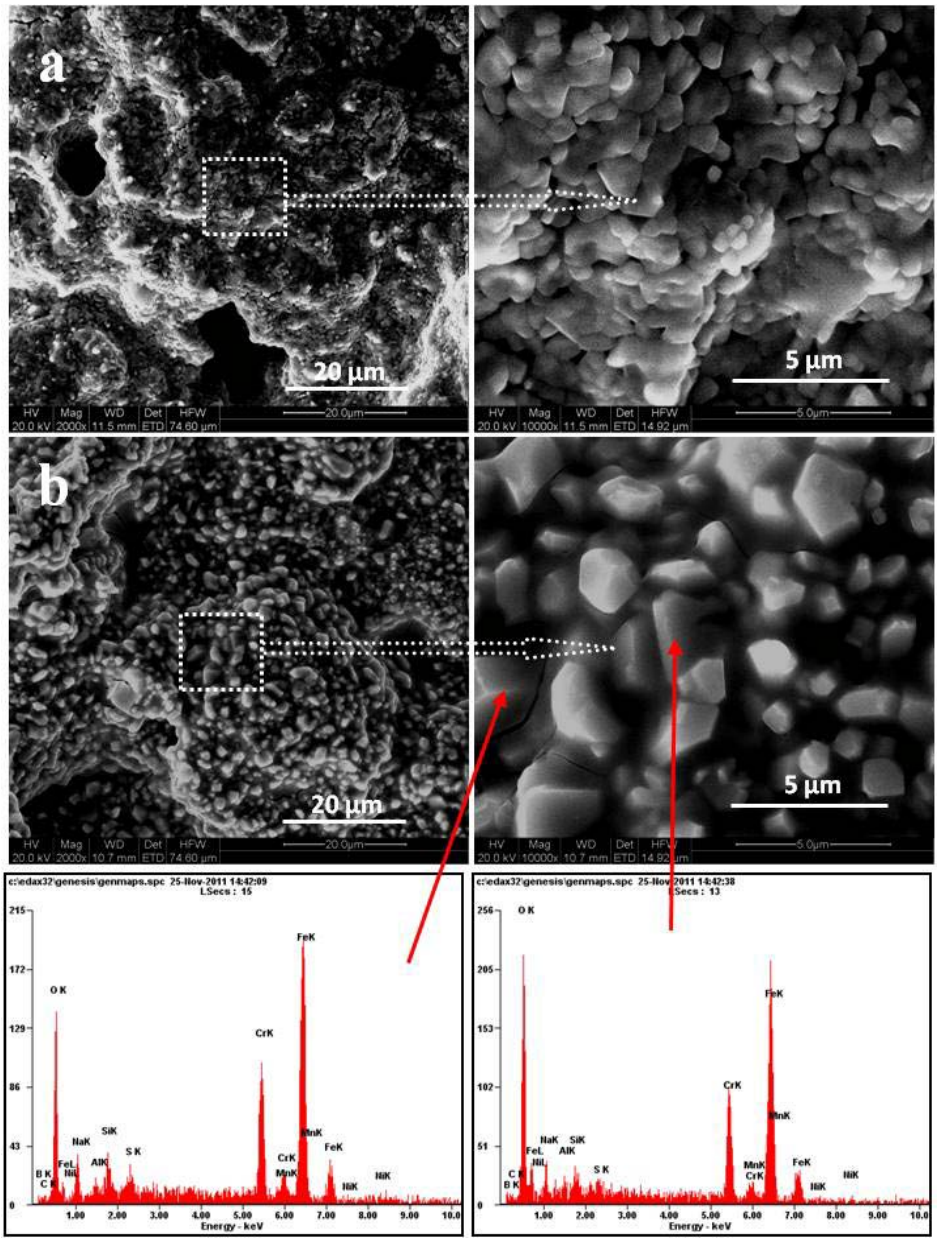

Fig 5.18: Surface scale morphology and EDS analysis for the coated specimens (CC) subjected to hot corrosion in molten salt (Na_2SO_4 - 82% $Fe_2(SO_4)_3$) environment at 700^0C for (a) 10 cycles and (b) 50 cycles.

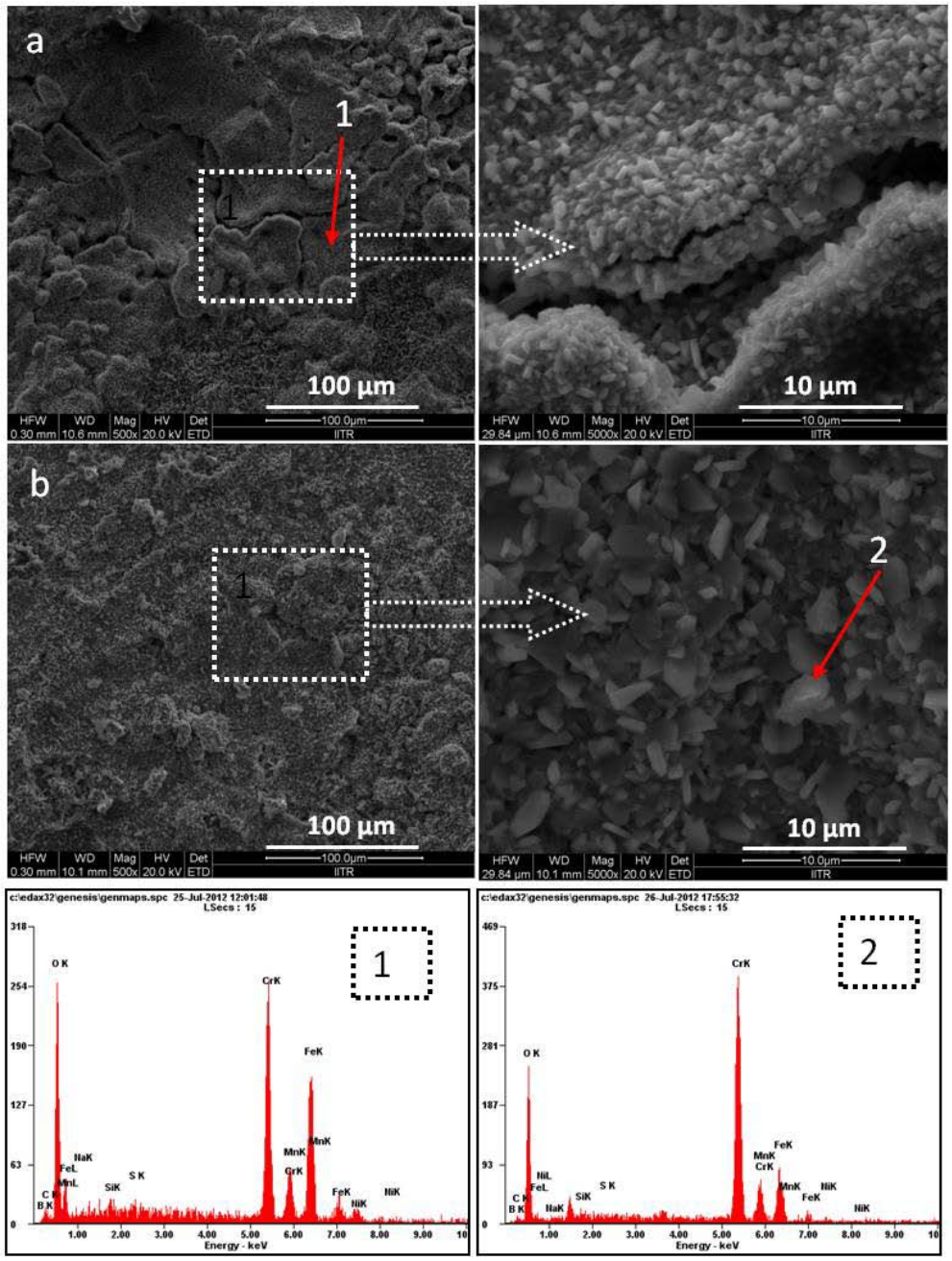

Fig 5.19: Surface scale morphology and EDS analysis for coated specimen (CC) subjected to hot corrosion in molten salt (Na_2SO_4 - 82% $Fe_2(SO_4)_3$) environment at 900^0C for (a) 10 cycles and (b) 50 cycles.

5.3.3.2.2 Cross-sectional analysis and X-ray mapping of the scale

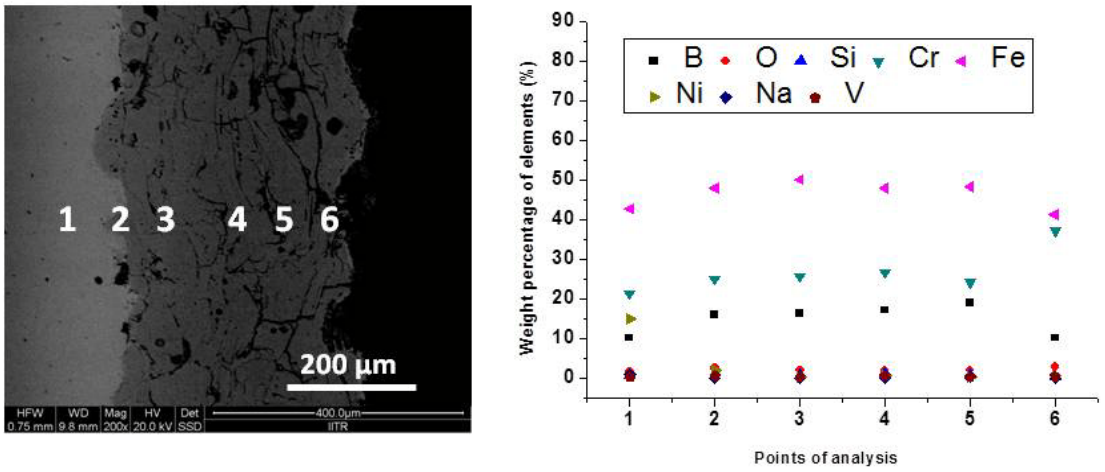

Fig 5.20: Morphology of oxide scale across the cross section of CC coated specimens, subjected to hot corrosion in molten salt (Na_2SO_4-60% V_2O_5) environment at 900^{0}C for 50 cycles.

Oxide scale morphologies along with elemental composition along the cross section of the coated specimens when exposed to cyclic oxidation for 50 cycles at 900 ^{0}C in Na_2SO_4-60% V_2O_5 and Na_2SO_4 - 82% $Fe_2(SO_4)_3$ environment are shown in Fig. 5.20-5.22 & 5.21-5.23 respectively. For the coated specimen, the oxide scale was dense and adherent and maintained continuous contact with the substrate even longer period of exposure of 50 cycles. The oxide scale contains Cr,Fe, and O. This suggests the possibility of formation of oxides of mainly chromium and iron in the scale. Nickel diffused from substrate to coating whereas chromium diffused from coating to substrate.

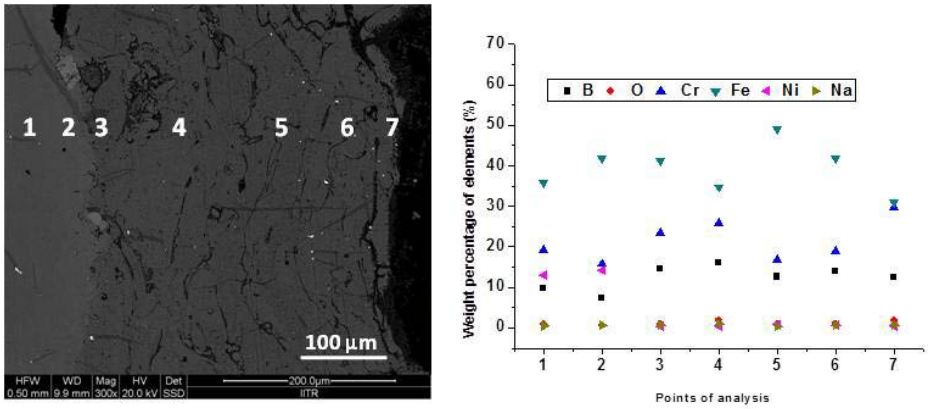

Fig 5.21: Morphology of oxide scale across the cross section of CC coated specimens, subjected to hot corrosion in molten salt (Na_2SO_4 - 82% $Fe_2(SO_4)_3$) environment at 900^{0}C for 50 cycles.

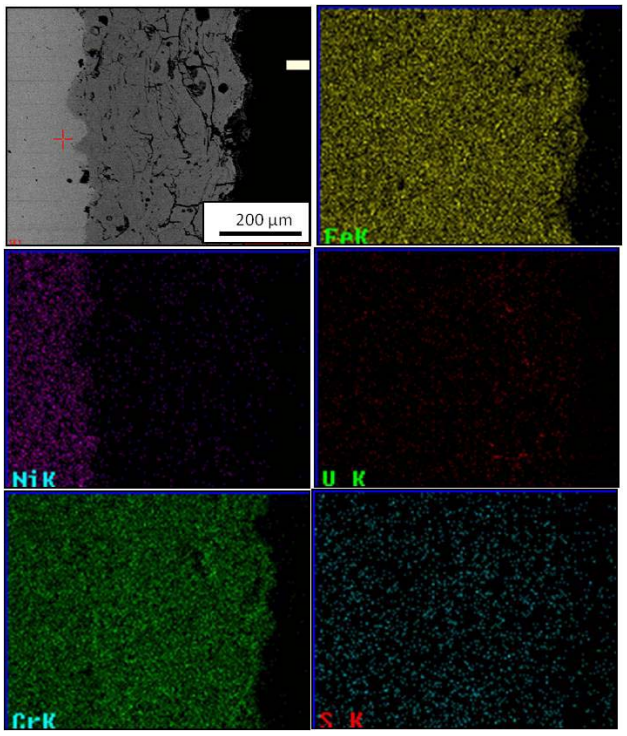

Fig 5.22: Composition image (SE) and X-ray mapping of the cross section of the coated specimen subjected to hot corrosion in molten salt (Na_2SO_4-60% V_2O_5) environment at 900^0C for 50 cycles.

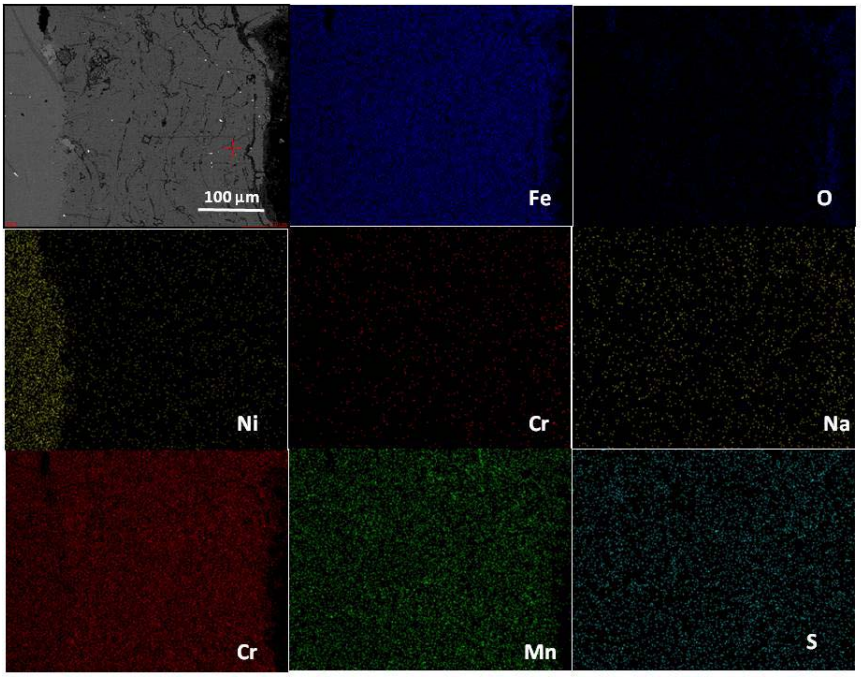

Fig 5.23: Composition image (SE) and X-ray mapping of the cross section of the coated specimen subjected to hot corrosion in molten salt (Na_2SO_4 - 82% $Fe_2(SO_4)_3$) environment at 900^0C for 50 cycles.

5.3.3.3 X-ray diffraction analysis (XRD) analysis

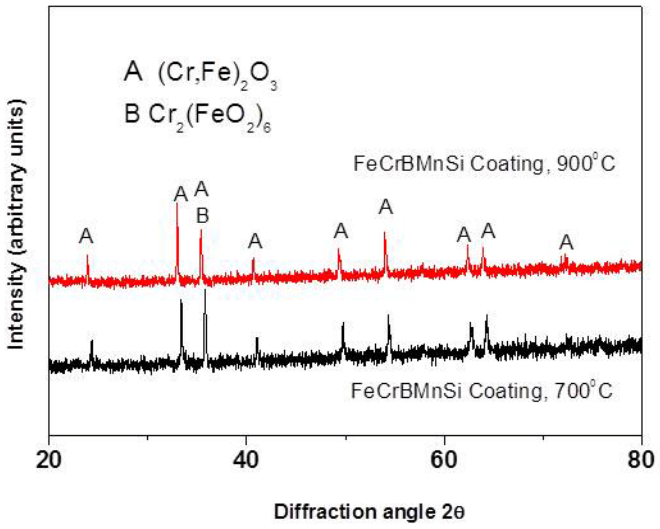

Fig 5.24: The XRD patterns of the scale formed on coated specimen (CC), subjected to hot corrosion in molten salt (Na_2SO_4-60% V_2O_5) environment at 700^0C & 900^0C for 50 cycles.

The XRD diffractograms for the coated specimen subjected to cyclic oxidation at 700 ^{0}C and 900^0C in Na_2SO_4-60% V_2O_5 (Fig. 5.24) revealed the formation of $(Cr,Fe)_2O_3$ as very strong phases, whereas $Cr_2(FeO_2)_6$ present as low intensity phases.The XRD diffractograms for the coated specimen subjected to cyclic oxidation at 700 ^{0}C and 900^0C in Na_2SO_4 - 82% $Fe_2(SO_4)_3$ revealed the formation of $(Fe_{0.6}Cr_{0.4})_2O_3$, and Mn_2O_3 as very strong phases, whereas Na_2FeO_4 present as low intensity phases (Fig. 5.25).

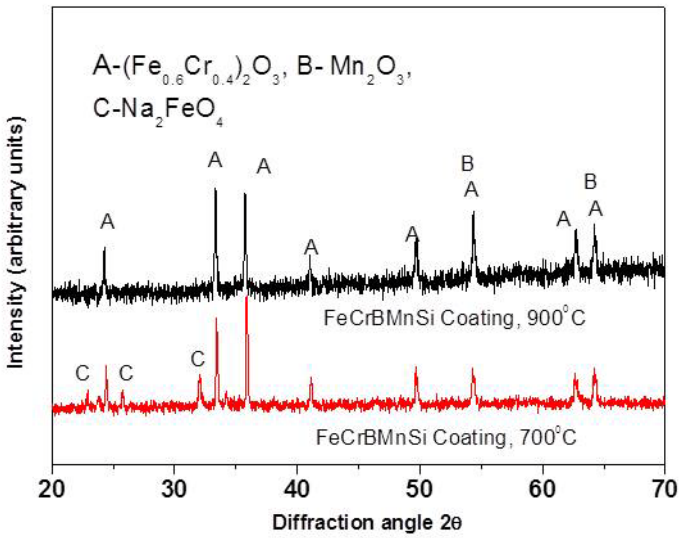

Fig 5.25: The XRD patterns of the scale formed on coated specimen (CC), subjected to hot corrosion in molten salt (Na_2SO_4 - 82% $Fe_2(SO_4)_3$) environment at 700^0C & 900^0C for 50 cycles.

5.3.4 Discussion

The weight gain curves for HVAS-sprayed FeCr based conventional coatings (CC) followed nearly a parabolic behavior (Fig. 5.15 & 5.16). A small deviation from the parabolic rate law might be due to the cyclic scale growth. The higher weight gain of the specimens during the first few cycles might be due to the rapid formation at the splat boundaries and within the open pores due to the penetration of oxidizing species, further, the subsequent increase in weight is gradual.

The various phases identified from the X-ray diffraction (XRD) patterns of the oxidized uncoated specimen subjected to cyclic oxidation in air at 700^0C & 900^0C in Na_2SO_4-60% V_2O_5 after 50 cycles are shown in Fig 5.24. The XRD diffractograms for the coated specimen subjected to cyclic oxidation at 700 ^{0}C and 900^0C in Na_2SO_4-60% V_2O_5 (Fig. 5.24) revealed the formation of $(Cr,Fe)_2O_3$ as very strong phases, whereas $Cr_2(FeO_2)_6$ present as low intensity phases. The XRD diffractograms for the coated specimen subjected to cyclic oxidation at 700 ^{0}C and 900^0C in Na_2SO_4 - 82% $Fe_2(SO_4)_3$ revealed the formation of $(Fe_{0.6}Cr_{0.4})_2O_3$, and Mn_2O_3 as very strong phases, whereas Na_2FeO_4 present as low intensity phases (Fig. 5.25).The surface composition analysis of coated substrate indicates that oxides of Cr & Fe mainly present in the oxide scale along with NiO, Fe_2O_3, and SiO_2, which clearly reveals the diffusion of these elements from substrate.

Cross-sectional EDAX analysis of corroded coated samples shows the variation in elemental composition after oxidation studies. The chromium rich elements are present in the uppermost part of coating. Fe and Si have diffused from the substrate into the coating. The oxide scale for the coated specimen seems to be dense and adherent and has retained its continuous contact with the substrate steel even after 50 cycles. The oxide scale contains Cr,Fe, and O. This indicates the possibility of formation of oxides of mainly Cr and Fe in the oxide scale (Fig. 5.20). Nickel has diffused from substrate to coating whereas chromium diffused from coating to substrate.

The formation of thermodynamically stable chromium oxide scale and its slow growth, might have acted as barrier to the inward diffusion of corrosion species into the coating. Fe and Si are clearly visible in top surface of the coating, which confirms the diffusion of this element from the substrate to the top coating surface.

The life of coating in oxygen containing atmosphere at high temperature is dependent upon the formation of a protective oxide scale, Cr_2O_3. The Cr_2O_3 phase is thermodynamically stable up to very high temperatures due to its high melting points as well as it forms a dense, continuous and adherent layers that grow relatively slow. The scale of this type forms a solid diffusion barrier that precludes further interaction of oxygen with the underlying coating. The reaction rate is rapid initially as oxygen and the reacting elements in the coating are in direct contact. Once the scale grows and becomes continuous,

diffusion of either species becomes increasingly difficult due to the growing diffusion barrier. As a result, the rate of mass gain due to oxygen uptake reduces with time. The growth of oxide scale typically displays a parabolic dependence with time and its longevity is dependent upon the concentration of the scale-forming element in the coating material, temperature, oxidizing conditions and alloy microstructure.

It may be mentioned based on the present investigation that coating can provide higher hot corrosion resistance at high temperature although it is traditionally specified for wear and erosion resistance applications. Schematic diagram of the proposed oxidation mechanism of FeCr based FeCrBSiMn coated 310S alloy substrate subjected to hot corrosion in molten salt (Na_2SO_4-60% V_2O_5) & (Na_2SO_4 - 82% $Fe_2(SO_4)_3$) environment at 900^0C for 50 cycles are shown in Fig. 5.26 & 5.27, respectively. Corrosion species such as S, O, V diffused into the coating through the microcracks and pores present in the coating. The presence of chromium and iron in the scale was noticed and small amount of alloying element such as Ni has migrated from the substrate into the coating. The diffusion controlled reaction upon formation of Cr_2O_3 films on the coatings surface limits the diffusion of aggressive species such as air and other impurities in to the coatings.

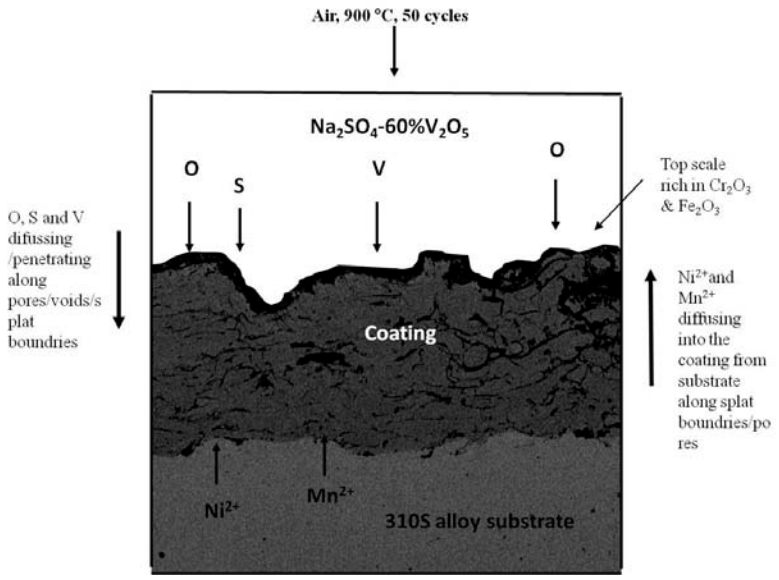

Fig 5.26: Schematic of the proposed oxidation mechanism of coated specimen (CC) subjected to hot corrosion in molten salt (Na_2SO_4-60% V_2O_5) environment at 700^0C & 900^0C for 50 cycles.

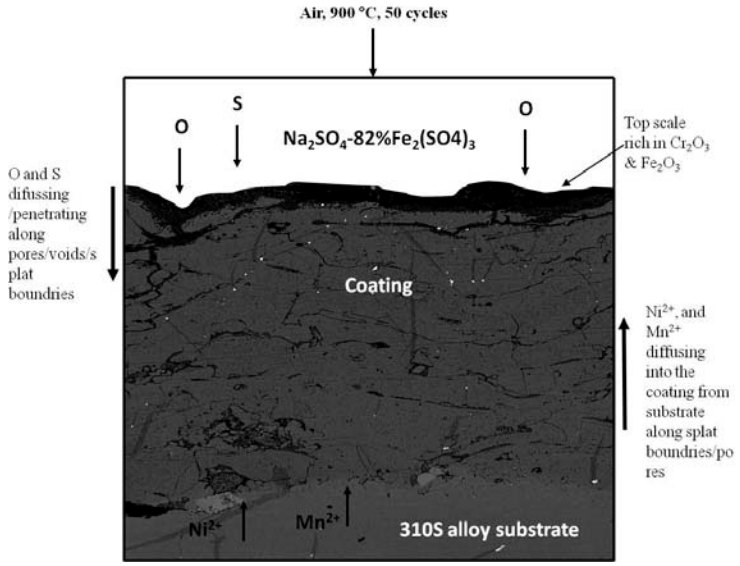

Fig 5.27: Schematic of the proposed oxidation mechanism of coated specimen (CC) subjected to hot corrosion in molten salt (Na_2SO_4 - 82% $Fe_2(SO_4)_3$) environment at 700^0C & 900^0C for 50 cycles.

5.3.5 Conclusions

- FeCrBSiMn alloy coatings were deposited successfully on 310 alloy substrate by the HVAS-spraying process.
- The coated specimen showed a higher hot corrosion resistance subjected to cyclic oxidation in air at 700 ^{0}C, 900^0C, and in molten salt environments after 50 cycles with its uncoated counterpart.
- The formation of protective dense oxides of chromium might have contributed for the better hot corrosion resistance in the coated specimen. The scale formed on the surface of the coating was adherent with some sign of minor cracks.
- The splat and globular morphology of the as deposited coatings provides relatively high density to the coatings, which is essential for achieving degradation resistance of the coatings.
- The formation of protective Cr_2O_3 oxide layers is responsible for imparting resistance against high temperature oxidation on the coated specimen.
- The diffusion controlled reaction upon formation of Cr_2O_3 films on the coatings surface limits the diffusion of aggressive species such as air and other impurities in to the coatings.
- The oxidation behavior of coated samples was found to obey parabolic rate law.

5.4 EROSION-CORROSION STUDIES IN ACTUAL INDUSTRIAL ENVIRONMENT

5.4.1 Experimental details

The substrate material, coating formulation and the oxidation studies are explained in detail in section 3.1, 3.2.3 and 3.4.1.

5.4.2 Results

5.4.2.1 Weight change measurements

The oxidation-erosion loss was measured in terms of coating due to scaling after 1500 hours of exposure. Rough estimate of the thickness lost for HVAS coatings was 0.25 mm, and the rate of thickness loss was 57.524 mpy. The weight gain per unit area for the HVAS coating was found to be 9.86 mg cm^{-2}. This small weight gain on the coated specimen is due to the degradation and ash particles deposition on exposed surfaces.

5.4.2.2 FE-SEM/EDS analysis

5.4.2.2.1 Surface morphology of the scales

In order to evaluate the degradation behavior of the FeCrBMnSi coating in real time boiler environments, coating coupons were kept in the industrial coal fired boiler for 1500 hours at 700 ± 10^{o}C, where fly ash particles continuously impinge on the specimen. Results indicate the coated specimens behaved very well in the boiler environment. FE-SEM analysis of the coated specimen after 1500 hours in such a boiler environment is shown in Fig. 5.28. Adherent oxide scale on the coatings with minor spalling was observed at edges of the coatings. It also indicates pull out of the particle from the oxidized coatings (Fig 5.28a, d). The pulled-out areas show the presence of Al, Si, O. It is because of high velocity fly ash particles erode the oxide surface of the coated specimen. The signatures of erosion caused by the fly ash particles appear as long, wider ploughs, and crater (Fig. 5.28). Cr, Fe and O and significant amount of Al, Si, Mn and Na are observed in the scales. EDS analysis confirms the deposition of ash on the coatings (Fig. 5.28d). The oxide scale on the coated specimen in coal fired boiler at 700 ±10^{o}C for 1500 hours was partially removed due to particle impact. The presence of FeCr, $(Cr, Fe)_2O_3$ phases is observed on the oxidized surface of the coatings exposed to boiler environment. During initial stages of hot corrosion, chromium exhibits higher affinity for oxygen to form Cr_2O_3 and offers improved resistance to oxidation. This is because of poor rate of growth and ability to act as barrier against ionic migration. Further, the Cr_2O_3 phase is known to be a hard phase and resists erosion.

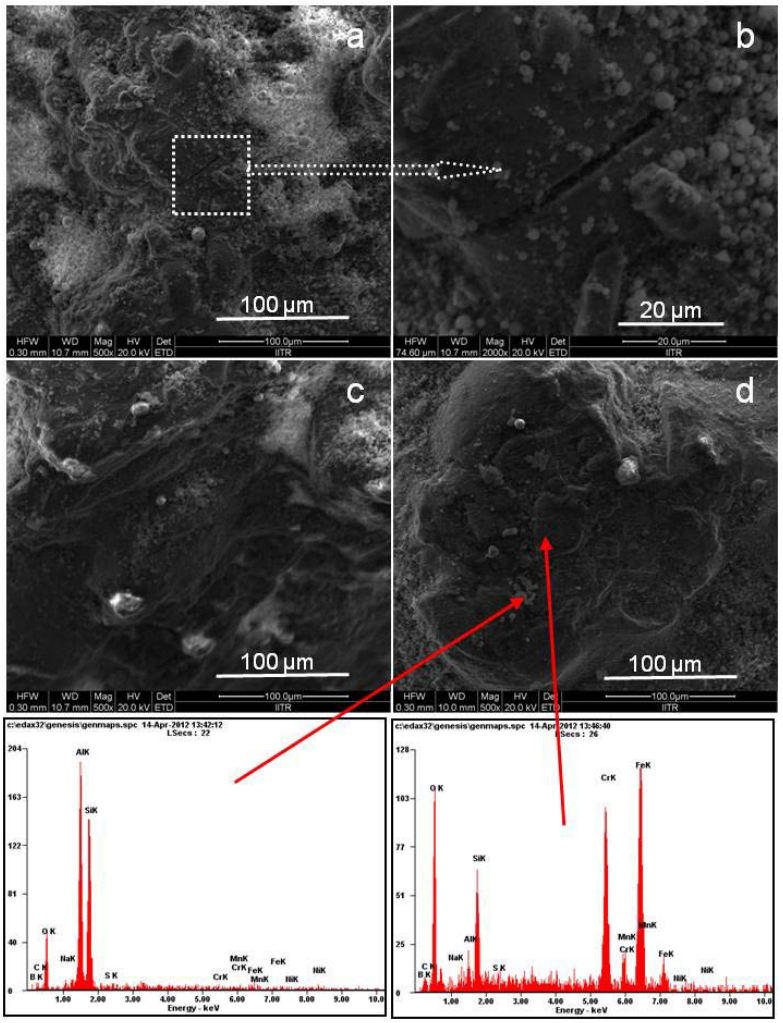

Fig 5.28: FE-SEM/EDS Surface analysis of coated specimen (CC) exposed to superheater of the coal fired boiler 700±10 ^{0}C for 1500 hours.

5.4.2.2.2 Cross-sectional analysis and X-ray mapping of the scale

The cross-sectional analyses by X-ray mapping of different elements of the coated specimens subjected to degradation in coal fired boiler at 700 ± 10 ^{o} C for 1500 hours are shown in Fig. 5.29. The scale mainly consists of oxides of Cr, Fe, whereas S and Na have diffused in to the coating. The coating performed well and protected the 310S substrate material. Corrosive species were able to penetrate some of the coatings and attack the substrate via interconnected network of voids and oxides at splat boundaries.

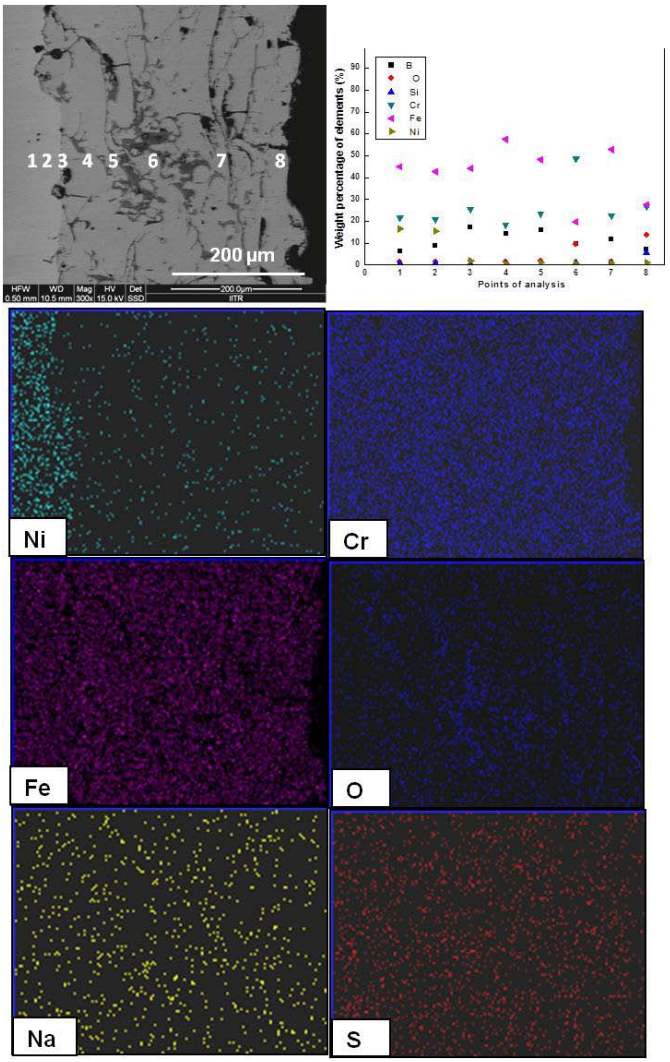

Fig 5.29: Composition image (SE), morphology of oxide scale across the cross section and X-ray mapping of the cross section of the coated specimen (CC) subjected to subjected to hot corrosion in actual boiler environment at 700±10 ^{0}C for 1500 hours.

5.4.2.3 X-ray diffraction analysis (XRD)

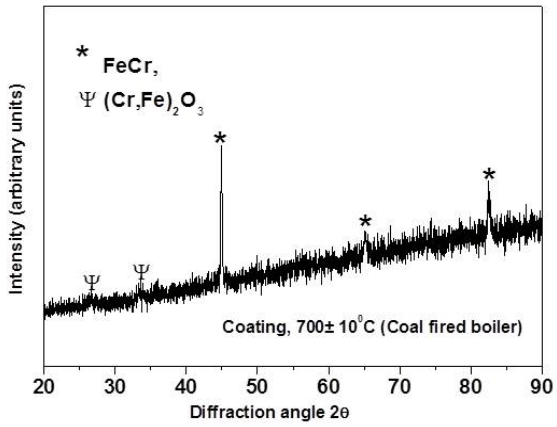

Fig 5.30: The XRD patterns of the scale formed on coated specimens (CC), subjected to hot corrosion in actual boiler environment at 700±10 ^{0}C for 1500 hours.

The XRD patterns of the scale formed on coated specimens (CC) subjected to hot corrosion in real boiler environment at 700±10 ^{0}C for 1500 hours are shown in Fig. 5.30. The major and minor phases detected at the surface of the specimens are shown in the XRD graph. The various phases identified from the X-ray diffraction (XRD) patterns of the corroded uncoated specimen subjected to actual boiler environment at 700±10 ^{0}C are shown in Fig 5.30. Cr_2O_3 and Fe_2O_3 were observed as the main phases.

5.4.3 Discussion

The less weight gain of bare alloy than coated specimen is attributed to oxide scale of spallaing in the real environment of the coal fired boiler and fluxing action of the molten salt along with erosion of oxide scale. The general ash deposit found on boiler super heaters is $Na_2O.V_2O_4.5V_2O_5$. This deposit melts at 550^{0}C. Above the melting point, this ash deposit material corrodes metals by long-term contact (Sidhu and Prakash, 2006P). The accumulation of low melting point salts from flue gas on the fire side surface of the boiler tubes indicates hot corrosion and is considered a route cause for the severe wastage of tube materials (Sidhu et al., 2005B).

5.4.4 Conclusions

- The HVAS sprayed CC coating was adherent to the steel in the real boiler environment at 700±10 °C. The surface scale was also found to be intact.
- The coated 310S alloy exhibited improved resistance to erosion and oxidation than uncoated specimen.
- The coatings exposed to industrial environment of thermal power plant showed the formation of oxides of FeCr, $(Cr, Fe)_2O_3$ phases, which imparts protection to the substrate.
- Coated specimens (CC) exhibited excellent oxidation and wear/spallation resistance.

CHAPTER - 6

FeCr based nanostructured coating

Characterization, oxidation and hot corrosion behavior of FeCr based nanostructured coatings deposited on 310S alloy substrate by High velocity arc spray process (HVAS) are described in this chapter. The cyclic oxidation r and hot corrosion studies were conducted at an elevated temperature of 700^0C and 900^0C in air, Na_2SO_4-60%V_2O_5, Na_2SO_4-82%$Fe_2(SO_4)_3$ molten salt environments for 50 cycles and coal fired real boiler environments at 700 $\pm 10^oC$ for 1500 hours, respectively. The weight change measurements for coated and bare substrate were made to substantiate its oxidation kinetics through the evaluation of the parabolic rate constants, thereby evaluating the protective nature of the coatings. The microstructural characteristics of the corroded products were analysed by using techniques such as XRD, FE-SEM/EDS and X-ray mapping to understand the mode of oxidation and hot corrosion.

6.1CHARACTERIZATION OF THE COATING

6.1.1 Introduction .

Thermally sprayed coatings have emerged as a viable solution for providing necessary protection against wear and corrosion (Liu et al., 1998, 2000, 2001, 2001A, 2006, Nerz et al., 1992; Nicholls et al., 2002; Nicholls and Stephenson, 1995). The high temperature oxidation resistance of Fe based high-chromium and nickel containing alloys are extensively used to fabricate corrosion and wear resistant coatings (Kamal et al., 2009, Murthy et al., 2006). These Fe-base coatings are deposited by different thermal spray techniques such as plasma spray process, detonation gun process and High velocity oxy-fuel process (HVOF). Among all these thermal spray processes, HVAS process is usually employed due to its cost effectiveness (operating lower cost), high deposit efficiency and less applications difficulties (Liu et al., 2001). HVAS process has a capability of producing dense coating with higher bond strength and lower oxide content. Thermally sprayed Fe base coatings have been used extensively to inhibit/mitigate wear, erosion and corrosion at elevated temperatures in gas turbines, steam turbine, power generation industry, and coal burning boiler tubes (Schuh et al., 2007, Park et al., 2007). Ni-based, Co-based and Fe-based super alloys have been developed to enhance their mechanical properties and oxidation resistance. Since these alloys are very costly, a composite system comprising of base material (steel) and wear/corrosion resistant protective surface layer has been proposed as most favorable choice of material for combining both mechanical and corrosion resistance properties as reported in the literature (Sidhu et al., 2006C). Literature reveals that the thermal spray process is widely used to produce wear and

corrosion-resistant coatings on the components used in hot section of power generation industry and coal fired boiler (Kaur et al., 2011, Nickel et al., 2002; Niranatlumpong et al., 2000).

Improvement is further required to enhance mechanical properties and resistance against oxidation, hot corrosion of the nanostructured coatings. There is very little published information on the application of HVAS sprayed nanostructured alloy (NC) coatings. In this study, the microstructure, porosity, coating thickness, phase formation, microhardness properties of the coatings were characterized using FE-SEM/EDS, X-ray mapping and XRD techniques to present an experimental evidence so as to broaden applications of HVAS sprayed FeC- based nanostructured alloy coatings in the coating industries.

6.1.2 Experimental Details

The details of the substrate material, coating formulation and characterization of the coating are discussed in chapter 3.

6.1.3 Results

6.1.3.1 Characterization of the coating powder

The morphology of the nanostructured wire material was investigated by TEM. The morphology of the nanostructured wire material was investigated by TEM. Fig. 6.1(a, b) shows the TEM images of the nanostructured wire material, which confirms nanometric size of the initial spherical powder particles. The size of nanostructured wire materials used for coating was found to be in the range 10-120nm.

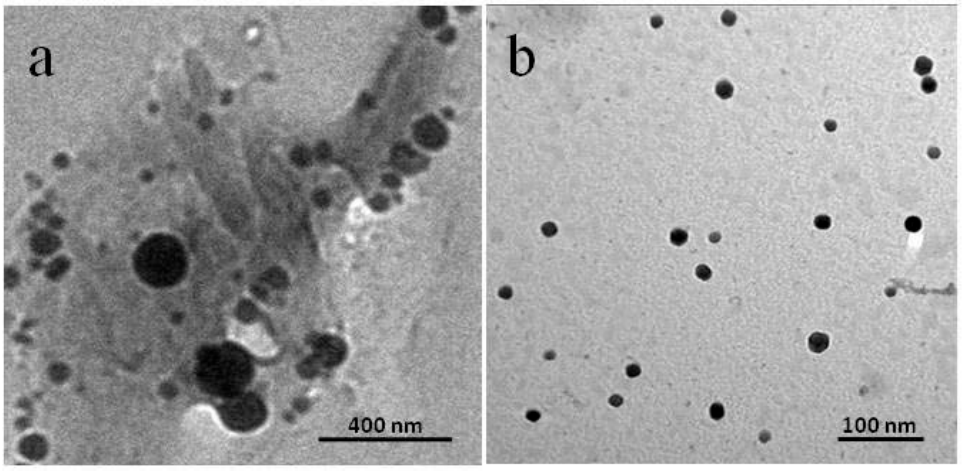

Fig 6.1: TEM image showing the morphology of the nanostructured wire material.

6.1.3.2 Characterization of the coating

The morphology of the as sprayed nanostructured coating was investigated by TEM. TEM image shown in Fig. 6.2(a, b) indicates the presence of nanocrystalline particles in the coating. Fig. 6.2(c) shows the concentric bright rings in the SAED pattern, which indicates the polycrystalline nature of nanostructured particles in the coating.

FE-SEM images of the nanostructured coating are shown in Fig. 6.3(a, b). The microstructures revealed that high-velocity arc sprayed nanostructured coating is dense, smooth and without any micro cracking. The coating surface was free of loose particles. Also, the coating surface consisted of the globules of sprayed splats. EDS analysis (see insets in Fig. 6.3 a, b) of the coating surface indicates the presence of Fe, Cr as major elements and Si, Nb, O, W, B as minor elements.

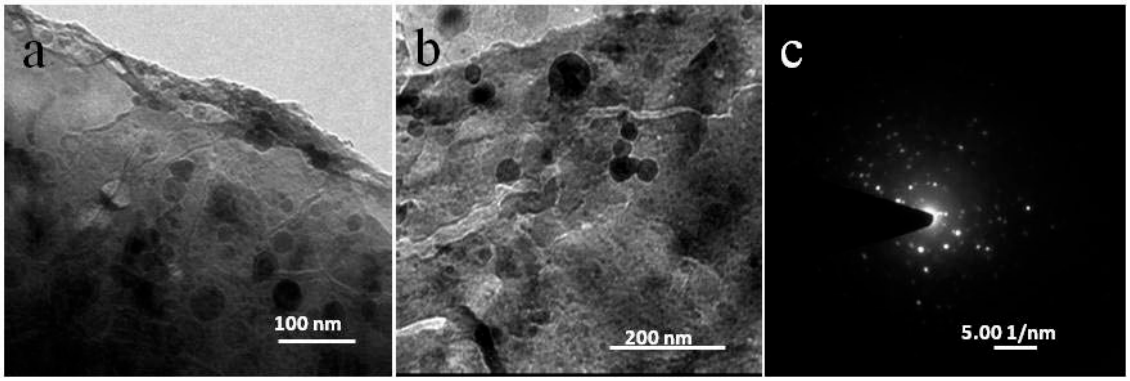

Fig 6.2: (a) TEM analysis showing the surface morphology for the as-sprayed coating on 310S substrate

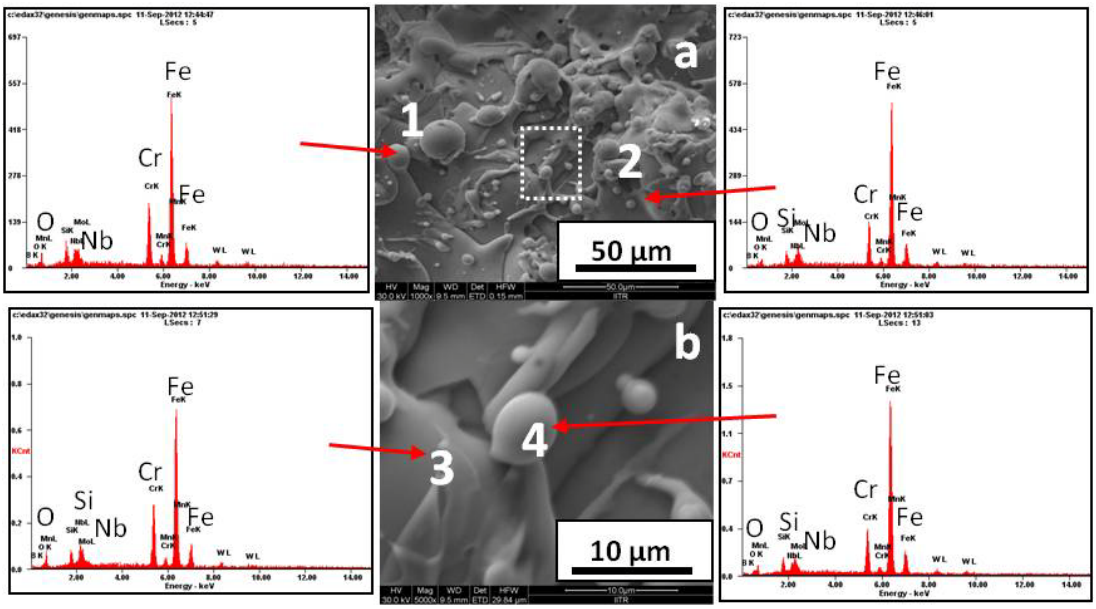

Fig 6.3: (a, b) FE-SEM/EDS with EDS analysis showing the surface morphology for the as-sprayed coating on 310S substrate.

6.1.3.3 Surface roughness of the coated specimen (NC)

The surface of the as-sprayed coated specimen was rough and the average surface roughness (R_a) was found to be 19.74 µm (Fig. 6.4).

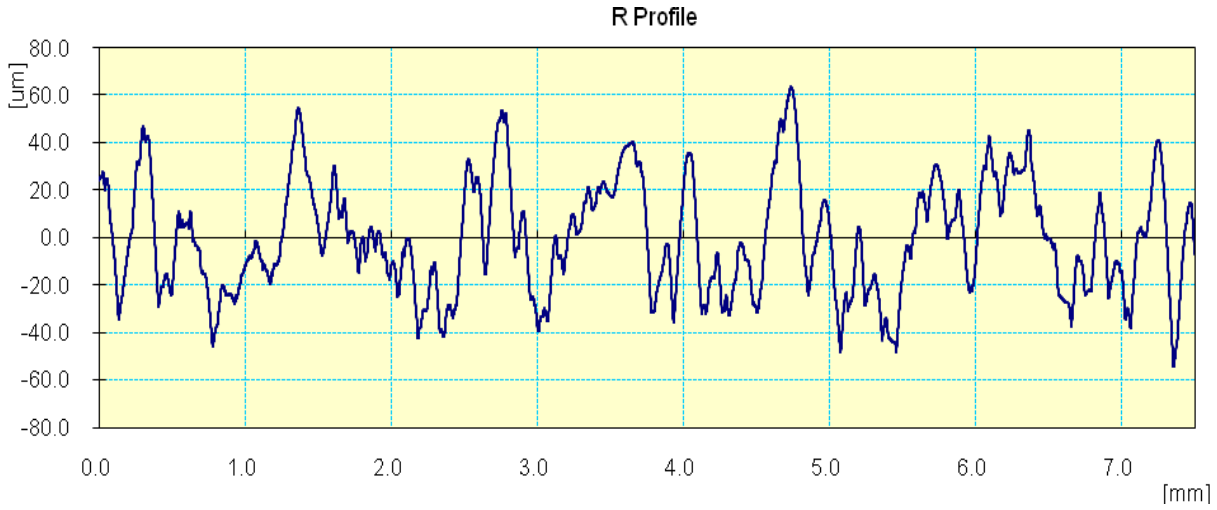

Fig 6.4: Surface roughness profile of the as-sprayed coating(NC).

6.1.3.4 Porosity of the coating

The porosities of the coatings play a important role in corrosion/high temperature oxidation as it provide preferential paths through which corrosion species can go through the coating to reach the substrate and may reduce the corrosion resistance of coating. Porosity of the HVAS coatings is found to be less than 2.5%, which reveals that coating is dense.

6.1.3.5 Bond strength of the coating

The bond strength of NC coating was measured on three specimens as discussed in section 3.3.4. Average bond strength of 6000 Psi was observed for the NC coating.

6.1.3.6 Microhardness of the coating

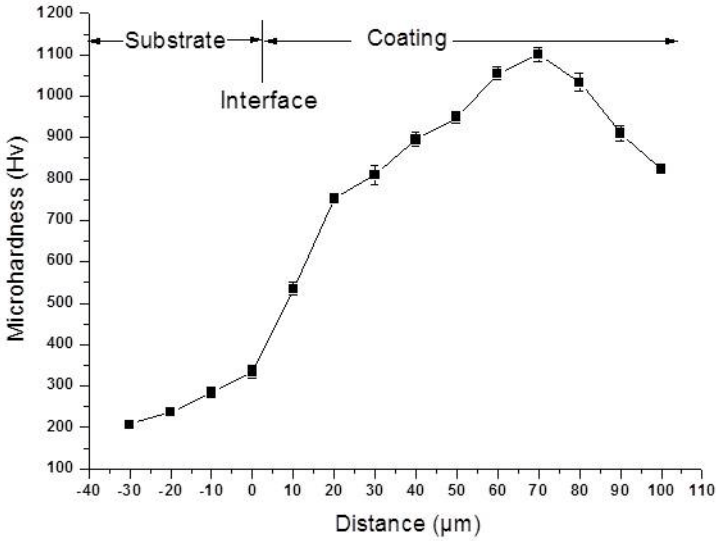

Fig.6.5 Variation of microhardness across the cross section of the coating

Micro hardness of the nanostructured alloy coating was determined across the cross-sectioned samples. The microhardness data of the coatings are compiled in Fig.6.5, it was found to be in the range of 520-1100 HV. It is high due to dense structure of the coatings consisting of nano-sized particles. The maximum microhardness measured for the coating is about 1100 Hv.

6.1.3.7 X-ray diffraction (XRD) analysis

XRD pattern of the as-deposited nanostructured coating shown in Fig. 6.6 reveals the presence of FeCr phase. The average crystallite size for the as-sprayed nanostructured coating was found to be 34 nm, which was calculated by using the Debye Scherer formula.

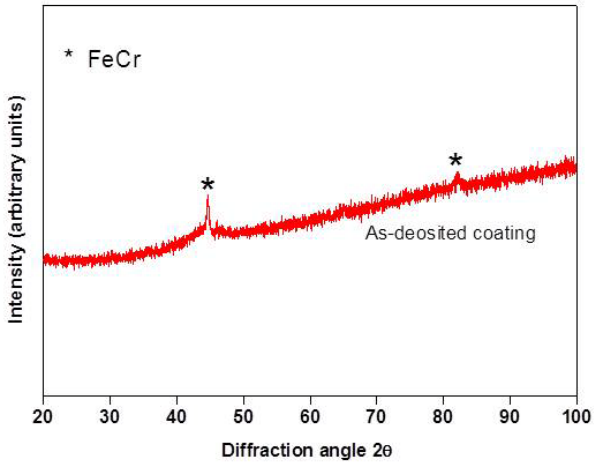

Fig 6.6: XRD diffraction for the as-sprayed coating

6.1.3.8 Cross-sectional analysis and X-ray mapping

The BSE images at the cross-section of NC coating on 301S alloy substrate by FE-SEM/EDS and the results are shown in Fig. 6.7. It clearly shows the formation of dense uniform and adherent splats like structure with some unmelted particles and pores. The major portion of NC coating is covered with Fe and Cr. Fig. 6.8 shows X-ray mapping of the coating area is rich with the major elemental constituents of the coating powder. Elemental mapping also indicates Ni diffusion from the substrate into the coating.

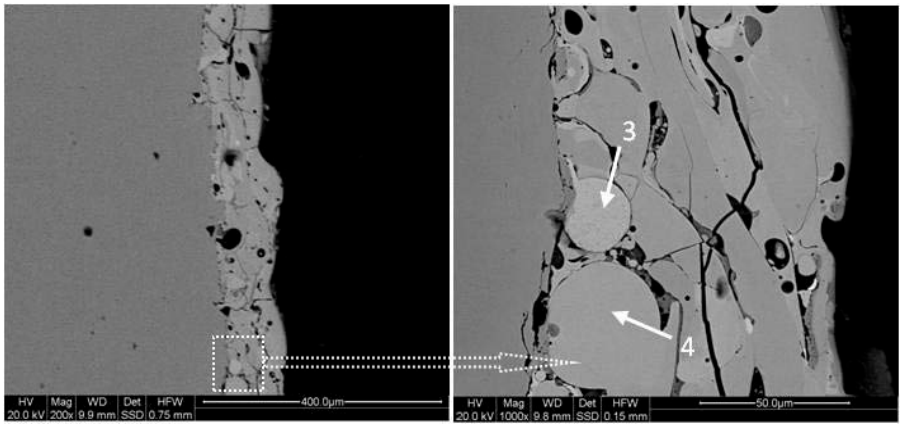

Fig 6.7: Cross sectional micrograph showing the morphology of the developed coating

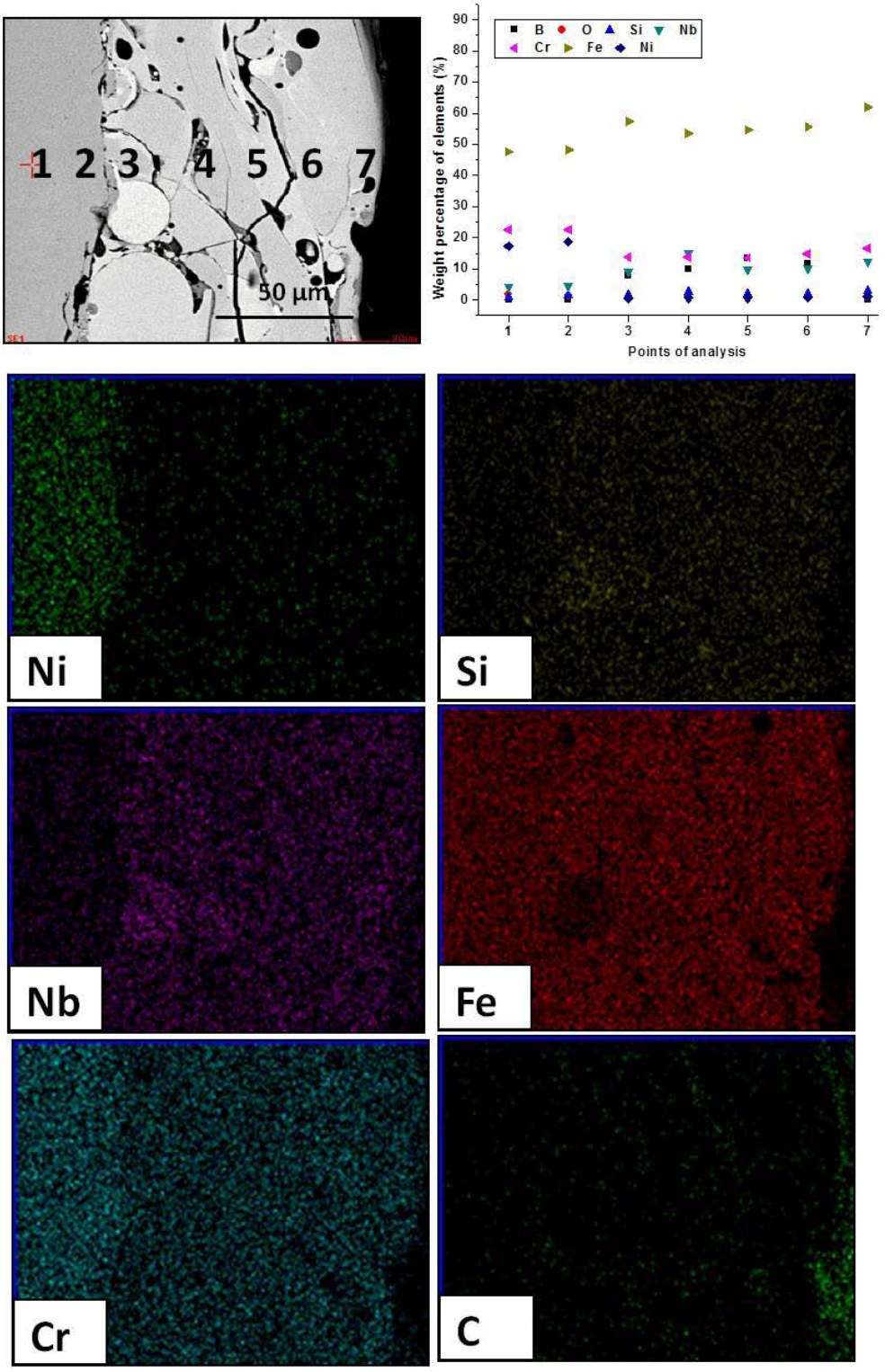

Fig.6.8 FE-SEM/EDS analysis at the cross-section and X-ray mapping of as-sprayed coated specimen (NC) on 310S alloy substrate.

6.1.4 Discussion

Uniform and almost crack-free surfaces are observed at the coated surface or edges. The micropores in the coatings have a significant role to play as far as the corrosion of thermal spray coatings is concerned, as they can provide a pathway to the reactive corrosive elements (Choi et al., 2002) through which the corrosion species can penetrate the coating to reach the substrate and may cause rapid corrosion attack. The microstructure also shows incompletely melted particles. Fig. 6.7 shows small amount of porosity as black contrast regions. Small amount of porosity indicates dense coatings provide corrosion resistance. The as-sprayed surface is fairly rough, dense, flat and free of cracks but shows the presence of partially melted particles (Fig.6.3). The microhardness of as sprayed coating has been found to be very high as compared to the alloy substrate (Fig.6.5). Some variation in microhardness values in the coating may be due to the presence of porosity, un-melted and partially melted particles.

6.1.5 Conclusions

The HVAS process wase used to deposit (NC) coatings on 310S alloy substrate and the coating were characterized for their microstructural features, and hardness in the present work. The major observations are presented here.

- FeCr- based nanostructured alloy (NC) coatings on 310S was fabricated by the HVAS-spraying process.
- The as-sprayed coatings consisted of smooth and dense structure.
- A good adhesion of the coatings with the substrate was evident as there is no sign of cracks and gaps at the interface.
- The microhardness of the as sprayed coating was found to be in the range of 520-1100 HV.

6.2 OXIDATION STUDIES IN AIR

6.2.1 Introduction

Degradation of metals in high temperature aggressive environment is a serious problem for boiler tubes of coal fired boilers. Huge amounts of material wastage in power generation plants due to combustion of fuels are reported (Sidhu et al., 2006E, Porcayo-Calderon et al., 1998; Prakash et al., 2001 and 2005). Literature reveals the wide contribution of thermal sprayed coatings for the safety of boiler tubes against high temperature corrosion attack (Kaur et al., 2009 & 2011, Chatha et al., 2012; Reid et al., 1971; Ren et al., 2005 & 2006; Sachs et al., 1958; Saunders et al., 1997).

Recently, there has been increasing interest in producing FeCr-based nanostructured alloy coatings due to their high strength and hardness, superior wear and corrosion resistance (Wang et al., 2001; Buchanan et al., 2008; Cheng et al., 2009). The influence of microstructural features on erosion-corrosion performance in actual coal fired boiler environment (at 700 ± 10^0C) and the oxidation behavior of HVAS nanostructured coatings is limited in the literature. The degradation mechanisms of nanostructured coatings exposed to high temperature environment (700ºC & 900^0C) is not subjected to detailed study so far. Therefore, the present work was focused to study the erosion-corrosion performance of HVAS nanostructured coatings deposited on 310S. The microstructural features and oxidation behavior of these coatings at 700ºC and 900^0C were investigated by using FE-SEM/EDS, XRD, and thermo gravimetric technique, respectively. The variations in microstructural morphology were correlated with the oxidation behavior of bare and coated specimens.

6.2.2 Experimental details

The substrate material, coating formulation and the oxidation studies are explained in detail in section 3.1, 3.2.3 and 3.4.1.

6.2.3 Results

6.2.3.1 Weight change measurements

Weight change per unit area (mg/cm^2) versus number of cycles plots for the coated specimen subjected to cyclic oxidation at 700ºC and 900^oC in air up to 50 cycles is shown in Fig. 6.9a. The plot reveals that coated specimen has undergone lesser overall weight gain at 700ºC as compared to that of the coatings at 900ºC. It is obvious from the plots that at 700ºC, the coated specimen shows a general tendency to approach a steady state after a gradual increase in weight during the initial 26 cycles of the study. However, high rate of increase in weight gain was observed with some spalling at high temperature (900ºC), up to 50 cycle of the study. It should be noted that in spite of the macro cracks observed on surface of the coated specimen after exposure at 700^oC for 50 hours (see Fig. 6.10), the weight gain did

not increase rapidly. This suggests superior resistance of high temperature oxidation of the nanostructured (FeCr)-based coatings. In Fig. 6.9b, the square of weight gain per unit area (mg^2/cm^4) versus number of cycles for coated and uncoated specimens is plotted. The trend in oxide growth at 700ºC and 900ºC can be approximated to a parabolic relationship. The parabolic rate constants, K_p values for the coated specimen subjected to cyclic oxidation in air for 50 hours at 700º C and 900^0 C were calculated and found to be 1.39 x 10^{-12} $g^2cm^{-4}s^{-1}$ and 2.69 x 10^{-12} $g^2cm^{-4}s^{-1}$, respectively. The K_p value for the coated specimen at 700ºC was found to be nearly one-half of the K_p value of the coated specimen at 900ºC.

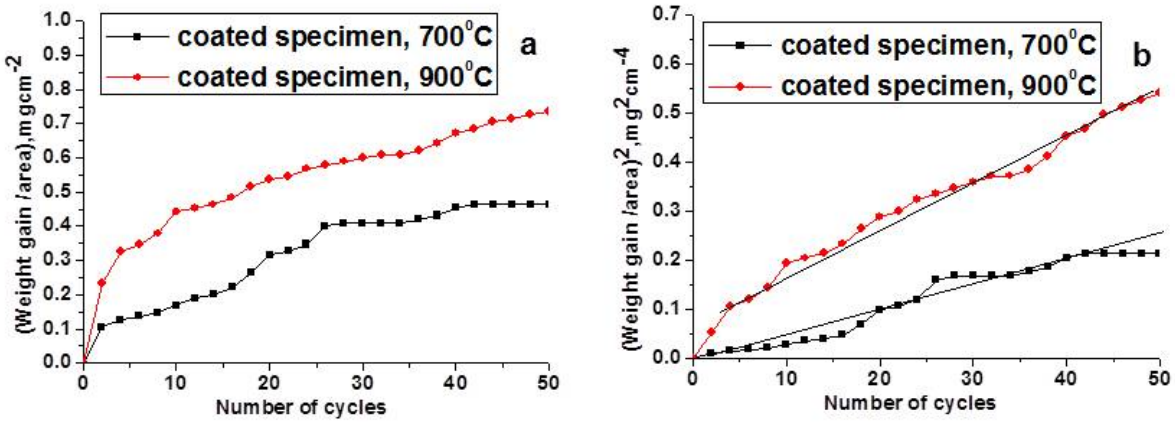

Fig 6.9: Weight gain/area versus number of cycles and (Weight gain/area)^2 versus number of cycles plot (a, b) for the coated specimen (NC), after cyclic oxidation of 50 cycles in air at 700º C and 900^0 C.

6.2.3.2 FE-SEM/EDS analysis

6.2.3.2.1 Surface morphology of the scales

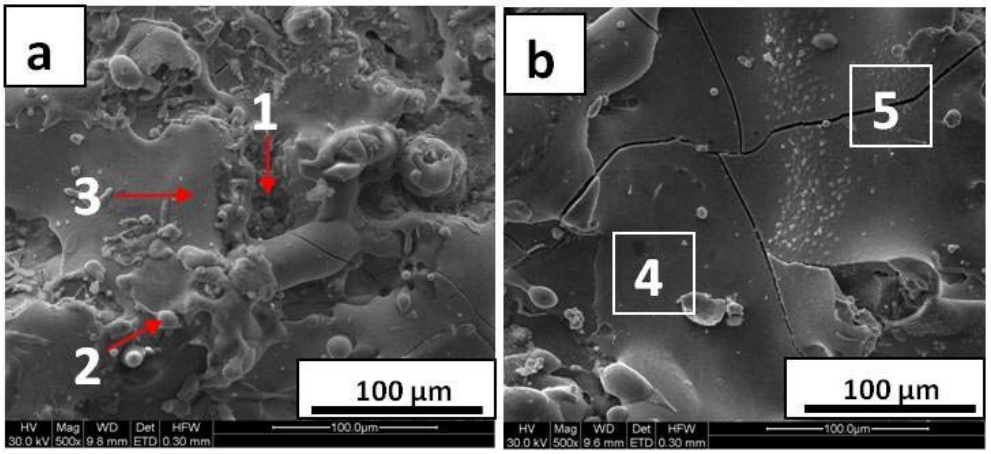

Fig 6.10: Surface morphology of coated specimen (NC) after (a) 10 hours, and (b) 50 hours oxidation cycles at 700^0C.

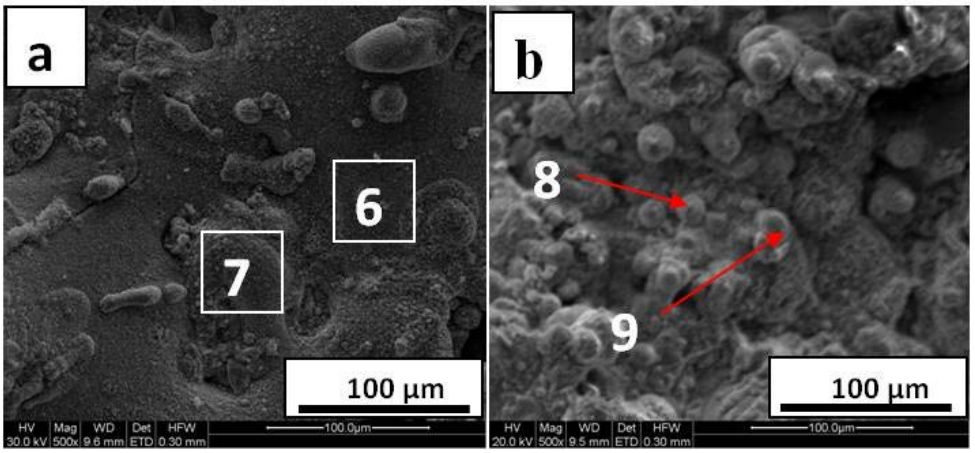

Fig 6.11: Surface morphology of coated specimen (NC) after (a) 10 hours, and (b) 50 hours oxidation cycles at 900^0C.

Table 6.1. EDS analysis results (wt. %) corresponding to Fig. 6.10 & 6.11 for the coated specimen subjected to cyclic oxidation in air at 700º C and 900^0 C.

Points	C	O	Si	Cr	Mn	Fe	Nb
1	0	4.34	3.4	17	1.59	60.62	13.05
2	0	2.37	3.3	17.02	0.85	63.86	12.6
3	1.81	4.64	5.69	15.92	1.02	55.2	15.5
4	0	7.76	4.30	20.47	1.44	57.55	8.76
5	0	6.20	3.17	19.57	0.68	64.53	5.85
6	4.85	20.25	20.51	11.59	1.72	37.68	3.39
7	0	8.19	1.28	22.12	2.18	61.51	3.60
8	4.22	26.39	2.01	26.26	1.44	36.83	1.24
9	2.32	17.89	3.12	29.37	2.10	43.04	1.51

Detailed analysis of surfaces of coated specimens after oxidization at 700ºC and 900^0C for 10 and 50 cycles is shown in Fig. 6.10 & 6.11. FE-SEM analysis of the coated surface at 700ºC indicates loosely bound oxide particles after 10 cycles of oxidation (Fig 6.10a), while the thick layers of oxides are found after oxidation at 30 and 50 cycles (Fig. 6.10b). EDS analysis listed in Table 2 indicates the major presence of Cr, O, Fe along with minor presence of Nb, C, Mn, and Si. The cracks observed after oxidation for 30 and 50 cycles indicate spalling of the oxide scales (Fig. 6.10 a, b).

The surface of the oxidized coated specimen at 900ºC shows the spongy nodules after oxidation for 10 cycles (fig 6.11a). EDS analysis of nodules indicates the presence of Cr, O, Fe. Minor amount of Nb, Si, and Mn are detected in the oxide scale. With increase in number of cycles to 30, the number of nodules has increased. The presence of cracks can also be observed on the surfaces after 10 and 50 cycles (fig 6.11 a, b). However, the surface is completely covered by the nodules after oxidation for 50 cycles. Further, EDS analysis of the nodules shows the major presence of Fe, Cr, O.

6.2.3.2.2 Cross-sectional analysis and X-ray mapping of the scale

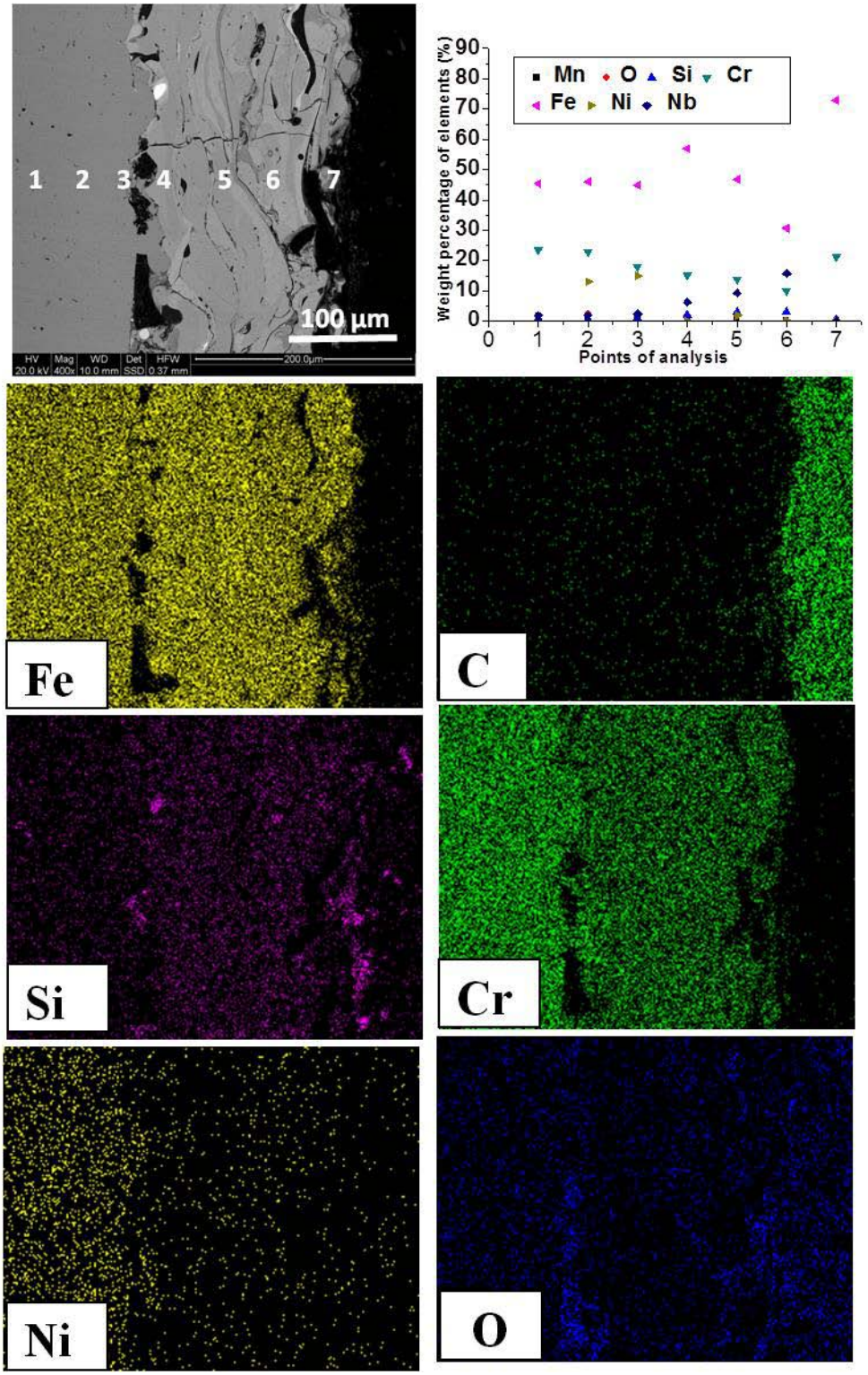

Fig.6.12 Fe-SEM/EDS analysis across the cross-section and X-ray mapping of the coated specimen (NC) subjected to cyclic oxidation at 900 ^{o} C in air after50 cycles

The cross-sectional analysis of the coated specimens subjected to cyclic oxidation in air at 900^{o}C after 50 cycles is shown in Fig. 6.12. Figure 6.12 shows that the scale mainly consists of oxides of Fe and Cr along with significant amounts of Ni. The oxide scale is found to be continuous, dense, and adherent. X-ray mapping of different elements are shown in Figure 6.12. The oxide scale is dense and uniform in thickness. The formation of oxides of chromium and iron might have acted as barrier to the inward diffusion of oxygen into the coating.

6.2.3.3 X-ray diffraction analysis (XRD) analysis

Different phases identified from XRD analysis of the oxidized coated specimen in air at 700^{o} C and 900^{0}C after 50 cycles are shown in Fig 6.13. XRD analysis of the surface of the coated specimen after 50 cycles at 700^{o}C and 900^{o}C revealed the presence of (Cr, Fe)$_2$O$_3$. Absence of any other oxides reveals strong resistance to oxidation of the coating in ambient conditions.

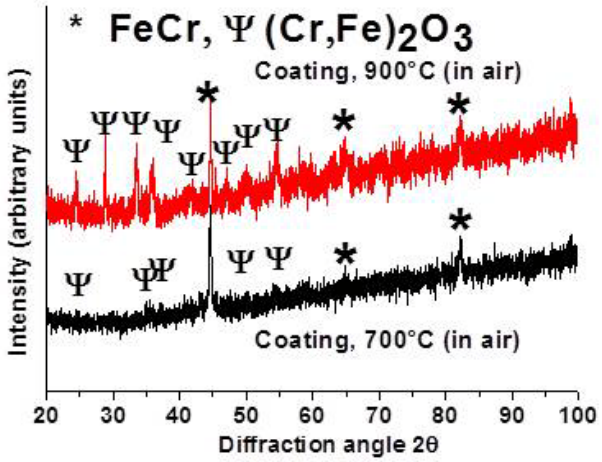

Fig 6.13: The XRD patterns of the scale formed on coated specimen (NC) after cyclic oxidation of 50 cycles in air at 700^{0} C and 900^{0} C.

6.2.4 Discussion

The formation of different phases, interdiffusivity of alloying elements, and protective nature of scales formed under shorter exposure periods to high temperature environment (700 ^{o}C & 900^{o}C) are completely different as compared to that of the conventional coatings, as evident from the XRD, SEM/EDS, and X-ray mapping results obtained in the present work. The nanosized grain morphology of the coating facilitated the formation of protective scales which is continuous, adherent, and non-porous due to the higher diffusivity of alloying elements in the coatings. It precludes high temperature oxidation by acting as a diffusion barrier between the environment and coating. The oxide scale is found to be continuous, dense, and adherent. Fig. 6.12 shows the scale mainly consists of oxides of Cr and Fe. X-ray

mapping of different elements is shown in Figure 6.12. The oxide scale is dense and uniform in thickness. Some alloying elements of the substrate such as Ni diffused into the coating. The corrosion resistance of the coatings is attributed to rapid formation of oxides at the coating splat boundaries due to penetration of the oxidizing species along the splat boundaries. After few cycles, once the oxides are formed at splat boundaries, the coating becomes dense; consequently the growth of the oxides becomes limited mainly to the surface of the specimen. Schematic representation of the possible oxidation mode of the coated specimen (NC) at 900^0C after 50 cycles is shown in fig. 6.14.

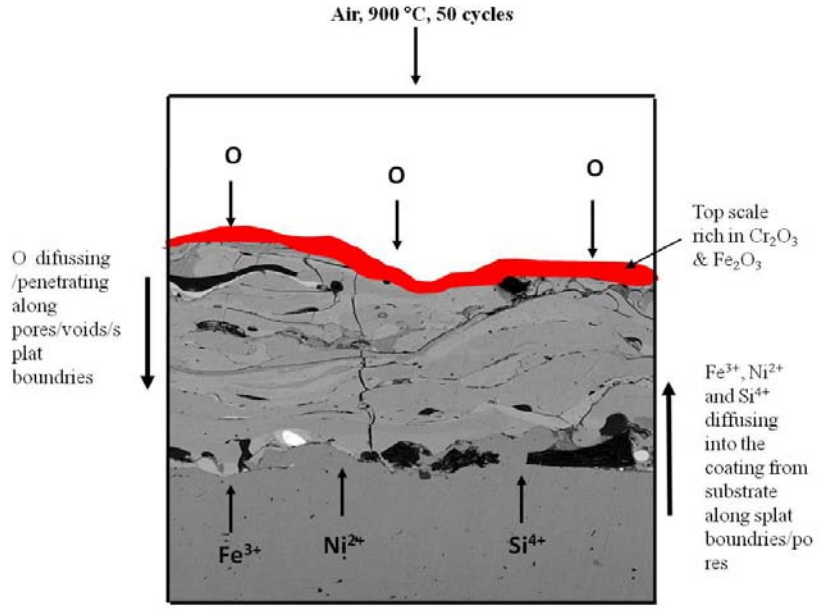

Fig 6.14: Schematic of the proposed oxidation mechanism of coated specimen (CC) at 900^0 C in Air after 50 cycles.

6.2.5 Conclusions

- The oxidation behavior of coating was found to obey parabolic rate law.
- The formation of shielding layers of chromium oxide and iron oxide imparts high temperature oxidation resistance on the coated specimen.
- The diffusion controlled reaction upon formation of Cr_2O_3 films on the coatings surface limits the diffusion of aggressive species such as air and other impurities in to the coatings.
- HVAS coated (NC) specimens exhibited excellent oxidation and wear/spallation resistance.

6.3 HOT CORROSION STUDIES IN MOLTEN SALT ENVIRONMENTS

6.3.1 Introduction

High velocity arc spray process (HVAS) is one of the most promising thermal spray technologies for high quality wear resistant coatings. This technique offers producing hard coatings with considerable adherence strength and compressive residual stresses.

The field of nanostructured materials and nanostructured coatings fabricated by different thermal spray techniques demonstrate development in last few years, owing to attractive combination of their novel properties. Nanostructured materials have received considerable interest for the enhanced corrosion and wear resistance (Rahman et al., 2013; Zhou et al., 2013; Chawla et al., 2011; Planche et al. 2004; Lee et al., 2006; Bansal et al., 2003; Basak et al., 2008; Georgiou 2013; Li et al., 2010; Kai et al., 2009). It can be anticipated that such wear resistant coatings will be used for structural parts in elevated temperature environments. The degradation mechanisms of high velocity arc sprayed FeCr based alloy coatings exposed to molten salt (Na_2SO_4-82%$Fe_2(SO_4)_3$) environment at 700^0C under cyclic conditions has not been studied so far. Knowledge of the reaction kinetics and microstructural changes of the oxide scales formed at high elevated temperatures in aggressive environment are important for evaluating the performance of materials in high temperature applications (Hussain et al., 1994; Matthews et al., 2003).Therefore, the present work has been focused to study microstructural changes and hot corrosion behavior of FeCr-based coatings after exposure of 10 and 50 hrs in molten salt (Na_2SO_4-60% V_2O_5) & (Na_2SO_4-82%$Fe_2(SO_4)_3$) environment at 700ºC & 900ºC by using FE-SEM/EDS, XRD and thermogravimetric techniques, respectively. The microstructural changes were characterized and correlated with the hot corrosion behavior of coatings.

6.3.2 Experimental details

The substrate material, coating formulation and the oxidation studies are explained in detail in section 3.1, 3.2.3 and 3.4.1.

6.3.3 Results

6.3.3.1 Weight change measurements

Weight change per unit area (mg/cm^2) versus number of cycles plots for the coated specimens (NC) exposed to molten salt (Na_2SO_4-60% V_2O_5) environment at 700^0C and 900^0C under cyclic conditions after 50 cycles is shown in Fig. 6.15a. It is obvious from the plots that at 700ºC, the coated specimens (NC) show a general tendency to approach a steady state after a gradual increase in weight during the initial 25 cycles of the study; whereas at high temperature (900ºC), there is a high rate of increase in weight gain up to 5 cycle after which it shows a gradual increase in weight up to 50 cycles of

the study. This suggests superior high temperature degradation resistance of NC coating. In Fig. 6.15b, the square of weight gain per unit area (mg^2/cm^4) versus number of cycles for coated specimens (NC) is plotted. The trend in oxide growth at 700ºC and 900ºC can be approximated to a parabolic relationship. The parabolic rate constants K_p values for NC was found to be 4.05 x 10^{-11} $g^2cm^{-4}s^{-1}$ and 5.36 x 10^{-11} $g^2cm^{-4}s^{-1}$, respectively. The K_p value for the CC was found to be nearly twice of the K_p value of the NC at 900ºC.

Weight change per unit area (mg/cm^2) versus number of cycles plots for the coated specimens (NC) exposed to molten salt (Na_2SO_4-82%$Fe_2(SO_4)_3$) environment at 700^0C and 900^0C under cyclic conditions after 50 cycles is shown in Fig. 6.16a. The plot reveals that NC coated specimens have undergone lesser overall weight gain at 700 & 900ºC as compared to uncoated counterpart. It is obvious from the plots that at 700ºC, the coated specimens show a general tendency to approach a steady state after a gradual increase in weight during the initial 10 cycles of the study; whereas at high temperature (900ºC) there is a high rate of increase in weight gain up to 5 cycle after which it show a gradual increase in weight up to 50 cycles of the study. This suggests superior hot corrosion resistance of NC coating. Square of weight gain per unit area (mg^2/cm^4) versus number of cycles for the uncoated and coated specimen were plotted (Fig 6.16b). The trend in oxide growth at 700ºC and 900ºC can be approximated to a parabolic relationship. The parabolic rate constants K_p values for the uncoated (310S ASS) subjected to cyclic hot corrosion in molten salt for 50 hours at 700º C and 900^0 C were calculated and found to be 8.6 x 10^{-11} $g^2cm^{-4}s^{-1}$ and 24.4 x 10^{-11} $g^2cm^{-4}s^{-1}$, respectively..Where as, the parabolic rate constants K_p values for NC was found to be 2.94 x 10^{-11} $g^2cm^{-4}s^{-1}$ and 4.72 x 10^{-11} $g^2cm^{-4}s^{-1}$, respectively. The K_p value for the NC was found to be nearly one-third and one-fifth of the K_p value of the uncoated specimen at 700 & 900ºC, respectively.

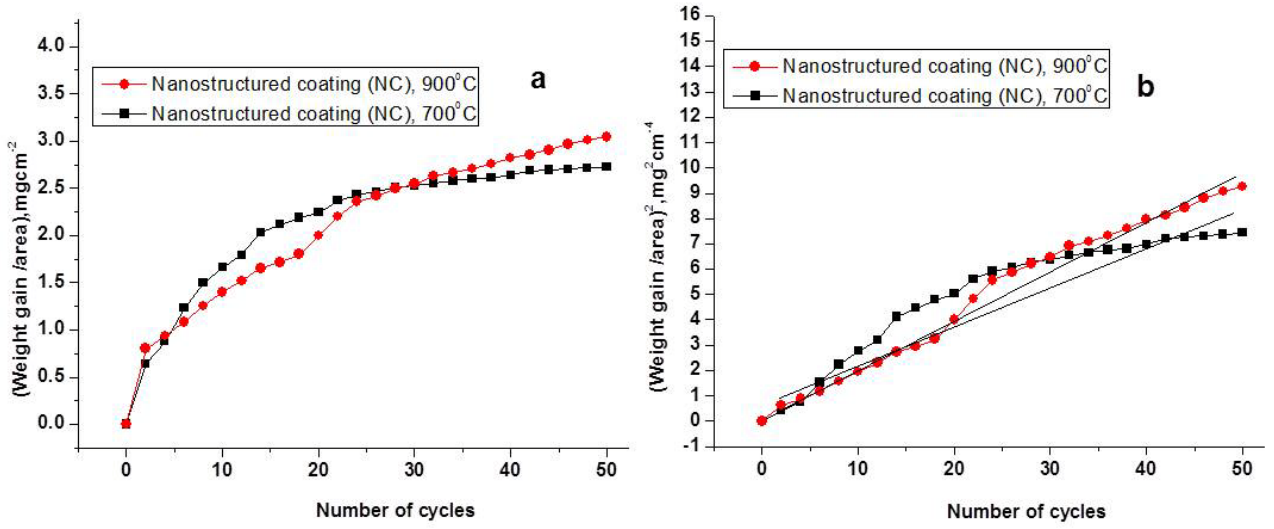

Fig 6.15: (a) Weight gain after oxidation per unit area versus number of cycles and (b) Weight gain afteroxidation per unit area)^2 versus number of cycles, for coated specimens (NC) subjected to hot corrosion in molten salt (Na_2SO_4-60% V_2O_5) environment at 700^{0}C & 900^{0}C for 50cycles.

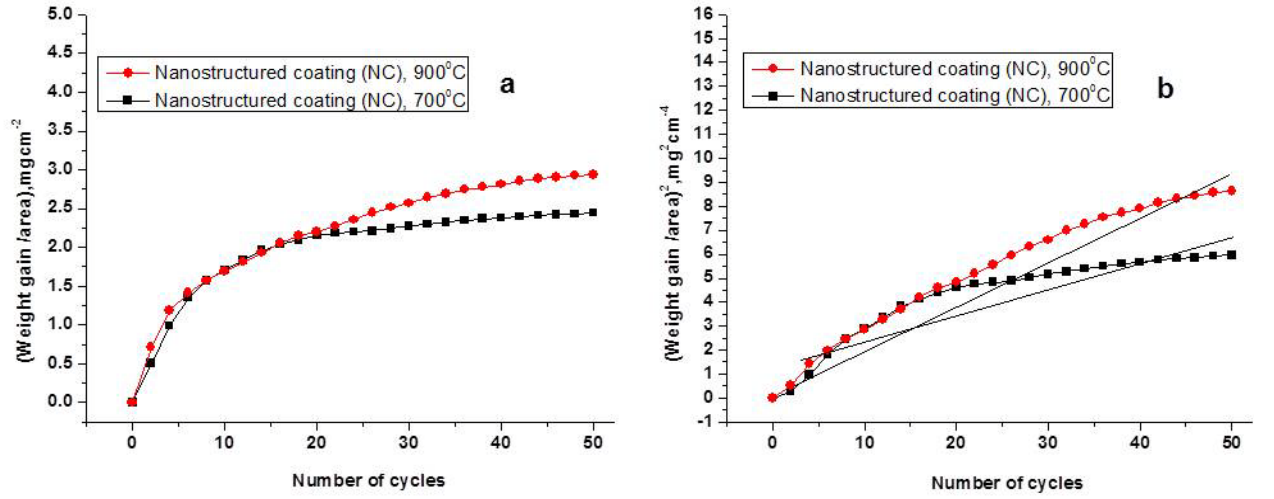

Fig 6.16: (a) Weight gain after oxidation per unit area versus number of cycles and (b) Weight gain after oxidation per unit area)^2 versus number of cycles, for the coated specimens (NC) subjected to hot corrosion in molten salt (Na_2SO_4-82% $Fe_2(SO_4)_3$) environment at 700^{0}C & 900^{0}C for 50 cycles.

6.3.3.2 FE-SEM/EDS analysis

6.3.3.2.1 Surface morphology of the scales

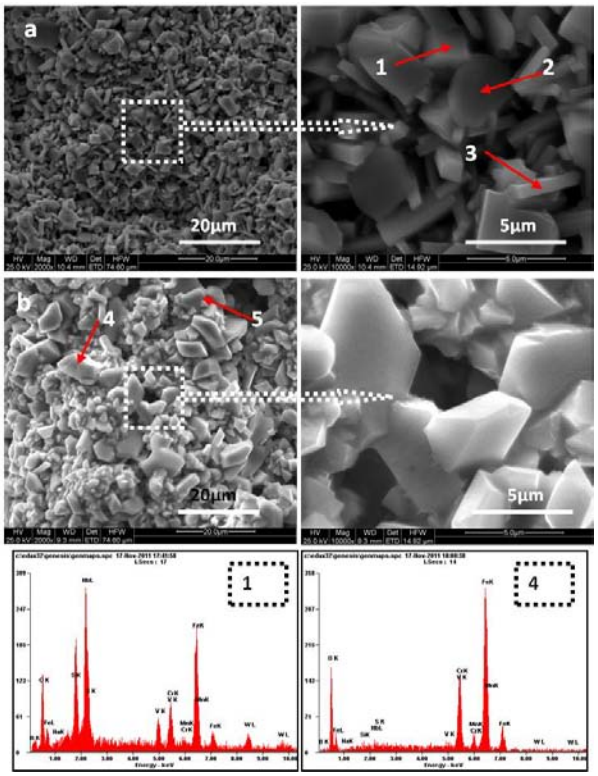

Fig 6.17: Surface scale morphology and EDS analysis for the coated specimens (NC) subjected to hot corrosion in molten salt (Na_2SO_4-60% V_2O_5) environment at 700^0C for (a) 10 cycles and (b) 50 cycles.

Table 6.2: EDS analysis results (wt.%) corresponding to Fig. 6.17 for the nano structured alloy coating exposed to molten salt (Na_2SO_4-60%V_2O_5) environment at 700^0C under cyclic condition (a) after 10 hours, (b) after 50 hours.

Elements	B	O	Na	Si	Nb	S	V	Cr	Mn	Fe	W
1	29.21	14.72	0.37	3.02	17.23	0.57	2.31	3.65	0.33	16.26	12.33
2	15.32	24.19	1.45	2.43	0.00	2.29	11.72	8.34	1.13	33.12	0.00
3	35.84	15.63	0.57	3.01	14.57	0.53	2.78	2.74	0.30	14.53	9.49
4	10.19	18.79	0.62	0.53	1.89	0.38	0.90	15.14	0.87	48.09	2.60
5	0.00	18.15	0.64	0.62	1.51	0.56	1.22	16.78	1.21	55.98	3.34

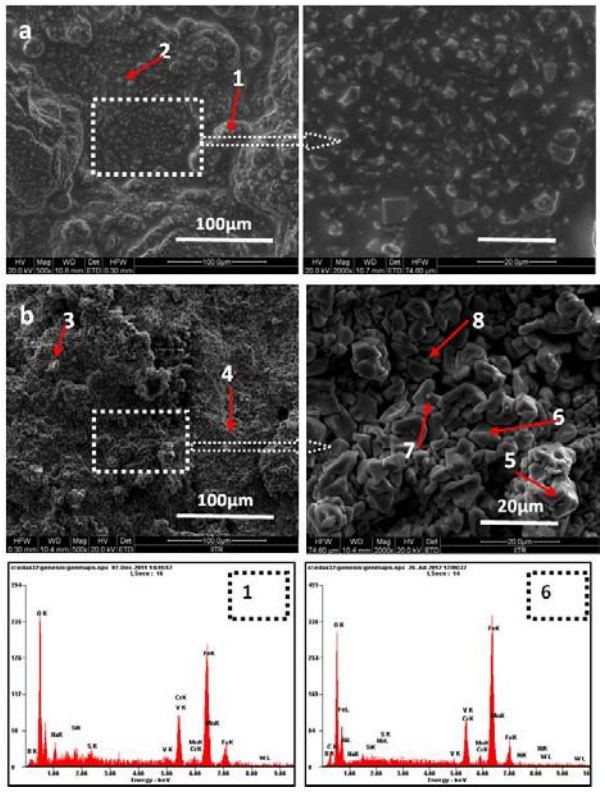

Fig 6.18: Surface scale morphology and EDS analysis for the coated specimens (NC) subjected to hot corrosion in molten salt (Na_2SO_4-60% V_2O_5) environment at 900^0C for (a) 10 cycles and (b) 50 cycles.

Table 6.3: EDS analysis results (wt.%) corresponding to Fig. 6.18 for the nano structured alloy coating exposed to molten salt (Na_2SO_4-60%V_2O_5) environment at 900^0C under cyclic condition (a) after 10 hours, (b) after 50 hours.

Elements	**B**	**O**	**Na**	**Si**	**Nb**	**S**	**V**	**Cr**	**Mn**	**Fe**	**W**
1	5.98	20.95	1.37	0.51	44.41	0.37	0.84	5.53	0.13	18.82	1.09
2	12.86	7.07	0.16	3.82	56.84	2.29	0.33	0.55	0.18	1.26	14.64
3	0.00	2.53	0.25	1.65	2.91	2.06	10.42	14.27	1.53	51.29	10.99
4	17.47	19.07	0.78	0.65	0.99	0.27	1.26	9.71	0.50	40.57	2.71
5	11.72	14.72	0.60	0.42	0.61	0.20	0.40	8.06	0.30	52.57	1.29
6	16.11	19.04	0.36	0.17	0.15	0.17	0.67	8.43	0.49	42.15	1.93
7	18.97	19.32	0.42	0.27	0.26	0.25	0.63	6.36	0.37	43.26	2.60
8	10.88	18.57	0.48	0.45	0.47	0.00	0.47	6.78	0.86	51.24	3.78

Detailed analysis of surfaces of coated specimens NC exposed to molten salt (Na_2SO_4-60%V_2O_5) environment at 700^0C and 900^0C under cyclic conditions for 10, and 50 cycles is shown in Fig. 6.17 and Fig. 6.18, respectively.

FE-SEM analysis of the coated surface of NC at 700ºC indicates some micro crack and loosely bound oxide particles after 10 cycles of oxidation (Fig 6.17a), while the thick layers of oxides are found after oxidation at 50 cycles (Fig. 6.17b). EDS analysis indicates (Table 6.2) the major presence of Cr, O, Fe, Nb, B, W along with minor presence of Si, Mn, S, V, and Na.

The surface of the oxidized coated specimen of NC at 900ºC appears as consisting of spongy nodules after oxidation for 10 cycles (fig 6.18a). EDS analysis (Table 6.2) of nodules indicates Cr, O, Fe, Nb, B and W. Minor amount of Si, Mn, S, V, and Na are detected in the oxide scale. With increase in number of cycles to 30, the number of nodules has increased. However, the surface is completely covered by the nodules after oxidation for 50 cycles (Fig 6.18b). Whereas in case of the coated specimens, NC exposed to molten salt (Na_2SO_4 - 82% $Fe_2(SO_4)_3$) environment at 700^0C and 900^0C under cyclic conditions for 10 and 50 cycles is shown in Fig. 6.19 and Fig. 6.20, respectively.

Detailed analysis of surfaces of coated specimens (NC) exposed to molten salt (Na_2SO_4-82%$Fe_2(SO_4)_3$) environment at 700^0C and 900^0C under cyclic conditions for 10 and 50 cycles is shown in Figs. 6.19 and Figs. 6.20, respectively. The oxide surfaces are relatively intact with the substrate. The microstructure after oxidation at 700^0C for 10 cycles consists of porous morphology of oxide surface (6.19a). The walls of the porous body are made with strongly connected particles of irregular shape. With increase in number of cycles to 50, increased bonding of particles and macrocracks in porous structures are observed (6.19b). There is no observable change in the EDS analysis of the oxide surfaces obtained after 10 and 50 cycles.

SEM images of nanostructured coated samples after heating at 900^0C for 10 cycles indicates considerable spalling and breaking of oxide surface. High magnification of the oxide surface in Fig. 6.20a shows cylindrical particles. The surface after heating for 50 cycles shows macrocracks (Fig. 6.20b) and large numbers of cylindrical and irregular shaped oxide particles are also observed after heating for 50 cycles (Fig. 6.20b). EDS analysis shows that particles are rich in chromium and oxygen after 50 cycles, whereas the presence of iron is also observed after 10 cycles.

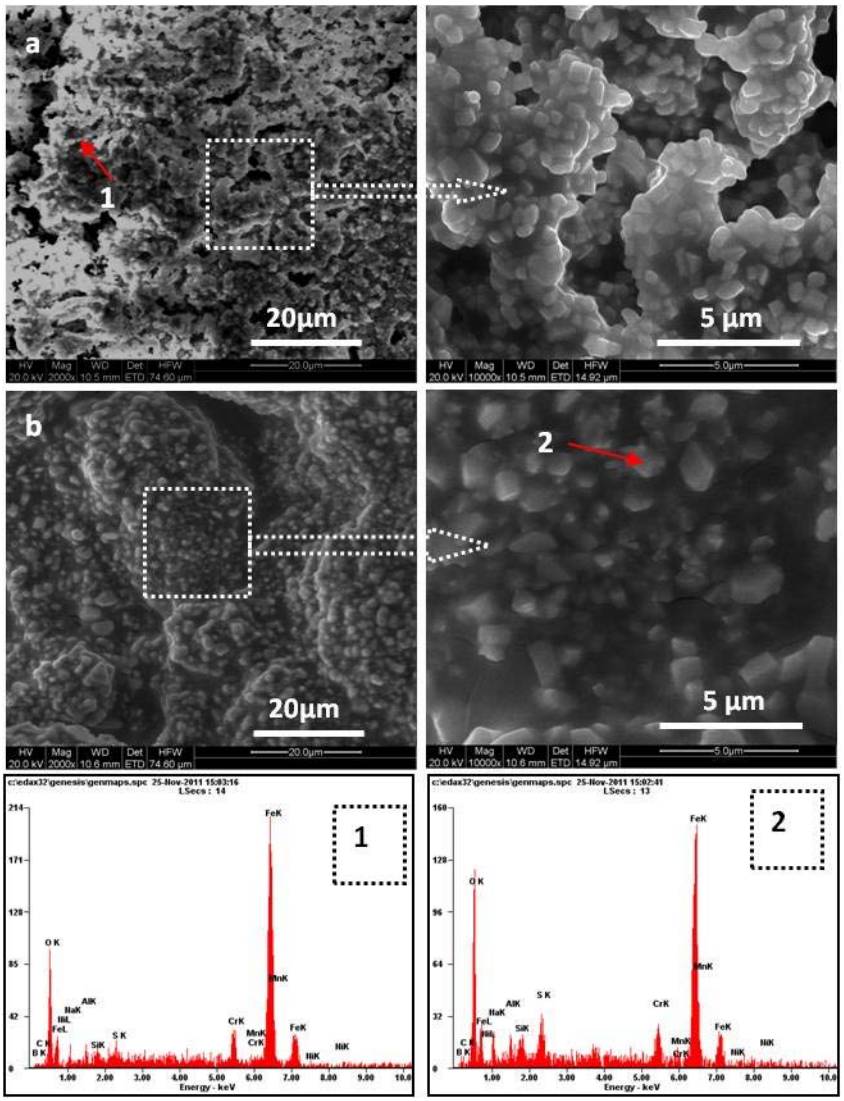

Fig 6.19: Surface scale morphology and EDS analysis for the coated specimens (NC) subjected to hot corrosion in molten salt (Na_2SO_4 - 82% $Fe_2(SO_4)_3$) environment at 700^0C for (a) 10 cycles and (b) 50 cycles.

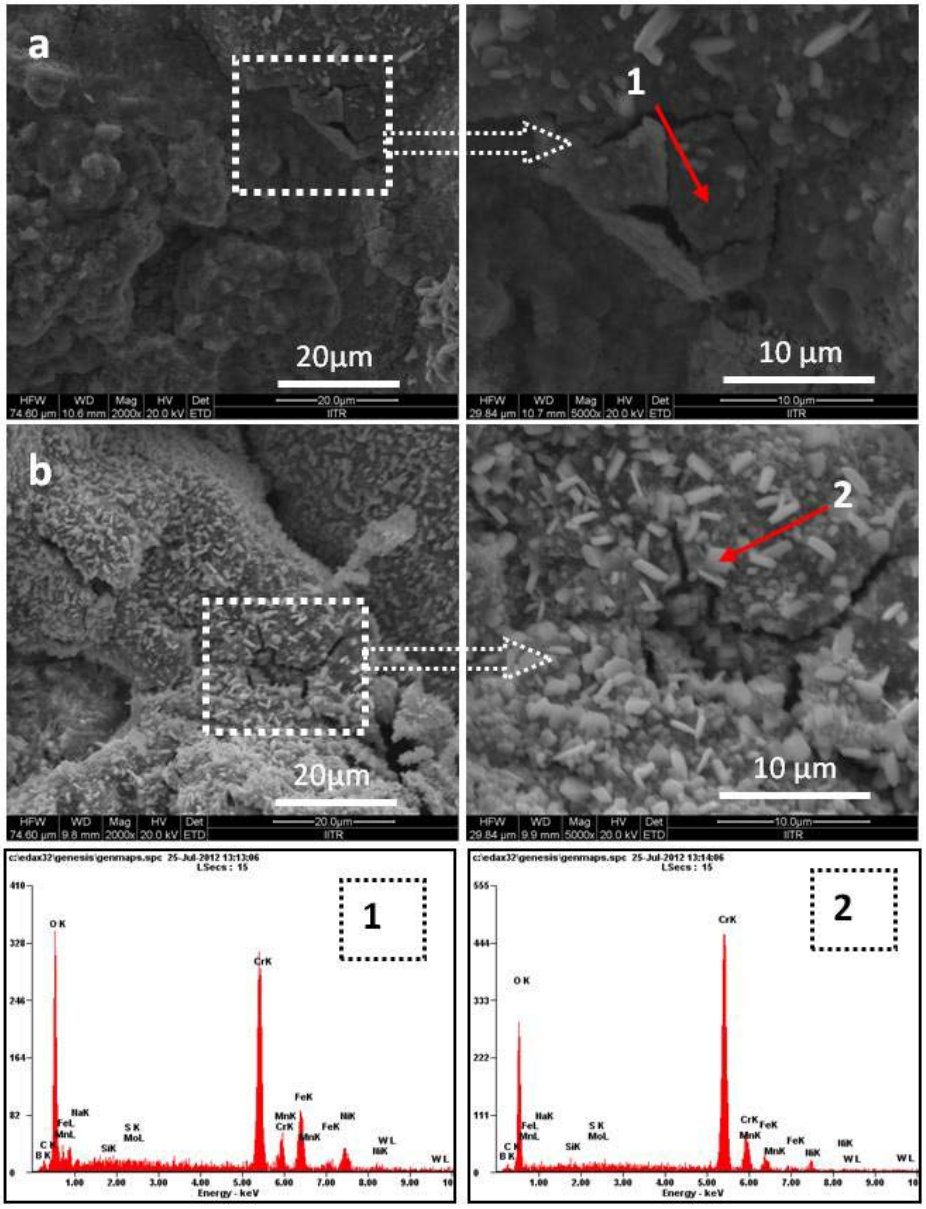

Fig 6.20: Surface scale morphology and EDS analysis for coated specimen (NC) subjected to hot corrosion in molten salt (Na_2SO_4 - 82% $Fe_2(SO_4)_3$) environment at 900^0C for (a) 10 cycles and (b) 50 cycles.

6.3.3.2.2 Cross-sectional analysis and X-ray mapping of the scale

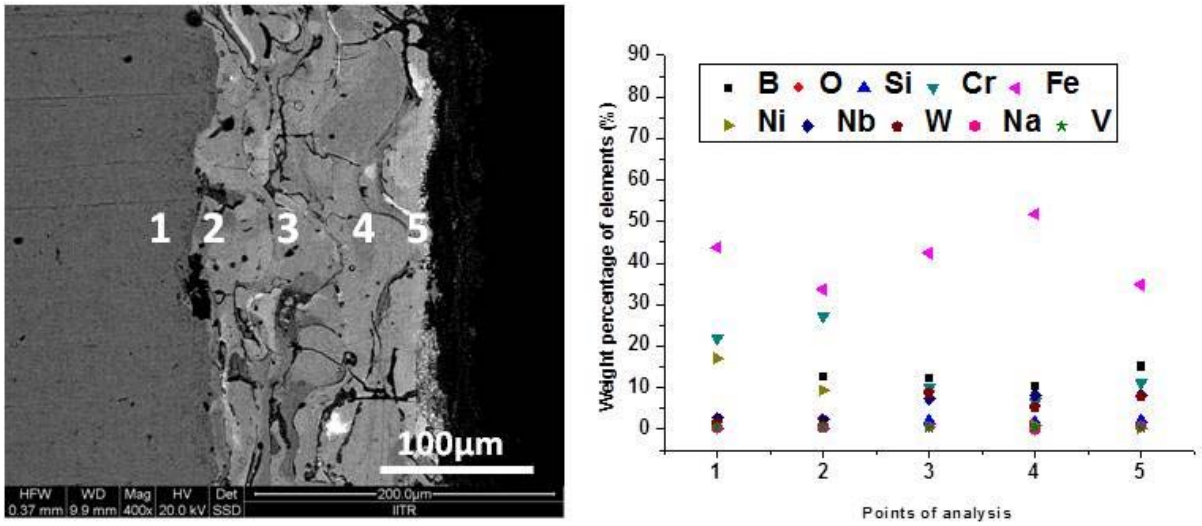

Fig 6.21: Morphology of oxide scale across the cross section of NC coated specimens, subjected to hot corrosion in molten salt (Na_2SO_4-60% V_2O_5) environment at 900^0C for 50 cycles.

The cross-sectional analyses and X-ray mapping of different elements of the coated specimens exposed to molten salt (Na_2SO_4-60%V_2O_5) environment at 900^0C under cyclic conditions after 50 cycles are shown in Fig.6.21. Figure 6.21 shows that the oxide scale mainly consist of Fe, Cr, B and O along with significant amounts of Nb, W, Si, Ni, Na and V (Fig. 6.21). Fig. 6.23 shows the X ray mapping of scale in NC, it mainly consists of Cr, Fe, Nb and O where as S, V and Na have diffused in to the coating.

The cross-sectional analyses and X-ray mapping of different elements of the coated specimens exposed to molten salt (Na_2SO_4 - 82% $Fe_2(SO_4)_3$) environment at 900^0C under cyclic conditions after 50 cycles are shown in Fig.6.22. It indicates that the oxide scale mainly consists of Fe, Cr, B and O along with significant amounts of Nb, W, Si, Ni and Na. Fig. 6.24 shows X-ray mapping of oxide scale in NC. It showed Cr, Fe, Nb and O where as S and Na have diffused in to the coating. In case of coated sample, the oxide surface is intact and adherent to the substrate. The removal of the oxide surface is less as compared to the uncoated specimen. The large amount of sulphur diffusion into the sample can be observed in case of uncoated sample, whereas sulphur is restricted to diffuse in to the substrate in case of coated surface. The formation of oxides of chromium and iron might have acted as barrier to the inward diffusion of oxygen into the coating.

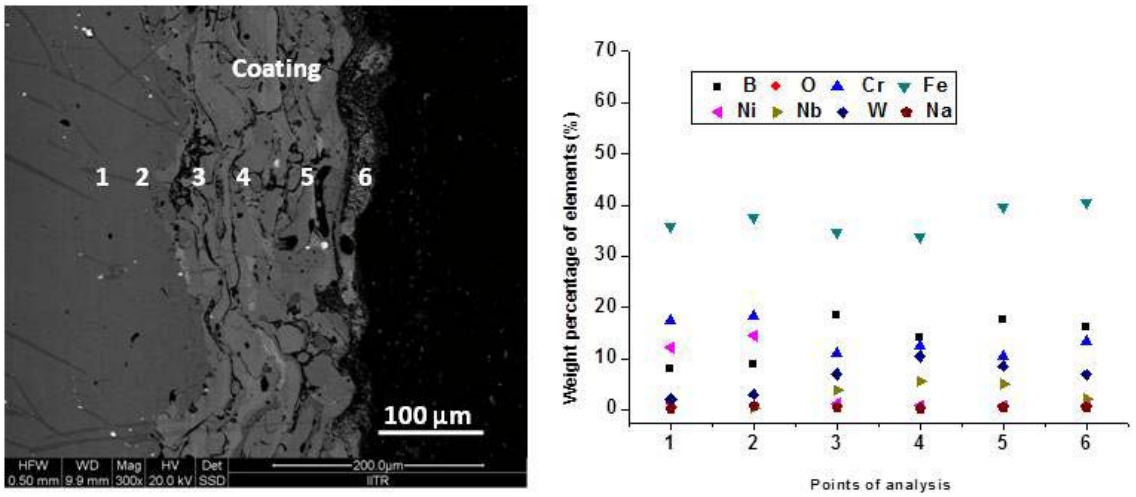

Fig 6.22: Morphology of oxide scale across the cross section of NC coated specimens, subjected to hot corrosion in molten salt (Na_2SO_4 - 82% $Fe_2(SO_4)_3$) environment at 900^0C for 50 cycles.

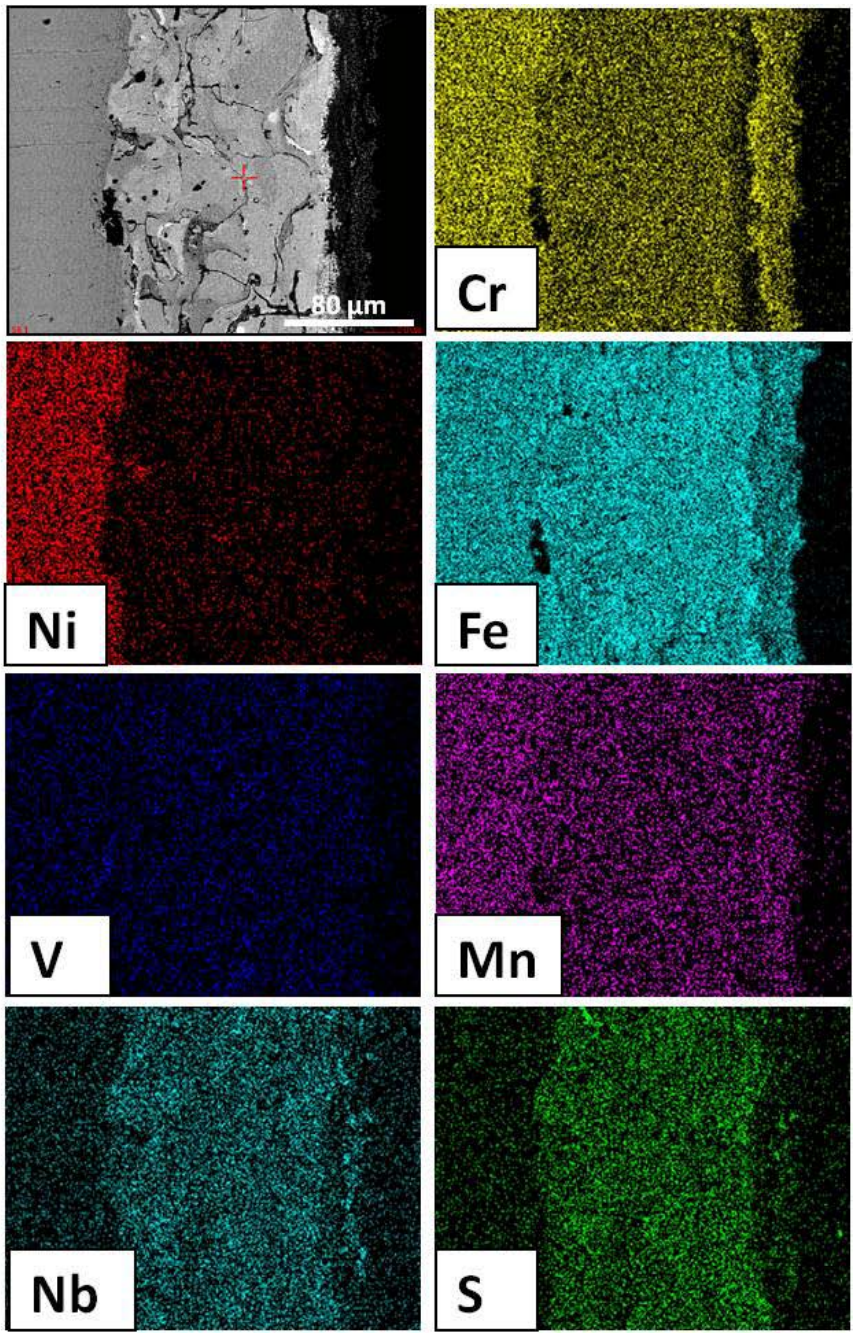

Fig 6.23: Composition image (SE) and X-ray mapping of the cross section of the coated specimen subjected to hot corrosion in molten salt (Na_2SO_4-60% V_2O_5) environment at 900^0C for 50 cycles.

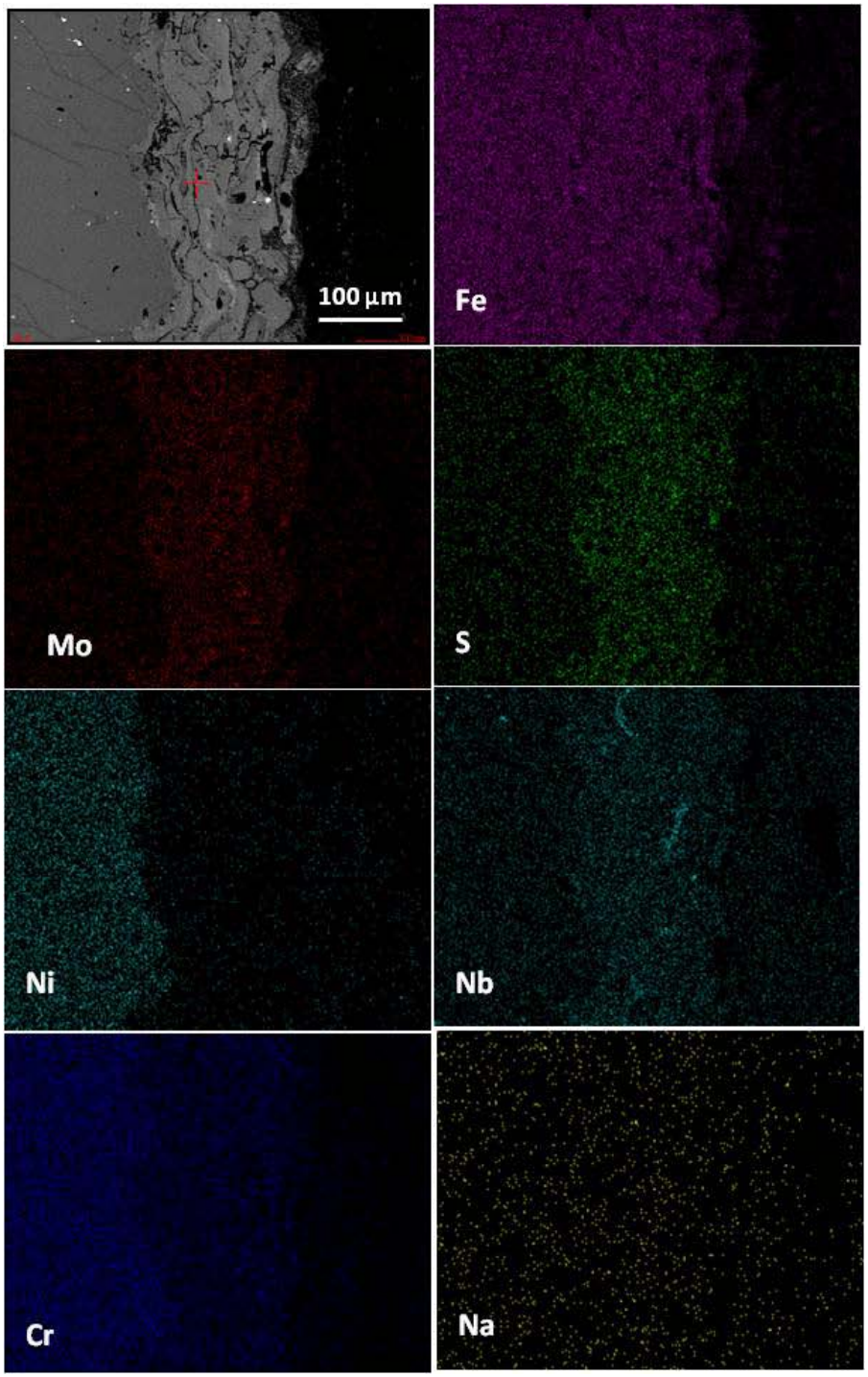

Fig 6.24: Composition image (SE) and X-ray mapping of the cross section of the coated specimen subjected to hot corrosion in molten salt (Na_2SO_4 - 82% $Fe_2(SO_4)_3$) environment at 900^0C for 50 cycles.

6.3.3.3 X-ray diffraction analysis (XRD) analysis

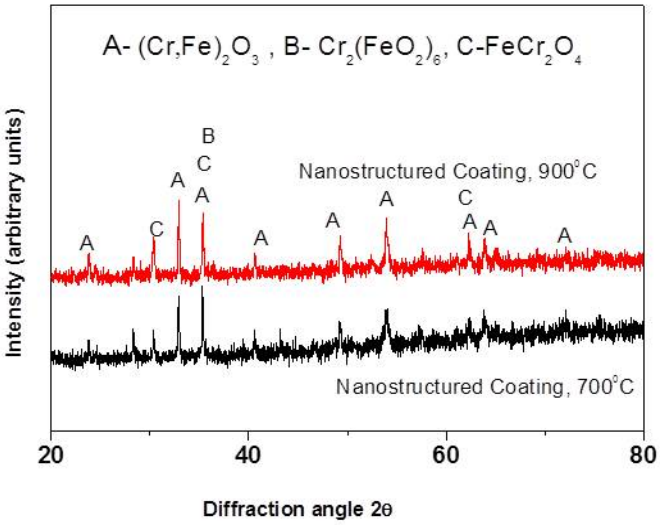

Fig 6.25: The XRD patterns of the scale formed on coated specimen (NC), subjected to hot corrosion in molten salt (Na_2SO_4-60% V_2O_5) environment at 700^0C & 900^0C for 50 cycles.

The XRD patterns of the scale formed on coated specimens (NC) exposed to molten salt (Na_2SO_4-60%V_2O_5) environment at 700^0C and 900^0C under cyclic conditions after 50 cycles are shown in Fig.6.25. The XRD diffractograms for the coated specimen (NC) revealed the formation of (Cr, Fe)$_2O_3$, $Cr_2(FeO_2)_6$ as very strong phases, $FeCr_2O_4$ as low intensity phases. The XRD patterns of the scale formed on coated specimens (NC) exposed to molten salt (Na_2SO_4 - 82% $Fe_2(SO_4)_3$) environment at 700^0C and 900^0C under cyclic conditions after 50 cycles are shown in Fig. 6.26. The XRD diffractograms for the coated specimen (NC) revealed the formation of ($Fe_{0.6}$, $Cr_{0.4}$)$_2O_3$, Mn_2O_3, and $Mn_2Cr_2O_4$ as very strong phases. Some additional phases of $Mn_2Cr_2O_4$ observed at 900^0C, the intensities of phases observed have increased with increase in temperature.

Chromium shows higher affinity for oxygen and form Cr_2O_3 during the initial stages of high temperature degradation, which offers better oxidation resistance owing to its low rate of oxide growth and ability and act as effective barriers against migration of ions.

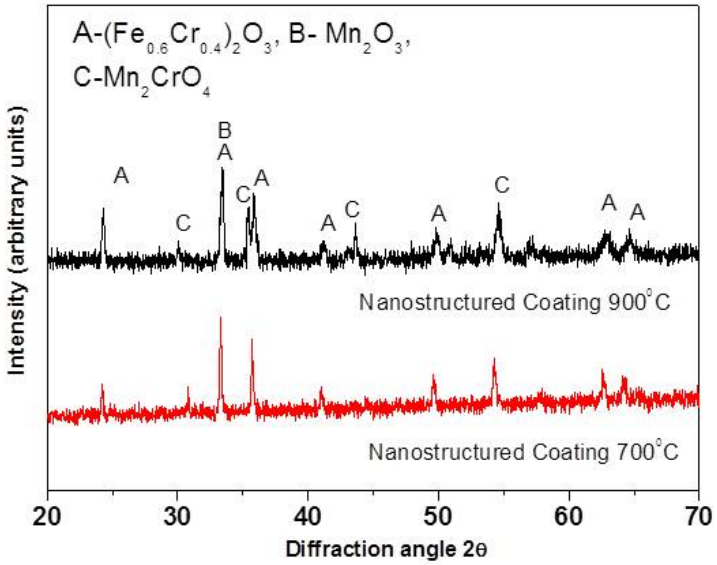

Fig 6.26: The XRD patterns of the scale formed on coated specimen (NC), subjected to hot corrosion in molten salt (Na_2SO_4 - 82% $Fe_2(SO_4)_3$) environment at 700^0C & 900^0C for 50 cycles.

6.3.3.4 Discussion

The failure of the protective oxide layer, which enables molten salt to access directly the substrate material. The failure may result from chemical reactions. The salt fluxing mechanism was originally proposed by Goebel and Pettit (Goebel et al., 1970A).

The shielding efficiency of oxide scale will be lost due to fluxing in molten salt. Fluxing is due to either by (i) combination of oxides with O^{-2} i.e. basic fluxing, or (ii) decomposition of oxides i.e. acidic fluxing. The reaction of alkali sulphates with iron oxides in the presence of SO_3 to form $(Na)_3Fe(SO_4)_3$, as per the following (Sidhu et al., 2006K).

$$2Fe_3O_4 + 9Na_2SO_4 + 9SO_3 + 1/2O_2 = 6\ Na_3Fe(SO_4)_3$$

$$Fe_2O_3 + 3\ Na_2SO_4 + 3SO_3 = 2\ Na_3Fe(SO_4)_3$$

The $(Na)_3Fe(SO_4)_3$ is thought to lead to the degradation of coal fired plant super heaters.

The present results indicate that HVAS-sprayed FeCr based nanostructured coatings (NC) exhibit high hot corrosion resistance. It showed better performance than 310S ASS due to the quick formation of uniform Cr_2O_3 scale, with a denser structure. The nanostructured coatings with high volume fraction of grain boundaries facilitate rapid Cr diffusion, leading to the reaction between Cr and oxygen in the air (Tao Kai, et al., 2009). The nanostructured coatings promote the formation of oxide scale, which is denser than its conventional coatings. It may be mentioned that there is no reported literature on high temperature oxidation studies in molten salt environment of FeCr based nanostructured coatings deposited by HVAS. The improved corrosion resistance of the nanostructured FeCr based nanostructured coatings as observed in the present work is in tandem with the similar studies made on the Ni based super alloy coatings deposited by other routes like sputtering and HVOF (Rahman et al., 2013). The reaction rate between alloying elements and oxygen for the formation of continuous oxide scale to cover the whole surface of the coated specimens is relatively high in case of nanostructured coatings as compared to 310S ASS or other conventional coatings. Rahman et al. reported that the critical alumiunium or chromium required for the development of a continuous Al_2O_3 or Cr_2O_3 is significantly lower for the nanostructured coatings than that of conventional coatings (Rahman et al., 2013). The nanostructured coatings with high volume fraction of grain boundaries facilitate rapid Cr diffusion, leading to the reaction between Cr and oxygen in the air. X-ray mapping analysis (Fig. 6.23 & 6.24) suggests that the nanostructured coatings are found to be dense and successful to maintain contact with the bare alloy. It is also evident from the oxygen map that the bare alloy did not undergo internal oxidation. This suggests effective shielding nature of the nanostructured coating. The nanostructured coating was good in resisting spallation.

The possible hot corrosion modes for the nanostructured coating subjected to the molten salt environments for 50 cycles at 900^0C are schematically represented in Fig. 6.27 & 6.28 respectively. Corrosion species such as S, O, V diffused into the coating through the microcracks and pores present in the coating. The presence of chromium and iron in the scale was noticed and small amount of alloying element such as Ni has migrated from the substrate into the coating. The diffusion controlled reaction upon formation of Cr_2O_3 films on the coatings surface limits the diffusion of aggressive species such as air and other impurities in to the coatings.

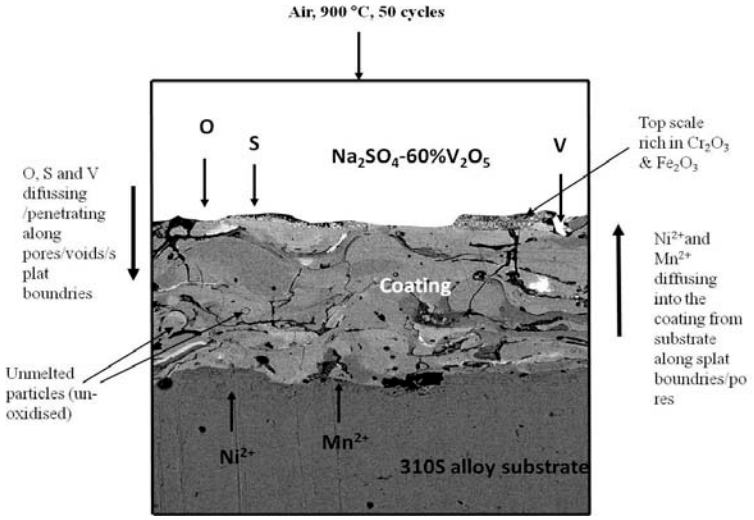

Fig 6.27: Schematic of the proposed oxidation mechanism of coated specimen (NC) subjected to hot corrosion in molten salt (Na_2SO_4-60% V_2O_5) environment at 900^0C for 50 cycles.

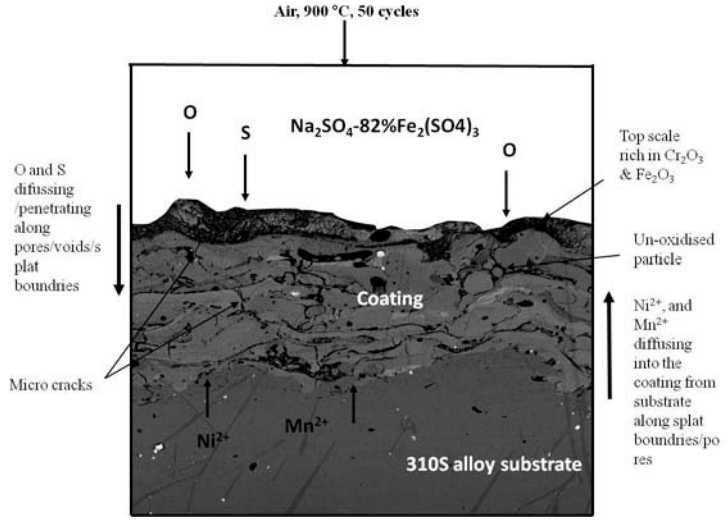

Fig 6.28: Schematic of the proposed oxidation mechanism of coated specimen (NC)subjected to hot corrosion in molten salt (Na_2SO_4 - 82% $Fe_2(SO_4)_3$) environment at 900^0C for 50 cycles.

6.3.3.5 Conclusions

- FeCr-based nanostructured alloy coatings were deposited successfully on 310 alloy substrate by the HVAS-spraying process.
- The scale formed on the surface of the coating was adherent with some sign of minor cracks.
- The splat and globular morphology of the as deposited coatings provides relatively high density to the coatings, which is essential for achieving degradation resistance of the coatings.
- The formation of protective Cr_2O_3 oxide layers is responsible for imparting high wear and corrosion resistance.
- The diffusion controlled reaction upon formation of Cr_2O_3 films on the coatings surface limits the diffusion of aggressive species such as air and other impurities in to the coatings.

6.4 EROSION-CORROSION STUDIES IN ACTUAL INDUSTRIAL ENVIRONMENT

6.4.1 Experimental details

The substrate material, coating formulation and the oxidation studies are explained in detail in section 3.1, 3.2.3 and 3.4.1.

6.4.2 Results

6.4.2.1 Weight change measurements

The extent of oxidation-erosion loss was measured in terms of coating layer lost due to scaling after 1500 hours of exposure. Rough estimate of the thickness lost for HVAS nanostructured coatings was 0.04 mm, and the rate of thickness loss was 9.2 mpy. The weight gain per unit area for the HVAS coating was found to be 7.81 mg cm^{-2}. This small weight gain on the coated specimen is due to the degradation and ash particles deposition on exposed surfaces.

6.4.2.2 FE-SEM/EDS analysis

6.4.2.2.1 Surface morphology of the scales

In order to assess the performance of nanostructured FeCr-based coating in the actual service conditions, the coated specimens were placed in the industrial coal fired boiler for 1500 hours at 700 ± 10^{o}C where fly ash particles continuously thrown on the specimen. Results indicate that the coatings deposited on 310S steel by the HVAS process do not degrade in the boiler environment. FE-SEM analysis of the coated specimen after 1500 hours of exposure in the boiler environment is shown in Fig. 6.29. The oxide scale was adherent and minor spalling was observed at edges of the coated specimen. The surface also shows the pull-out of nodules. The periphery of the pulled-out areas indicates white contrast, the EDS analysis of which confirms the fly ash elements Al, Si, O. This indicates that the high velocity fly ash particles erode the oxide surface of the coated specimen. Further, the long and wider ploughs, craters and rough areas on the surface are signatures of erosion caused by the fly ash particles (Fig. 6.29 c, d and e). The scale consisted mainly of Cr, Fe and O, with significant amount of Al, Si, Mn and Na. The presence of ash deposited on the surface of coating was confirmed by EDS analysis (table 6.4). The oxide scale formed on the surface of coated specimen subjected to cyclic oxidation in coal fired boiler at 700 ±10^{o}C for 1500 hours was partially removed due to particle impact.

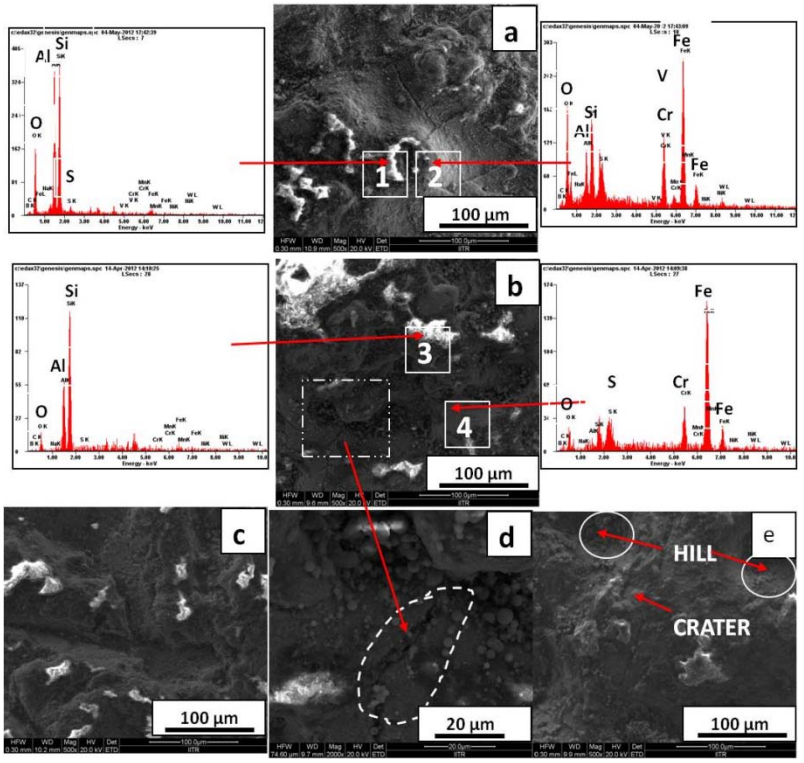

Fig 6.29: FE-SEM/EDS Surface analysis of coated specimen (NC) exposed to superheater of the coal fired boiler 700±10 ^{0}C for 1500 hours.

Table 6.4: EDS analysis results (wt. %) corresponding to Fig. 6.29 for the coated specimen subjected to cyclic oxidation in coal fired boiler at 700 ± 10 ^{o} C for 1500 hours.

	B	C	O	V	Al	Si	S	Cr	Mn	Fe	Ni	W	Nb
1	0	5.0	30.22	0.41	20.33	23.32	1.28	0.21	0	3	0.17	0.97	14.54
2	4.64	1.68	7.75	0.23	0.39	1.25	0.77	10.67	0.34	12.94	0.21	4.06	54.91
3	0	0	13.13	0	24.74	54.21	0	0.93	0	6.99	0	0	0
4	1.08	1.76	3.08	0	0.13	0.57	0.62	3.51	0.44	17.96	0.39	3.15	67.26

6.4.2.2.2 Cross-sectional analysis and X-ray mapping of the scale

The cross-sectional analysis of the coated specimens subjected to cyclic oxidation in coal fired boiler at 700 ± 10 ^{o} C for 1500 hours was performed and shown in Fig. 6.30. Figure 6.30 shows that the scale mainly consists of oxides of Fe and Cr along with significant amounts of Ni. The oxide scale is found to be continuous, dense, and adherent. Fig. 6.30 show the scale mainly consists of oxides of Cr and Fe. X-ray mapping of different elements is shown in Figure 6.30. The oxide scale is dense and uniform in thickness. However, in case of coal fired boiler, the scale mainly consists of oxides of Cr, Fe, whereas S and Na have diffused in to the coating. The formation of oxides of chromium and iron might have acted as barrier to the inward diffusion of oxygen into the coating.

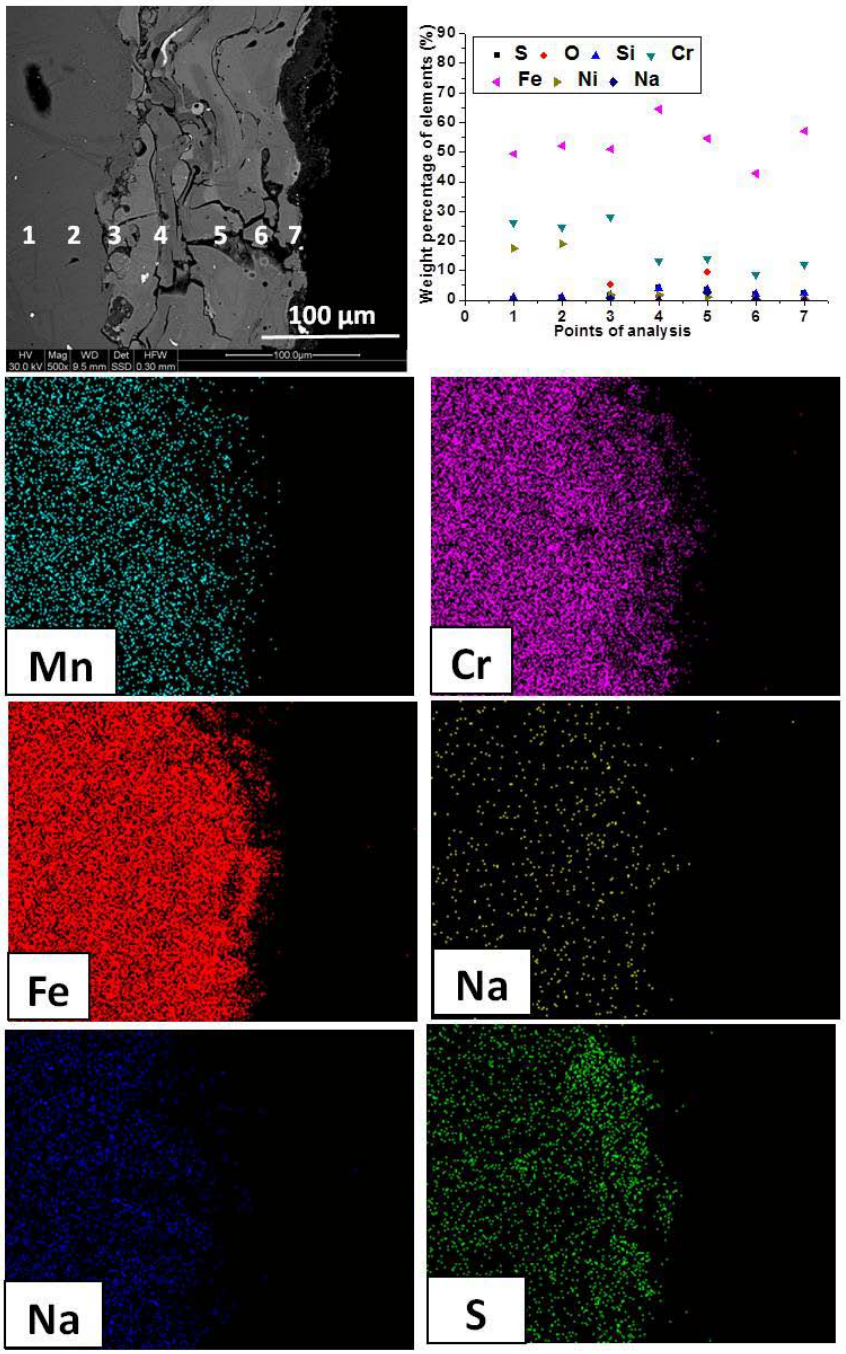

Fig 6.30: Composition image (SE), morphology of oxide scale across the cross section and X-ray mapping of the cross section of the coated specimen (NC) subjected to hot corrosion in actual boiler environment at 700±10 ^{0}C for 1500 hours.

6.4.2.2.3 X-ray diffraction analysis (XRD) analysis

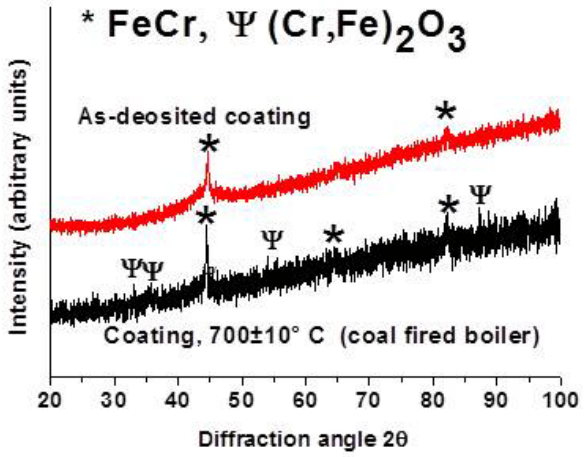

Fig 6.31: The XRD patterns of the scale formed on coated specimens (CC), subjected to hot corrosion in actual boiler environment at 700±10 ^{0}C for 1500 hours.

The XRD patterns of the scale formed on coated specimens (NC) subjected to hot corrosion in actual boiler environment at 700±10 ^{0}C for 1500 hours are shown in Fig. 6.31. The major and minor phases detected at the surface of the specimens are shown in the XRD graph. XRD analysis of the oxidized surface of the coated specimen after 1500 hours of exposure, in coal fired boiler environment, shows the presence of FeCr, (Cr, Fe)$_2$O$_3$ phases.

6.4.3 Discussion

The FeCr based nanostructured coatings deposited on 310S behaved very well in the boiler environment at 700 ± 10^{0}C. Due to the very low porosity of the developed coating, there was hardly any penetration of corrosive species into the coating. Coating was unaffected by any attack. The attack was limited to edges only otherwise coating acted as a shield between the corrosive species/environment and the metallic substrate and effectively hindered the corrosive species from migrating into substrate. Coating remained essentially adherent to the substrate. Continuous impact of fly ash and other particles entrapped in the air blast resulted in thickness loss of the coatings. Presence of Al_2O_3, SiO_2 and CaO is an indicative of fly ash on the surface of exposed samples, which was verified by EDS analysis. The detection of Si, Ca, Na, Fe along with O is an indication of embedded ash. There is a presence of hills and craters on the surface along with pits and cracks which is a clear indication of combined effect of erosion and corrosion caused by combined action of flue gases and fly ash. Hills and craters were formed on the surface indicating effect of erosion, which was limited to the surface only. The coating has protected the surface very well by covering surface of the alloy substrate 310S. This may be due to the fact that Cr_2O_3 probably

hinders the grain boundary diffusion of the elements. The compact and protective Cr_2O_3 layer separated the metal substrate from the boiler environment. As a result, the coating improved the wear and corrosion resistance. From weight gain and thickness loss data, it can be inferred that the protection to the base metals has been provided by the coating. The lower weight gain of bare alloy substrate than its coated counterpart might be attributed to spallation of the oxide scale in the actual environment of the coal fired boiler and fluxing action of the molten salt along with erosion of oxide scale. The most common deposit found on boiler super heaters is sodium vanadyl vandate, $Na_2O.V_2O_4.5V_2O_5$, which melts at a relatively low temperature, 550^0C. Above the melting point, the ash material corrodes metals by long-term contact (Sidhu and Prakash, 2006P). The more compact and less porous the coating, the higher is its erosion-corrosion resistance (Wang et al., 1992). The nanostructured coating was no longer oxidized and acted as an effective inert barrier to improve the isothermal and cyclic oxidation resistance of alloys exposed to boiler environment for 1500 hours. The nanostructured coatings show very dense structure , high thermal stability and excellent cracking/spallation resistance.

6.4.4 Conclusions

- The HVAS sprayed nanostructured coating maintained adherence to the steel substrate in the real boiler environment at 700±10 °C. The surface scales were also found to be intact.
- The coated 310S alloy substrate exhibited improved resistance to oxidation and erosion when compared against bare specimen.
- The coatings exposed to industrial environment of thermal power plant showed the formation of oxides of FeCr, $(Cr, Fe)_2O_3$ phases, which imparts protection to the substrate.
- Coated specimens (NC) exhibited excellent oxidation and wear/spallation resistance.

CHAPTER - 7

COMPARATIVE DISCUSSION

In this chapter, the performance of 310S alloy substrate, HVOF & HVAS spray coatings deposited on the 310S alloy substrates subjected to high temperature air oxidation,aggressive environments such as Na_2SO_4-60%V_2O_5, Na_2SO_4-82%$Fe_2(SO_4)_3$ *and in actual boiler environments , under cyclic conditions, is compared.*

7.1 Oxidation in air

The bar charts showing the overall weight gains in air at 700 & 900^0C cycles for the coated and bare specimens are presented in Fig. 7.1. The bare alloy substrate exhibits lower oxidation resistance than the coated specimens. The nanostructured coating (NC) exhibits highest oxidation resistance among all coatings deposited by different techniques. The development of oxides of chromium on the NC coatings imparts high oxidation resistance. Further, the scales developed on coatings were thin, dense and compact, which led to the less weight gain, as represented by the less value of parabolic rate constant. In the sub-scale region of coating, alloying elements remain in the un-reacted state and when oxides globules in the surface oxides allows penetrations of O little dipper in to the coating, it oxidize the coatings along the Ni reach splat boundaries. Further, Cr shows a tendency to form a thick band along the interface of coating and substrate. The oxidation behavior of all the coatings follow nearly a parabolic rate law (Table 7.1), excluding bare substrate, as it is slightly deviates as shown in fig 4.10.

Nanostructured coating (NC) provides the maximum oxidation resistance and is found successful in reducing weight gain as compare to the bare substrate 310S. It is due to the formation of oxides of Cr, and Fe on the coatings. The as deposited coatings seem to have good adhesion with the substrate as no cracks and pores are seen at the interface. Further, the scales formed on the nanostructured coatings are observed to be fine, dense and compact which contributes to the lower weight gain as evident from the lower parabolic rate constant. The slight deviation from the parabolic rate of cyclic oxidation is attributed to the formation and rapid growth of inhomogeneous oxides during oxidation process (Choi et al., 2002). The accelerated weight gain of the coated specimens was noted only during initial cycles. This is probably due to the rapid formation of oxides at the coating-splat boundaries and penetration of oxidizing species along the splat boundaries/open pores. However, weight gain was minimized subsequently due to densification and obstructed movement of oxidizing species to the inner portion of the coating.

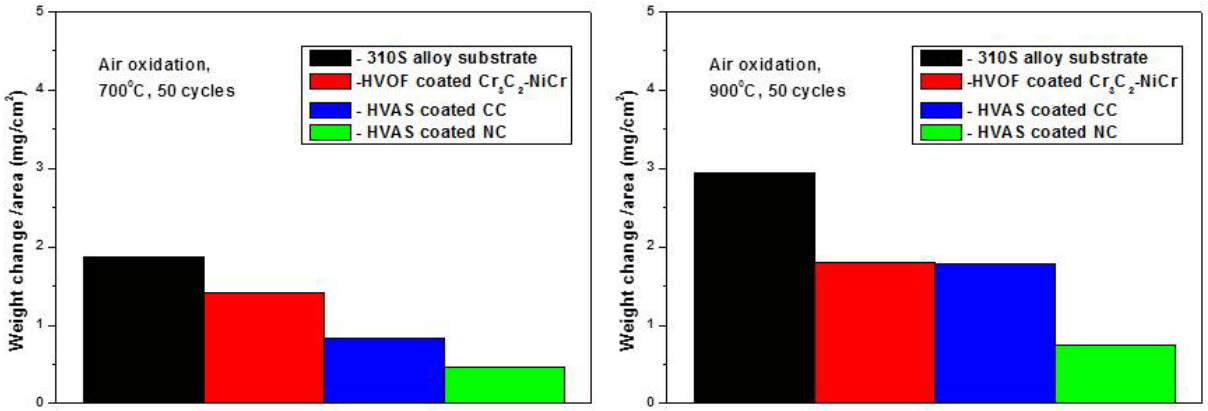

Fig. 7.1 Bar chart showing cumulative weight gain (mg/cm^2) for bare and coated specimens subjected to cyclic oxidation in air at 700 & 900^{0}C for 50 cycles

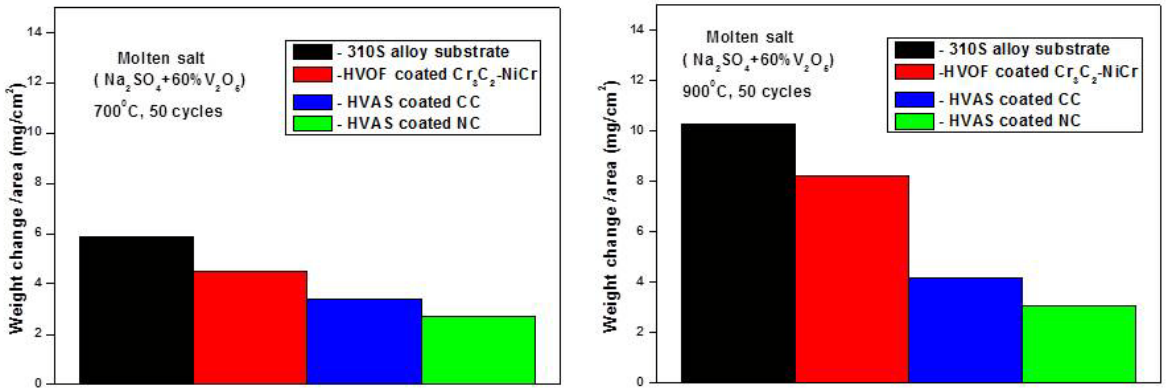

Fig. 7.2 Bar chart showing cumulative weight gain (mg/cm^2) for bare and coated specimens subjected to cyclic oxidation in Na_2SO_4-60%V_2O_5 at 700 & 900^{0}C for 50 cycles

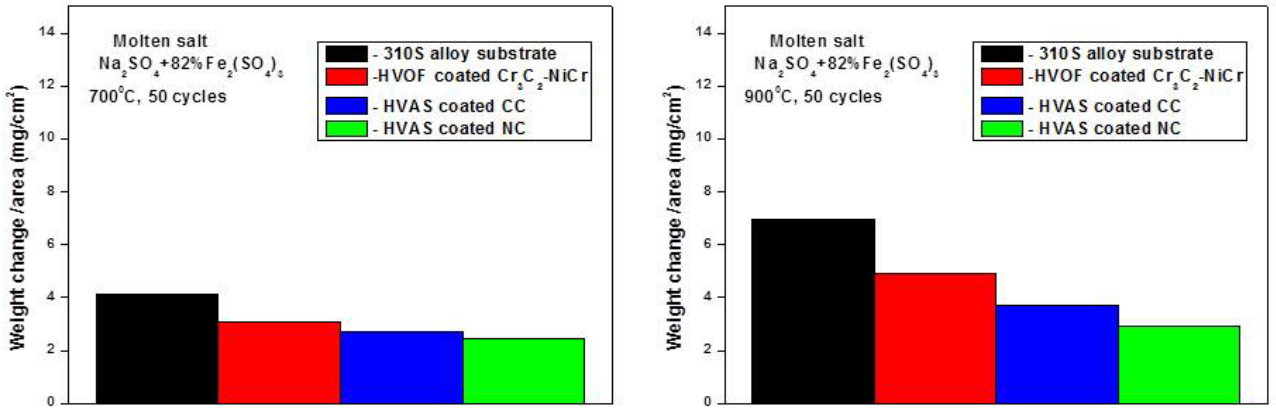

Fig. 7.3 Bar chart showing cumulative weight gain (mg/cm^2) for bare and coated specimens subjected to cyclic oxidation in Na_2SO_4-82%$Fe_2(SO_4)_3$ at 700 & 900^{0}C for 50 cycles

Table 7.1 Parabolic rate constant (Kp) values for 310S alloy substrate and coated specimen subjected to cyclic oxidation for 50 cycles at 700 & 900^0C

Substrate	Kp X 10^{-11} $gm^2cm^{-4}s^{-1}$
310S bare alloy substrate, 700^0C (Air)	1.5
310S bare alloy substrate, 900^0C (Air)	4.1
Coated specimen Cr3C2-NiCr, 700^0C (Air)	0.84
Coated specimen Cr3C2-NiCr, 700^0C (Air)	1.3
Coated specimen CC, 700^0C (Air)	0.36
Coated specimen CC, 900^0C (Air)	1.5
Coated specimen NC, 700^0C (Air)	0.13
Coated specimen NC, 900^0C (Air)	0.25
310S bare alloy substrate, 700^0C (Na_2SO_4-60%V_2O_5)	18.3
310S bare alloy substrate, 900^0C (Na_2SO_4-60%V_2O_5)	55
Coated specimen Cr3C2-NiCr, 700^0C (Na_2SO_4-60%V_2O_5)	10.2
Coated specimen Cr3C2-NiCr, 900^0C (Na_2SO_4-60%V_2O_5)	33.8
Coated specimen CC, 700^0C (Na_2SO_4-60%V_2O_5)	5.9
Coated specimen CC, 900^0C (Na_2SO_4-60%V_2O_5)	9.36
Coated specimen NC, 700^0C (Na_2SO_4-60%V_2O_5)	4.05
Coated specimen NC, 900^0C (Na_2SO_4-60%V_2O_5)	5.36
310S bare alloy substrate, 700^0C (Na_2SO_4-82%$Fe_2(SO_4)_3$)	8.6
310S bare alloy substrate, 900^0C (Na_2SO_4-82%$Fe_2(SO_4)_3$)	24.4
Coated specimen Cr3C2-NiCr, 700^0C (Na_2SO_4-82%$Fe_2(SO_4)_3$)	5
Coated specimen Cr3C2-NiCr, 900^0C (Na_2SO_4-82%$Fe_2(SO_4)_3$)	12.7
Coated specimen CC, 700^0C (Na_2SO_4-82%$Fe_2(SO_4)_3$)	4.14
Coated specimen CC, 900^0C (Na_2SO_4-82%$Fe_2(SO_4)_3$)	7.61
Coated specimen NC, 700^0C (Na_2SO_4-82%$Fe_2(SO_4)_3$)	2.94
Coated specimen NC, 900^0C (Na_2SO_4-82%$Fe_2(SO_4)_3$)	4.72

7.2 Na_2SO_4-60%V_2O_5 & Na_2SO_4-82%$Fe_2(SO_4)_3$ molten salt Environment

The bar chart showing the overall weight gain for bare and coated specimens after 50 cycles in molten salt (Na_2SO_4-60%V_2O_5) & (Na_2SO_4-82%$Fe_2(SO_4)_3$) environment is presented in Fig 7.2 and 7.3, respectively. It is evident that the bare alloy substrate shows a higher weight gain as compared to coated specimens under cyclic conditions. The bare substrate exhibits a lower resistance to the molten salt environment, as clear from the higher parabolic rate constant (Table 7.1) as well as higher weight gain (fig. 7.2 & 7.3). The degradation behavior of all the coatings follows nearly a parabolic rate law, except for bare substrate, which shows slightly deviation as shown in fig 4.21 & 4.22 respectively.

7.3 Actual Industrial coal fired Boiler Environment

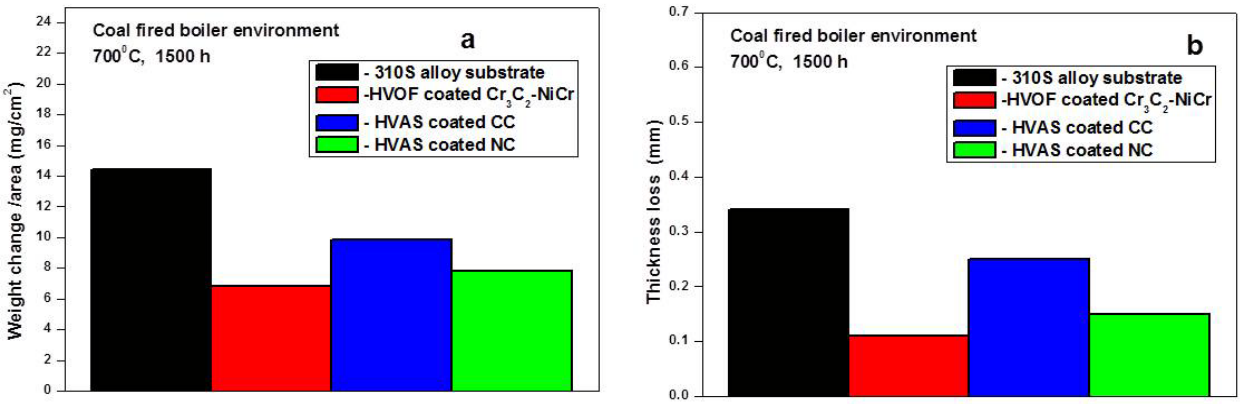

Fig. 7.4 (a) Bar chart showing net weight change (mg/cm^2) and thickness loss (b) for bare and coated boiler at specimens after exposure to coal fired 700^{0}C for 1500 hours.

All the coatings have shown good hot corrosion resistance in the boiler environment consisting of actual working condition of the coal –fired boiler. The bare substrate has suffered hot corrosion, erosion and ash deposition with internal corrosion attack in the coal–fired boiler environment at 700^{0}C. Erosion combined with oxide scale spallation attributed to lower weight gain of bare substrate, within average internal corrosion attack up to 0.34 mm from the scale substrate interface (Fig.7.4 a, b). All the coated specimens show a better adhesion to the substrate during entire 1500 hours of exposure in the following order Cr_3C_2-NiCr > NC > CC > 310S bare alloy substrate. All coated specimens have shown weight gain due to the formation of the oxides scale ash deposition as evident from increase in scale thickness (fig 7.4a). The fluctuation in weight gain data during the experiment can be attributed to the fly ash deposition and rapid thermal cycling, which leads to falling off scale due to the erosion and the regeneration of ash deposit and the oxide scale. In general, all the coatings which are partially oxidized under study show no internal corrosion attack, whereas bare substrate shows internal corrosion attack. Fig. 7.4a shows the highest weight change (weight loss) due to the formation of discontinuous, porous and fragile oxide scale when exposed to real boiler environment for 1500 hours at 700±10^{0}C, whereas, the coated specimens show small weight change (weight gain).

CHAPTER - 8

CONCLUSIONS

The key findings pertaining to oxidation behavior of Cr_3C_2-25%NiCr coatings formulated by HVOF and FeCr-based conventional and nanostructured coatings by HVAS process on the 310S alloy substrate are presented in this chapter. Bare alloy substrate (310S) and coated specimens were subjected to high temperature air oxidation, aggressive environments such as Na_2SO_4-60%V_2O_5 and Na_2SO_4-82%$Fe_2(SO_4)_3$ under cyclic conditions, in a laboratory furnace, at an elevated temperature of 700 & 900^0C for an oxidation run of 50 cycles in all the cases. In addition to the laboratory tests, an attempt has been made to assess the performance of coatings in the real environment of coal fired boiler. The outcomes of the present study are summarized below:

1. The HVOF thermal spray process with kerosene as fuel could be used successfully to deposit Cr_3C_2-25%NiCr coating on the given 310S alloy substrate. FeCr-based conventional (CC) and nanostructured (NC) coatings were deposited successfully by using HVAS spray process.

2. HVOF sprayed Cr_3C_2-25%NiCr coating exhibits lower porosity (< 1%) as compared to HVAS sprayed coatings (<4%).

3. HVOF sprayed Cr_3C_2-25%NiCr coating exhibits lower surface roughness (<7 µm) as compare to HVAS sprayed coatings (<25 µm).

4. The average thickness of Cr_3C_2–25%NiCr coating was found to be 265±19 µm; where as, average thickness of CC and NC was found to be 491±10.39 µm and 95±2.02 µm, respectively.

5. The maximum microhardness for Cr_3C_2-25%NiCr, CC and NC is found to be 1014, 1060 and 1100 Hv, respectively.

6. The bond strength for Cr_3C_2-25%NiCr was found to be 10000 Psi, whereas CC and NC coatings exhibit 6000 Psi.

7. The interdiffusion of alloying elements from the substrate to the HVOF/HVAS sprayed coatings was observed to be marginal as indicated by cross-sectional X-ray mapping analysis. It shows that the adhesion between the coating and the substrate is due to mechanical interlocking and metallurgical bonding effect.

Oxidation in air

8. 310S bare alloy substrate exhibits lower oxidation resistance than the coated specimens. The nanostructured coating (NC) exhibits highest oxidation resistance among the all coatings deposited by different techniques.

9. Based on the thermogravimetric (weight change with respect to time) data, the relative oxidation resistance attained by the various coatings under study can be arranged in the following sequence:

$$NC > CC > Cr_3C_2\text{-}25\%NiCr$$

10. The better protection provided by HVAS sprayed NC coating may be attributed to very fine grains in the nanoscale range. The fine grains helps in rapid diffusion of the elements from the deposited coating such as chromium, thus providing selective oxidation of the elements. This helps in forming a uniform oxide layer on the exposed surface and prevents the further diffusion of oxidizing species into the base alloy.

11. For HVOF sprayed Cr_3C_2-25%NiCr coating, the development of protective oxide layers like Cr_2O_3 and spinel of Ni and Cr is thought to be responsible for high temperature oxidation resistance.

12. The oxidation behavior of coated samples obeyed parabolic rate law.

Na_2SO_4-60%V_2O_5 & Na_2SO_4-82%$Fe_2(SO_4)_3$ molten salt Environment

13. Based on the oxidation rates calculated for the bare substrate and coated specimens after 50 cycles of oxidation in the molten salt environment, the relative hot corrosion resistance attained by the various coatings under study can be arranged in the following sequence:

$$NC > CC > Cr_3C_2\text{-}25\%NiCr$$

14. Rate of hot corrosion was high during initial stages of oxidation in the given environment for all types of coatings. During transient period of oxidation, the corroding species probably have penetrated into the coating along the splat boundaries and the open pores to cause rapid oxidation. However, once all these possible diffusion paths are blocked by the formation of the oxides, the oxidation is then restricted mainly to coating surface resulting in a steady state.

15. The cumulative weight gain in case of HVOF sprayed Cr is relatively high as compared to the HVAS sprayed coatings. The higher weight gain in case of HVOF sprayed coating may be due to the observed microspalling of thin scale during the early stages of exposure to the molten salt environment thereby exposing a fresh surface to the corrosive species.

16. The HVAS sprayed nanostructured coating (NC) has provided best protection in the given aggressive environment under study. The enhanced protection against hot corrosion may be due to the possible formation of uniform protective scale covering the whole surface of the coatings facilitated by the nanosized grain morphology of the coatings. The higher volume fraction of grain boundaries in the nanostructured coatings facilitated the formation of relatively denser oxide scale at a higher rate as compared to conventional coatings.

Actual Industrial Coal fired Boiler Environment

17. The samples were hanged in the low temperature Superheater zone (700 ± 10^0C) for 1500 hrs and negligible effect was observed on all the coatings.

18. Based on the overall weight gain and thickness loss, the relative erosion-corrosion resistance attained by the various coatings after 1500 hrs of oxidation in the low temperature, superheater zone (700 ± 10^0C) can be arranged in the following sequence:

$$Cr_3C_2\text{-}25\%NiCr > NC > CC$$

19. The weight gain in case of HVOF sprayed Cr_3C_2-25%NiCr is lowest, which may be attributed to high bond strength of Cr_3C_2-25%NiCr coating.

20. The Cr_2O_3 rich oxide scale formed in the boiler environment probably contributed to the superior resistance to oxidation–erosion in the coated alloy substrate.

21. Bare 310S alloy substrate has undergone increased oxidation rate in the form of severe spalling of the scale in the real boiler environment at 700±10 °C. The bare alloy suffered larger weight loss when compared against coated specimen.

22. All the coatings were strongly adherent on the 310S alloy substrate in the real boiler environment at 700±10 °C.

23. Cr_3C_2-25NiCr coated specimens exhibited excellent oxidation and wear/spallation resistance.

SUGGESTIONS FOR FUTURE WORK

In light of the significant results obtained in the present study, some of the recommendations for future work are as follows:

1. All the investigated coatings showed promising results in laboratory and in actual coal fired boiler environment. High temperature erosion studies of the coated specimens may also be evaluated in the laboratory.

2. A mathematical model could be developed using the laboratory and industrial coal fired boiler environment data.

3. Hot stage microscopy may also be used to understand the development of the scale as well as mechanism of transport of species during the oxidation and hot corrosion runs.

4. The tailoring of coating powder compositions especially by alloying the coating powders with rare earth elements could be made prior to the coating.

5. The coatings behavior can be studied in the actual running boiler environment for longer duration may be for few years by providing these coatings on the actual boiler tubes.

6. Studies may be conducted to investigate the degradation behavior of the thermal spray coatings obtained by other thermal spray process such as cold spraying, kinetic spraying etc.

7. The porosity of these coatings can be eliminated so as to enhance their corrosion resistance through judicious choice of post coating treatment.

REFERENCES

1. **Abedini**, A., Pourmousa, A., Chandra, S., Mostaghimi, J., (2006), "Effect of substrate temperature on the properties of coatings and splats deposited by wire arc spraying," Surface & Coatings Technol., Vol. 201, pp. 3350–3358.
2. **Backman,** R., Hupa, M. and Uppstu, E., (1987), "Fouling and Corrosion Mechanisms in the Recovery Boiler Superheater Area," Tappi Journal, Vol. 70, pp. 123-127.
3. **Bakare**, M.S., Voisey, K.T., Chokethawai, K., and McCartney, D.G., (2012), "Corrosion behaviour of crystalline and amorphous forms of the glass forming alloy $Fe_{43}Cr_{16}Mo_{16}C_{15}B_{10}$," Journal of Alloys and Compounds Vol. 527, pp. 210– 218.
4. **Bala,** N., Singh, H., Prakash, S. and Karthikeyan, J. (2012), "Investigations on the Behavior of HVOF and Cold Sprayed Ni-20Cr Coating on T22 Boiler Steel in Actual Boiler Environment," Journal of Thermal Spray Technology, Vol. 21, No. 1, pp. 144-158.
5. **Bansal**, P., Padture, N.P. and Vasiliev, A., (2003), "Improved interfacial mechanical properties of Al2O3- 13wt%TiO2 plasma-sprayed coatings derived from nanocrystalline powders," Acta Materialia, Vol. 51, pp. 2959-2970.
6. **Barbooti,** M.M., Al-Madfai, S.H. and Nassouri, H.J., (1988), "Thermochemical Studies on Hot ash Corrosion of Stainless Steel 304 and Inhibition by Magnesium Sulphate," Thermochemical Acta, Vol. 126, pp. 43-49.
7. **Basak**, A.K., Achanta, S., Celis, J.P., Vardavoulias, M. and Matteazzi, P., (2008), "Structure and mechanical properties of plasma sprayed nanostructured alumina and FeCuAl–alumina cermet coatings," Surf. & Coat. Technol., Vol. 202, pp. 2368-2373.
8. **Beltran**, A.M. and Shores, D.A., (1972), "Ch. 11: Hot Corrosion," in 'The Superalloys,' Eds. Sims, C.T. and Hagel, W.C., Wiley Publ., John Wiley and Sons, N. Y.
9. **Bhat,** R.R. and Rao, P.P., (1994), "High strength Cu-Ni-Cr alloys by thermo mechanical treatment," Indian Journal of Engineering and Materials Sciences, Vol. 1, pp. 41-47.
10. **Buchanan**, V.E., McCartney, D.G. and Shipway, P.H., (2008), "A comparison of the abrasive wear behaviour of iron-chromium based hardfaced coatings deposited by SMAW and electric arc spraying," Wear, Vol. 264, pp. 542-549.
11. **Bunshah,** Rointan F., (2001), "Ch.3: Thermal spraying and Detonation Gun Process", In 'Handbook of Hard Coatings, Deposition Technologies, Properties and applications,' William Andrew Publishing, LLC, Newyork, U.S.A.
12. **Bhushan**, B. and Gupta, B.K. (1991), 'Handbook of Tribology: Materials, Coatings and Surface

Treatments,' McGraw-Hill, N.Y.

13. **Birks**, N. and Meier, G.H., (1983), "Introduction to High Temperature Oxidation of Metals", London: Edward Arnold.
14. **Bittel**, J.T., Sjodahl, L.H. and White, J.F., (1969), "Oxidation of 304L Stainless Steel by Steam and by Air," Corros., Vol. 25, No. 1, pp. 7-14.
15. **Blum**, R., (1997), "Advance (700 °C) PF Power Plant," EC Contact No Sf/1001/97/DK.
16. **Bluni**, S. T. and Mardar, A. R., (1996), "Effects Of Thermal Spray Coating Composition and Microstructure on Coating Response and Substrate Protection at High Temperatures," Corrosion, Vol.52, No. 3, pp. 213-218.
17. **Bornstein**, N.S. and DeCrescente, M.A., (1969), "Relationship Between Compounds of Sodium and Sulfur and Sulfidation," Met. Soc. AIME-Trans., Vol. 245, No. 9, pp. 1947-1952,
18. **Bornstein**, N.S. and DeCrescente, M.A., (1970), "The Role of Sodium and Sulfur in the Accelerated Oxidation Phenomena-Sulphidation," Corros., Vol. 26, No. 7, pp. 209-214.
19. **Bornstein**, N.S., Decrescente, M.A. and Roth, H.A., (1975), "Effect of Vanadium and Sodium Compounds on the Accelerated Oxidation of Nickel Base Alloys," Proc. Conf. on Turbine Mater. In the Marine Environment, MMIC-75-27, Columbus, Ohio, USA, pp. 115-160.
20. **Castello**, P., Guttmann, V., Farr, N. and Smith, G., (2000), "Laboratory-Simulated Fuel-Ash Corrosion of Superheater Tubes In Coal Fired Ultra Supercritical-Boiler" Meter, corros., Vol. 51, No. 11, pp.786-790.
21. **Chatha**, S.S., Sidhu, H.S., Sidhu, B.S., (2012), "High temperature hot corrosion behavior of NiCr and Cr_3C_2-NiCr coatings on T91 boiler steel in an aggressive environment at 750 °C," Surface & Coating technol., Vol. 206, pp. 3839-3850.
22. **Chatterjee**, U.K„ Bose, S.K. and Roy, S.K., (2001), "Environmental Degradation of Metals," Pub., Marcel Dekker, 270 Madison Avenue, N.Y.
23. **Chattopadhyay**, B. and Wood, G.C., (1970), "Transient Oxidation of Alloys" Oxid. Met., Vol 2, No. 4, pp. 373-399.
24. **Choudhury,** S.G., Mukhopadhyay, N.K., Das, G., Das, S.K. and Bhattacharya, D.K., (1998), "Failure Analysis of Weld Repaired Steam Turbine Casing", Engineering Failure Analysis, Vol. **5**, pp. 205-218.
25. **Cheruvu** N.S., Chan K.S., and Viswanathan R., (2006), "Evaluation, degradation and life assessment of coatings for land based combustion turbines," Energy Mater., Vol. 1, No. 1, pp. 33-47.
26. **Chawla, V**, Chawla, A., Sidhu, B.S., Prakash S. and Puri, D., (2011**)**, "Performance of

Nanostructured Metal Nitride Coated T-22 Boiler Steel in Na_2SO_4–60% V_2O_5 Environment at 900°C under Cyclic Conditions," Journal of Minerals & Materials Characterization & Engineering, Vol.10 No.7, pp.583-608**.**

27. **Chawla, V.**, Chawla, A., Puri, D., Prakash, S., Gurbuxani, P.G. and Sidhu, B.S., (2011A), "Hot Corrosion & Erosion Problems in Coal Based Power Plants in India and Possible Solutions – A Review", Vol. 10, No.4, pp.367-385.
28. **Chen**, Y.X., Xu, B.S., Liu, Y., Liang, X.B., and Xu, Y., (2008), "Structure and sliding wear behavior of 321 stainless steel/Al composite coating deposited by high velocity arc spraying technique," Trans. Nonferrous Met. Soc. China, Vol. 18, pp. 603-609.
29. **Cheng**, J., Liang, X., Xu, B., (2009), "Microstructure and wear behavior of FeBSiNbCr metallic glass coatings," J. mater. Sci. Technol., Vol. 25, pp. 687-690.
30. **Choi**, H., Yoon, B., Kim, H. and Lee, C., (2002), "Isothermal Oxidation of Air Plasma Spray NiCrAlY Bond Coatings," Surf. Coat. Technol., Vol. 150. No. 2-3. pp. 297-308.
31. **Choquet**, P. Indrigo, C. and Mevrel, R., (1987), "Microstructure of oxide scales formed on cyclically oxidized M-Cr-Al-Y Coatings," Mater. Sci. Eng. Vol.88. pp.97-101.
32. **Colot**, D., Petelot, D., Hoch, P. and Beranger, G., (1997), "Mechanisms of Hot Corrosion in Coal Fired Boilers Gas T91 and EM12 Steels," Mater. Sci. Forum, Vol. 251-254, pp. 641-648.
33. **Conner**, J.A. and Connor W.B., (1994), "Ranking Protective Coatings: Laboratory Vs. Field Experience." JOM, Dec., pp. 35-38.
34. **Coze**, L.J., Franzoni, U, Cayla, O., Devisme, A. and Lefort, A., (1989), "The Development of High-Temperature Corrosion-Resistant Aluminium-Containing Ferritic Steels," Mater. Sci. Eng. A-Struct., Vol. 120, pp. 293-300.
35. **Cuevas-Arteaga**, C.. Porcavo-Calderon, J., Izquierdo, G., Martinez-Villafane, A. and Gonzalez-Rodriguez. J.G., (2001), "Study of Hot Corrosion of Alloy 800 using Linear Polarazation Resistance and Weight Loss Measurement," Mater. Sci. Technol., Vol.17, No. 7, pp. -885.
36. **Cullity**, B.D., Elements of X-ray Diffraction, Addison-Wesley, 1970.
37. **Das**, D., Balasubramaniam, R. and Mungole, M.N., (2002), "Hot Corrosion of Carbon-Alloyed FeAl-Based Iron Aluminides," Mater. Sci. Eng. A., Vol.338, No. 1-2, pp. 24-32.
38. **DeMasi-Marcin**, J.T. and Gupta, D.K., (1994), "Protective Coatings in The Gas Turbine Engine," Surf. Coat. Technol., Vol. 68-69, pp. 1-9.
39. **Deshpande,** S., Sampath, S. and Zhang, H., (2006), "Mechanisms of Oxidation and its Role

in Micro structural Evolution of Metallic Thermal Spray Coatings-Case Study For Ni-Al," Surf. Coat. Technol., Vol.200, pp.5395-5406.

40. **Dieter,** L., (2007), "Corrosion and Surface Chemistry of Metals," EPFL Press, Lausanne, Switzerland.
41. **Dooley,** R.B. and Wilson, J.R., (1975), "The Coirosion of 50Cr-50Ni Alloy in Liquid Vanadate Systems in the Temperature Range 750-950^{0}C," Trans. ASME, July, pp. 422-428.
42. **Eliaz,** N., Shemesh, G. and Latanision, R.M., (2002), "Hot Corrosion in Gas Turbine Components," Eng. Fail. Anal., Vol. 9, pp. 31-43.
43. **Erning,** U. and Nestler, M., (1999), "HVOF Coatings for Hard-Chrome Replacement-Properties And Applications," in: Proceedings of United Thermal Spray Conference (UTSC 99), Dusseldorf. Marzo, pp. 462-466.
44. **Eroglu,** S. and Duran, C., (1997), "Processing and Properties of a 85% Cr3C;-10.5%Ni-4.5%Fe Cermet," Scripta Materialia, Vol.37, No.7, pp. 991-997.
45. **Fairman,** L., (1962), "Technical Note: Mechanism of Accelerated Oxidation by Vanadium-Containing Fuel Ash," Corros. Sci., Vol. 2, pp. 293-296.
46. **Fernando, J.,** Monceau, D., Tetard, D., Pieraggi, B., and Vahlas,C., (2003), "Chemical Vapor Deposition of Ruthenium on NiCoCrAlYTa Powders Followed by Thermal Oxidation of the Sintered Coupons," Surf. Coat. Technol., Vol. 163-164., pp.44-49.
47. **Frances,** M., Steinmetz. P., Steinmetz, J., Duret. C. and Mevrel, R., (1985), "Hot Corrosion Behavior of Low Pressure Plasma Sprayed NiCoCrAlY+Ta Coating on Nickel Based Superalloys," J. vacuum sci. Technol. A, Vol. 3 No.6, pp.2537-2544.
48. **Fu, B.Y.**, He, D.D., and Zhao L., (2009), "Effect of heat treatment on the microstructure and mechanical properties of Fe-based amorphous coatings," Journal of Alloys and Compounds, Vol. 480, pp. 422-427.
49. **Fontana**, M.G., "Corrosion Engineering", Tata McGraw-Hill Publishing Company Limited, Third Edition, (2005), Chapter 1, pp. 1-4.
50. **Gang,** C.J., Chang-Jiu Li, Yu-Yue Wang and Wen-Ya Li, (2006), "Microstructural Characterization and Abrasive Wear Performance of HVOF Sprayed Cr_3C_2-NiCr Coating," Surf. Coat. Technol., Vol. 200, pp. 6749-6757.
51. **Gesmundo,** F. and Viani, F., (1988), "The Mechanism of Low-Temperature Corrosion of Pure Iron and Manganese at 600-800°C," Mater. Chem. Phys., Vol. 20, pp. 513-528.
52. **Gitanjaly,** (2003), "Role of Inhibitors on Hot Corrosion of Superalloys in Na_2SO_4-V_2O_5

Environment," Ph. D. Thesis, Met. and Mat. Engg. Deptt., IIT, Roorkee, India.

53. **Gitanjaly,** Prakash, S. and Singh, S., (2002), "Effects of MgO and CaO on Hot Corrosion of Fe Base Superalloy Superfer 800H in Na_2S0_4-60%V_20_5 Environment," Brit. Corros. J Vol. 37, No. 1, pp. 56-62.

54. **Gledhill,** H.C., Turner, I.G. and Doyle, C., (1999), "Direct Morphological Comparison Of Plasma Sprayed and Detonation Gun Sprayed Hydroxyapatite Coatings for die Applications," Biomaterials, Vol. 20, pp. 315-322.

55. **Goebel,** J.A., and Pettit, F.S., (1970A), "Na_2SO_4 - Induced Accelerated Oxidation (Hot Corrosion) of Nickel," Metall. Trans., Vol. 1, pp. 1943-1954.

56. **Geobel,** J.A. and Pettit, F.S., (1970B), "The Influence of Sulphides on the Oxidation behaviour of Nickel-base Alloys," Metall Trans, Vol. 1, pp.3421 -3429.

57. **Geobel,** J.A., Pettit, F.S. and Goward, G.W., (1973), "Mechanisms for the Hot Corrosion of Base Alloys," Metall. Trans., Vol. 4, pp. 261-275.

58. **Georgiou**, E.P., Achanta, S., Dosta, S., Fernandez, J., Matteazzi, P., Kusinski, J., Piticescu, R.R. and Celis, J.P., (2013), "Structural and tribological properties of supersonic sprayed Fe–Cu–Al–Al2O3 nanostructured cermets," Applied Surface Science, Vol. 275, 142-147.

59. **Goward,** G.W., (1998), "Progress in Coatings for Gas Turbine Airfoils," Surf. Coat. Technol., Vol. 108-109, pp.73-79.

60. **Grainger,** S. and Blunt, J., (1989), "Ch.2: Mechanism of Wear and Corrosion," in 'Engineering Coatings-design and application,' Abington Publishing, England.

61. **Grewal**, H.S., Singh, H. and Agrawal, A., (2013), Microstructural and mechanical characterization of thermal sprayed nickel–alumina composite coatings, Surface & Coatings Technology, Vol. 216, pp. 78-92.

62. **Grunling,** H.W. and Bauer, R., (1992), "The Role of Silicon in Corrosion-Resistant High Temperarature Coatings," Thin Solid Films, Vol.95, pp.3-20.

63. **Guilemnay,** J.M., Espallargas, N., Suegama, P.H. and Benedetti A.V., (2006), "Comparative study of Cr_3C_2-NiCr coatings obtained by HVOF and hard chromium coatings," Corro. Sci., pp. 2998-3013.

64. **Guilemany,** J.M., Nutting, J. and Llorca-Isem, N., (1994), "Characterisation of Cr_3C_2-NiCr Powder for High Velocity Oxyfuel Spraying," Powder Metallurgy, Vol. 37 No.4, pp. 289-292.

65. **Guilemany,** J.M., Nutting, J. and Llorca-Isem. N., (1996), "Microstructural Examination of HVOF Chromium Carbide Coatings for High-Temperature Applications," J. Therm. Spray Technol., Vol.5 No.4, pp. 483-489.
66. **Guilemany**, J.M., Miguel, J.M., Vizcaino, S., Climent, F., (2001), "Role of three-body abrasion wear in the sliding wear behaviour of WC-Co coatings obtained by thermal spraying", Surf. Coat. Technol., Vol. 140, pp. 141–146.
67. **Guo**, H., Peng, D., Cui, Y. and Gong, S., (2011), "High-temperature oxidation and hot-corrosion behaviour of EB-PVD β-NiAlDy coatings," Corrosion Science, Vol. 53 pp. 1050–1059.
68. **Guo**, R.Q., Zhang, C., Chen, Q., Yang, Y., Li, N., Liu, L., (2011A), "Study of structure and corrosion resistance of Fe-based amorphous coatings prepared by HVAF and HVOF," Corrosion Science, Vol. 53, pp. 2351–2356.
69. **Gurrappa,** I. and Sambasiva Rao, A., (2006), "Thermal Barrier Coatings for Enhanced Efficiency as Turbine Engines," Surf. Coat. Technol., Vol. 201, No. 6, pp 3016-3029.
70. **Gurrappa**, I., (1999), "Hot Corrosion Behavior of CM 247 LC Alloy in Na_2SO_4 and NaCl Environments," Oxid. Met., Vol. 51, No. 5, pp. 353-382.
71. **Gurrappa,** I., (2000), "Hot Corrosion of Protective Coatings," Mater. Manuf. Process., Vol. 15, No. 5, pp. 761-773.
72. **Gurrappa,** I., (2001), "Identification of Hot Corrosion Resistant MCrAlY Based Bond Coatings for Gas Turbine Engine Applications," Surf. Coat. Technol., Vol. 139, pp. 272-283.
73. **Gurrappa,** I., (2003), "Influence of Alloying Elements on Hot Corrosion of Superalloys and Coatings: Necessity of Smart Coatings for Gas Turbine Engines," Mater. Sci. and Technol., Vol. 19, no.2. pp. 178-183.
74. **Hancock,** P., (1987), "Vanadic and Chloride Attack of Superalloys," Mater. Sci. Technol., Vol. 3, pp. 536-544.
75. **Hao Du,** Chao S., Hua, W., Wang, T., Gong, J., Jiang, X. and Lee, S.W., (2007), "Structure, Mechanical and Sliding Wear Properties of WC-Co/MoS_2-Ni Coatings by Detonation Gun Spray,'' Mater. Sci. Eng A, Vol. 445-446, pp. 122-134.
76. **Hara,** M., Hisaichi, T., Itoh, K. and Shinata, Y., (1991), "Effects of SO_3, SO_2 and O_2 Gasses on Hot Corrosion of Ni and Ni-Cr Alloys in Molten Na_2SO_4," J. Jpn. I. Met., Vol. 55, No. 11, pp. 1207-1215.
77. **Harris,** G.T., Child, H.C. and Kerr, J.A., (1955), "Effect of the Composition of Gas-Turbine

Alloys on Resistance to Scaling and to Vanadium Pentaoxide Attack," ISIJ Int., Vol. 179, pp. 342-347.

78. **Haugsrud,** R., (2003), “On the High-Temperature Oxidation of Nickel,” Corros. Sci., Vol. 45, No. l, pp. 211-235.
79. **Hawthorne,** H.M., Arsenault B., Immarigeon J.P., Legoux J.G. and Parameswaran V.R., (1999), “Comparison of Slurry and Dry Erosion Behaviour of Some HVOF Thermal Sprayed Coatings,” Wear, Vol. 225-229, pp. 825-834.
80. **Hazoor,** S.S, Sidhu, B.S. and Prakash, S., (2006), “Mechanical and Microstructural Properties of HVOF Sprayed WC-Co and Cr_3C_2-NiCr Coatings on the Boiler Tube Steels Using LPG as the fuel gas,” J. Mate. Pro. Technol., Vol.171, pp. 77-82.
81. **He,** J.L., Yu, C.H., Leyland, A., Wilson, A.D. and Matthews, A., (2002), “A Comparative Study of the Cyclic Thermal Oxidation of PVD Nickel Aluminide Coatings,” Surf. Coat. Technol., Vol. 155, No. 1, pp. 67-79.
82. **He**, J.H., Ice, M., Schoenung, J.M., Shin, D.H. and Lavernia, E.J., (2001), “Thermal stability of nanostructured Cr_3C_2-NiCr coatings,” J. Therm. Spray Technol., Vol. 10, pp. 293–300.
83. **He,** J., Ice, M. and Lavernia, E.J., (2000), “Synthesis of Nanostructured Cr_3C_2-(Ni20Cr) Coatings,” Meta. Mater. Trans. A, Vol. 31 A, pp. 555-564.
84. **Heath,** G. R., Heimgartner, P., Irons, G., Miller, R. and Gustafsson, S., (1997), “An Assessment of Thermal Spray Coating Technologies for High Temperature Corrosion Protection,” Mater. Sci. Forum, Vol. 251-54, pp. 809-816.
85. **Herman,** H., “Plasma Sprayed Coatings,” (1988), Scientific American, Vol. 259, No. 3, pp.78 -83.
86. **Hocking,** M.G. and Sidky, P.S., (1987), “The Hot Corrosion of Nickel-Based Ternary Alloys and Superalloys for gas Turbine Applications-II. The Mechanism of Corrosion in SO_2/O_2 Atmospheres,” Corro. Sci., Vol. 27, No. 2, pp. 205-214.
87. **Hocking,** M.G., (1993), “Coatings Resistant to Erosive/Corrosive and Severe Environments,” Surf. Coat. Technol., Vol. 62, pp. 460-466.
88. **Hsu**, H.W. and Tsai W.T., (2000), “High temperature corrosion behavior of siliconized 310 stainless steel,” Mater. Chemistry and Phy., Vol. 64, pp. 147-155.
89. **Hussain,** N., Shahid, K.A., Khan, I.H. and Rahman, S., (1994), “Oxidation of High-Temperature Alloys (Superalloys) at Elevated Temperatures in Air: I,” Oxid. Met., Vol. 41, No. 3-4, pp. 251-269.

90. **Hwang,** Y.S. and Rapp., R.A., (1989), "Thrmochemistry and Solubilities of Oxides in Sodium Sulfate-Vanadate Solutions," Corros., Vol. 45, No. 11, pp. 933-937.

91. **Iyer,** S.R., Iyer, K.J.L. and Radhakrishan, V.M., (1987), "High Temperature Corrosion of a Ni-Base Superalloy by Vanadium," Proc. of 10th ICMC, Madras, India, Vol. 4, pp. 3665-3670.

92. **Iyer,** S.R., Iyer, K.J.L. and radhakrishan, V.M., (1987A), "Hot Corrosion Cracking of Nimonic 80A," High Temp. Technol., Vol. 5, No.3, pp. 145-150.

93. **Jandin**, G., Liao, H., Feng, Z.Q. and Coddet, C., (2003), "Correlations between operating conditions, microstructure and mechanical properties of twin wire arc sprayed steel coatings," Mater. Sci. and Engg. A, Vol. 349, pp. 298-305.

94. **Jena,** A.K and Chaturvedi, M.C., (1984), "Review the Role of Alloying Elements in the Design of Nickel-Base Superalloys," J. Mate. Sci., Vol. 19, pp.3121-3139.

95. **Johnson,** D.M., Whittle, D.P. and Stringer, J., (1978), "The Hot Corrosion of Directionally Solidified Ni-Cr-Nb-Al Eutectic Alloys," Oxid. Met., Vol. 12, No. 3, pp. 273-291.

96. **Kai,** W., Leu, C.J. and Wu, Y.J., (1998), "Effects of Mo and A1 Additions on the Sulfidation Behavior of 310 Stainless Steel," Oxid. Met. Vol. 50, pp. 89-122.

97. **Kai**, T., Zhou Xiang-lin, Cui Hua and Zhang Ji-shan, (2009), "Oxidation and hot corrosion behaviors of HVAF-sprayed conventional and nanostructured NiCrC coatings," Trans. Nonferrous Met. Soc. China, Vol. 19, pp. 1151-1160.

98. **Kamal,** S., Jayaganthan, R. and Prakash, S., (2009), "Characterisation of Detonation Gun Sprayed Cr_3C_2-25NiCr Coatings on Ni and Fe Based Superalloys," Surf. Engg., Vol. 25, No. 4, pp. 287-294.

99. **Kamal,** S., Jayaganthan, R. and Prakash, S., (2009A). "High Temperature Oxidation Studies Of Detonation-Gun-Spraved Cr_3C_2-25NiCr Coating on Fe and Ni-Based Superalloys in air Under Cyclic Condition at 900 °C," J Alloys Comp., Vol. 472, pp. 378-389.

100. **Kamal,** S., Jayaganthan, R. and Prakash, S., (2009B), "Evaluation of Cyclic Hot Corrosion Behaviour of Detonation Gun Sprayed Cr_3C_2-25NiCr Coatings on Nickel- and Iron-Based Superalloys," Surf. Coat. Technol., Vol.203, pp. 1004-1013.

101. **Kamal,** S., Jayaganthan, R., Prakash, S., and Kumar, S., (2008A), "Hot Corrosion Behavior of Detonation Gun Sprayed Cr_3C_2-25NiCr Coatings on Ni and Fe-based Superalloys in Na_2SO_4-60% V_2O_5 Environment at 900°C," J. Alloys Comp., Vol. 463, pp. 358-372.

102. **Kaur**, M., Singh, H. and Prakash, S., (2009), "High-Temperature Corrosion Studies of HVOF-Sprayed Cr_3C_2-25NiCr Coating on SAE-347H Boiler Steel," J. of Thermal Spray Technol., Vol. 18, No. 4, pp. 619-632.
103. **Kaur**, M., Singh, H. and Prakash, S., (2011), "Surface engineering analysis of detonation-gun sprayed Cr_3C_2-NiCr coating under high-temperature oxidation and oxidation–erosion environments," Surf. Coat. Technol. Vol. 206, pp. 530-541.
104. **Kerby,** R.C. and Wilson J.R., (1973), "Corrosion of Metals by Liquid Vanadium Pentoxide and the Sodium Vanadates," Trans. ASME, Jan., pp. 36-44.
105. **Kerby,** R.C. and Wilson J.R., (1972), "Electrical Conduction Properties of Liquid Vanadates: II The Sodium," Canadian journal of chemistry. Vol. 58. pp. 2871-2876.
106. **Khajavi,** M.R. **and** Shariat, M.H., (2004), "Failure of First Stage Gas Turbine Blades," Eng. Fail .Anal., Vol. 11, pp. 589-597.
107. **Khalid,** F.A., Hussain, N. and Shahid, K.A., (1999), "Microstructure and Morphology of High Temperature Oxidation in Superallovs." Mater. Sci. and Engg. A- Struct., Vol. 265, pp. 87- 94.
108. **Khanna,** A.S. and Jha, S.K., (1998), "Degradation of Materials Under Hot Corrosion Conditions," Trans. Indian Inst. Metals, Vol. 51, No. 5, pp. 279-290.
109. **Khanna,** A.S., (2002), "High Temperature Oxidation-Basics" in 'Introduction to High temperature Oxidation and corrosion,' Pub., ASM International, U.S.A.
110. **Khanna**, A.S., (2005), Ch-6: "Handbook of environmental degradation of Materials," Pub., William Andrew, 13 Eaton Avenue, N.Y.
111. **Kim,** D.Y, Han, M.S. and Youn, J.G., (1998), "Characterisation of Erosion Resistant Cr_3C_2-NiCr Plasma Sprayed Coatings," in Thermal Spray: Practical Solutions for Engineering Problems. ASM International, U.S.A.
112. **Kim,** D.Y., Han, M.S. and Youn, J.G., (1996), in: C.C. Berndt Ed. Thermal Spray: Practical Solutions for Engineering Problems, ASM International, Materials Park, Ohio,U.S.A., pp. 123- 128.
113. **Kim,** G.M., Yanar, N.M., Hewitt, E.N., Pettit, F.S. and Meier, G.H., (2002), "The Effect of the Type of Thermal Exposure on the Durability of Thermal Barrier Coatings," Scripta Materialia, Vol. 46, pp. 489-95.
114. **Kim** H.S., Estrin, Y., (2008), "Strength and strain hardening of nanocrystalline materials," Mater. Sci. and Engg. A, Vol. 483-484 No. 2, pp. 127-130.
115. **Kim** S.K., Cha, B.C., (2004), "Deposition of CrN-MoS_2 thin films by D. C. magnetron

sputtering," Surf. and Coat. Technol., Vol. 188-189, pp. 174-178.

116. **Klimenko,** V.S., (1979), "Detonation Spray-Deposition of Alumina of Various Degrees of Filling of The Barrel With Carrier Gas," Puroshkovaya Metallurgiya, No. 10, pp. 47-49.
117. **Knotek**, O., (2001), "Chapter 3: Thermal Spraying and Detonation Spray Gun Processes," in 'Handbook of Hard Coatings: Deposition Technologies, Properties and Applications,' Ed. Bunshah, R.F., Noyes Pub. Park Ridge. New Jersey, U.S.A. William Andrew Publishing, LLC, Norwich, N.Y., U.S.A., pp. 77-107.
118. **Ko,** P.L. and Robertson, M.F., (2002), "Wear Characteristics of Electrolytic Hard Chrome and Thermal Sprayed WC-10 Co-4 Cr Coatings Sliding Against Al-Ni-Bronze in Air at 21°C and at -40 °C," Wear, Vol. 252, pp. 880-893.
119. **Koch,** G.H., Brongers, M.P.H., Thompson, N.G., Virmani, Y.P. and Payer, J.H., (2002), "Historic Congressional Study: Corrosion Costs and Preventive Strategies in the United States," Supplement to Mater. Perfor., July, pp. 1-11.
120. **Kofstad,** P., (1966), "Chapter 1: General Introduction" in 'High Temperature Oxidation of Metals,' John Wiley & Sons Inc. U.S.A.
121. **Kofstad,** P., (1988), "Chapter 14" in 'High Temperature Corrosion,' Elsevier Applied Science, London & N.Y., pp. 465.
122. **Kofstad.** P., (1990), "High Temperature Corrosion of Metals." Proc. of Conf. on Microscopy of oxidation, London, pp. 1-9.
123. **Kohi,** F.J., Stearns, C.A. and Fryburg, G.C., (1979), "The Role of NaCl in Flame Chemistry Deposition Process, and its Reaction With Protective Oxides", Proc. 4th US/UK Navy Conf. on Gas Turbine Materials in a Marine Environment, Vol. II. U.S. Naval Sea Command, annapolis, MD, pp. 565.
124. **Kolta,** G.A., Hewaidy, L.F. and Felix, N.S., (1972), "Reactions between Sodium Sulphate and Vanadium Pentoxide." Thermochim, Acta. Vol. 4, pp. 151-164
125. **Korpiola,** K. and Vuoristo, P., (1996). "Effect of HVOF Gas Velocity and Fuel to Oxygen Ratio on the Wear Properties of Tungsten Carbide Coating," in: Bernt, C. C. edi.. Thermal Spray: Practical Solutions for Engineering Problems. Cincinnati. U.S.A., 11 - 17 October. ASM.
126. **Krishna,** B.V. and Sidhu. R.K., (2002), "Pitting Corrosion of Steel Tubes in an Air Preheater, Practical Failure Analysis,'' ASM Int., Vol. 2. No. 5. pp. 61-66.
127. **Kuiry.** C., Seal. S., Bose, S.K. and Roy. S.K., (1994), "Effect of Surface Preparation on the High-Ternperature Oxidation Behaviour of AIS1 316 Stainless Steel." ISO Int. Vol. 34,

No. 7, pp. 599-606.

128. **Kuroda,** S., Kawakita, J., Watanabe, M. and Katanoda, H. (2008), "Topical Review Warm spraying- A Novel Coating Process Based on High-Velocity Impact of Solid Particles," Sci. Technol. Adv. Mater., Vol. 9, pp. 1-17.

129. **Lai**, G.Y., "Oxidation-High Temperature Corrosion of Engineering Alloys", Pub. ASM International (1990) Chapter 3, pp. 15.

130. **Lambert,** P., Champagne, B. and Arseneault, B., (1991). "Oxidation and Hot Corrosion in Na_2SO_4,-10%V_20_5 of Ni-17Cr-6Al-0.5Y and Ni-I6Cr-5.7Al-0.47V-5Si, MCrAlY Alloys at 700°C," Can. Metall. Quart., Vol. 30, No. 2. pp. 125-130.

131. **Lee,** S.Y. and McNaiian, M.J., (1990). "Inhibition of Oxidation of Iron in Environments Containing Chlorine at 1100 and 1200K." J. Electrochem. Soc., Vol. 137. No. 2, pp. 472- 479.

132. **Lee,** W.H. and Lin, R.Y., (2002), "Hot Corrosion Mechanism of Intermetallic Compound Ni_3Al," Mater. Chem. Phys., Vol. 77, pp. 86-96.

133. **Lee**, C.H. and Hwang,S.Y., (2006), "Development and properties of nanostructured thermal spray coatings," Current Applied Phy., Vol. 6, pp. 1002-1006.

134. **Levy,** A.V., (1993), "The Erosion-Corrosion of Tubing Steels in Combustion Boiler Environments," Corrosion Sci., Vol. 35, No. 5-8, pp. 1035-1043.

135. **Levy,** M., Huie, R. and Pettit, F., (1989), "Oxidation and Hot Corrosion of Some Advanced Superalloys at 1300 to 2000°F (704 to 1093 °C),''Corr. Sci., Vol. 45, No. 8, pp. 661-674.

136. **Li,** J.F., Wang X.Y., Liao H., Ding C.X. and Coddet, C., (2004), "Indentation Analysis of Plasma-Sprayed Cr_3C_2-NiCr Coatings," J. mate. Sci. letters, Vol.39, pp. 7111-7114.

137. **Li**, C.J., and Ohmori, A., (1996), "The Lamellar Structure of a Detonation Gun Sprayed Al_2O_3 Coating," Surf. Coat. Technol., Vol. 82, pp. 254-258.

138. **Li,** C.X., Sun, Y. and Bell, T., (2000), "Shot Peening of Plasma Nitrided Steel for Fretting Fatigue Strength Enhancement," Mate. Sci. Technol., Vol. 16, pp. 1067-1072.

139. **Li,** L., Zhu, R. and Gesmundo, F., (1996), "Hot Corrosion of Iron in the Presence of Salt Mixture Deposit containing NaCl and V_2O_5 at 600°C," J. Mater. Sci. Technol., Vol. 12, No. 6, pp. 445-451.

140. **Li**, C.J., Ji, G. C., Wang, Y. Y., Sonoya, K. (2002), "Dominant effect of carbide rebounding on the carbon loss during high velocity oxyfuel spraying of Cr_3C_2–NiCr," Thin Solid Films, Vol. 419, pp. 137–143.
141. **Li,** M.H., Sun, X.F., Li, J.G., Zhang, Z.Y., Jin, T., Guan, H.R. and Hu, Z.Q., (2003A), "Oxidation Behavior of a Single-Crystal Ni-Base Superalloy in Air-I: At 800 and 900°C," Oxide. Met., Vol. 59, No. 5-6, pp.591-605.
142. **Lima,** C.R.C. and Guilemany, J.M., (2007), "Adhesion Improvements of Thermal Barrier Coatings With HVOF Thermally Sprayed Bond Coats," Surf. Coat. Technol., Vol. 201, pp. 4694-4701.
143. **Lindgren,** J.R. and. Johnson, W.R., (1987), "Friction and Wear Behavior of Chromium Carbide Coatings," Surf. Coat. Technol., Vol. 32, pp. 249-260.
144. **Liu,** G., Li, M., Zhou, Y. and Zhang, Y., (2006), "Influence of Pre-Oxidation on The Hot Corrosion of Ti_3SiC_2 in the Mixture of Na_2SO_4-NaCl melts," Corro. Sci., Vol.48, pp. 650-661.
145. **Liu,** J. and Ding, C., (2000), "Improvement in the Properties of Plasma-Sprayed Chromium Carbide Coatings Using Nickel-Clad Powders," Surf. Coat. Technol., Vol. 130, pp. 15-19.
146. **Liu,** M., (1998), "Study on the Spray Processes and Characteristics of Cr_3C_2-NiCr Coating," In Thermal Spray: Meeting the Challenges of the 21st Century, Nice, France: ASM International, Materials Park, OH-U.S.A.
147. **Liu,** P.S., Liang, K.M., Zhou, H.Y., Gu, S.R., Sun, X.F., Guan, H.R., Jin, T. and Yang, K.N., (2001A), "Cyclic Oxidation Behavior of Aluminide Coatings on the Co-Base Superalloy DZ40M," Surf. Coat. Technol., Vol. 145, pp. 75-79.
148. **Luthra,** K.L. and Shores, D.A., (1980), "Mechanism of Na_2SO_4 Induced Corrosion at 600-900 °C," J. Electrochem. Soc., Vol. 127 No. 10, pp. 2202-2210.
149. **Luthra,** K.L., (1985), "Kinetics of the Low Temperature Hot Corrosion of Co-Al Alloys," J. Electrochem. Soc., Vol. 132, No. 6, pp. 1293-1298.
150. **Luthra,** K.L. and Spacil, H.S., (1982), "Impurity Deposits in Gas Turbines from Fuels Containing Sodium and Vanadium," J. Ele. Soc., Vol. 129, No. 3, pp. 649-656.
151. **Madhu Chittora**. Project Monitor, Economic Research India Ltd., January 28 - February 3, (2008).
152. **Mahesh**, R.A., Jayaganthan, R. and Prakash, S., (2008), "Characterization of HVOF

Sprayed NiCrAlY-0.4 wt%CeO_2 Coatings on Superalloys," Surf. Engg., Vol.24, N0.5, pp.366-373.

153. **Maledi,** N.B., Potgieter, J.H., Sephton, M. Cornish, L.A., Chown, L. and Suss, R., (2006), "Hot Corrosion Behaviour of Pt-Alloys for Application in the Next Generation of Gas Turbines," International Platinum Conference 'Platinum Surges Ahead', the Southern African Institute of Mining and Metallurgy, 2006, pp. 81-90.
154. **Malik,** A.U. and Ahmad, S., (1983), "Na_2SO_4-Induced Corrosion of Some Nimonic Alloys at 650 to 1000°C," Metallkd., Vol. 74, No. 12, pp. 819-824.
155. **Malik,** A.U. and Mobin, M., (1987), "Studies on Some Solid State Reactions Relevant to Hot Corrosion," Proc. of 10^{lh} ICMC, Madras, India, Vol. 4, pp. 3345-3365.
156. **Malik,** A.U., Asrar, N., Ahmad, S. and Siddiqi, N.A.B., (1988), "Hot Corrosion Behaviour of Some Industrially Important Nickel-base Alloys in Presence of Na_2SO_4(S) and NaCl(S)," Metallkd., Vol. 79, No.5, pp. 285-295.
157. **Manoj Kumar**, B. V., and Basu, B., (2005), "Evaluation in friction and wear of fretting wear of Mg-SiC composites: influence of fretting duration," Journal of materials research, Vol. 20, pp. 801-812.
158. **Manoj Kumar**, B. V., Basu, B**.**, Murthy, V. S. R., Gupta, M, (2005A), "The Role of Tribochemistry on Fretting wear of Mg-SiC Particulate Composites," Composites: Part A Vol. 36, pp. 13-23.
159. **Marriot,** J.B., (1990), "Future Materials Requirements for High Temperature Power Engineering Component," Materials & Design, Vol. 11, No. 3, pp. 122-128.
160. **Matthews** S. J., (2004) "Erosion-Corrosion of Cr3C2-NiCr High Velocity Thermal Spray Coatings," Ph.D. Thesis, The University of Auckland.
161. **Matthews**, S., James, B. and Hyland, M., (2013), "High temperature erosion–oxidation of Cr_3C_2–NiCr thermal spray coatings under simulated turbine conditions," Corrosion Science, Vol. 70, pp. 203–211.
162. **Matthews,** S., Hyland, M. and James, B., (2003), "Microhardness Variation in Relation to Carbide Development in Heat Treated Cr_3C_2-NiCr Thermal Spray Coatings," Acta Materialia, Vol.51, pp. 4267-4277.
163. **Matthews,** S., James, B. and Hyland, M., (2008), "Erosion of oxide scales formed on Cr_3C_2–NiCr thermal spray coatings," Corrosion Science, Vol. 50, pp. 3087–3094.
164. **Matthews** S., James, B. and Hyland, M., (2009), "The role of microstructure in the high temperature oxidation mechanism of Cr_3C_2–NiCr composite coatings," Corrosion Science,

Vol. 51, pp. 1172–1180.

165. **Meier,** G.H., (1989), “A Review of Advances in High-temperature Corrosion”. Mate. Sci. Engg. A., Vol. 120, pp. 1-11.

166. **Metals Handbook,** (1975), ‘Failure Analysis and Prevention,’ Vol. 10, ASM Publication, Metals Park Ohio, U.S.A.

167. **Metals Handbook,** (1990), "Properties and Selection; Iron, Steel and High Performance Alloys, 10th Edition,” Vol. l**,** ASM Publication, Metals Park Ohio, U.S.A.

168. **Mevrel,** R., (1989), “State of the Art on High-temperature Corrosion-resistant Coatings,” Mater. Sci. Engg. A, Vol. 120, pp. 13-24.

169. **Misra,** A.K., (1986), “Mechanism of Na_2SO_4-Induced Corrosion of Molybdenum Containing Nickel-Base Superalloys at High Temperatures,” J. Electrochem. Soc., Vol. 133, No. 5, pp. 1029-1037.

170. **Mitra,** S.K, Roy, S.K. and Bose, S.K., (1993), “Influence of Superficial Coating of CeO_2 on the Oxidation Behavior of A1SI 304 Stainless Steel,” Oxid. Met, Vol. 39 (3-4), pp.22-229.

171. **Mobin,** M., Malik, A.U., Ahmad, S., Hasan, S.K. and Ajmal, M., (1996), “Studies on the Interactions of Metal Oxides and N Na_2SO_4 at 1100 and 1200 K in Oxygen,” Bull. Mater. Sci., Vol. 19, No. 5, pp. 807-821.

172. **Mohanty,** Smith, R.W., De Bonte, M., Celis, L.P. and Lugscheider E., (1996), “Sliding Wear Behavior of Thermally Sprayed 75/25 Cr_3C_2/NiCr Wear Resistant Coatings,” Wear, Vol. 198, pp. 251-266.

173. **Morimoto.** J., Yoh S., Shinji F., Nobuyuki A. and Masahiro T., (2006), "’Surface Modification of Cr_3C_2-NiCr Cermet Coatings by Direct Diode Laser,” Vacuum, Vol. 80, pp. 1400-1405.

174. **Moujahid,** S.E., (1987), “High Temperature Corrosion of Cast Iron-Chains by Coal Ash,” Proc. Of 10th 1CMC, Madras, India, Vol. 1, pp. 857-860.

175. **Murthy,** J.K.N. and Venkataraman, B., (2006), “Abrasive Wear Behaviour of WC-CoCr and Cr_3C_2-20(NiCr) Deposited by HVOF and Detonation Spray Processes,” Surf. Coat. Technol., Vol.200, pp. 2642-2652.

176. **Murthy,** J.K.N., Bysakh, S., Gopinath, K. and Venkataraman, B., (2007), “Microstructure Dependent Erosion in Cr_3C_2-20(NiCr) Coating Deposited by a Detonation-Gun,”Surf. Coat. Technol., Vol. 202, No. 1, pp. 1-12.

177. **Murthy**, J.K.N., Venkataraman, B., (2006), “Abrasive wear behavior of WC-CoCr and

Cr3C2-20(NiCr) deposited by HVOF and detonation spray processes," Surface and Coatings Technology., Vol. 200, pp. 2642-2652.

178. **Mukhopadhyay,** N.K., Chowdhury,S.G., Das, G., Chattoraj, I., Das S.K. and Bhattacharya, D.K., (1998), "An Investigation of the Failure of Low Pressure Steam Turbine Blades",Engineering Failure Analysis, Vol. **5**, pp. 181-193.
179. **Mukhopadhyay**, N.K.**,** Chowdhury S.G., Sinha, R.K.., Bhattacharys D.K., and Chaudhuri, S., (1999), "An analysis of remaining life estimation of a service exposed economiser tube of 60 MW boiler," Engineering Failure Analysis, Vol. 6, pp. 233-243.
180. **Nanni,** P., Buscaglia, V., Asmundis, C.D. and Roy, S.K., (1987), "Sodium Sulphate Induced Hot Corrosion of Pure Fe, Mn and Cr in Combustion Gas," Proc. of 10th ICMC, Madras, India, Vol. 4, pp. 3413-3422.
181. **Natesan,** K., (1976), "Corrosion-Erosion Behavior of Materials in a Coal-Gasification Environment," Corros., Vol. 32, No. 9, pp. 364-370
182. **Natesan,** K., (1985) "High-Temperature Corrosion in Coal Gasification Systems," Corros.,Vol. 41 No. 11,pp. 646-655.
183. **Nelson**, H.W., Krause, H.H., Ungar, E.W., Putnam. A.A., Slunder, C.J., Miller, P.D., mmel, J.D. and Landry, B.A., (1959), "A Review of Available Information on, Corrosion and Deposits in Coal- and Oil-Fired Boilers and Gas Turbines," Report of ASME Research Committee on Corrosion and Deposits from Combustion Gases. Pub. Pergamon Press and ASME, N.Y.
184. **Nerz,** J.E., Kushner B.A. and Rotolico, A.J., (1992), "Microstructural Evaluation of Tungsten Carbide-Cobalt Coatings," ASM International (U.S.A.), pp. 115-120.
185. **Nicholls,** J.R. and Stephenson, D.J., (1995), "Chapter- 22: High-Temperature Coatings for Gas Turbines," in 'Intermetallic Compounds, Principles and Practice, Vol. 2-Practice,' Eds. Westbrook, J.H. and Fleischer, F.L., Pub. John Wiley & Sons Ltd. England.
186. **Nicholls**, J.R., Simms, N.J., Chan, W.Y. and Evans, H.E. (2002), "Smart Overlay Coatings- Concept and Practice," Surf. Coat. Technol., Vol. 149, pp. 236-244.
187. **Nickel**, H., Quadakkers, W.J. and Singheiser. L., (2002), "Analysis of Corrosion Layers on erective Coatings and High Temperature Materials in Simulated Service Environments of Modern Power Plants Using SNMS, SIMS, SEM, TEM. RBS and X-ray Diffraction studies." Anal. Bioanal. Chem., Vol. 374, pp. 581 -587.
188. **Nicoll,** A.R., (1984), "Chapter 13: The Production and Performance Evaluation of High temperature Coatings," in 'Coatings and Surface Treatment for Corrosion and Wear

esistance,' Eds. Strafford, K.N. Datta, P.K. and Googan. C.G., (1984), Institution of Corros. Sci. and Technol., Birmingham, Pub. Ellis Horwood Ltd., Chichester.

189. **Niranatlumpong,** P., Ponton, C.B. and Evans H. E. (2000), "The Failure of Protective oxides on Plasma-Sprayed NiCrAlY Overlay Coatings," Oxid. Met, Vol. 53, No. 3-4, pp. 41-258.
190. **Otsuka**, N, (2002), "Effects of Fuel Impurities on the Fireside Corrosion of Boiler Tubes in Advanced Power Generating Systems-A Thermodynamic Calculation of Deposit Chemistry," Corros. Sci., Vol 44, pp. 265-283.
191. **Pantony**, D.A. and Vasu, K.I., (1968A), "Studies in the Corrosion of Metals under Melts-1," J. Inorg. Nucl. Chem., Vol. 10, pp. 423-432.
192. **Pantony**, D.A. and Vasu, K.I., (1968B), "Studies in the Corrosion of Metals under Melts-III," J. Inorg. Nucl. Chem., Vol. 10, pp. 755-779.
193. **Park**, S.Y., Kimb, M.C. and Park, C.G., (2007), "Mechanical Properties and Microstructure Evolution of the Nano WC-Co Coatings Fabricated by Detonation gun Spraying with Post Meat Treatment," Mate. Sci. Engg. A, Vol. 449-451, pp. 894-897.
194. **Pettit**, F.S. and Giggins, C.S., (1987). "Hot Corrosion, Chapter 12," in 'Superalloys II,' Eds. Sims, C.T., Stollof, N.S. and Hagel, W.C., Pub. Wiley Pub., N.Y.
195. **Pettit**, F.S. and Meier, G.H., (1984), ":Oxidation and Hot corrosion of Superalloys," M. Gell, C.S. Karlovich, R.H. Bricknel, W. B. Kent, J. F. Radovich (Eds.),The Met. Soc. of AIME, Warrendale, Pensylvania, pp. 651-687.
196. **Pettit,** F.S. and Meier, G.H., (1985), "Oxidation and Hot corrosion of Superalloys," Juperalloys 85, Eds. Gell, M., Kartovich, C.S., Bricknel, R.H., Kent W.B. and Radovich, I.F., Met. Soc. of AIME, Warrendale, Pensylvania, pp. 651-687.
197. **Pettit,** F.S., (1977), "Design of Structural With High Temperature Corrosion Resistance, Fundamental Aspects of Structural Alloy Design," N.Y. : Plenum press, pp. 597-621
198. **Planche**, M.P., Liao, H. and Coddet, C., (2004), "Relationships between in-flight particle characteristics and coating microstructure with a twin wire arc spray process and different working conditions," Surf. and Coat. Technol., Vol. 182, pp. 215-226.
199. **Porcayo-Calderon,** J., Gonzalez-Rodriguez, J.G. and Martinez, L., (1998), "Protection of Carbon Steel against Hot Corrosion using Thermal Spray Si- and Cr-Base Coatings," J. Mater. Engg. Perform., Vol. 7, pp. 79-87.
200. **Prakash,** S., Puri, D. and Singh, H., (2005), "Hot Corrosion Behaviour of Plasma Sprayed Coating on Ni-Based Superalloys in Na2S04-60%$V_2$05 Environment" ISIJ Int., Vol. 45,

No.6, pp. 886-895.

201. **Prakash,** S., Singh, S., Sidhu, B. S. and Madeshia, A., (2001), “Tube Failures in Coal Fired Boilers,” Proc. National Seminar on Advances in Material and Processing, Nov., 9-10, I1TR, Roorkee, India, pp. 245-253.

202. **Priyantha,** N., Jayaweera, **P.,** Sanjurjo, A., Lau, K., Lu, F. and Krist, K., (2003), “Corrosion-Resistant Metallic Coatings for Applications in Highly Aggressive Environments,” Surf. Coat. Technol., Vol. 163-164, pp. 31-36.

203. **Rapp**, R.A. and Goto, K.S., (1981), "The Hot Corrosion of Metals by Molten Salts,” Sympos. Fused Salts, Eds. Braunstein, J. and Selman, J. R., The Electrochem. Soc., Pennington, N. J., pp. 159.

204. **Rapp**, R.A., (1986). “Chemistry and Electrochemistry of the Hot Corrosion of Metals,” Corros., Vol. 42, No. 10, pp. 568-577.

205. **Rapp**, R. A., (2002), "Hot Corrosion of Materials: A Fluxing Mechanism,” Corros. Sci, Vol.44, No. 2, pp. 209-221

206. **Rapp**, R.A., Devan, J.H., Douglass, D. L., Nordine, P.C., Pettit, F.S. and Whittle, D.P., (1981), "High Temperature Corrosion in Energy Systems,” Mater. Sci. Engg., Vol. 50, pp. 1-17.

207. **Rahman,** A., Jayaganthan, R., Chandra, R. and. Ambardar R., (2013), “High temperature degradation behavior of sputtered nanostructured Co–Al coatings on superalloy,” Applied Surface Science, Vol. 265, pp. 10-23.

208. **Rajan**, A., Davenport A.J., Geoff M.S. and Andreas A., (2006), “Effect of iron-containing intermetallic particles on the corrosion behavior of aluminium,” Corrosion Science, Vol. 48, pp. 3455-3471.

209. **Reid**, W.T., (1971), “External Corrosion and Deposits-Boilers and Gas turbines,” Elsevier, N.Y., pp. 115-143

210. **Ren**, X. and Wang, F., (2006), “High-temperature Oxidation and Hot-Corrosion Behavior of A Sputtered NiCrAlY Coating With and Without Aluminizing,” Surf. Coat. Technol., Vol. 201. pp.30-37

211. **Ren**, X., Wang, F. and Wang, X., (2005), “High-temperature Oxidation and Hot Corrosion Behaviors of the NiCr-CrAl Coating on a Nickel-based Superalloy,” Surf. Coat. Technol., Vol. 198, pp. 425-431.

212. **Sachs,** K., (1958), “Accelerated High Temperature Oxidation due to Vanadium Pentoxide,” Metallurgia, Apr., pp. 167-173.

213. **Sahraoui,** T., Guessasma, S., Fenineche, N.E., Montavon, G. and Coddet, C., (2004),"Friction and Wear Behaviour Prediction of HVOF Coatings and Electroplated Hard Chromium Using Neural Computation," Mater. Letters, Vol. 58, pp. 654- 660.

214. **Salmenoja,** K., Makela, K., Hupa, M. and Backman, R. (1996), "Superheater Corrosion in Environments Containing Potassium and Chlorine," J. Inst. Energy, Vol.69, pp. 155-162.

215. **Sarkar**, D, Manoj Kumar B. V., and Basu, B**.**, (2006), "Understanding the fretting wear of Ti_3SiC_2," Journal of the European Ceramic Society, Vol. 26, pp. 2441-2452.

216. **Saunders,** S.R.J., Gohil, D.D., Banlcs, J.P., Sheriff, M.U., Tortorelli, P.F., Van, J.H.D. and Wright, I.G., (1997), "Behaviour of FeCr alloy and Iron Aluminides Alloys in Coal Gasification Atmospheres Containing HC1," Mater. Sci. Forum, Vol. 251-254, pp. 583-90.

217. **Scrivani,** A., Ianeili, S., Rossi, A., Groppetti, R., Casadei, F. and Rizzi, G., (2001), "A Contribution to the Surface Analysis and Characterization of HVOF Coatings for Petrochemical Application," Wear, Vol. 250, pp. 107-113.

218. **Schuh**, C.A., Hufnagel, T.C. and Ramamurty, U., (2007), "Mechanical behavior of amorphous alloys," Acta Mater., Vol. 55, pp. 4067-4109.

219. **Seal,** S., Bose, S.K. and Roy, S.K., (1994), "Improvement in the Oxidation Behaviour of Austenitic Stainless Steels by Superficially Applied, Cerium Oxide Coatings," Oxid. Met., Vol. 41, No. 1-2, pp. 139-178.

220. **Sedriks**, A.J., (1996), "Corrosion of stainless steels," 2nd ed., John Wiley & Sons, New York.

221. **Seo,** D., Ogawa, K., Tanno, M., Shoji, T. and Murata S., (2007), "Influence of Heat Exposure Time on Isothermal Degradation of Plasma Sprayed CoNiCrAlY Coatings," Surf. Coat. Technol., Vol. 20, pp. 7952-7960.

222. **Sharma**, R.N., (1996), "Hot Corrosion Behaviour of Iron- and Nickel-Base Superalloys in Salt Environments at Elevated Temperatures," Ph.D. Thesis. Met. & Mat. Engg. Dept., University of Roorkee, Roorkee, India.

223. **Shi**, L., (1993), "Accelerated Oxidation of Iron Induced by Na_2SO_4 Deposits in Oxygen at 750°C- A New Type Low-Temperature Hot Corrosion," Oxid. Met., Vol. 40, No. 1-2, pp. 197-211.

224. **Shi,** L., Zhang, Y. and Shih, S., (1993A), "The Low Temperature Hot corrosion of Iron and Iron-AIuminium Alloys," Corros. Sci., Vol. 33, No, 9, pp. 1427-1438.

225. **Shih**, S., Zhang, Y. and Li, X., (1989), "Sub-Melting Point Hot Corrosion of Alloys and Coatings," Mater. Sci. Eng. A., Vol. 120, pp. 277-282.

226. **Shirvani**, K., Saremi, M., Nishikata, A. and Tsuru, T., (2003), "Electrochemical Study on Hot Corrosion of Si-modified Aluminide Coated In-738LC in Na_2SO_4-20 wt.% NaCI melt at 750 °C," Corrosion Science, Vol.45, pp. 1011-1021.

227. **Shukla**, V.N., Tewari, V.K., Jayaganthan, R., (2011), "Comparison of tribological behavior of Cr_3C_2-NiCr coatings deposited by different thermal spray Techniques: a review," International journal of materials science and engineering, Vol. 2, pp. 55-58.

228. **Shukla**, V.N., Jayaganthan, R., Tewari, V.K., (2012), "Hot corrosion studies of HVOF-sprayed Cr_3C_2-NiCr coating on 310S stainless steel in an actual environment of a coal fired boiler," Advanced Materials Research, Vol. 585, pp. 483-487.

229. **Shukla**, V.N., Jayaganthan, R., Tewari, V.K., (2013), "Degradation Behavior of Nanostructured Coatings Deposited by High-Velocity Arc Spraying Process in an Actual Environment of a Coal-Fired Boiler," JOM, Vol. 65(6), pp. 784-791.

230. **Sidhu**, B.S., (2003), 'Studies on the Role of Coatings in Improving Resistance to Hot Corrosion and Degradation,' Ph.D. Thesis, Met. & Mat. Eng. Dept., Indian Institute of Technology Roorkee, Roorkee.

231. **Sidhu,** B.S., Puri, D. and Prakash, S., (2004), "Characterisations of Plasma Sprayed and Laser Remelted NiCrAlY Bond Coats and Ni_3Al Coatings on Boiler Tube Steels," Mater. Sci. Eng. A-Struct., Vol. 368, No. 1-2, pp. 149-158.

232. **Sidhu,** B.S. and Prakash, S., (2006P), "Erosion-Corrosion of plasma as sprayed and laser remelted Stellite 6 coatings in a coal fired boiler," Wear, Vol. 260, pp. 1035-1044.

233. **Sidhu,** T.S., Prakash, S. and Agravval, R.D., (2005A), "Studies on the properties of high-velocity oxy-fuel thermal spray coatings for higher temperature applications,"Mater. Sci., Vol.41. No. 6, pp. 805-823.

234. **Sidhu,** T.S., Prakash, S. and Agrawal, R.D., (2006A), "Performance of High Velocity Oxy Fuel -Sprayed Coating on an Fe-Based Superalloy in Na_2SO_4–V_2O_5 Environment at 900 °C Part II: Hot Corrosion Behaviour Of Coating," J. Mate. Engg. Perf., Vol. 15, pp. 130-138.

235. **Sidhu,** T.S., Prakash, S. and Agrawal, R.D., (2006B), "Hot corrosion studies of HVOF sprayed Cr_3C_2-NiCr and Ni-20Cr coatings on nickel-based superalloy at 900 °C," Surf. Coat. Technol., Vol. 201, No. 3-4, pp. 792-800.

236. **Sidhu,** T.S., Prakash, S. and Agrawal R.D., (2006C), "Hot Corrosion Behaviour of HVOF-Sprayed NiCrBSi Coatings on Ni and Fe-based Superalloys in Na_2SO-60% V_2O_5

Environment at 900 °C," Acta Materialia, Vol.54, pp. 773-784.

237. **Sidhu,** T.S., Prakash, S. and Agrawal R.D., (2006D), "Hot corrosion and performance of nickel-based coatings", Current science, Vol. 90, No. 1, pp. 41-47.

238. **Sidhu,** T.S., Prakash, S. and Agrawal R.D., (2007), "Study of Molten Salt Corrosion of High Velocity Oxy-Fuel Sprayed Cermet and Nickel-Based Coatings at 900°C," Metar. Mate. Trans. A., Vol. 38, pp. 77-85.

239. **Sidhu,** T.S., Prakash, S. and Agrawal, R.D. (2006E), "Hot Corrosion Studies of HVOF NiCrBSi and Stellite-6 Coatings on a Ni-based Superalloy in an Actual Industrial Environment of a Coal Fired Boiler," Surf. Coat. Technol., Vol. 201 No.3-4, pp. 1602-1612

240. **Sidhu,** T.S., Prakash, S. and Agrawal, R.D. (2006F), "Studies of the Metallurgical and Mechanical Properties of High Velocity Oxy-Fuel Sprayed Stellite-6 Coatings on Ni- and Fe- Based Superalloys,"Surf. Coat. Technol., Vol. 201 No. 1-2, pp. 273-281.

241. **Sidhu,** T.S., Prakash, S. and Agrawal, R.D. (2006G), "Characterizations of HVOF Sprayed NiCrBSi Coatings on Ni- and Fe-based Superalloys and Evaluation of Cyclic Oxidation Behaviour of Some Ni-based Superalloys in Molten Salt Environment," Thin Solid Films, Vol. 575 No. l, pp. 95-105.

242. **Sidhu,** T.S., Prakash, S. and Agrawal, R.D., (2005B), "Hot Corrosion Performance of a NiCr Coated Ni-based alloy," Scripta Materialia, Vol. 55, pp. 179-182.

243. **Sidhu,** T.S., Prakash, S. and Agrawal, R.D., (2006H), "Evaluation of Hot Corrosion Resistance of HVOF Coatings on a Ni-based Superalloys in Molten Salt Environment," Mater. Sci Eng. A., Vol. 430**,** No.2, pp. 64-78.

244. **Sidhu,** T.S., (2006K), "Studies on the Hot corrosion Behaviour of HVOF Coatings on Some Ni-and Fe- Based Superalloys," Ph.D. Thesis, Dept, of Met. & Mat. Engg. Dept., Indian Institute of Technology Roorkee, Roorkee.

245. **Sidky,** P.S. and Hocking, M.G., (1987), "The Hot Corrosion of Ni-Based Ternary Alloys and Superalloys for Application in Gas Turbines Employing Residual Fuels," Corros. Sci., Vol. 27, No. 5, pp. 499-530.

246. **Sidky,** P.S., Hocking, M.G., (1999), "Review of Inorganic Coatings and Coating Processes For Reducing Wear and Corrosion," Brit. Corros. J., Vol. 34, No. 3, pp. 171-183.

247. **Singh,** H., Prakash, S. and Puri, D., (2006), "Some observations on the high temperature oxidation behaviour of plasma sprayed Ni_3Al coatings," Mater. Sci. Engg. A, Vol. 444, pp. 242-250.

248. **Singh**, H., Puri, D. and Prakash, S., (2005A), "Some Studies on Hot Corrosion

Performance of Plasma Sprayed Coatings on a Fe-Based Superalloy," Surf. Coat. Technol., Vol. 192, No. 1, pp. 27-38.

249. **Singh**, H., Puri, D. and Prakash, S., (2005B), "Corrosion Behaviour of Plasma Sprayed Coating on Ni based Supcralloys in $Na2S0_4$-60%V_2O_5 Environment at 900°C" ISIJ Int., Vol. 45, No.6, pp. 886-895.

250. **Smeggil,** J.G. and Bornstein, N.S., (1983), "Study of 'Interdiffusion Effects on Oxidation/Corrosion Resistant Coatings for Advanced Single Crystal Superalloys," Proc. sympos. High-Temperature Protective Coatings, March 7-8, Atlanta, GA, U.S.A., Ed. Singhal, S.C., Pub. Metall. Soc of AIME, Warrendale, PA, USA, pp. 61-74.

251. **Smith,** C.D., Patel, S.J., Farr, N.C. and Hoffmann, M., (1999), "The Corrosion Resistance of Nickel Containing Alloys In Coal Fired Boiler Environments [A]," Corrosion 99[C] NACE International, Houston, pp. 12.

252. **Sobolev,** V.V., Guilemany.J. M. and Nutting, J., (2004), "HVOF spraying," B0655, Maney, IOM3, pp. 5.

253. **Sophie Roure**, Frank Czerwinski, and Anthony Petrie, (1994), "Influence of $Ce0_2$-Coating on the High-Temperature Oxidation of Chromium," Oxid. Met., Vol. 42, pp. 75-102.

254. **Souza,** V.A.D. and Neville A., (2007), "Aspects of Microstructure on the Synergy and Overall Material Loss of Thermal Spray Coatings in Erosion-Corrosion Environments," Wear, Vol. 263, pp. 339-346.

255. **Stein**, K.J., Schorr, B.S. and Marder, A.R., (1999), "Erosion of thermal spray MCr-Cr_3C_2 cermet coatings," Wear, Vol. 224, pp. 153-159.

256. **Stringer**, J., (1972), "The functional form of rate curves for the high temperature oxidation of dispersion-containing alloys forming Cr_2O_3 scale," Oxid. Of Met., Vol. 5 (1), pp. 49-58.

257. **Stringer**, J., (1998), "Coatings in the Electricity Supply industry: Past, Present, and Coatings", Surface and Coating Technology, Vol. 108-109, pp. 1-9.

258. **Streief** R., (1993), "Databases and expert systems for high temperature corrosion and coatings," Corros. Sci., Vol. 35. No. 5-8, pp. 1177-1187.

259. **Stott,** F.H., Chong, F.M. and Stifling, C.A. in M. F. Rothman (ed.), (1985), "High Temperature Corrosion in energy Systems," AIME, Warrendale, PA, PP. 253.

260. **Stott**, F. H., (1998), "The role of oxidation in the wear of alloys," Trib. Int., Vol. 31, No. 1-3, pp. 61-71.

261. **Sundararajan,** T., Kuroda, S., Itagaki, T. and Abe F., (2003), "Steam Oxidation Resistance of Ni-Cr Thermal spray Coatings on 9Cr-1Mo Steel. Part 1:80 Ni-20Cr," ISIJ Int., Vol. 43, No. 1, pp. 95-103.

262. **Thilkan,** H.R., Lahiri, A.K. and banerjee, T., (1967), "Studies on the resistance of alloys steels against oil ash corrosion-part I," NML technical Journal, May, pp. 20-25.

263. **Tiwari,** S.N. and Prakash, S., (1996), "Hot corrosion behavior of an Iron base Super alloys in salt environment at elevated temperature," Proc. Of Sympos. Metals and Materials Research, IIT Madras, Madras, 4-5th July, pp. 107-117.

264. **Tiwari,** S.N., (1997), "Investigations on hot corrosion of some FE, Ni and Co-Base Super alloys in Na_2SO_4-V_2O_5 Environment under cyclic conditions," Ph.D. Thesis, Met. & Mat. Dept., University of Roorkee, Roorkee, India.

265. **Toma D.,** Brandi W. and Koster U., (2000), "The Characteristics of Alumina Scales Formed on HVOF-Sprayed MCrAlY Coatings," Oxid. Met., Vol.53. No. 1-2, pp. 125-137.

266. **Viswanathan** R.,(1989), " Damage mechanism and life assessment of high-temperature components", ASM International, ISBN: 0-87170-358-0, pp. 1-483.

267. **Wagner,** N., Gnadic K., Kreye, H. and Kronewetter, H., (1984), "Particle velocity in Hypersonic Flame Spraying of WC-Co," Surf. Coat. Technol., Vol.22, pp. 61-71.

268. **Wang**, B.Q., Shui, Z.R., (2002), "The hot erosion behavior of HVOF chromium carbide-metal cermet coatings sprayed with different powders," Wear, Vol. 253, pp. 550–557.

269. **Wang**, B., (1996), "Erosion-corrosion of thermal sprayed coatings in FBC boilers," Wear, Vol. 199, pp. 24-32.

270. **Wang**, B.Q., Geng, G.Q., Levy, A.V. and Buchanan, E.R., (1992), "Elevated temperature erosion of carbide-Metal composite, Proceedings of the International Thermal Spray Conference and Exposition," C.C. Berndt, Ed., Materials Park, OH, U.S.A.: ASM International, PP. 735-742.

271. **Wang**, D., (1988), "Corrosion Behaviour of Chromized and/ or Aluminized 21/4Cr-1Mo Steel in medium-BTU Coal Gasifier Environments," Surf. Coat. Technol., Vol. 36, pp. 49-60.

272. **Wang**, B.Q., Seitz, M.W., (2001), "Comparison in erosion behavior of iron-base coatings sprayed by three different arc-spray processes," Wear, Vol. 250, pp. 755-761.

273. **Wielage**, B., Hanna Pokhmurska, Mykhajlo Student, Volodymyr Gvozdeckii, Taras Stupnyckyj, Vasyl Pokhmurskii, (2013), "Iron-based coatings arc-sprayed with cored wires for applications at elevated temperatures," Surf. Coat. Technol., Vol. 220, pp. 27–35.

274. **Wirojanupatump**, S., Shipway, P.H., McCartney, D.G., (2001), "The influence of HVOF powder feedstock characteristics on the abrasive wear behaviour of CrxCy–NiCr coatings," Wear, Vol. 249, pp. 829–837.

275. **Wright**, I.G., (1987), "High temperature corrosion," in "metal handbook", Vol. 13, 9th ed., metals park, ASM, pp. 97-103.

276. **Wu,** C. and Okuyama, M., (1996), "Evaluation of High temperature Corrosion Resistance of Al Plasma Spray Coatings in Molten Sulphates at 1073 K by Electrochemical Measurements," Mater. Trans., JIIM, Vol.37, No. 5, pp. 991-97.

277. **Xiong**, C.Y., Binshi, X. and Yi, X., (2008), "Structure and sliding wear behavior of 321 stainless steel/Al composite coating deposited by high velocity arc spraying technique," Trans. of nonferrous Metal soc. of china, Vol. 18, pp. 603-609.

278. **Xue J.M.**, Ezhilvalavan S., Gao X. S. and Wang J., (2002), "Strontium titanate doped lead metaniobate ferroelectric thin films," Applied Physics letter, Vol. 81, pp. 877-879.

279. **Zhang**, T and Li, D.Y., (2000), "Effects of Cerium on Dry Sand Erosion and Corrosive Erosion Aluminide coating on 1030 steel," J. Mate. Sci. letters, Vol. 19, pp. 429-432.

280. **Zhou**, C., Zhang, Q. and Li, Y., (2013), "Thermal shock behavior of nano structured and microstructured thermal barrier coatings on a Fe-based alloy", Surf. Coat. Technol., Vol. 217, pp. 70-75.